The Application of Heterogenous Supported Catalysts for the Treatment of Greywater via *In-situ* Generated H₂O₂

Thesis submitted in accordance with the requirements of Cardiff University for the degree of Doctor of Philosophy by:

Thomas Edward Harry Richards

School of Chemistry

Cardiff University

2022

Summary.

The work presented within this thesis looks primarily into developing a catalyst with the ability to synthesise H_2O_2 as well as reactive oxygen species that can act in combination as a biocide towards common bacteria and degrade an antibiotic. The current method for the synthesis of H_2O_2 on an industrial scale is the anthraquinone process, however this method necessitates large scale production to be economically viable due to the unselective hydrogenation of the carrier molecule resulting in the need for its periodic replacement alongside the overall complexity of the process. This large-scale production means that concentrated H_2O_2 (70 wt.%) then needs to be transported safely to the desired site of use. This leads to acid/halide stabilisers being added prior to transportation, which then makes the once environmentally friendly oxidant become a hazard as well as the solution needing to be diluted, given the desired concentration for common H_2O_2 use is around 3-5 wt.% H_2O_2. All these factors point towards the desire for a smaller-scale, more efficient method to produce H_2O_2 that could overcome all the drawbacks, including cost of stabilizers, dilution, transport, and storage, with the current industrial route. Water disinfection is currently reliant on chlorination, but ideally requires a route that avoids the formation of chemical residues. H_2O_2, a broad-spectrum biocide, can offer such an alternative, but is typically less effective than traditional approaches to water remediation. However, the results held within this thesis show that a catalytic approach to generating all H_2O_2 reactive oxygen species could form the basis of an alternative method for water disinfection.

The first part of this work investigates the efficacy of AuPd catalysts prepared by an industrially relevant excess chloride wet co-impregnation procedure to synthesise H_2O_2 from molecular H_2 and O_2 in a batch regime. Subsequently, pelleted analogues of these materials were investigated for their activity towards H_2O_2 production and the remediation of *Escherichia coli* K12 JM109. The generation of reactive oxygen species, which include hydroxyl, hydroperoxyl and superoxide radicals (identified by electron paramagnetic spectroscopy), over the 1 wt.% AuPd/TiO$_2$ catalyst during the synthesis of hydrogen peroxide was found to offer extremely high biocidal efficacy (8.1 $\log_{10}$). Comparison to traditional biocides, such as preformed H_2O_2 and NaOCl further demonstrated the efficacy of the catalytic approach, achieving rates of microorganism kill over 10^7 times more potent than conventional disinfectants. This approach could form the basis of an alternative method for water disinfection, particularly in communities not currently served by traditional means of water remediation or where access to potable water is scarce.

Building on earlier studies into bactericidal and virucidal performance of a catalytic approach to water remediation this approach to oxidation was broadened to determine efficacy towards the remediation of organic contaminants found in water bodies via *in-situ* H_2O_2 generation. With a focus on the antibiotic metronidazole, a common antibiotic for the treatment of skin and mouth infections. Initial studies, using the optimal AuPd catalyst from previous investigations to microorganism kill, seemed to indicate the efficacy of the catalytic approach with *in-situ* H_2O_2 achieving far greater rates of conversion compared to that observed using commercial H_2O_2 However, extensive studies revealed that that while there may be a minor contribution from oxidative pathways the primary cause for the observed conversion of metronidazole was the catalysed hydrogenation of the metronidazole.

Finally, extensive catalyst design was investigated with an aim to both improve the performance and stability of the AuPd catalyst studied for bactericidal efficacy and lower catalyst costs by find an alternative to Au. In this work a focus was placed on catalytic performance towards H_2O_2 production, in a batch regime. Initial studies into the well-established AuPd system demonstrated the key role of Pd: Au ratio on catalytic activity, under conditions that have previously been found to be optimal for H_2O_2 formation. Further investigations using the optimal Pd: Au ratio identified the role of the catalyst support in controlling particle size and Pd oxidation state and thus catalytic performance. Building on these studies, Pd was alloyed with a range of abundant secondary metals is subsequently explored. The performance of all catalysts towards H_2O_2 production was subsequently established under conditions approximating those used within earlier studies for water remediation. With an aim to ultimately transition into the flow regime previously utilised, the effect of pelleting the catalytic series was evaluated.

Acknowledgments.

Initially I would like to thank my supervisor Professor Graham Hutchings, for giving me the opportunity to pursue my research for such a prestigious group as the Cardiff Catalysis Institute. His support over the past 4 years has been exceptional and I couldn't have asked for a better supervisor.

Secondly, I would like to thank Cardiff University itself for having me for the last 8 years, it has been a wonderful university to both study at and now work for and I would not have wished to pursue my academic journey anywhere else. I would also like to thank all the academic staff at the university that have both taught me as well as provided me support over my 8 years at this university.

Additionally, I would like to thank all the staff in the CCI for their help within the labs, as well as Steve Morris and Greg Shaw for all their help designing, building, and maintaining all my and the communal CCI reactors, your aid was always greatly appreciated. Furthermore, I would like to thank the analytical services at the university, primarily Dr Thomas Davies, Simon Waller, and Dr David Morgan for all your help in aiding in my comprehension of the analytical techniques as well as providing me with the highest quality of data for me to interpret.

I would also like to thank everyone over in Pharmacy for your help in welcoming me into an unfamiliar environment and making me feel somewhat like a pharmacist, even if I never believed it myself. However, I would like to specifically thank Professor Jean-Yves Maillard, for allowing a chemist into his laboratory, as well Andrew Robertson and Grzegorz Suldecki for training me and answering any stupid questions I may have asked.

Furthermore, I would also like to thank my Postdoctoral researcher Dr Rich Lewis for your endless support through this PhD, I can safely say this body of work would not be half as a good as it is without your continued aid, I am very grateful for both your aid in and outside of university. Additionally, I would like to thank everyone inside the 'hydrogen peroxide team' over my 4 years here Alba Santos, Alex Barnes, Caitlin Crombie, David Kovacic, Joe Brehm, Ash Ward and Greg Sharp for all your help over these past years and for helping me maintain a slither of my sanity.

I would like to thank my landlord and housemate Sina Jamalfar for all your support over the past few years. Additionally, I would like to thank my other housemates. Joe Coombes, for providing me with hours of entertainment and distractions away from Chemistry. Matt Edwards, we came into this PhD together and we will finish this together. Finally, an honourable mention to the guinea pigs of 41 Inverness Place, Ole and Alex, you were the best guinea pigs anyone could have asked for and the 18 months we spent together were never boring. (RIP Alex)

Additionally, I would like to say a big thanks to Dr Richard Champ, Sarah Hamilton, Jo Perkins, and Sarah Spencer-Chapman for their physical and mental support over the past two years.

Finally, I would like to thank my family who none of us this would have been possible without. I am very sad that Grandad Bill, Auntie Claire, and Granny Richards aren't here to see me finish this, but I hope I've done them proud. To Mum, Dad and James, thank you for constantly supporting me throughout these past 8 years. It hasn't been the easiest of times, but this wouldn't have been possible without you all. Finally, I would like to thank Lottie for her constant support over these last 4 year, allowing me to get to the fortunate position I am now.

Publication List.

1. T. Richards, J.H. Harrhy, R.J. Lewis, A.G.R. Howe, G.M. Suldecki, A. Folli, D.J. Morgan, T.E. Davies, E.J. Loveridge, D.A. Crole, J.K. Edwards, P. Gaskin, C.J. Kiely, Q. He, D.M. Murphy, J.Y. Maillard, S.J. Freakley, G.J. Hutchings, Nat. Catal. (2021). **Contribution:** All experimental work held within this thesis was undertaken by myself, apart from the suspension tests, biofilm testing, ethanol *E. coli* testing and EPR experiments.

2. Richards, T., Lewis, R.J., Morgan, D.J. *et al.* The Direct Synthesis of Hydrogen Peroxide Over Supported Pd-Based Catalysts: An Investigation into the Role of the Support and Secondary Metal Modifiers. *Catal Lett* (2022). **Contribution:** All experimental work held within this thesis was undertaken by myself.

Table Of Contents.

1 Introduction.

1.1 General Overview.

The first known use of catalysis can be dated back to 1552 when Valerius Cordus used sulphuric acid to catalyse the conversion of alcohol to ether.[1] However, this scientific discovery wasn't named until 1836 when Jöns Jakob Berzelius published his report 'Catalytic Force' and coined the term catalysis.[2] The term originated from the ancient Greek words' *kata* and *lyein* meaning down and loosen respectively.[1] In this report, he explained the term as:

> "When new compounds are formed in unorganized substances
> in consequence of action between different bodies, it is the result
> of the mutual tendency of these bodies to comply, in a more perfect
> way, with their affinities. On the one hand, those substances
> whose affinities are the strongest combine; and, on the other,
> those which have the weaker affinities are expelled."

hereby introducing the concept of catalysis to the scientific world. Fast forward to modern day and endless industries have evolved and emerged, with catalysts playing a vital role. Currently over 90% of all chemicals produced have a catalyst involved in their synthesis.[3] Aluminosilicates are used in the petrochemical industry for "catalytic cracking" to produce small hydrocarbons, iron is used in the Haber Process for the synthesis of ammonia and nickel is used in the production of syngas looking towards alternative fuels. The utilisation of catalysts towards environmental application is currently paramount, with CO_2 levels, global temperatures and sea levels collectively reaching all-time highs, with no signs of decreasing. Thereby, wherever possible, catalysts are being utilised to increase the efficiency of industrial processes to control pollution and avoid the use of toxic chemicals.

1.2 Theory of Catalysis.

The modern-day definition of a catalyst is a substance that increases the rate of a reaction without modifying the overall standard Gibbs energy change in the reaction.[4] The substance will be able to do this reaction multiple times while not being consumed. The catalyst increases the rate of reaction by providing an alternate reaction pathway with a lower activation energy, in turn decreasing the activation energy (E_a) of the reaction (Figure 1.1). While it can be

observed that the activation energy of the reaction decreases with the addition of the catalyst it is also noticeable that the Gibbs free energy of the system (G) stays consistent. The overall Gibbs free energy of any given reaction is independent of the presence of a catalyst, remaining the same.
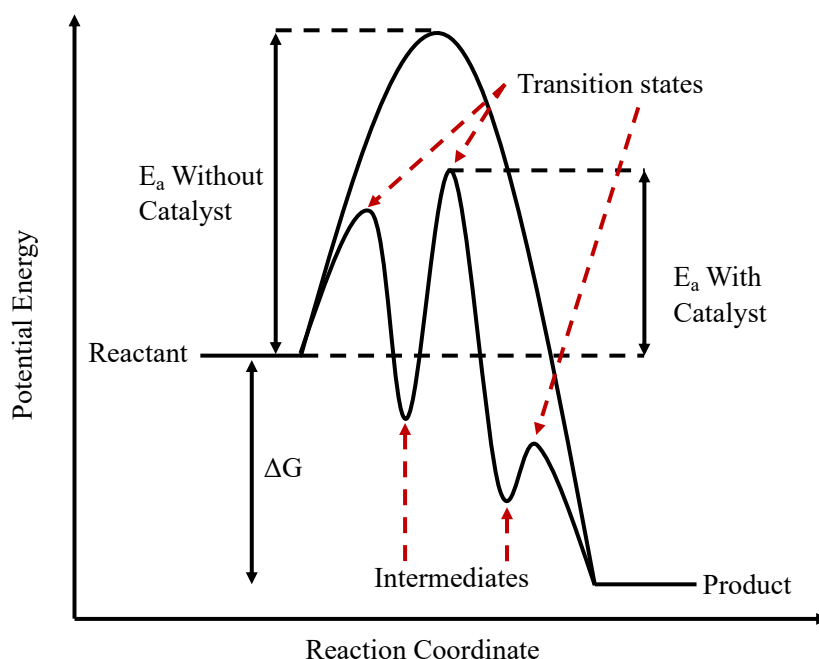
Figure 1.1: Energy diagram comparing the potential energy diagrams for a single-step reaction in the presence and absence of a catalyst. Figure reproduced as image rights are in the public domain.[5]

Every chemical reaction has initial reactants that undergo chemical changes which subsequently lead to the formation of reaction intermediates and transition states, before forming the reactions products. Transition states are molecules formed during the initial stages of a reaction and are very short-lived surviving around one bond vibration cycle. Whereas an intermediate is the state prior to the formation of a new molecule and has a discrete lifetime lasting anywhere from nanoseconds to days. Any given reaction can have multiple intermediates and transition states; however, all these must be surpassed energetically (E_a) before the products of the reaction can be formed, illustrated in Figure 1.1. This energetic barrier, known as the activation energy (E_a), can be overcome by the injection of energy into the reaction either by increasing reactant concentration, temperature and/or pressure. These increases lead to an increase in energy and likelihood of a reaction occurring. Another way to overcome the energetic barrier is to lower the activation energy of the reaction entirely, this can be done by utilising a catalyst. This is done by creating an alternate pathway which requires

less energy to produce the same products. All the above can be condensed into the Arrhenius Equation (Equation 1), which combines all the reaction conditions and produces a rate constant which assigns a value to the rate of any given reaction.

$$k = Ae^{\frac{-E_a}{RT}}$$

(1)

k – Rate Constant – A proportionally factor relating to the rate of a chemical reaction

A – Pre-exponential Factor

E_a – Activation Energy

R – Gas Constant (8.3145 J mol^{-1} K^{-1})

T – Temperature (Kelvin)

Equation 1: The Arrhenius Equation.

1.3 Types of Catalyst.

Catalysts can be present in different physical states in a reaction however can nominally be categorized into one of three classes, they are either a biocatalyst, a homogenous or a heterogeneous catalyst. Biocatalysts implement natural proteins known as enzymes or nucleic acids to catalyse chemical reactions outside of the living cell. There are many advantages to their use, with these catalysts having high catalytic output, and mild reaction conditions. However, they also have their disadvantages, with product and catalyst recovery post reaction being very complex as well as being very unstable when commercially applied. Some progress however has been made using a technique known as immobilization which can aid in increasing many aspects of the catalyst including stability, activity, specificity, recovery and selectivity, as well as a reduction in its inhibition.[6] This can be achieved in a variety of ways by using a multipoint covalent attachment[7] or immobilising upon a hydrophobic or porous support.[8,9]

The main issue with biological catalysts is their high specificity. To reproduce these reactions in a laboratory is a complicated procedure. Enzymes will only work in extremely narrow temperature and pH regions and if the reactions are subject to conditions out of these regions they denature, the biological version of catalyst deactivation.[10] Even with these downfalls enzymes still have their place in catalysis, with certain enzymes being applied to certain heterogenous catalytic reactions. Unspecific peroxygenases (UPOs) are a branch of enzymes

3

that are utilised for the selective oxidation of hydrocarbons due to the use of only H_2O_2 as both an oxygen donor and a final electron acceptor to generate the oxygen species needed for the oxidation to occur.[11] With this being the resolution to an issue that most other heterogenous catalysts have due to low regioselectivity leading to over oxidation of the substrate.[11] Thus allowing the enzymes to be employed in a variety industrial synthesis reaction; with lipase being used to produce biodiesel,[12] rennet for cheese production[13] and proteases for a variety of uses such as detergent and leather manufacturing.[14]

Homogenous catalysis however refers to catalytic reactions in which both the catalyst and reactants are in the same phase. This homogeneity leads to characterisation being very easy and catalytic activity and selectivity being high. However, this also becomes an issue when the catalyst needs to be recovered for re-use as catalyst/product separation can be intricate. The first instance of homogenous catalysis in industry was in the 1750s implementing a NO molecule to assist in the oxidation of SO_2 to SO_3 for the production of sulphuric acid.[15] However, nowadays the application of homogenous catalysis applies to the utilisation of organometallic or coordination complexes such as the Wacker process (Pd catalyst) for olefin oxidation or the Ziegler-Natta process (Ti catalyst) for ethylene polymerisation.[16]

Finally, and where my research will be centred around, is heterogenous catalysis. This is when the catalyst and reactants are in separate phases, typically using a solid phase catalyst alongside gas and/or liquid phase reactants. The catalyst operates by adsorption in which the adsorbate (reactants) binds to the adsorbent (catalyst). There are two types of adsorption that can occur during a heterogenous catalysed reaction; physisorption, in which the adsorbate becomes weakly bound to the adsorbent via Van der Waals forces or chemisorption, where the adsorbate forms a chemical bond with the adsorbent by the sharing of electrons. There are also three mechanisms by which these surface reactions occur, Langmuir-Hinshelwood, Mars-Van Krevelen, or Eley-Rideal mechanism. The Langmuir-Hinshelwood mechanism proceeds with the two reactant molecules (1 + 2) adsorbing to the catalysts' surface simultaneously, once adsorbed they react with each other to form the product before desorbing (Figure 1.2).

The Eley-Rideal mechanism starts with a reactant molecule (1) adsorbing to the catalysts' surface. The second reactant molecule (2) then reacts with 1 to form the product yet does this without adsorbing to the catalysts' surface. Finally, The Mars-Van Krevelen mechanism proceeds by a reactant (1) forming a chemical bond with the catalysts surface. The second

reactant (2) then joins and reacts with the atoms present in the surface to form the product. This then desorbs leaving a vacancy which is then filled with the succeeding reactant.
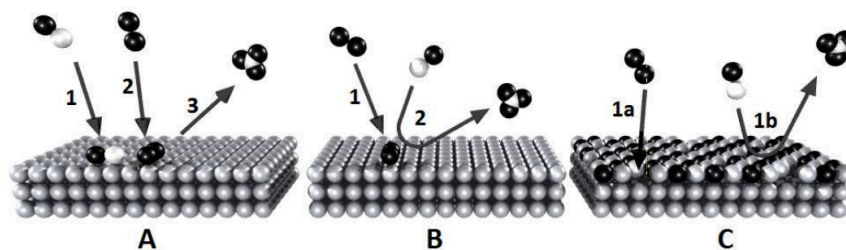
Figure 1.2: Generalised Langmuir-Hinshelwood (a), Eley-Rideal (b) and Mars-Van Krevelen (c) Mechanism. Figure use granted in accordance with copyright by Elsevier.[17]

Heterogenous catalysts are used in many large-scale industrial processes. An Iron catalyst supported on Al_2O_3 is used to synthesise ammonia using the Haber-Bosch process,[18] Ag/Al_2O_3 is used to synthesise ethylene oxide[19] and vanadium oxides are used to synthesise sulphuric acid,[20] to name just a few. However, there is now a demand to make industrial processes 'greener' that adhere to the principles of green chemistry.

1.4   Green Chemistry.

The manufacture and designing of products and processes that eliminate or minimize the use and generation of substances that are in any way hazardous to the environment is an idea known as "Green Chemistry". It was a concept developed in 1998 by Paul Anastas and Nicolas Eghbali[21] and was a way to inspire scientists and engineers alike to take a greener approach towards a sustainable future. Currently, the concept consists of 12 principles,[21] and these are displayed below:

1. **Prevention –** It is better to prevent waste than it is to clean up afterwards: So chemical processes should be designed to minimise waste.

2. **Atom Economy -** Synthetic procedures should be devised to maximise the incorporation of all materials used in the process into the final product.

3. **Less Hazardous Chemical Synthesis –** Synthetic methodologies should use and produce substances that pose little or no toxicity to human health and the environment.

4. **Designing Safer Chemical** – Products should preserve efficacy (i.e., be fit for purpose) while reducing toxicity.

5. **Safer Solvents and Auxiliaries** – Auxiliary substances in chemical procedures (solvents, separation media etc) should be made unnecessary whenever possible and, when used, should be innocuous in the environment.

6. **Design for energy efficiency** – Energy requirements for chemical processes should be recognised for their environmental and economic impact and should be minimised. Processes conducted at ambient temperature and pressure are to be preferred over alternatives.

7. **Use of Renewable Feedstocks** – A raw material should be renewable rather than depleting whenever technically and economically practicable.

8. **Reduce Derivatives** – Derivatisation (use of blocking groups, protection/deprotection steps etc) generate side product waste and so should be avoided.

9. **Catalysis** – Catalytic reagents (as selective as possible) reduce energy and waste requirements and so should be used in preference to stoichiometric reagents.

10. **Design for Degradation** – Chemical products should be designed so that at the end of their lifetime/function they break down into innocuous degradation products.

11. **Real-Time Analysis for Pollution Prevention** – Analytical methodologies need to be further developed to allow for real-time in-process monitoring and control prior to the formation of hazardous substances.

12. **Inherently Safe Chemistry for Accident Prevention** – Substances and the form of a substance used in a chemical process should be chosen to minimise the potential for chemical accident, including releases, explosions, and fires.

1.5   Heterogenous Catalyst Preparation Methods.

The designing of a catalyst must be methodically thought out, making sure to cover all the details associated with the catalyst and the reaction. Catalyst design should begin with the reaction itself, looking into which pathway you want the catalyst to promote and what are the desirable and undesirable products of this route. Yet, promoters or selective poisons can be added to improve performance by increasing catalyst stability, activity and/or selectivity.[22] These are molecules which alone have no catalytic ability and can be added deliberately or accidently to a reaction however when they are introduced they can interact with active components of catalysts and alter their chemical effect on the catalysed substance. However, all these should be considered with cost in mind, which leads to a majority of catalyst being a compromise between cost and catalytic performance.[23] A heterogenous catalyst can be described by shape, size, pore distribution, surface area and the requisite number of components (e.g. active species, promoters and support).[22] The catalysts preparation conditions can also have significant effect on its performance, with the following have a significant effect;[24]

1. Precursor concentration
2. Precursor volume/concentration; support mass ratio
3. Support type
4. Temperature
5. pH
6. Presence of stabilisers
7. Ageing Time
8. Filtration/washing/drying method
9. Choice of Treatment (flow rate, ramp rate, flow gas, temperature)
10. External conditions (light, humidity, contaminants)

1.5.1   Sol-Gel.

One of the most well-established synthetic methods towards the production of metal oxide nanoparticles as well as mixed oxide composites is the sol–gel method. The formation of the metal oxide nanoparticles involves different consecutive steps, initially the corresponding metal precursor undergoes rapid hydrolysis to produce the metal hydroxide solution. This is followed by an immediate condensation which leads to the formation of a three-dimensional

gel. Finally, this gel is subjected to a drying process which produces either an Xerogel, if dried by evaporation, or an Aerogel, if dried supercritically (Figure 1.3).[25] The sol–gel method can be classified into two routes, aqueous sol–gel, if water is used as reaction medium, and nonaqueous sol–gel method, if an organic solvent is used.
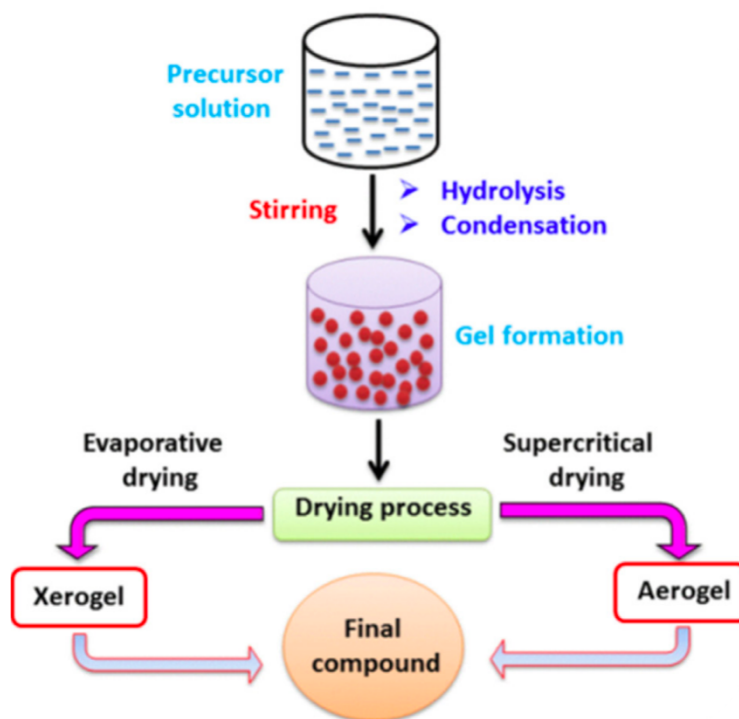
Figure 1.3: Pathway towards the production of metal oxide catalysts using the sol-gel method Figure use granted in accordance with copyright by Elsevier.[25]

For the aqueous sol–gel method, oxygen is a necessity for the formation of metal oxides, with the oxygen being supplied by the solvent, water. Generally, metal acetates, nitrates, sulphates, chlorides, and metal alkoxides are employed as the metal precursors for this method, with the alkoxides dominating due to the high reaction affinity of alkoxides towards water.[26,27] For the nonaqueous or nonhydrolytic sol–gel method, the oxygen required for the formation of the metal oxides is supplied either from the solvents, such as alcohols, ketones, aldehydes, or by the metal precursors. Additionally, the organic solvents also tune several of the catalyst's components like morphology, surface properties, particle size, and composition of the final oxide material.[25]

1.5.2 Chemical Vapour Impregnation (CVI).

Chemical vapour impregnation was first developed in 1962 by Bickerdike[28] for increasing the density of porous carbon. Following this, developments were made when Jenkin,[29] patented the

process for infiltrating porous alumina with chromium carbide in 1964. Commercialization of the CVI process was then implemented by Du Pont (USA) and Société Europeènne de Propulsion (SEP) for the manufacturing of ceramic matrix composites. The CVI method involves the metal precursor penetrating the supports preformed pores, in a gaseous state at ~1000 °C, and undergoing a chemical reaction, before eventually depositing onto the support pores. In this manner the matrix material grows into the fibrous porous structure (preform) in a continuous layer by layer way, thus forming the composite matrix.[30]

1.5.3 Sol-Immobilisation.

In the production of catalysts, the activity and selectivity of the catalyst are correlated by a variety of parameters; morphology, dispersion and interaction of the metal particles and the support.[31] Many varieties of synthesis methods including incipient wetness, impregnation often fail to produce high metal dispersion, mostly depending on the support used in synthesis.[32] Implementing a sol-immobilisation catalytic synthesis however allows a greater control over the metal particle size by the formation of a pre-formed metallic colloid, in turn reducing the effect the support has on the metal particles dispersion.[32] The metallic sol is prepared in the presence of a stabilising agent before immobilising upon the selected support.[33,34] Once the sol is prepared to produce the catalyst the support is then added to the sol and the metal particles adsorb out of solution onto the support. For optimum metal dispersion a support with increased functionality should be chosen e.g. OH, NH, SH.[35]

1.5.4 Coprecipitation.

The coprecipitation synthetic method involves the formation of simultaneous nucleation, growth, coarsening, and/or agglomeration processes to take place. The coprecipitation method proceeds by following stages;[36]

1. The products are obtained as an insoluble species in supersaturation conditions.
2. Nucleation process helps to form many small particles.
3. Post nucleation process takes place due to Ostwald ripening processes which lead to aggregation, dramatically affecting the particle size, shape, morphology, and, with other applications, properties.
4. The supersaturation helps to induce precipitation at the reaction scale.

The advantage of implementing this method is that there is no solid waste, however there are many disadvantages including toxic liquid waste, high capital cost and a readjustment of pH.

1.5.5 Supercritical Antisolvent Synthesis.

The Supercritical Anti Solvent technique is a technique implemented for the micronization of pharmaceutical and natural compounds. The technique itself is established upon the contact of an organic solution alongside supercritical carbon dioxide (SC-CO_2).[37] During the process, SC-CO_2 is quickly dissolved in the organic solution, causing the precipitation of solutes by the antisolvent effect. Following this, SC-CO_2 efficiently extracts the organic solvent, which allows the solvent-free products to be obtained. The technique itself has also been used to synthesise catalysts, with the objective to generate high stability and active catalysts. This was reported by Hutchings & co-workers[38] in which zincian georgeite, an amorphous copper–zinc hydroxycarbonate, was prepared by the aforementioned technique and has demonstrated that it can be used to prepare Cu/ZnO catalysts that are highly active and stable for the WGS reaction. This observed enhanced stability enables the removal of the previous necessary alumina into the catalyst. Furthermore, this technique allows the processing of high-purity materials free from residual catalyst poisons, including nitrates[39] and alkali metals[40] and does not require delicate control of a broad range of conditions such as pH.

1.5.6 Wet Impregnation.

An impregnation catalyst is made in a 3-step process. Initially a solution containing a prerequisite volume of precursor(s) and solvent is generated and is then incorporated alongside the catalysts support for a specific time. Secondly, the mixture is dried to remove the solvent, before finally calcining the catalyst.[41] Impregnation catalysts can be separated into wet-impregnation and incipient wet-impregnation, with the amount of precursor(s) and solvent solution being the only substantial difference. In wet-impregnation an excess amount of this solution is used in respect to the pore volume of the support, while in incipient wet-impregnation either the same or less than the pore volume of the support is added.

1.6 Hydrogen Peroxide.

In chemical synthesis, hydrogen peroxide (H_2O_2) is regarded as a significant reagent due to water and oxygen being the only by-products and its direct synthesis being theoretically 100% atom efficient, acknowledging green chemistry principles 2 and 10. Hydrogen peroxide is an

inorganic peroxide with the formula H_2O_2. It is the simplest of the peroxides, consisting of two hydroxyl groups covalently bound by a single O-O bond. It appears in its purest form as a clear, colourless liquid, which is miscible with water. The non-planar geometric structure of H_2O_2 was eluded to by Antoine Giguère in 1950 using infra-red spectroscopy.[42] However, this structure changes depending on the state of the molecule, due to the hydrogen bonding not being present when in the gaseous state[43] (Figure 1.4).
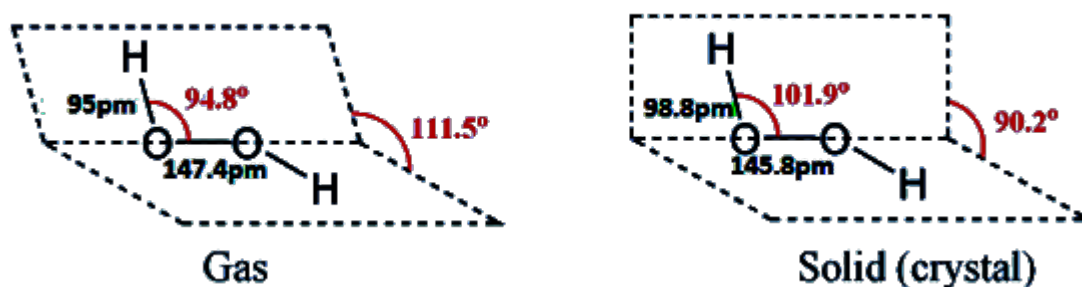
Figure 1.4: Gaseous and solid-state structure of hydrogen peroxide. Figure use granted in as image rights are in the public domain.[43]

Hydrogen peroxide has many industrial applications and as of 2015 its global market value was set at \$3.9 billion.[44] The dominant industries that utilise H_2O_2 are the pulp/paper bleaching and textiles industries in which it is being used as an environmentally friendly alternative to chlorine.[45] Furthermore it can be applied to the destruction of toxic chemicals present in industrial waste as it can efficiently destroy thiocyanate, chlorine and other toxic chemicals.[45] Sodium hypochlorite can also be destroyed with the reaction forming O_2, H_2O and NaCl. It is also prevalent in the mining industry, in the extraction of gold and the extraction and purification of uranium, as well as many other heavy metals.[45]

H_2O_2 is also used in a variety of oxidative processes, such as the Hydrogen Peroxide to Propylene Oxide (HPPO) process for propene oxide synthesis, used for the production of polyurethane and unsaturated resins[46] and, unlike other oxidants, where large amounts of waste are produced requiring separation from the desired product, H_2O_2 only produces water as a by-product.[47,48] In addition, H_2O_2 has the highest active oxygen content of all the most commonly used industrial oxidants (Table 1.1), exemplifying the efficacy of using H_2O_2 as an oxidant.[48]

Table 1.1: Most used oxidants available. Table use granted in accordance with copyright by John Wiley and Sons.[48]

Oxidant	Active Oxygen Content (% w/w)	By-Product
H_2O_2	47.1	H_2O
tBuOOH	17.8	tBuOH
HNO_3	25	NO_x,N_2O,N_2
N_2O	36.4	N_2
NaClO	21.6	NaCl
$NaClO_2$	35.6	NaCl
NaBrO	13.4	NaBr
"$KHSO_5$"[(a)]	10.5	"$KHSO_4$"
$NaIO_4$	29.9[(b)]	NaI
PhIO	7.3	PhI

(a) stabilised and marketed as the triple salt 2 $KHSO_5.KHSO_4.K_2SO_4$ (oxone).

(b) Assuming that all four oxygen atoms are used.

1.6.1 Manufacturing H_2O_2.

The initial procedure to produce H_2O_2 on an industrial scale can be traced back to J. Thenard in 1818,[49] reacting barium peroxide with nitric acid. The process could be improved by replacing nitric with hydrochloric acid, due to the ability of H_2O_2 to be synthesised in combination with barium chloride (Equations 2-4).

$$BaO_2 + 2HCl \longrightarrow BaCl_2 + H_2O_2 \qquad (2)$$

$$BaCl_2 + H_2SO_4 \longrightarrow BaSO_4 + 2HCl \qquad (3)$$

$$BaO_2 + H_2SO_4 \longrightarrow BaSO_4 + H_2O_2 \qquad (4)$$

Equations 2 - 4: Synthesis of H_2O_2 from barium peroxide and hydrochloric acid. Equations reproduced as image rights are in the public domain.

This method of synthesising H_2O_2 was still in production into the 20th century before becoming phased out due to very high production costs and the discovery by Meidinger that H_2O_2 could be generated electrolytically from aqueous sulphuric acid[50] (Equations 5-8). This became an economically viable process for synthesising high purity, concentrated and stable H_2O_2.

However, this still wasn't sufficient, as industry now requires much higher efficiency and reaction rates, while keeping production costs low.

$$2H_2SO_4 \longrightarrow H_2S_2O_8 + H_2 \tag{5}$$

$$H_2S_2O_8 + H_2O \longrightarrow H_2SO_5 + H_2SO_4 \tag{6}$$

$$H_2SO_5 + H_2O \longrightarrow H_2O_2 + H_2SO_4 \tag{7}$$

$$2H_2O \longrightarrow H_2O_2 + H_2 \tag{8}$$

Equations 5-8: The electrochemical synthesis of aqueous H_2O_2. Equations reproduced as image rights are in the public domain.

In 1901, Manchot observed that oxidising hydroquinones or hydrazobenzenes, under alkaline condition, yield peroxides.[51] However, this reaction was insufficient and was then replaced in 1945 by the anthraquinone process and is the method industry still uses to this day. The process was developed by Reidl-Pfeider[52] and uses a 2-alkylanthraquinone (AQ) dissolved in an appropriate solvent and catalytically hydrogenated to the corresponding 2-alkylanthra-hydroquinone (AHQ). AHQ then becomes the hydrogen carrier inside the working solution. The AHQ is then separated from the hydrogenation catalyst and reacted with an oxygen-containing gas, primarily compressed air, to reform AQ and generate H_2O_2 (Figure 1.5).
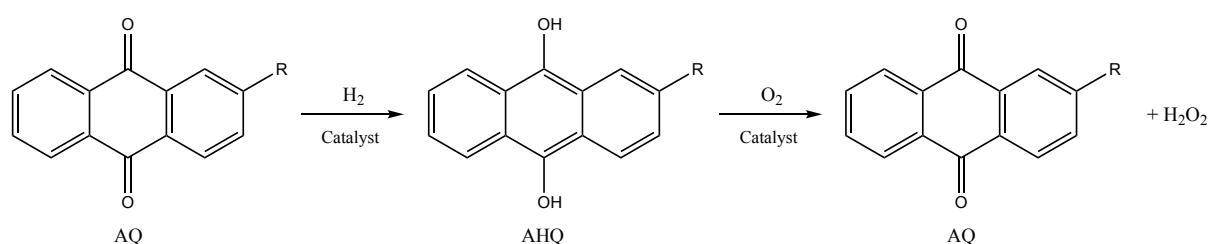
Figure 1.5: The anthraquinone process. Figure use granted in accordance with copyright by Elsevier.[53]

The H_2O_2 is then extracted from the working solution by demineralising water to form a crude solution, with a H_2O_2 concentration of between 25-40 wt.%. This aqueous H_2O_2 is then distilled to remove impurities and generate the commercial grade H_2O_2, with a concentration between 35-70 wt.%.[45]

The advantages to the AQ process are that the reaction occurs under mild conditions (< 80 °C and < 5 bar pressure)[54] and the direct contact between H_2 and O_2 is avoided, with the aforementioned high yields of H_2O_2 generated per cycle. The reaction however is still not without its flaws. There is a need for the quinones, and their reaction products, to have good solubility as well as high resistance to any non-specific oxidation reactions. This is due to the possibility of many by products being generated during the hydrogenation of AQ and oxidation of AHQ (Figure 1.6) leading to the carrier molecule being degraded and preventing the reaction proceeding. This leads to a net consumption of AQ, which to counteract requires constant removal and subsequent reintroduction of fresh AQ. All this causes the process having to be done on a large scale to become commercially viable, which means that concentrated H_2O_2 (70 wt.%) solutions need to be stabilised, stored, and then transported and diluted upon requirement. This transport step generates safety concerns as the H_2O_2 must be transported to its site of use leading to H_2O_2 becoming a potential hazard. This step also causes the need for acid/halide stabilisers to be added to allow transportation of the highly concentrated H_2O_2, leading to this oxidant no longer being environmentally friendly. Stabilisers are added to H_2O_2 to minimise its decomposition over time during under storage, transportation, and/or handling conditions. Common stabilisers used for this process include colloidal stannate, sodium pyrophosphate, organophosphates, nitrates, and phosphoric acid, however the quantities of these stabilisers present in solution are unknown given their industrial application but can range anywhere from a 1:10,000 to 1:1 ratio of stabiliser to H_2O_2.[55] These complications led to research into alternative small-scale routes for the production of 3-5 wt.% H_2O_2, which is the required concentration for most household, dental and cosmetic applications of H_2O_2.[56]
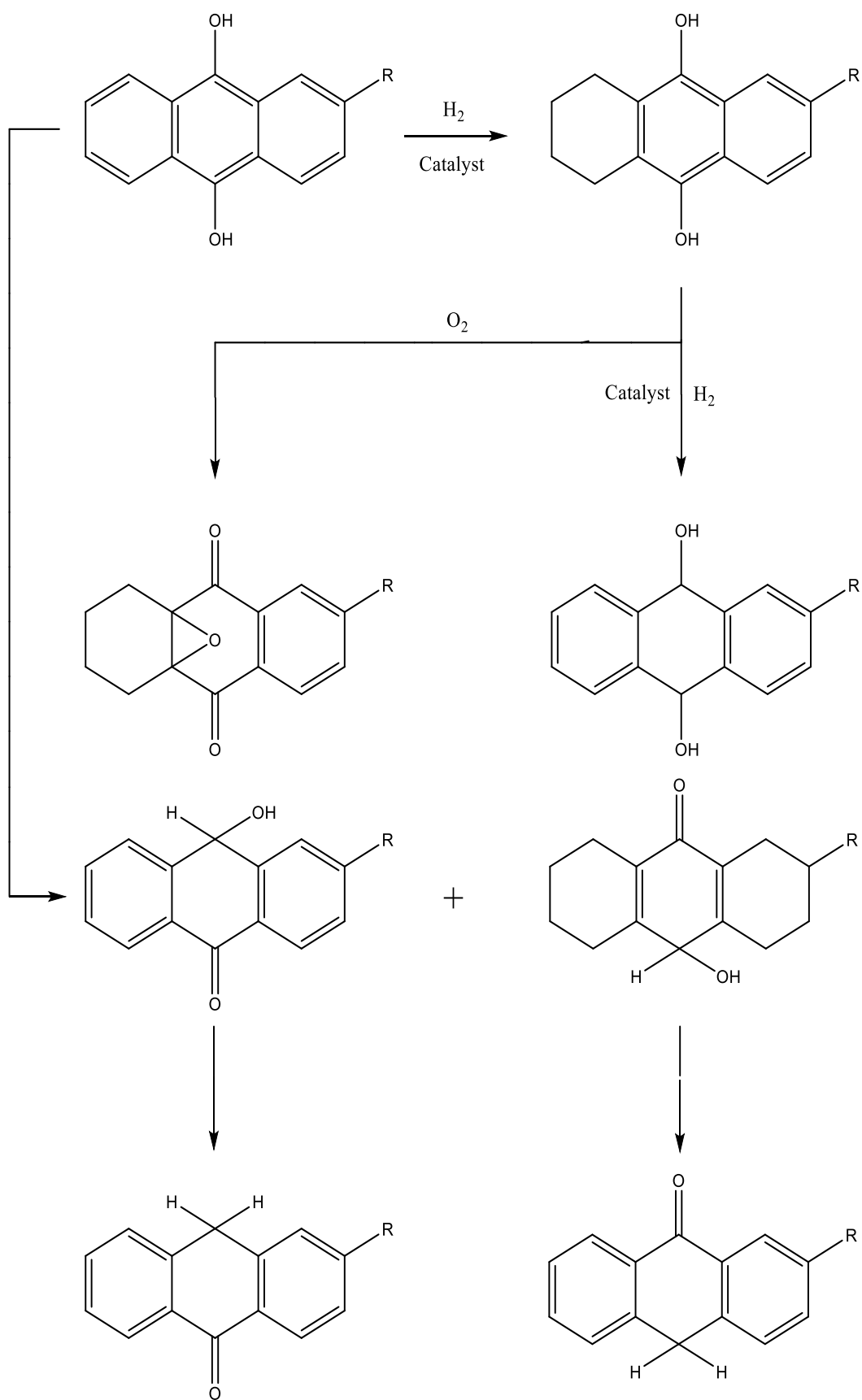
Figure 1.6: Potential by-products produced during the anthraquinone process. Figure reproduction granted in accordance with copyright by Elsevier.[54]

1.6.2   Electrolytic Synthesis of H_2O_2.

Electrochemistry offers an economical and environmentally friendly alternative to the anthraquinone process, producing H_2O_2 from either H_2O or O_2.[57] This can be achieved at either end of an electrolytic cell, the anode or the cathode, and enables the production of "useful"[56] concentrations of H_2O_2 over continued electrolysis. The initial publication into the electrosynthesis of H_2O_2 came from Traube in 1887, in which a Hg-Au electrode was used to synthesise H_2O_2.[58] The reaction however is not without its complications as the majority of electrode materials favour competing oxidation reactions. This is observed in Figure 1.7 as the $4e^-$ reduction of O_2 (the oxygen reduction reaction (ORR)) and the $4e^-$ oxidation of H_2O (the oxygen evolution reaction (OER)) are not required in this reaction as we only desire the $2e^-$ pathways which lead towards the reduction/oxidation of H_2O/O_2. This leads to an overcomplication towards the synthesis of H_2O_2 as the process involves reversible redox reactions for all products, starting materials and reaction intermediates, making the formation of stable H_2O_2 very challenging.
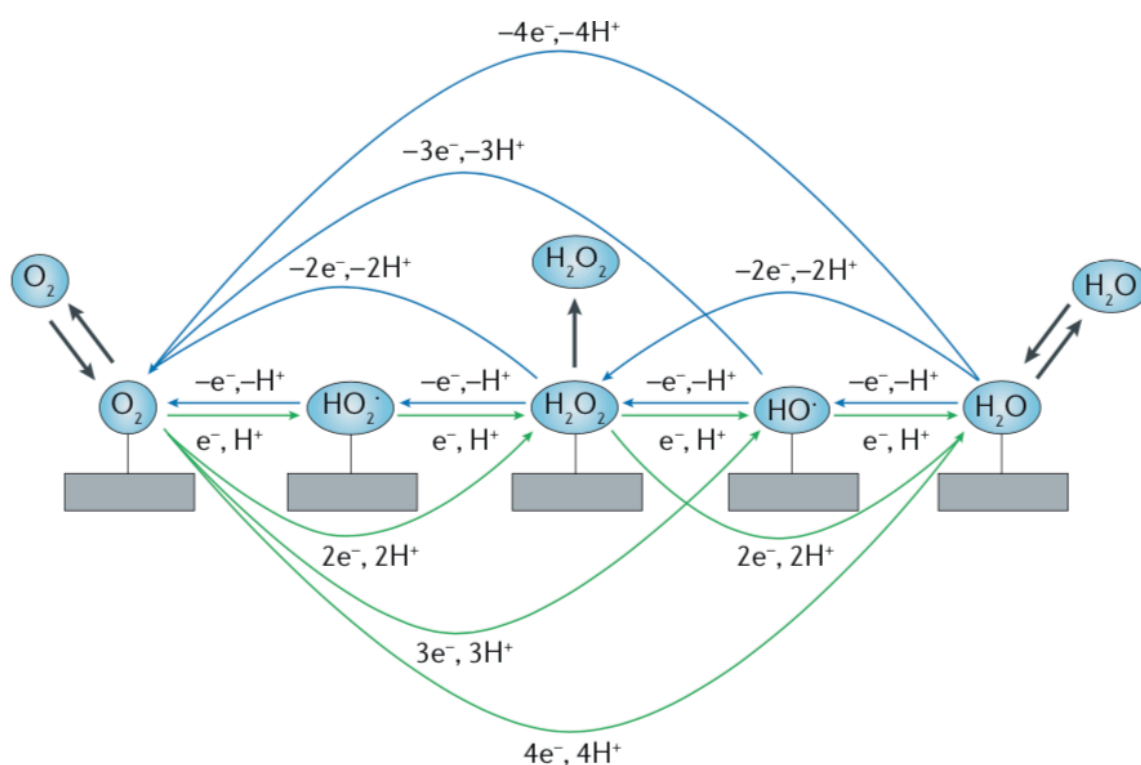
Figure 1.7: Pathway to produce H_2O_2 from H_2O (Blue). Figure use granted in accordance with copyright by Springer Nature.[57]

1.6.3 Direct Synthesis of H_2O_2.

The direct synthesis of H_2O_2 from molecular O_2 and H_2 represents the potential to offer a more economical and environmental alternative to the anthraquinone process, with the synthesis being potentially 100% atom efficient alongside using green solvents in MeOH, H_2O etc. The direct synthesis of H_2O_2 originates back to 1914 with Henkel and Weber experimenting with noble metal catalysts (Pd, Pt, Ni) in a gas stream of H_2 and O_2.[59] Fast forward to modern day and still no industrial application exists for the formation of H_2O_2 via its direct synthesis. This comes down to two issues, safety of operation and H_2O_2 degradation. The combination of H_2 and O_2, are explosive over a wide range of concentration (5-95% of H_2 in O_2), therefore dilution in inert gases (CO_2, N_2) must occur until below the explosive limit. Additionally, the majority of catalysts synthesised for the direct synthesis of H_2O_2 are also active for its decomposition,[60] as both reactions that make up decomposition are thermodynamically favoured, $\Delta G^\circ_{298K} = -211.5$ kJ mol^{-1} for hydrogenation and $\Delta H^\circ_{298K} = -105.8$ kJ mol^{-1} for its decomposition, over its direct synthesis ($\Delta H^\circ_{298K} = -135.8$ kJ mol^{-1})[47]. A free energy diagram showing this can be seen below in Figure 1.8. However, it has also been concluded that a catalyst can be produced that does not degrade any H_2O_2, as proven by Edwards et al[61] in which a 5 wt.% AuPd/C catalyst, pre-treated with 2 vol.% HNO_3, had a decomposition activity of 0 mol$_{H2O2}$ kg$_{cat}^{-1}$ h^{-1}.
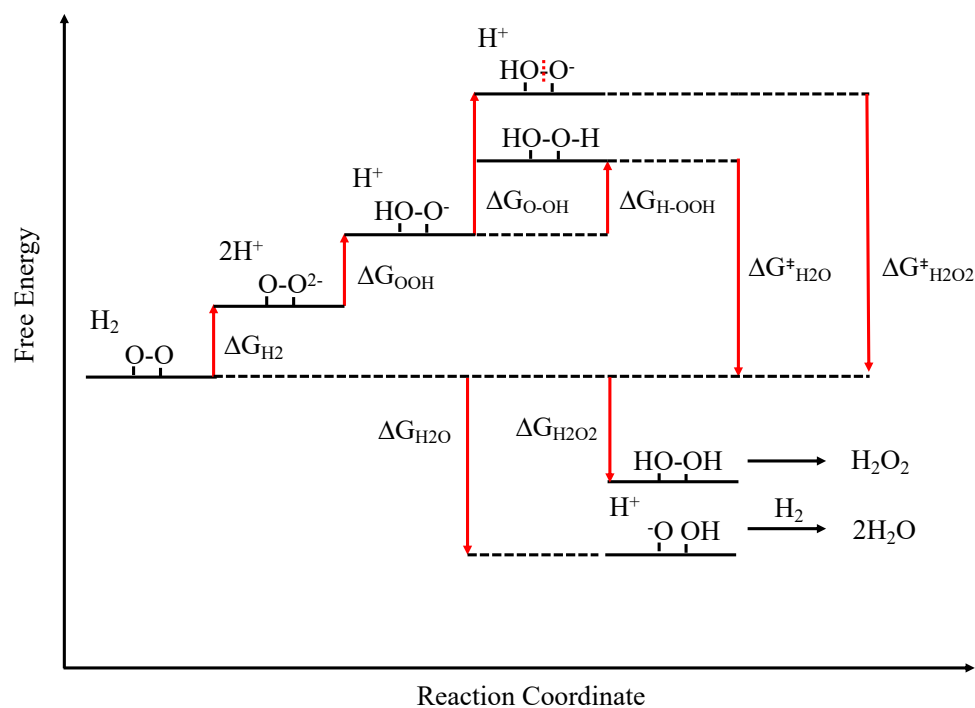
Figure 1.8: Free Energy Diagram for the direct synthesis of H_2O_2. Figure reproduction granted in accordance with copyright by The Journal of American Chemical Society.[62]

This degradation of H_2O_2 must be supressed as much as possible as a high H_2 selectivity (> 95%) is required for any industrial process.[60] To aid in this, modifications to the catalyst can be made. Acidic and halide promoters can be added to the reaction to improve H_2 selectivity, as Pospelova[63–65] and later on Choudhary[66] concluded in their research that the addition of an acid was required to achieve a high H_2O_2 yield employing reduced 5 wt.% Pd catalyst. This response to the inclusion of acid is expected as the decomposition of H_2O_2 is a base catalysed reaction.

1.6.4 Mechanism for the Direct Synthesis of H_2O_2.

The general assumption is that the mechanism for the direct synthesis of H_2O_2 is via a two-step hydrogenation mechanism, with several competitive side reactions also present. To fully comprehend the mechanism many studies have been undertaken. Lunsford & co-workers [67] undertook an isotopic labelling experiment using a mixture $^{16}O_2$ and $^{18}O_2$ to understand whether O_2 is dissociated prior to H_2O_2 formation or if it remained in its diatomic form throughout synthesis, as hypothesised by Pospelova.[63–65] Raman spectroscopy was utilised to determine the isotropic distribution in the product. Results returned showing only two peaks, a $H_2^{16}O_2$ peak at 879 cm^{-1} and a $H_2^{18}O_2$ peak at 830 cm^{-1}, indicating that H_2O_2 is produced from a diatomic form of O_2. This can be concluded as a peak at 852 cm^{-1}, representative of $H_2^{16}O^{18}O$, would also be present if oxygen dissociation was present in synthesis.

The mechanism for the direct synthesis towards H_2O_2, was hypothesised by Hutchings & co-workers[68] and Flaherty et $al,$[69] leading to the production of a reaction scheme which included the steps towards the synthesis of H_2O_2, the undesired side products and the dissociative adsorption of O_2 (Equations 9-18).

$$H_2 + 2^* \longrightarrow 2H^* \quad (9) \qquad O_2 + 2^* \longrightarrow 2O^* \quad (14)$$

$$O_2 + 2^* \longrightarrow O_2^* \quad (10) \qquad O^* + H^* \longrightarrow OH^* + * \quad (15)$$

$$H^* + O_2^* \longrightarrow O_2H^* + * \quad (11) \qquad OH^* + H^* \longrightarrow H_2O^* + * \quad (16)$$

$$O_2H^* + H^* \longrightarrow H_2O_2^* + * \quad (12) \qquad H_2O^* \longrightarrow H_2O + * \quad (17)$$

$$H_2O_2^* \longrightarrow H_2O_2 + * \quad (13) \qquad H_2O_2^* \longrightarrow H_2O^* + O^* \quad (18)$$
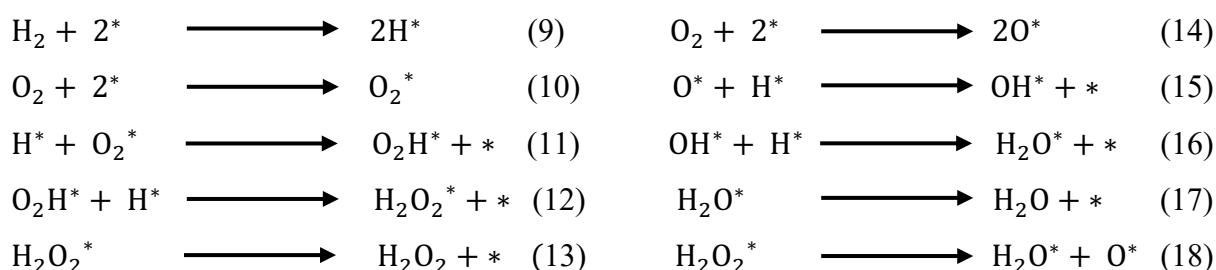
Equations 9–18: Reaction scheme to produce H_2O_2 (9-13), undesired side products (14-18) and dissociative adsorption O_2 (10), with * denoting a vacant site. Equations granted in accordance with copyright by Royal Society of Chemistry.[68]

In this kinetic scheme it can be deduced that the direct synthesis of H_2O_2 is simply a 2-step hydrogenation of O_2, supporting the research by Pospelova [63–65]. Another approach to the production of H_2O_2 could be the combination of 2 adsorbed hydroxyl radicals, formed during the adsorption molecular O_2 binding to two vacant surface sites (6). However, it is kinetically more favourable to form H_2O in this situation via sequential hydrogenation (8-9).

Jun Li *et al*[70] undertook a theoretical approach to aid in the comprehension of the mechanism for H_2O production from H_2O_2, using a Pd (111) and an Au@Pd (111) surface alongside periodic DFT calculations. It was discovered that the main reactions leading to the production of H_2O are the decomposition of H_2O_2 and the hydrogenation of OH, with the dissociation of H_2O_2 being identified as the key step in the production of H_2O. Furthermore, it was discovered that the Au present on the Au@Pd (111) surface were able to encourage the release of H_2O_2, while supressing the dissociation of H_2O_2. The effects of unreacted H atoms present on the catalytic surface were also evaluated and it was discovered that these were, in the same manner as Au, able to encourage the release of H_2O_2 and supress H_2O_2 dissociation, which leads to a net increase in H_2O_2 selectivity.

Further theoretical studies were launched by Staykov *et. al*[71] into developing a study into the direct interaction of H_2 and O_2 on a Pd(111), to be able to propose a reaction mechanism and explain the observe high selectivity of bimetallic AuPd catalysts. The first step in the formation of H_2O_2 upon Pd(111) is the superoxo molecule interacting with the hydrogen atom situated over the nearest 3-fold position forming the first step intermediate, which is then followed by this intermediate reacting with the second hydrogen in the nearest 3-fold position leading to the formation of H_2O_2 (Figure 1.9).
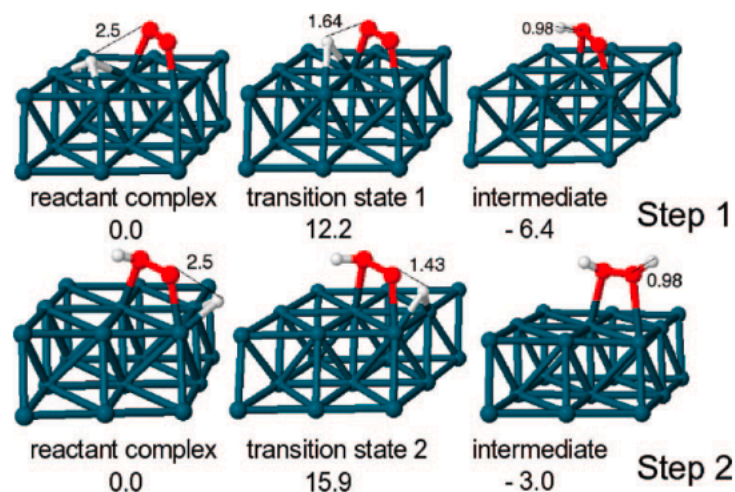
Figure 1.9: The formation of H_2O_2 upon the Pd(111) surface, with bond lengths being in Å and energies in Kcal mol^{-1}. Figure use granted in accordance with copyright by The Journal of American Chemical Society.[71]

When Au is added to the catalyst surface the adsorption of O_2 is the same as on the Pd(111), however the presence of Au significantly suppresses the oxygen dissociation. This absence in atomic oxygen increases the amount of H_2O_2 produced and reduces the pathways that leads to the formation of H_2O. For the dissociation of H_2 however, it is essential that this same presence of Au doesn't also block the dissociation of H_2, which it was determined to not be the case because its presence does not block the reaction and allows formation of atomic H. Therefore, it is concluded that the theoretical study shows that the presence of Au blocks the dissociation of H_2O_2 and increases the selectivity towards it.

1.6.5   Key Points.

- H_2O_2 is produced from a diatomic form of O_2 rather than the O_2 being dissociated prior.[67]
- Direct synthesis of H_2O_2 is simply a 2-step hydrogenation of O_2.[68]
- The main reactions leading to the production of H_2O are the decomposition of H_2O_2 and the hydrogenation of OH, with the dissociation of H_2O_2 being identified as the key step in the production of H_2O.[70]
- The presence of Au alongside Pd blocks the dissociation of H_2O_2 and increases the selectivity towards it.[71]

1.7   Direct Synthesis of H_2O_2 Utilising Pd catalysts.

Pd as a catalyst for the direct synthesis of H_2O_2 was initially reported by Henkel and Webber.[59] They patented the cathode manufacturing of H_2O_2 in an electrolyte containing O_2 or an O_2 containing species, alongside water, gaseous H_2 and a Pd catalyst. The issue with the direct synthesis of H_2O_2 is the explosive limit on H_2. The safety rating assigned to H_2 is the highest available rating on the flammability scale, NFPA 704, due to high H_2 diffusion rate in air and still being flammable when mixed with air in a volumetric ratio as low as 4%. This was observed when DuPont developed a pilot plant utilising a supported Pd-based catalyst to synthesise H_2O_2 in 10% H_2 and O_2, yet due to frequent explosion over time the plant never reached commercialisation and to its eventual decommissioning.[56] This concluded that to be able to work towards synthesising H_2O_2 directly, the reaction must be done outside of the explosive region, with an O_2:H_2 ratio of 2:1 and a dilution of H_2 in inert gas to below 4%.

Colloidal Pd can also be utilised as a catalyst for the direct synthesis of H_2O_2, even due to its homogenous characteristics and their associated drawbacks around separation. Lunsford *et. al*[67,72] investigated into colloids by utilising a 5 wt.% Pd/SiO_2 catalyst for the direct synthesis of H_2O_2. The catalyst was tested in an HCl acidified water solution, alongside H_2 and O_2. The catalyst was shown to be active for H_2O_2 synthesis however, it was concluded that it was not the supported Pd/SiO_2 catalyst that was synthesising H_2O_2 but rather $PdCl_4^{2-}$ that was generated during the reaction and found to be present in the liquid phase (Figure 1.10).
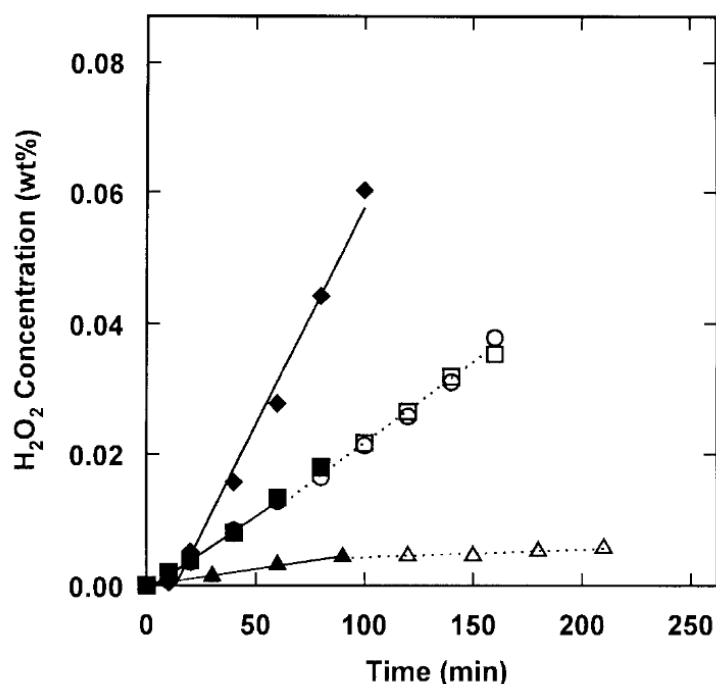
Figure 1.10: Catalytic formation of H_2O_2 in an aqueous phase before and after the removal of 2.2 mg of 5 wt.% Pd/SiO$_2$. (■) before and (□) after the removal of the solid phase from a 1 M HCl solution; (●) before and (○) after the removal of the solid phase from an 0.1 M HCl solution; (▲) before and (△) after the removal of the solid phase from an 0.01 M HCl solution. Peroxide formation in a nominally 1.0×10^{-4} M PdCl$_4^{2-}$ solution containing 1 M HCl is depicted by (◆). **Reaction Conditions:** 2.2 mg 5 wt.% Pd/TiO$_2$, Solvent = 10 cm^3 of 1M HCl Acidified H_2O, P = 14.6 Psi, O$_2$:H$_2$ 2:1, Gas Flow Rate O$_2$ = 20 cm^3 min^{-1}, Gas Flow Rate H$_2$ = 10 cm^3 min^{-1}, T = 25 °C and Time = 1 h. Figure use granted in accordance with copyright by Elsevier.[72]

This was observed as when the supported catalyst was removed (□) from solution there was no loss in catalyst activity. Furthermore, it was apparent that the presence of HCl and O$_2$ were both key to a high H_2O_2 production as when both were removed H_2O_2 formation diminished rapidly (△), indicating that the high concentration of HCl and O$_2$ together encouraged Pd colloid formation. Although these results are positive, the eventual industrial application of a Pd colloid would be ineffective due to lack of control over the size and structure of the colloid as well as its removal from the product stream.

The active phase in supported Pd catalysts, for the synthesis of H_2O_2, is something that has been debated for years and is still not agreed upon. Research into this area was pursued by Lunsford *et. al*[73] in which a Pd^0/SiO$_2$, PdO/SiO$_2$ and (PR) partially reduced PdO/SiO$_2$ were generated and tested for the direct synthesis of H_2O_2, with the form of oxidation state of Pd

being confirmed by XRD and XPS. For H_2O_2 synthesis, Pd^0/SiO_2 was observed to be the only catalyst able to produce H_2O_2. With both PdO/SiO_2 and (PR) PdO/SiO_2 unable to produce a measurable amount in a gaseous mixture of H_2 and O_2. These results support that Pd^0 is the active phase for H_2O_2 and not PdO, however this directly contradicts the conclusions made by Choudhary *et. al.*[74,75]

The research conducted by Choudhary into the influence of the Pd oxidation state by using 2.5 wt.% Pd[74,75] deposited upon a variety of supports. In the initial study it was concluded that when supported upon CeO_2, ThO_2 or Ga_2O_3 the reduced Pd was unable to synthesise H_2O_2. However, upon oxidising, the reduced Pd was converted to an entirely PdO phase and H_2O_2 synthesis drastically improved due to an increase in H_2O_2 selectivity and a decrease in degradation. Both of which are correlated to the propensity of H_2O_2 bind to reduced Pd sites over PdO.[75] However, during reactions the PdO phases are reduced upon producing H_2O_2 and return to a reduced Pd state, this continues throughout an entire reaction and leads to the formation of a mixed phased catalyst and explains the drop off in a catalysts activity over time. It was also observed that the properties of the reduced catalyst (e.g. particle size[76], distribution, surface area etc) had much less of an effect on the catalyst's ability to successfully synthesise H_2O_2, due to the catalysts extremely high H_2O_2 decomposition overshadowing all of these. These results further indicate that it is still vastly misunderstood what active phase is in fact the reason for Pd's excellent activity towards the direct synthesis of H_2O_2 from H_2 and O_2, with all current research seemingly contradicting each other.

Ouyang *et. al*[77] studied the origins of active sites for the direct synthesis of H_2O_2 on Pd/TiO_2 catalysts. A range of Pd catalysts supported upon TiO_2 (1–5 wt.%) were prepared using incipient wetness impregnation before being tested for the direct synthesis of H_2O_2. The 1 wt.% Pd was the optimum catalyst showing the highest H_2O_2 selectivity of 61% and the lowest H_2 conversion of 10.2%, corresponding to a H_2O_2 productivity of 2.99 mol_{H2O2} kg_{cat}^{-1} h^{-1} and a rate in TOF of 630 h^{-1}. The 5 wt.% Pd however exhibited the lowest H_2O_2 selectivity of 41% yet had the highest H_2 conversion, which yielded the lowest H_2O_2 productivity of 1.24 mol_{H2O2} kg_{cat}^{-1} h^{-1} and a rate of 296 in TOF h^{-1}. These results indicate that the rise in Pd loading leads to an increase in H_2 conversion at the expense of H_2O_2 selectivity, productivity, and rate values. Regarding degradation, it was found that the hydrogenation rate decreased with an increase in Pd loading from 6.39 mol_{H2O2} kg_{cat}^{-1} h^{-1} for 1 wt.% Pd to 2.94 mol_{H2O2} kg_{cat}^{-1} h^{-1} for 5 wt.% Pd. When researching into the active sites it was revealed that both Pd^0 and Pd^{2+} coexist in a freshly

reduced catalyst. It was reported that with the reduction of 1 wt.% PdO, the surface ratio of Pd^0 increases from 34.3% to 52.4%, while the ratio of Pd^{2+} decreases from 65.7% to 47.6%, with this enhancing both selectivity and productivity of H_2O_2. Yet, on the surface of the 1 wt.% PdO catalyst, there are not enough metallic Pd sites for the dissociative activation of H_2, and a portion of H_2O is probably formed via this reduction of the surface PdO species. In addition, the Pd and PdO interfaces were formed when more metallic Pd species are exposed, providing active sites both for H_2 activation and for activation of O_2 without dissociation. When Pd loading increased a rise in the Pd^{2+}/Pd^0 ratio was presented and could be responsible for the drop of H_2O_2 selectivity and productivity. This work concludes that the active sites for H_2O_2 synthesis should not be assigned simply to metallic Pd or oxidized Pd species, rather that the synthesis of H_2O_2 should be a consequence of the interaction between Pd and PdO due to Pd cycling through its oxidation states (Figure 1.11).
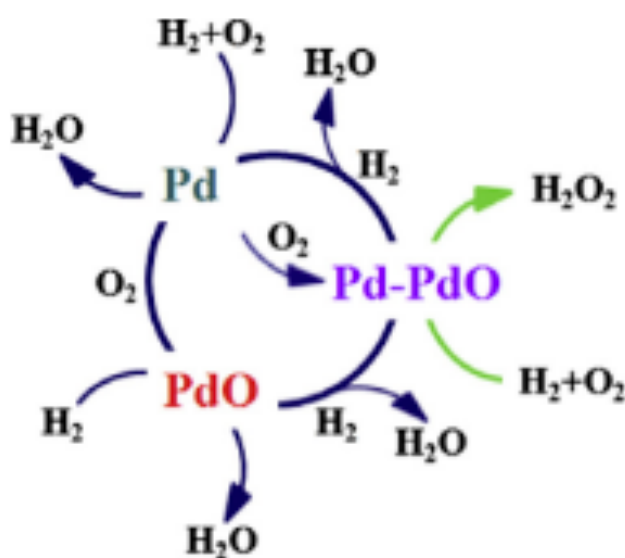
Figure 1.11: The reaction mechanism of H_2O_2 synthesis on a Pd/TiO$_2$ catalyst. Figure use granted in accordance with copyright by Elsevier.[77]

Given the relatively high decomposition and poor selectivity of Pd towards H_2O_2, methods have been developed to research and improve upon these negatives. Positive results have returned with the introduction of halide promoters, either being added straight into reaction medium[66,78,79] or into the catalyst itself.[32,78] This is another topic that both Lunsford[80–82] and Choudhary[66,83] have once again dedicated part of their research to. Lunsford *et. al*[80] started by comparing the effect of HCl and H_2SO_4 on the reaction mixture. In a reaction mixture of ethanol, 0.06-0.12 M H_2SO_4 showed an improvement at increasing the ability of the catalyst to

synthesise H_2O_2 compared to HCl. But, when the reaction mixture was water, 0.06-0.12 M HCl was much more effective than H_2SO_4 in increasing the ability of the catalyst towards the formation of high concentrations of H_2O_2. It is hypothesised that chlorine in water, and at a sufficiently high concentration, is capable of blocking the Pd sites that promote the dissociation of O_2, which in turn result in the formation of H_2O.[82] In ethanol however, a common solvent for the direct synthesis of H_2O_2, it is assumed that the ethanol itself is responsible due to halide adsorption either blocking sites that promote O−O bond scission or reducing the density of states near the Fermi level and consequently making metal surfaces less reactive for O−O cleavage, both of which increase H_2O_2 production.[62] Flaherty *et. al*[69] continued to support the case for the positive effect that protic solvents have on the synthesis of H_2O_2 by concluding that H_2O_2 only forms in protic solvents and not in aprotic solvents, which was hypothesised to be due to their protonated forms cocatalysing the proton−electron transfer steps by providing low barrier pathways to shuttle protons. The beneficial effects of H_2SO_4 were supported further by Choudhary *et. al*[83] who concluded that H_2O_2 decomposition decreased with first order rate constant upon increasing the concentration of H_2SO_4, from 0–10 mol L^{-1}, and temperature, from 8-40 °C (Figure 1.12).
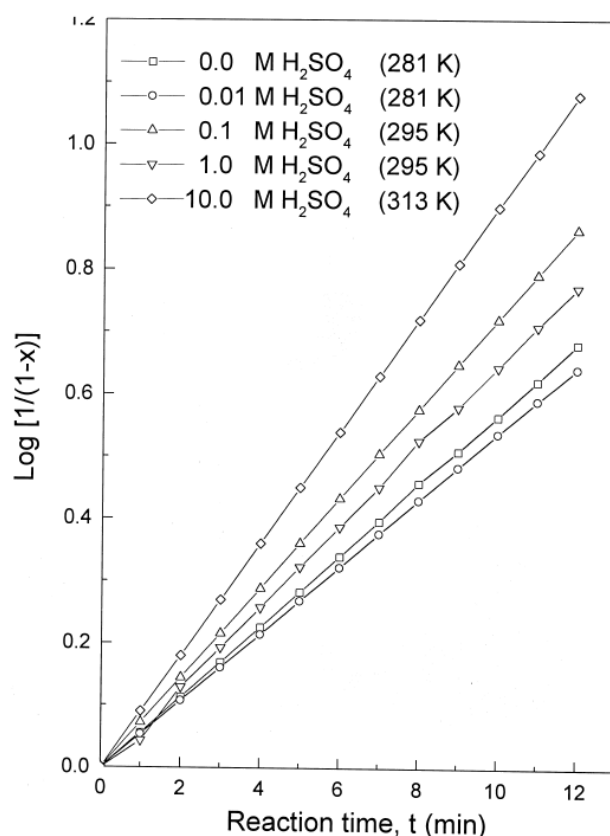
Figure 1.12: Linear kinetic plot of the decomposition of H_2O_2 with increasing temperature and H_2SO_4 concentration. **Reaction Conditions:** 20 mg 5 wt.% Pd/C, P = 14 Psi, Gas Flow Rate H_2 = 10 cm^3 min^{-1}, Solvent = 0-10 M H_2SO_4 and T = 8-40 °C. Figure use granted in accordance with copyright by Springer Nature.[83]

Furthermore, Lunsford *et. al*[81] showed that it is not just the halide ion that increases production but also the associated proton. A proton is described as a critical promoter for H_2O_2 synthesis and does this by increasing the reactivity of the Pd surface, while not being directly involved.[69] The study commenced by initially removing any protons from the reaction mixture, with the results showing that all the gaseous H_2 was consumed in the production of H_2O. However, in the opposite scenario, when an excess of H^+ was added to the reaction mixture, a drastic increase in the production of H_2O_2 was observed, which led to the blocking of the Pd active sites which inhibits the scission of molecular H_2, the rate determining step in the synthesis of H_2O_2 [84]. Furthermore, while it has been concluded that protons are important in increasing the synthesis of H_2O_2, their partnering halide ions still do play a role in H_2O_2 synthesis. Br⁻ and Cl⁻ were both shown to increase the selectivity towards H_2O_2, binding to the sites associated with H_2O_2 combustion and reduction. Of the two halide ions tested Br⁻ was shown to be the more effective of the two, due to a stronger binding energy towards Pd. However, not all halide ions

are beneficial to H_2O_2 production with F^- and I^- both having negative effects on production.[66] F^- was shown to increase H_2 production to H_2O_2, yet this increase was minimal as was outweighed by the additional increase of both the decomposition and hydrogenation of H_2O_2. I^- had a similar outcome by completely deactivating the Pd catalyst, due to its strong coordination to all Pd active sites.

Another approach to the introduction of acidic promoters is to incorporate the halide ions into the catalyst itself. Choudhary and co-workers[78] approached this by impregnating their 5 wt.% Pd/C catalyst with ammonium halide salts ($NH_4^+Cl^-$, $NH_4^+F^-$, $NH_4^+Br^-$, $NH_4^+I^-$) via wet impregnation method. It was concluded that neither pre-bromination nor pre-chlorination caused an increase in net H_2O_2 productivity in comparison to when they were added separately to the reaction medium, due to a much smaller decrease in H_2O_2 decomposition. When this result was compared to no halogenation a marked improvement was observed. For pre-fluorination, a drastic increase in activity towards H_2 combustion was expressed, but not towards H_2O_2 production. With pre-iodination, complete deactivation of the catalyst occurred, in the same manner as iodination of the reaction medium, due to complete occupancy of all Pd active sites. Choudhary *et. al*[79] also trialled the effects of pre-halogenation on a 2.5 wt.% Pd catalyst adsorbed upon various supports (Al_2O_3, ZrO_2, Ga_2O_3, H-β, SiO_2). They discovered that after bromination H_2O_2 yield and selectivity increased drastically, while H_2 conversion showed a negligible decrease for all the supports. Iodine once again exhibited complete deactivation. While chlorination and fluorination both increased H_2 conversion and H_2O_2 decomposition, leading to no overall net gain of H_2O_2. Bromine was shown to be the primary halogen for increased H_2O_2 production, with the optimum amount of bromine added to the catalyst being 0.2 mmol g^{-1}, with any further quantity showing no positives to H_2O_2 yield or reduced H_2O_2 decomposition. This work has contributed to the synthesis of most, if not all, non-Au containing catalysts to produce H_2O_2 containing an acidic promotor, whether it's in the reaction medium or in the catalyst itself. With the aim to improve overall production of H_2O_2 by suppressing the degradation pathways.

However, Biasi *et. al*[85] looked into the effect that the absence of halides and acids in the reaction medium have on the degradation and direct synthesis of H_2O_2, using a 5 wt.% Pd/C. Temperature effects and subsequent hydrogen addition were also investigated without using the aforementioned promoters, with all reactions being undertaken in a batch autoclave reactor. It was observed that increasing the temperature of a reaction from -5 to 40 °C increased

the production of H_2O 2.5x over 400 minutes. Yet, the production of H_2O_2 decreased 3.5x over the same time, with the production of H_2O_2 at 40 °C completely halting after 180 minutes due to the degradation pathway proceeding so readily. In response to the replacement of H_2, an enhanced H_2O_2 selectivity was observed before it was consumed for the reaction to proceed.

The effect of the support was studied further for the direct synthesis of H_2O_2 by Bernardini *et. al.*[86] Their research looked into the effect that supporting Pd on mixed oxides (ZrO_2 and CeO_2) and rare earth elements (Y_2O_3 and La_2O_3), predominately due to their capabilities of increasing metal dispersion and O_2 mobility. CO chemisorption concluded that all the samples achieved very high dispersion, ranging from 48.5%, for Pd supported on ZrO_2/CeO_2 (82.5 wt.%/17.5 wt.%), to 99.1%, for Pd supported on either CeO_2 or ZrO_2. With this high dispersion being due to a very small average particle size, varying from 1-2.6 nm. Once characterised, these catalysts were then tested for the direct synthesis of H_2O_2 in a high-pressure semi batch reactor. The Pd catalysts supported with predominately ZrO_2 were shown to have a H_2 conversion of around 20% after 5 hours, with the other catalysts failing to reach any higher than 9%. The catalysts with higher H_2 conversion also contained half the amount of Pd than the others, therefore their activity was much higher than the other catalysts. With respect to H_2O_2 production, the same catalysts that had large H_2 conversion also showed the highest H_2O_2 specific concentrations producing between 3.5–8.5 mol_{H2O2} kg_{cat}^{-1} h^{-1} after 300 minutes. It was correlated that these catalysts contained smaller pore diameters and in turn larger Pd particles. These supports that contained the larger Pd particles were more selective toward H_2O_2, suggesting that the highly unsaturated sites, such as Pd atoms at a corner or an edge largely present on small particles, cleave the O-O bond, leading to water. However, the supports with the higher reducibility favoured the production of H_2O_2, which was hypothesised to be due to an easier reduction of the active metal leading to the observed high selectivity. These observations led to the conclusion that the highly reducible supports give larger metal particles and are the most desirable when it comes to the preparation of catalysts for the H_2O_2 direct.

Further study into supports was undertaken by Park *et. al*[87] in which Pd catalysts, supported on mesostructured cellular foam (MCF) $Cs_{2.5}H_{0.5}PW_{12}O_{40}$ and prepared by incipient wetness impregnation at various wt.% (X = 14.3 – 38), were tested for the direct synthesis of H_2O_2. All reactions were carried out in an autoclave reactor with the results showing volcano-shaped curves with respect to $Cs_{2.5}H_{0.5}PW_{12}O_{40}$ content for both yield and selectivity (Figure 1.13). It was also discovered that the acidity of the Pd/CsPW-MCF-X catalysts increased in a similar

manner to the volcano-shaped curve observed for H_2O_2 yield and selectivity. Among the catalysts tested the Pd/CsPW-MCF-21.8 catalyst exhibited the largest acidity and additionally showed the highest yield for H_2O_2 synthesis. The Pd/CsPW-MCF-X catalysts efficiently acted as an alternate acid source and as an active metal catalyst in the direct synthesis of H_2O_2.
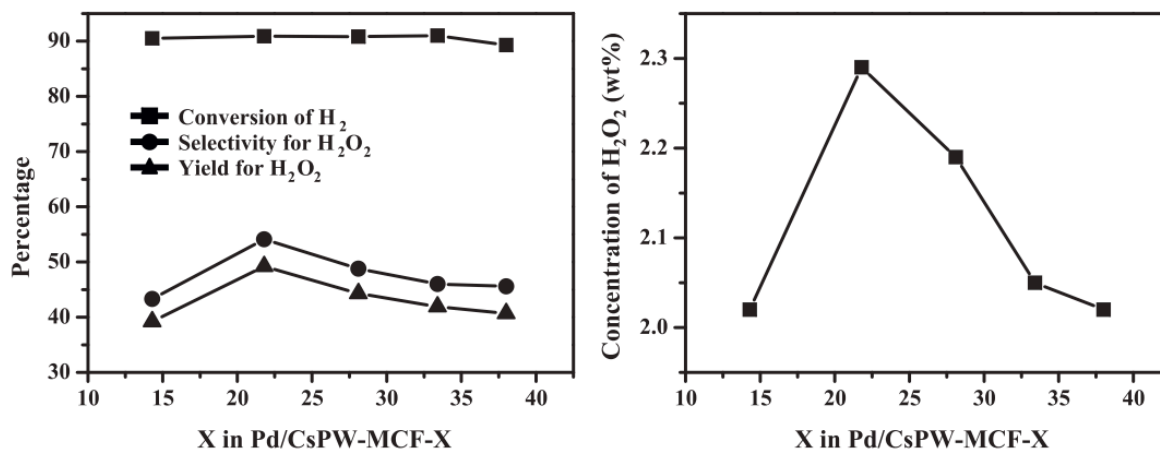
Figure 1.13: Catalytic performance of the various wt.% of Pd/CsPW-MCF-X catalyst towards the direct synthesis of H_2O_2 over 6 hours. **Reaction Conditions:** 1 g of Pd/CsPW-MCF-X, P = 147 Psi, Solvent = Methanol (80 mL) and NaBr (6.32 mg), H_2:O_2 0.4:1, Gas Flow Rate = 44 cm^3 min^{-1}, T = 28 °C, T = 6 h and 1000 rpm. Figure use granted in accordance with copyright by Elsevier.[87]

1.7.1 Key Points.

- Industrial application of a Pd colloid would be ineffective due to lack of control over the size and structure of the colloid as well as difficulty in its removal from the product stream. [67,72]

- The active sites for H_2O_2 synthesis are not the metallic Pd or oxidized Pd species but are a consequence of the interaction between Pd and PdO. [77]

- Both halide ions and their associated protons are able to increase the production whether in the reaction medium or in the catalyst structure itself. [78,81]

- Supports with higher reducibility favoured the production of H_2O_2, which was hypothesised to be due to an easier reduction of the active metal, essential to achieving high selectivity. [86]

- Mesostructured cellular foam catalysts can efficiently act as an alternate acid source and as an active metal catalyst in the direct synthesis of H_2O_2. [87]

1.8   Direct Synthesis of H_2O_2 Utilising Gold Catalysts.

Au was never thought of as a metal that could undertake catalytic reactions, due to it being inert in its standard, bulk, form. This changed in the 1970's when Bond *et. al*[88] reported that olefins could be hydrogenated by a supported Au catalyst prepared by thermal decomposition of chloroauric acid and in the presence of molecular H_2. Following this it was discovered that Au could be used for the low temperature oxidation of CO as well as the hydrochlorination of ethyne to vinyl chloride, with these reactions being discovered by Haruta[89] and Hutchings[90] respectively.

Au can also be used as a homogenous catalyst, however as there is only a limited number of highly volatile gold compounds most of the reactions are undertaken in the liquid phase or as a dissolved substrate and dissolved catalyst.[91] Additionally, Au can be utilised as a catalyst in oxidation reactions and this was discovered by Natile and co-workers[92–95] when tetrachloroaurate ($AuCl_4$) was able to synthesise isoxazoles and selectively oxidize thioethers. It has also been shown that Au can catalyse C-C bond formation in the asymmetric aldol condensation reaction developed by Ito *et. al.*[96]

The research by Haruta *et. al*[97] utilised a supported 5 wt.% Au/Fe_2O_3 catalyst, prepared by co-precipitation, with the results showing that the catalyst was very effective for the oxidation of CO with 100% conversion at 30 °C and 0 °C. Initially it was hypothesised that this activity was due to the Fe_2O_3 support. This was not the case and the activity was due to the small size of the Au nanoparticles, between 2-4 nm.[98] For the first time it was clear that a supported Au catalyst could be utilised for a range of reactions which were previously believed to be inconceivable, including selective oxidation, hydrogenation,[99] epoxidation[100] and C-H bond activation.[101] This led to a drastic influx in publications in Au catalysis, with 8x times the number of publications on "Gold catalysis" being produced in 2006 compared to the discovery by Haruta in 1987 (Figure 1.14).
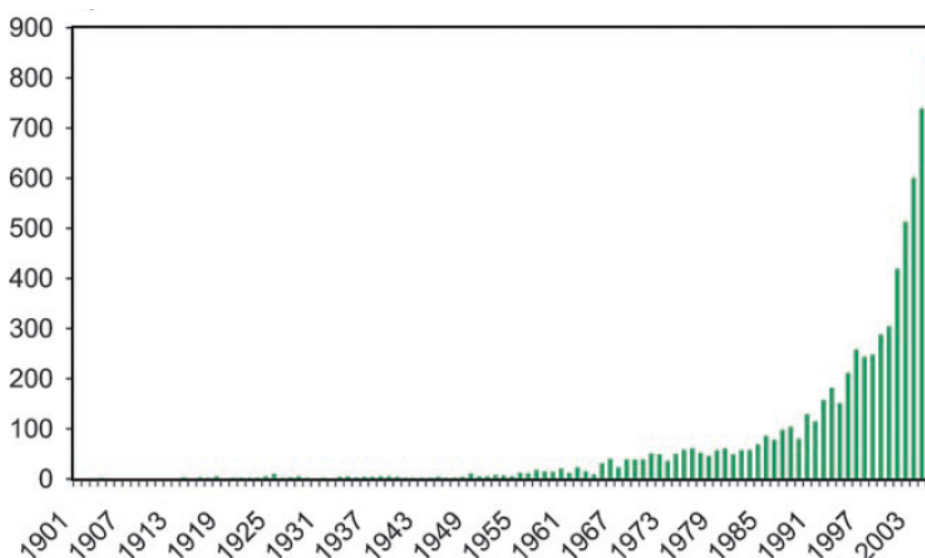
Figure 1.14: Number of publications on "Gold catalysis" from 1900-2006. Figure use granted in accordance to open access license.[98]

Following this discovery, Au was tested for the direct synthesis of H_2O_2, outside of the explosive limit. Landon *et. al*[102] used 5 wt.% Au, Pd and AuPd, supported on ZnO, at 35 °C with supercritical CO_2 as the reaction medium to overcome the issue of poor diffusion for H_2. Results showed that 5 wt.% Au/ZnO and 2.5 wt.% Au-2.5 wt.% Pd/ZnO both produced H_2O_2, albeit at a low rate of ~10 mol_{H2O2} kg_{cat}^{-1} h^{-1}. Yet this was greater than Pd/ZnO, which was unable to synthesise H_2O_2, only producing H_2O. It was concluded that at 35 °C any H_2O_2 produced was degraded just as readily. Thus, even though using supercritical CO_2 enabled the subjugation of the diffusion limit of H_2, at this temperature the instability of H_2O_2 prevented the fulfilment of the supercritical conditions. Temperature was subsequently reduced to 2 °C and the solvent changed to aqueous methanol in an attempt to increase solubility and reduce the degradation pathways, encouraging results followed. The rate of H_2O_2 production increased across the board, with 5 wt.% Au/Al_2O_3 producing more H_2O_2 than 5 wt.% Pd/Al_2O_3, producing 1530 and 370 mol_{H2O2} kg_{cat}^{-1} h^{-1} respectively.

Extending on their previous work, Landon *et. al*[103] continued in their testing of 5 wt.% supported Au catalysts by comparing them alongside supported Pd and AuPd (1:1 by wt.%) for the direct synthesis of H_2O_2 again in supercritical CO_2. The catalysts were all supported upon Al_2O_3 via impregnation using the incipient wetness method. Prior to comparisons the reaction conditions were screened to allow optimum production in H_2O_2, with catalyst mass, stirring rate, reaction time and temperature all tested. It was revealed that > 800 rpm the stirring

rate had no effect on the conversion of H_2. With increasing catalyst mass, H_2O_2 selectivity exhibits no correlation levelling out at 70%. However, both H_2 conversion and H_2O_2 yield increased alongside mass, as an influence of the mass transfer effect. To minimise this effect 0.05 g of catalyst was used. Reaction time and temperature were the final two parameters tested and regarding time, a linear increase in H_2 conversion is observed, however yield reaches its maximum at 45 minutes before decreasing. This can be explained as initially large amount of H_2O_2 is being produced yet when this concentration gets too high the same catalyst then degrades that same H_2O_2 limiting the amount of H_2O_2 that can be synthesised. The effect of temperature is simple, with an increase in reaction temperature resulting in a decrease in H_2O_2 selectivity and reactant gas solubility, yielding an increase in the degradation of H_2O_2. The 3 catalyst variants were then tested and the $AuPd/Al_2O_3$ catalyst showed a high production for H_2O_2 in comparison to the Au/Al_2O_3 and Al_2O_3 Pd/Al_2O_3, producing 4460 $mol_{H2O2}\ kg_{cat}^{-1}\ h^{-1}$ compared to 1530 and 370 $mol_{H2O2}\ kg_{cat}^{-1}\ h^{-1}$, for Au and Pd respectively (Table 1.2).

Table 1.2: Comparison of 5 wt.% Au, Pd and $AuPd/Al_2O_3$ for the synthesis of H_2O_2, selectivity of H_2O_2 and H_2 conversion.

Catalyst	O_2/H_2 Ratio	H_2 Conversion (%)	H_2O_2 (wt.%)	H_2O_2 Selectivity (%)	H_2O_2 Production / $mol_{H2O2}\ kg_{cat}^{-1}\ h^{-1}$
Au/Al_2O_3	1.2	6	0.031	53	1530
Pd/Al_2O_3	1.2	80	0.0008	1	370
$AuPd/Al_2O_3$	1.2	63	0.09	14	4460

Reaction Conditions: 50 mg catalyst, P = 1400 Psi, O_2:H_2 6:5, Solvent = Methanol (5.6 g) and H_2O (2.9 g), T = 2 °C, T = 0.5 h and 1200 rpm. Table use granted in accordance with copyright by Royal Society of Chemistry.[103]

This is an indication that a synergistic effect may exist between the Au and Pd, with the Pd acting as a promoter for the Au. These results also confirm that Au/Al_2O_3 is an effective catalyst for H_2O_2 production, mostly due to its high H_2O_2 selectivity of 53% when compared to AuPd and Pd's 63% and 6%.

Continuing this work, Okumura *et. al*[104] investigated the catalytic properties of the Au catalyst for H_2O_2 synthesis by changing the catalysts preparation method and supports. This was achieved using the deposition-precipitation and gas-phase grafting (GG) methods to deposit

Au onto various supports, including MgO, Al_2O_3, SiO_2, TiO_2, ZrO_2, SiO_2-AlO_2, MCM-41 and activated carbon (AC). The productivity of the Au deposited on the various supports was tested initially. Results indicated that SiO_2-Al_2O_3 and MgO are the worst for producing H_2O_2, therefore not suited for this reaction. However, 1 wt.% Au/SiO_2 was the optimum support for H_2O_2 synthesis producing 0.265 mol_{H2O2} kg_{cat}^{-1} h^{-1} at a pressure of 1 bar. This supports the proposition that the catalytic activity of an Au catalyst is dependent on the support, with the strength of the metal-support interaction dictating the reaction efficacy. Next, the H_2O_2 productivity was tested for different size Au particles deposited on MCM-41 and SiO_2. The results expressed that the rate of H_2O_2 formation decreased with an increase in the mean diameter of Au nanoparticles, indicating that the high dispersion of nanoparticles is essential for high H_2O_2 productivity. Finally, preparation methods were compared for H_2O_2 productivity, using the same Au/AC catalyst. Results previously showed that Au nanoparticles of less than 10 nm can be highly dispersed upon AC when using the GG. The results expressed that Au/AC was much more active for H_2O_2 production, with a value of 0.270 mol_{H2O2} $kgcat^{-1}$ h^{-1}, when using GG preparation method compared to the deposition-impregnation method, which returned a value of 0 mol_{H2O2} kg_{cat}^{-1} h^{-1} due to low Au particle dispersion. These findings indicate that preparation method, particle size and support are all key aspects in optimising an Au supported catalysts production of H_2O_2. These findings were affirmed by Ishihara *et. al*[105] who also concluded that 1 wt.% Au/SiO_2 was the optimal catalysis for H_2O_2 formation. The catalyst was active for H_2O_2 synthesis in the absence of a halide promoter with the key step in the formation of H_2O_2 upon supported Au catalysts being identified as the activation of H_2, with this being affirmed by the increase in H_2O_2 alongside an increase in H_2 partial pressure (Figure 1.15).
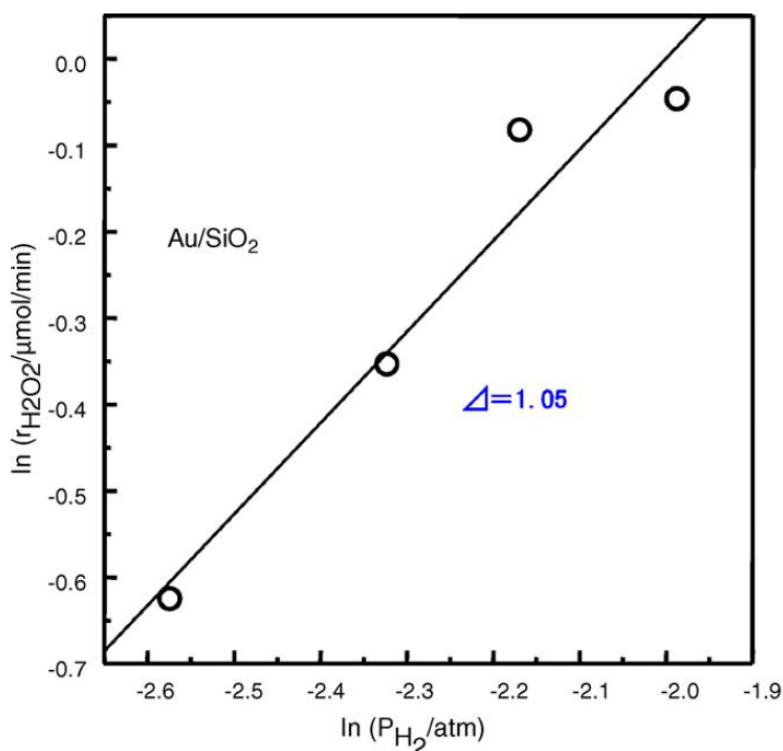
Figure 1.15: Dependence of H_2O_2 synthesis on the partial pressure of H_2. **Reaction Conditions:** 1 g Au/SiO₂, pH 6.0, $H_2/(H_2 +O_2)$ = 0.15, T = 10 °C and Time = 0.25 h. Figure use granted in accordance with copyright by Elsevier.[105]

In addition, Edwards *et. al*[106] tested for the effect of calcination temperature and preparation method on the direct synthesis of H_2O_2 and the low temperature oxidation of CO using 5 wt.% Au/Fe₂O₃ supported catalyst. They discovered that the catalysts generated by co-precipitation synthesised H_2O_2 an order of magnitude below those generated by impregnation, however the impregnation method generated better catalysts for low temperature CO oxidation indicating that the active sites for H_2 activation differ to those active for CO oxidation. Additionally, it was alluded to that to generate a stable and reusable catalyst the calcination temperature must be ≥ 400 °C, with catalysts calcined below this temperature leaching the metal off the supports surface leading to catalyst deactivation over time. While these catalysts synthesised H_2O_2, the addition of Pd to the Au/Fe₂O₃ significantly enhanced the catalysts performance from 0.54 $mol_{H2O2} \, kg_{cat}^{-1} \, h^{-1}$ to 16 $mol_{H2O2} \, kg_{cat}^{-1} \, h^{-1}$, which was also greater than 5 wt.% Pd/Fe₂O₃ which recorded a productivity of 3.6 $mol_{H2O2} \, kgcat^{-1} \, h^{-1}$.

1.8.1 Key Points.

- Catalytic activity of an Au catalyst is highly dependent on the support.[104]
- Rate of H_2O_2 formation decreases with an increase in the mean diameter of Au nanoparticles, indicating that the high dispersion of nanoparticles is essential for high H_2O_2 productivity.[104]
- To generate a stable and reusable catalyst the calcination temperature must be ≥ 400 °C, with catalysts calcined below this temperature leaching the metal from the support surface.[106]

1.9 Direct Synthesis of H_2O_2 Utilising AuPd Catalysts.

While it is well known that supported Pd catalysts are active for H_2O_2 and supported Au catalyst are selective for H_2O_2, it is also recognised that it is difficult to obtain a monometallic catalyst that exhibits both high H_2O_2 selectivity and yield. The concept of combining Au and Pd to form a supported bimetallic catalyst became important in the early 2000's due to the synergistic effect between the metals, which gave a significant increase in selectivity, activity and stability relative to their monometallic analogues. The bimetallic catalysts can be prepared in a similar way to the monometallics, however correct incorporation of the secondary metal is key. This enrichment towards the catalyst is caused by two alloy effects,[107] ensemble and ligand. The ensemble effect is the dilution of Pd on the surface of the support by the inclusion of Au. This is predominantly required due to the H_2O_2 side reactions that the contiguous Pd ensembles facilitate. With this increase in Au coverage, the bordering Pd ensembles are dismantled and replaced with isolated Pd ensembles, which for H_2O_2 synthesis leads to an increase in net H_2O_2 production. The ligand effect is an electronic perturbation of Pd, achieved by Au filling Pd's d-band, in turn moving its d-band centre away from the Fermi level. This leads to the Pd nanoparticles acting atomic, leading to weaker binding of reactants and products preventing self-poisoning of the catalyst surface. The overall objective of these bimetallic catalysts is to achieve high concentrations of H_2O_2, in company with a large activity and selectivity for H_2O_2 and a low affinity for degradation.

Initial studies were undertaken by Hyung *et. al*[108] in which a computational approach was taken into examining the role that Pd ensembles have for the selective formation of H_2O_2. For this study they considered three Pd ensembles; monomer (M), Dimer (D) and Trimer (T), shown in Figure 1.16. The formation energies per Pd atom were calculated to be 0.07, 0.11 and 0.15 eV

for the Pd monomer, dimer, and trimer respectively. These low values indicate that at sufficiently high temperatures a random distribution would occur, however surrounded by Au would be the energetically favoured position for all the ensembles. The total energy changes and activation barriers for the hydrogenation and decomposition for H_2O_2 for each ensemble were then tested, with the results indicating that the arrangement of the Pd atoms influences these values with each ensemble returning a different value. It was concluded that the arrangement of Au and Pd has a strong on effect on the selectivity of H_2O_2 directly from H_2 and O_2, with Pd monomers surrounded by less active Au atoms tending to enhance the suppression of O-O bond scission which leads to less net H_2O_2 decomposition.
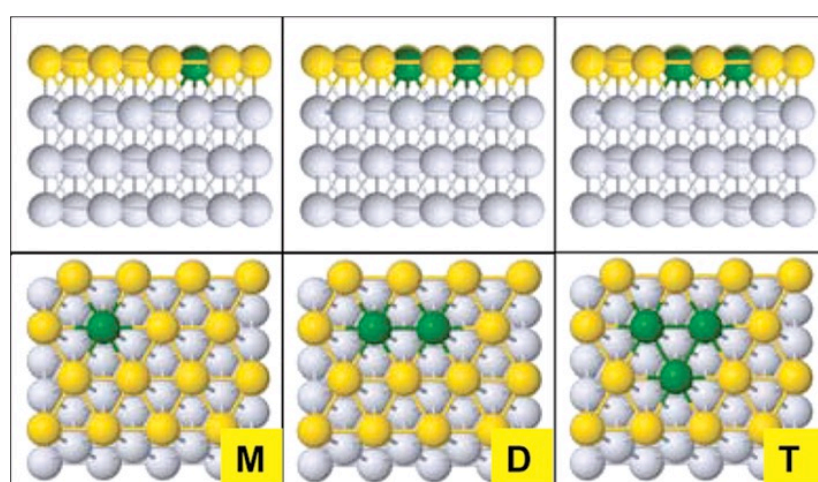
Figure 1.16: Side and aerial view of the model AuPd surfaces, Pd monomer (M), dimer (D), trimer (T) and pure (P) (green = Pd, yellow = Au, grey = subsurface Pd atoms). Figure use granted in accordance with copyright by American Chemical Society.[108]

The preparation method used to generate a catalyst can have a drastic effect on its catalytic properties towards any given reaction. This was discovered by Lopez-Sanchez *et. al*[109] who compared the differences between a bimetallic 1 wt.% AuPd made by sol immobilisation and conventional wet impregnation for H_2O_2 production and hydrogeneration. The positives towards using sol immobilised catalysts for H_2O_2 synthesis is that a greater control over particle size is possible, allowing a narrower range of nanoparticle production (4-7 nm) compared to most impregnation catalysts which can produce nanoparticles up to 200 nm in size.[110] In addition, STEM-ADF confirms that both the sol immobilised and conventional wet impregnation catalysts have a controlled Au/Pd composition, with all particles being an alloy of both Au and Pd (Figure 1.17).
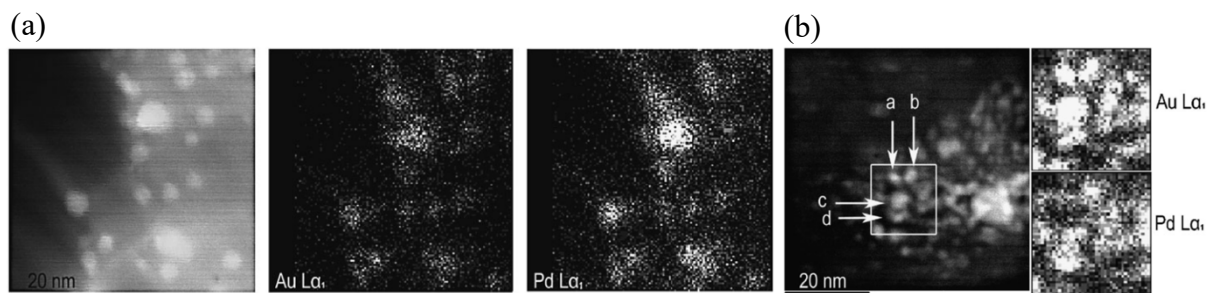
Figure 1.17: STEM-ADF image alongside the corresponding Au $L_{\alpha 1}$ and Pd $L_{\alpha 1}$ elemental maps of the (a) impregnation and (b) sol immobilised AuPd/C catalyst. Images used and reproduced in accordance with copyright by Royal Society of Chemistry.[109]

The impregnation catalysts were showed to contain more of a bimodal particle distribution, with large Au-rich nanoparticles and smaller Pd-rich nanoparticles. This difference in composition can be seen on the testing of H_2O_2 synthesis, with the bimodal distribution preventing the alloying of the two metals which in turn allows for a high production of H_2O_2 alongside a greater suppression towards its degradation. It was observed that the 1 wt.% sol immobilised catalyst was more active, producing 54 mol_{H2O2} kg_{cat}^{-1} h^{-1} compared to 12 mol_{H2O2} kg_{cat}^{-1} h^{-1}. Unfortunately, this catalyst was also the more active for the hydrogenation of H_2O_2, degrading 27% of the H_2O_2 produced compared to 4% for the conventional impregnation catalyst. Pritchard[111] furthered the study of sol immobilized 1 wt.% AuPd catalysts by testing different Au:Pd ratio catalysts supported on activated carbon for the synthesis of H_2O_2. He discovered that increasing the Pd content in the Au:Pd ratio from 1:0 to 1:7 led to an increase in the median, mean particle size and H_2O_2 degradation, with the 1:2 (Au: Pd) ratio catalyst synthesising the most H_2O_2 (188 mol_{H2O2} kg_{cat}^{-1} h^{-1}). This catalyst, when compared to the same catalyst prepared using impregnation, is just as active towards H_2O_2 synthesis while using 20% less total metal loading, indicating that this preparation method utilises the metal more effectively.

As discussed above it is clear there is a need for an impregnation catalyst preparation method that allows for greater elemental and size control of the metal particles and this is where the research by Sankar *et. al*[112] into developing a preparation method in which high H_2O_2 production could be available alongside a narrow particles size distribution. The method involved modifying the conventional impregnation method by adding an excess of Cl^- to generate both $AuCl_4^-$ and $PdCl_4^{2-}$, allowing greater control over the particle size distribution

and nanoparticle composition. This modification led to a more homogenous mixing of the two metals and a more active and stable catalyst. The optimum amount of HCl added to the impregnation solution was determined to be 0.58 M as this concentration held the best balance between reusability and activity. The catalyst was them compared to a sol immobilised and conventional impregnation catalyst of the same AuPd wt.% for H_2O_2 synthesis. A productivity of 99 mol_{H2O2} kg_{cat}^{-1} h^{-1} returned for the excess chlorine wet co-impregnation catalyst, with this result being 3 times more active than the sol immobilised catalyst and 4 times as active as the conventional impregnation catalyst. This catalyst however required reduction to become reusable, which was concluded to be associated with the removal of the excess of chloride ions.

The effect of changing the amount of H_2O present in the impregnation mixture was explored by Pritchard $et.$ al[113] for 1 g mixtures of 2.5 wt.% Au-2.5 wt.% Pd/TiO_2. This was then tested for its effect on the catalyst's activity towards the synthesis of H_2O_2. Upon increasing H_2O dilution from 2 to 15 mL a drop-in activity from 117 to 112 mol_{H2O2} kg_{cat}^{-1} h^{-1} was observed. This minor effect is due to an absence of any synergistic effects due to the bimodal distribution of the metal particles, forming small Pd-rich and large Au-rich metal particles. Yet, if no dilution occurs and a thick paste forms a more active catalyst is observed, due to the presence of the synergetic effects produced by the smaller bimetallic AuPd alloyed nanoparticles. However, this catalyst does not maintain this activity, slowly deactivating after continuous runs due to the variation in preparation method leading to a substantial effect in the catalyst stability and activity. Confirming that as the concentration of the metal salts is reduced, so is the catalysts activity. Further testing was done in which the dried catalyst (110 °C, 48 h) was then re-wetted (2-25 mL H_2O) and re-dried (110 °C, 48 h) before testing for H_2O_2 synthesis, however this had no effect on the catalyst's activity.

The effects on the degradation pathways associated with H_2O_2 via additives was studied by Villa $et.$ al[114] by functionalizing the surface of carbon nanofibers (CNFs) supported catalyst via acidification. To increase the acidity of the CNFs surface oxygen functionalities have been added and subsequently used to support Pd and AuPd nanoparticles. It was observed that the introduction of these oxygen functionalities on the surface of CNFs is beneficial in the reduction of the decomposition pathways associated with H_2O_2 (Table 1.3), removing any residual amorphous carbon. The table shows that the 1 wt.% AuPd/O-CNFs catalyst was able to produce a greater amount of H_2O_2 when compared to the 1 wt.% AuPd/CNFs catalyst while also reducing both the hydrogenation and decomposition rate. In addition to the above, it was

expressed that a substantial amount of control was given regarding the amount and the nature of the functionalities present on the supports surface.

Table 1.3: Activity of the CNF supported catalysts.

Catalyst	H$_2$O$_2$ Production / mol$_{H2O2}$ kg$_{cat}^{-1}$ h^{-1}	H$_2$O$_2$ Hydrogenation / mol$_{H2O2}$ kg$_{cat}^{-1}$ h^{-1}	H$_2$O$_2$ Decomposition / mol$_{H2O2}$ kg$_{cat}^{-1}$ h^{-1}
CNFs	5	60	198
O-CNFs	5	39	48
1% Pd/CNFs	21	472	77
1% Pd/O-CNFs	6	95	65
1% AuPd/CNFs	12	316	196
1% AuPd/O-CNFs	18	17	135

H$_2$O$_2$ Production Reaction Conditions: 10 mg Catalyst, 5% H$_2$/CO$_2$ (420 psi), 25% O$_2$/CO$_2$ (160 psi), Solvent = H$_2$O (2.9 g), MeOH (5.6 g), T = 2 °C, Time = 0.5 h and 1200 rpm. **H$_2$O$_2$ Hydrogenation & Decomposition Conditions:** 10 mg Catalyst, 5% H$_2$/CO$_2$ (420 psi), Solvent = H$_2$O (2.9 g), MeOH (5.6 g), T = 2 °C, Time = 0.5 h and 1200 rpm. Table reproduced in accordance with copyright by Royal Society of Chemistry.[114]

Li *et. al*[115] took a theoretical approach by examining the Pd(111) and Au@Pd(111) surfaces and their effect on the direct synthesis of H$_2$O$_2$. They established that the direct synthesis of H$_2$O$_2$ is a simple competition of competing reactions, with all side reaction being dependent on the O-O bond and the direct synthesis being dependent on O-M bond, where M is Pd for Pd(111) and Au for Au@Pd(111). In regard to Pd(111) the O-Pd bond is usually stronger than the O-O bonds, therefore leading to the side reactions exceeding the main reactions. To achieve the catalytic activity experimentally however, the Pd(111) surface should be pre-treated with a strong acid or halide ion to weaken the O-M bond. For the Au@Pd(111) surface, the O-Au bond is so weak that it does not compare to the strength of the O-O bond; in turn, the direct synthesis reaction dominates. Surface H atoms also play a role in the synthesis of H$_2$O$_2$. The co-adsorbed H atoms decrease the interaction between the metal surface and the reagents, aiding the main reactions. In addition, the H atoms occupy the Pd sites on the Au@Pd(111) surface, making the Au sites on the Au@Pd(111) surface the predominant sites available for binding which leads to the adsorption of O$_2$ upon one Pd atom and one Au atom. This adsorption is very important for the subsequent hydrogenation reactions.

Further studies were completed by Edwards *et al*[116,117] into acid treatment, with 5 wt.% Au, Pd and AuPd supported upon both TiO_2 and SiO_2 before being washed in 2 Vol.% HNO_3 (Table 1.4). The effect of acid treatment upon TiO_2 increased H_2O_2 production for all 3 catalysts with this was concluded to be due to the acidic pre-treatment removing any impurities and reducing the average particle size, via the improving of Au distribution into the nanoparticles. For the catalysts supported on SiO_2 however there is only an increase in productivity for the 5 wt.% Pd, and AuPd, as the 5wt.% Au showed no enhancement with productivity consistent at 7 mol_{H2O2} kg_{cat}^{-1} h^{-1}.

Table 1.4: Activity of mono and bimetallic 5 wt.% Au and Pd catalysts supported on TiO_2 and SiO_2.[116,117]

Catalyst	Pre-Treatment	H_2O_2 Production / mol_{H2O2} kg_{cat}^{-1} h^{-1}	H_2O_2 Hydrogenation / mol_{H2O2} kg_{cat}^{-1} h^{-1}
5% Au/TiO_2	Un-Treated	7	-
5% Au/TiO_2	2% HNO_3	7	-
5% Au/SiO_2	Un-Treated	7	112
5% Au/SiO_2	2% HNO_3	7	104
2.5% Au-2.5% Pd/TiO_2	Un-Treated	64	-
2.5% Au-2.5% Pd/TiO_2	2% HNO_3	110	-
2.5% Au-2.5% Pd/SiO_2	Un-Treated	53	275
2.5% Au-2.5% Pd/SiO_2	2% HNO_3	83	127
5% Pd/TiO_2	Un-Treated	30	-
5% Pd/TiO_2	2% HNO_3	33	-
5% Pd/SiO_2	Un-Treated	74	488
5% Pd/SiO_2	2% HNO_3	85	359

H_2O_2 Production Reaction Conditions: 50 mg Catalyst, 5% H_2/CO_2 (420 psi), 25% O_2/CO_2 (160 psi), Solvent = H_2O (2.9 g), MeOH (5.6 g), T = 2 °C, Time = 0.5 h and 1200 rpm. **H_2O_2 Hydrogenation & Decomposition Conditions:** 10 mg Catalyst, 5% H_2/CO_2 (420 psi), Solvent = H_2O (2.9 g), MeOH (5.6 g), T = 2 °C, Time = 0.5 h and 1200 rpm. Table reproduced in accordance with copyright by John Wiley and Sons and Royal Society of Chemistry.[116,117]

Ntainjua *et. al*[118] compared acid and halide treatment between a carbon and MgO supported AuPd catalyst. It was observed that for the MgO supported catalyst that the inclusion of 0.005-0.3 M HNO_3 to the reaction mixture decreased hydrogenation pathway as well as H_2O_2 production. Yet for the carbon support the hydrogenation activity increased with the inclusion

of acid, due to the halide poisoning the catalysts activity. For the inclusion of 0.00058-0.3 M bromide (NaBr), it is seen that hydrogenation activity decreases for both catalysts, due to the bromide blocking the hydrogenation sites as well as increasing the Pd^{2+}/Pd^0 ratio. However, there is a limit to the amount of bromide that can be added, as too much can poison the catalysts. Further testing by Edwards *et. al*[116] concluded from her work that acid treatment to oxide supported AuPd catalysts increases H_2O_2 activity and reduces H_2O_2 decomposition due to the dispersion of the Au on the support. The acid treatment was concluded to improve nucleation of nanoparticles and favour the formation of smaller AuPd particles. With these particles preventing the formation of the hydrogenation active sites, suppressing the decomposition pathways.

1.9.1 Key Points.

- The arrangement of Au and Pd has a strong on effect on the selectivity of H_2O_2 directly from H_2 and O_2, with Pd monomers surrounded by less active Au atoms tending to enhance the suppression of O-O bond scission which leads to less net H_2O_2 decomposition.[108]

- The inclusion of excess Cl^- into the conventional impregnation method to generate both $AuCl_4^-$ and $PdCl_4^{2-}$, allowed a greater control over the particle size distribution and nanoparticle composition, leading to a more homogenous mixing of the two metals and a more active and stable catalyst.[112]

- The dilution of the impregnation mixture leads to the absence of any synergistic effects due to the bimodal distribution of the metal particles, forming small Pd-rich and large Au-rich metal particles.[113]

- If no dilution occurs and a thick paste forms a more active catalyst is observed, due to the presence of the synergetic effects produced by the smaller bimetallic AuPd alloyed nanoparticles.

- The direct synthesis of H_2O_2 is a simple competition of reactions, with all decomposition reactions being dependent on the O-O bond of the O_2 molecule and the direct synthesis being dependent on O-M bond between catalyst surface and the O_2 molecule.[115]

- Acid treatment to oxide supported AuPd catalysts increases H_2O_2 activity and reduces H_2O_2 decomposition due to the removal of any impurities, reducing the average particle size and the dispersion of the Au on the support.[116,117]

1.10 Direct Synthesis of H_2O_2 Utilising Alternative Metals to Au and Pd.

While Pd has been considered to be the most promising catalytic metal for the direct synthesis of H_2O_2 and Au an excellent partner for increasing the selectivity of Pd towards H_2O_2, it has also been reported that we could look towards other metals that can also enhance the selectivity for Pd ensembles but at a cheaper price.[119] A study by Edwards & co-workers[120] looked into a 5 wt.% Pd/TiO_2 catalyst and the effect the addition of silver (Ag) would have on the direct synthesis and decomposition of H_2O_2, with the aim of these catalysts being used in the treatment of wastewater. It was observed that the activities of the reaction associated with H_2O_2 were highly dependent on the Ag:Pd ratio, with an increase in Ag content in the catalyst leading to a decrease in the rate of H_2O_2 synthesis and hydrogenation and an increase in decomposition. The optimal catalysts, 1 wt.% Ag–4 wt.% Pd/TiO_2 and 2 wt.% Ag–3 wt.% Pd/TiO_2, produced 194 and 222 ppm of H_2O_2 respectively, which is a sufficient amount to be used in the treatment of greywater[120]. In addition, these catalysts also exhibited higher decomposition activities, which further supports their application in wastewater treatment as the OH radicals formed during H_2O_2 decomposition exhibit excellent biocidal activity.

Further research into Ag was pursued by Gu *et. al*[121] in which incremental amounts of Ag, Pd/Ag molar ratios of 60:1, 40:1, 20:1, and 10:1, were introduced to a fixed 1 wt.% Pd/C catalyst for the direct synthesis of H_2O_2. The addition of Ag to the Pd/C caused a decrease in synthesis of H_2O_2 but an increase in the selectivity, similar to the results observed for Edwards & co-workers[120] for the 5 wt.% AgPd/TiO_2. With these results being explained by the ensemble effect, a dilution in the number of contiguous Pd ensembles and an increase in the number of Pd monomer sites preventing H_2O formation, and the electronic effect, the addition of Ag modifying the electronic properties of Pd by charge transfer. However, contrary to the work by Edwards & co-workers[120] the increase in Ag content led to a decrease in both the hydrogenation and degradation of H_2O_2, this was due to the addition of Ag leading to the formation of more Pd^{2+} sites, with these sites subsequently being assigned to lower H_2O_2 decomposition and hydrogenation activities than their corresponding Pd^0, as H_2O_2 is more inclined to be absorbed on Pd^0 sites. Furthermore, the addition of Ag also decreased the H_2 conversion, which was hypothesised to be due to the increased coverage of Ag blocking the adsorption of the reactants on the Pd adsorption sites.

The application of zinc (Zn) alongside Pd has exhibited high selectivity for the dehydrogenation of propane to propylene,[122] with this research leading to Wang $et.al$[123] inquiring into the effect that Zn additives have on the direct synthesis of H_2O_2 for a Pd/Al_2O_3. The study indicated that the addition of the Zn led to a smaller Pd size and higher Pd dispersion than the monometallic Pd, confirmed by CO chemisorption and TEM. With these properties coinciding with an increase in catalytic activity, due to the more exposed Pd atoms increasing the adsorption capacity towards molecular H_2 and O_2. In addition, the fraction of Pd^0 upon the surface of the support increased with the loading of Zn, confirmed by XPS and CO-DRIFTS, which was assigned to the increased charge transfer observed between the two metals with the increased presence of Zn. However, these characteristics also lead to a higher rate of H_2O_2 decomposition over monometallic Pd, as the high dispersion of Pd^0 provides an increased number of sites for H_2 adsorption, increasing H_2O_2 hydrogenation, and an increased propensity for H_2O_2 adsorption over the Pd^{2+} state.

Wang $et. al$[124] continued to look into alternate metals to enhance a monometallic Pd/TiO_2 catalyst by developing both a Pd_2Ga/TiO_2 and a Pd_2In/TiO_2 catalyst, via sol immobilisation. It was observed that upon the inclusion of Ga there was a significant drop in the degradation of H_2O_2 of around 35%, from 1056 to 695 mol_{H2O2} kg_{cat}^{-1} h^{-1}, and a moderate increase in H_2O_2 synthesis, from 103 to 111 mol_{H2O2} kg_{cat}^{-1} h^{-1}, due to a reduction in the size of the Pd ensembles. In comparison to Ga, when In was included into the catalyst structure there was a moderate drop-off in both productivity and degradation, to ~98 and ~780 mol_{H2O2} kg_{cat}^{-1} h^{-1} respectively, due to a reduction in Pd^0 content compared to monometallic Pd. Furthermore, when evaluating the catalytic selectivity of both Ga and In, an improvement is observed up to 30 and 34% respectively, compared to 24% for monometallic Pd, due to a reduction in the amount of isolated Pd sites which are frequently related to the degradation of H_2O_2. Consequently, it is concluded that while both Ga and In express an increased catalytic selectivity towards H_2O_2 over monometallic Pd, it is the introduction of small amounts of Ga to Pd that demonstrates the more dramatic change towards supressing the degradation of H_2O_2.

Furthering the study, Maity $et. al$[125] compared a monometallic Pd nanostructure catalyst with two bimetallic nanostructure catalysts, $Ni_{0.4}Pd_{0.6}$ and $Au_{0.5}Pd_{0.5}$, for the direct synthesis of H_2O_2. The two catalysts were prepared using a simple sodium borohydride reduction method[126] (Figure 1.18), before testing using the conditions described by Chinta & Lunsford.[127] The results returned showing that the inclusion of Ni leads to a 3-fold increase the production of

H_2O_2 over a 72 hours, from 114 to 356 mM, when compared to its monometallic counterpart. Furthermore, when they compared the $Ni_{0.4}Pd_{0.6}$ catalyst against the previously superior $Au_{0.5}Pd_{0.5}$ catalyst the $Ni_{0.4}Pd_{0.6}$ catalyst came out on top, with the $Au_{0.5}Pd_{0.5}$ catalyst producing only ~140 mM of H_2O_2 after 72 hours. With both documented increases in H_2O_2 production being due to the Ni in the bimetallic NiPd catalyst electronically modifying the Pd, enhancing its activity towards the synthesis of H_2O_2.
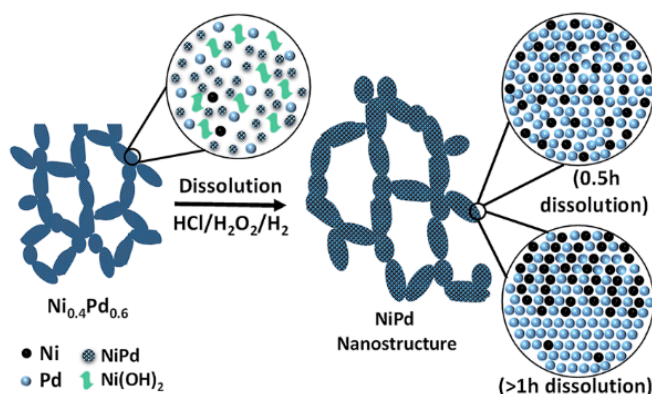
Figure 1.18: Schematic reconstruction of the formation of the $Ni_{0.4}Pd_{0.6}$ nanostructure catalyst using the simple borohydride method. Figure use granted in accordance with copyright by Royal Society of Chemistry.[125]

Ruthenium (Ru), in a similar manner to Pd, is known to be an effective hydrogenation catalyst, therefore its application towards the synthesis of H_2O_2 should be encouraged.[75] Although the only negative, again similarly to Pd, it has been documented that the hydrogenation function can become too pronounced and lead to the promotion of the sequential hydrogenation of H_2O_2. Ntainjua *et. al*[128] experimented with this by researching into the effect the inclusion of Ru has on the ability of bimetallic and trimetallic 5 wt.% catalysts to synthesise H_2O_2. Initially Ru was added to a 5 wt.% Au/TiO_2 catalyst, varying the Au/Ru ratio but keeping the total metal loading consistent at 5 wt.%. The results are expressed in Figure 1.19 and show a similar synergistic effect that is observed for $AuPd/TiO_2$ catalysts, with the 4.25 wt.% Ru-0.75 wt.% Au/TiO_2 catalyst producing the most H_2O_2 (69 mol_{H2O2} kg_{cat}^{-1} h^{-1}). A similar experiment was done for a 5 wt.% Pd/TiO_2, with the results differing as the most active catalyst was now a 4.5 wt.% Pd-0.5 wt.% Ru/TiO_2 catalyst producing 143 mol_{H2O2} kg_{cat}^{-1} h^{-1}, with any increase in Ru reducing catalytic activity.
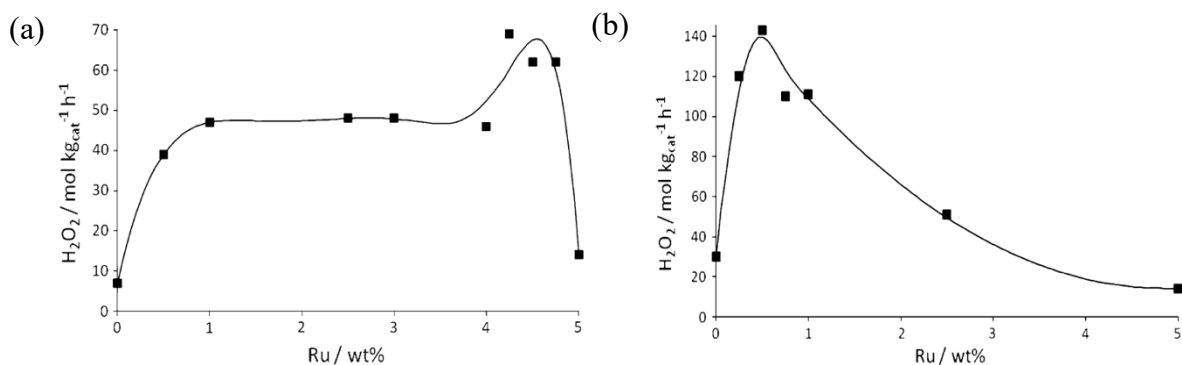
Figure 1.19: the effect of Ru content on the performance of (a) 5 wt.% Au-Ru/TiO$_2$ and (b) 5 wt.% Pd-Ru/TiO$_2$ catalyst for H$_2$O$_2$ synthesis. **H$_2$O$_2$ Production Reaction Conditions:** 50 mg Catalyst, 5% H$_2$/CO$_2$ (420 psi), 25% O$_2$/CO$_2$ (160 psi), Solvent = H$_2$O (2.9 g), MeOH (5.6 g), T = 2 °C, Time = 0.5 h and 1200 rpm. Figure use granted in accordance with copyright by Springer Nature.[128]

To conclude the study Ru was then added to a 5 wt.% AuPd/TiO$_2$. The AuPdRu/TiO$_2$ catalysts were predominately more active than their bimetallic counterparts, ranging from 109 – 153 mol$_{H2O2}$ kg$_{cat}^{-1}$ h^{-1}, with the 153 mol$_{H2O2}$ kg$_{cat}^{-1}$ h^{-1} being assigned to a 4.5 wt.% Pd-0.45 wt.% Ru-0.05 wt.% Au/TiO$_2$ catalyst. With these results indicating that trimetallic catalysts have the capacity to outperform the currently dominant bimetallic regarding synthesising H$_2$O$_2$, with further study needed into the origin of this observed activity.

Edwards *et. al*[129] experimented further by trialling the inclusion of a third metal to the catalysts structure. This was achieved by preparing catalysts upon CeO$_2$ with a total metal loading of 5 wt.% and including different metal ratios of Au, Pt and Pd, before testing for their ability to both synthesis and decompose H$_2$O$_2$. Initially the activities of the bimetallics were ranked as follows; PdPt > Pd > AuPd > AuPt > Pt > Au, indicating that Pd is the most active component required for the synthesis of H$_2$O$_2$. However, for the hydrogenation of H$_2$O$_2$ the results were ranked slightly differently as follows; Pd > PdPt > AuPd > Pt > Au > AuPt, indicating that the synergistic effect of Pt to Au has a more apparent effect on both reactions compared to the addition of Pd to Au. As the results for the bimetallics were encouraging, a wide range of metal combinations were then tested for the direct synthesis and hydrogenation of H$_2$O$_2$ (Figure 1.20).
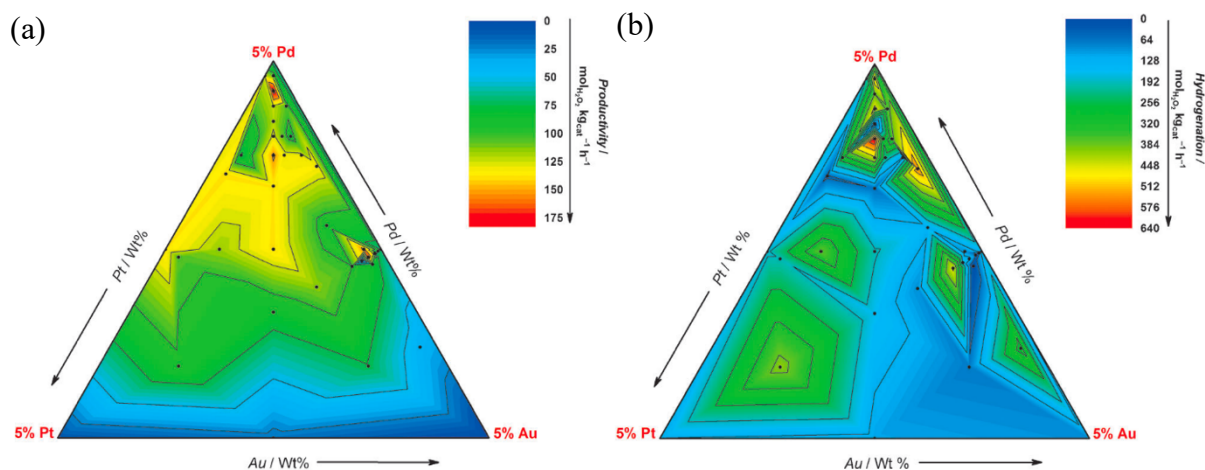
Figure 1.20: The rates of (a) synthesis and (b) hydrogenation of H_2O_2 for 5 wt.% CeO_2 supported Au/Pd/Pt catalysts. **H_2O_2 Production Reaction Conditions:** 50 mg Catalyst, 5% H_2/CO_2 (420 psi), 25% O_2/CO_2 (160 psi), Solvent = H_2O (2.9 g), MeOH (5.6 g), T = 2 °C, Time = 0.5 h and 1200 rpm. **H_2O_2 Hydrogenation & Decomposition Conditions:** 10 mg Catalyst, 5% H_2/CO_2 (420 psi), Solvent = H_2O (2.9 g), MeOH (5.6 g), T = 2 °C, Time = 0.5 h and 1200 rpm. Figure use granted in accordance with copyright by John Wiley and Sons.[129]

From Figure 1.20a, the image expressed three areas of high activity: (1) a composition predominately of Pd with a small addition of Au and Pt; (2) a catalyst that comprises mainly of Pd but contains slightly more Au and Pt and (3) a predominately bimetallic Au and Pd catalyst with a small amount of Pt. All these areas exhibit higher activity towards H_2O_2 production that bimetallic AuPd/CeO_2, indicating a clear promotional effect due to the addition of Pt. For hydrogenation (Figure 1.20b) however, of the 3 compositions, composition 1 and 2 also exhibit high H_2O_2 hydrogenation. Yet composition 3 shows a reduced value, indicating that this catalyst shows some real promise for the direct synthesis of H_2O_2 and the area of trimetallic catalysts as a whole.

1.10.1 Key Points.

Table 1.5: Activity of bi-metallic and tri-metallic catalysts for the direct synthesis of H_2O_2, prepared by different preparation methods.

Catalyst	Preperation Method	H_2O_2 Productivity / $mol_{H2O2} \, kg_{cat}^{-1} \, h^{-1}$	Catalyst Notes	Reference
0.5% Au-0.5% Pd/C	Sol Immobilisation	54	-	Lopez-Sanchez[109]
0.5% Au-0.5% Pd/C	Wet Impregnation	12	-	Lopez-Sanchez[109]
1%AuPd/C	Sol Immobilisation	188	1:2 Au:Pd Ratio	Pritchard[111]
0.5% Au-0.5% Pd/TiO$_2$	Wet Impregnation	99	Excess HCl (0.58M)	Sankar[112]
2.5% Au-2.5% Pd/TiO$_2$	Wet Impregnation	117	2mL Water in Preperation	Pritchard[113]
1% AuPd/O-CNFs	Wet Impregnation	18	Surface Functonalised (OH)	Villa[114]
2.5% Au-2.5 % Pd/TiO$_2$	Wet Impregnation	110	Acid Treatment (HCl)	Edwards[116,117]
1% AuPd/C	Wet Impregnation	139	Bromide Treatment (0.005M)	Ntainjua[118]
1% AuPd/MgO	Wet Impregnation	83	Bromide Treatment (3M)	Ntainjua[118]
1% Ag-4% Pd/TiO$_2$	Wet Impregnation	11	Ag Used	Edwards[120]
1% Pd2Ga/TiO$_2$	Sol Immobilisation	111	Ga Used	Wang[124]
1% Pd0.5In/TiO$_2$	Sol Immobilisation	78	In Used	Wang[124]
0.5% Ru-4.5% Pd/TiO$_2$	Wet Impregnation	143	Ru Used	Ntainjua[128]
2.4% Au-2.4%Pd-0.2%Pt/TiO$_2$	Incipient Wetness	170	Au and Pt Used	Edwards[129]

H_2O_2 Production Reaction Conditions: 50 mg Catalyst, 5% H_2/CO_2 (420 psi), 25% O_2/CO_2 (160 psi), Solvent = H_2O (2.9 g), MeOH (5.6 g), T = 2 °C, Time = 0.5 h and 1200 rpm.

1.11 Reaction Conditions for the Direct Synthesis of H_2O_2.

The conditions for the majority of reactions, including temperature, pressure, time and concentration of reactants can have a detrimental effect on the chosen path of a reaction. These conditions, when their quantities are varied, can change the feasibility of a reaction taking place. This is primarily due to the effect these conditions have on the high energy barriers of given reaction pathways, with certain conditions allowing these energy barriers to be met. All these variables associated with the conditions of a reaction should be studied in order to allow any given reaction to take the correct pathway towards producing the desired product, with the direct synthesis of H_2O_2 being no exception. Wilson *et. al*[62] examined the effects of H_2 and O_2 pressures and solvent H^+ concentrations on the production rates of H_2O_2 and H_2O for silica supported Pd clusters. These experiments were done in the absence of artefacts from mass transport and secondary decomposition of H_2O_2, with these rates being interpreted to evaluate their effect on the mechanism towards the direct synthesis of H_2O_2. To begin with, they experiments were left to run in solvents with varying H^+ concentrations and the results expressed that the presence of H^+ is essential for H_2O_2 synthesis, whereas the respective counterion is much less important. However, the dependence on the rates of H_2 and O_2

pressures provided information that the synthesis undertakes a heterolytic reaction pathways, similar to the two-electron oxygen reduction reaction (ORR). The above results allowed a greater comprehension of the mechanistic approach towards H_2O_2 synthesis, which included proton-electron transfer to form H_2O_2 and O-O bond scission, when in OOH state, to from H_2O. They also concluded that H_2O formation is more sensitive to the electronic structure than H_2O_2 is, thereby an increase in the coordinated: uncoordinated surface atom ratio can increase the selectivity towards H_2O_2 synthesis.

Continuing the study further, Santos *et. al*[130] explored the effect that changing the reaction conditions and Pd content has on H_2O_2 synthesis and degradation of a 1 wt.% AuPd/TiO$_2$ catalyst, prepared by excess chlorine wet co-impregnation.[112] Initially the reaction temperature was set to 2 °C and H_2O_2 productivity and degradation was measured for the different Pd content catalysts, Figure 1.21. Results showed that H_2O_2 synthesis increases up to 0.25% Pd before declining down to between 80-90 mol_{H2O2} kg_{cat}^{-1} h^{-1} upon further increasing the Pd content. For degradation however a constant increase in rate is shown, with increasing Pd content up to monometallic Pd returning a degradation value of ~400 mol_{H2O2} kg_{cat}^{-1} h^{-1}.
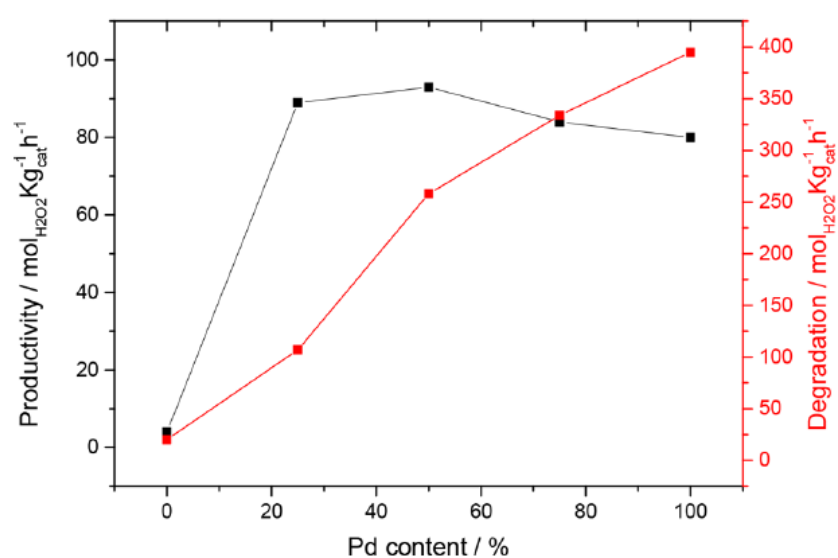
Figure 1.21: Activity of 1 wt.% AuPd/TiO$_2$, at varying Pd weight loading, towards the direct synthesis and degradation of H_2O_2 at 2 °C. **H_2O_2 Production Reaction Conditions:** 50 mg Catalyst, 5% H_2/CO$_2$ (420 psi), 25% O$_2$/CO$_2$ (160 psi), Solvent = H_2O (2.9 g), MeOH (5.6 g), T = 2 °C, Time = 0.5 h and 1200 rpm. **H_2O_2 Hydrogenation & Decomposition Conditions:** 10mg Catalyst, 5% H_2/CO$_2$ (420 psi), Solvent = H_2O (2.9 g), MeOH (5.6 g), T = 2 °C, Time = 0.5 h and 1200 rpm. Figure use granted in accordance with copyright by American Chemical Society.[130]

Increasing reaction temperature to 25 °C increased degradation as well as decreased H_2O_2 activity, indicating synthesis should be done at lower temperatures to inhibit the H_2O_2 decomposition pathways. A similar trend was observed when the solvent mixture was changed to water, with H_2O_2 productivity reduced drastically and H_2O_2 degradation being increased by a factor of 1.5, due to a combination of a decrease in H_2 solubility in water and an increased stability of H_2O_2 in methanol. Additionally, when the diluent gas was also changed to N_2 from CO_2 a further decrease in H_2O_2 activity and increase in degradation due to the loss of the acidification effect brought in by CO_2. It was concluded that the 0.5 wt.% Au-0.5 wt.% Pd/TiO_2 catalyst was the optimum Pd weight loaded catalyst for H_2O_2 synthesis and was hence tested for the effect of varying reaction time on H_2O_2 synthesis. The yield of H_2O_2 was shown to trend away from a linear relationship with respect to time, rising from 0.0085 wt.% after 5 minutes up to 0.020 wt.% after 30 minutes, with this observed pattern attributed to the catalytic activity of the catalyst towards H_2O_2 degradation.

1.11.1 Key Points.

- Protons are essential for H_2O_2 synthesis, whereas the respective counterion is much less important.[62]

- H_2O formation is more sensitive to the electronic structure of the support than H_2O_2 is, thereby an increase in the coordinated: uncoordinated surface atom ratio can increase the selectivity towards H_2O_2 synthesis.[62]

- Increasing reaction temperature increased degradation as well as decreased H_2O_2 activity, indicating synthesis should be done at lower temperatures.[130]

- When the diluent gas is N_2 over CO_2 a decrease in H_2O_2 activity and increase in degradation is observed, due to the loss of the acidification effect brought in by CO_2.[130]

1.12 The Effect of Solvent on the Direct Synthesis of H_2O_2.

One of the major issues with the direct synthesis of H_2O_2 is that the catalysts that are capable of synthesising H_2O_2 are also capable of degradation it just as readily, therefore it is of paramount interest to try and increase the selectivity of these catalyst towards H_2O_2 wherever possible. One of the ways to achieve this is to optimise the conditions of the direct synthesis, with one of these parameters being the solvent. Paunovic *et. al*[131] reported on the influence different groups of solvents had on the direct synthesis of H_2O_2, either added alone or as a co-

solvent alongside water. It was observed that the solvents nature has a strong effect on the activity and selectivity of the catalyst, with the addition of some solvents (acetone, isopropanol) to an already present aqueous phase increasing selectivity towards peroxide. It was suggested that the most suitable solvents are water miscible (methanol, ethanol, isopropanol), having an optimal balance between high selectivity and moderate/high conversions. Some water non-miscible solvents (hexane) show a high H_2 solubility however, they are not suitable for the direct synthesis due to poor selectivity. This being explained by Lunsford *et. al* who states that while H_2O_2 is 1st order with respect to H_2, it is also 1st order with respect to its hydrogenation.[132] Aprotic solvents (acetone, acetonitrile, DMSO) in contrast exhibit very high selectivity, due to the solvent interaction with the catalysts surface. However, at high solvent and reacting gas concentrations the aprotic solvent can act as a poison towards the catalyst, binding non-selectively to the catalyst's active sites.[131] These observations provide evidence that protic solvents co-catalyse the formation of H_2O_2.[69] These results concluded that methanol, when used a solvent or co-solvent and in concentrated H_2 and O_2, was shown to be the most suitable solvent, returning very high H_2O_2 yields.

Further investigations were undertaken by Lunsford *et. al*[133] in which the effect of solvent composition was tested for its effect on the production of H_2O_2. They used a 5 wt.% Pd/SiO$_2$ catalyst to comprehend the effects of having ethanol or water as the solvent phase in the direct synthesis of H_2O_2. When in ethanol, H_2O_2 production consistently increased up to 2 wt.% after 8 hours, with a rate of 22 mol$_{H2O2}$ kg$_{cat}^{-1}$ h^{-1}. When H_2O was the solvent a similar consistent increase in productivity was observed over the 8 hours, however only to a net H_2O_2 production of 1 wt.% and rate constant 80% that of ethanol (Figure 1.22a), due to the increased stability of H_2O_2 in ethanol a decrease in H_2 solubility in H_2O.
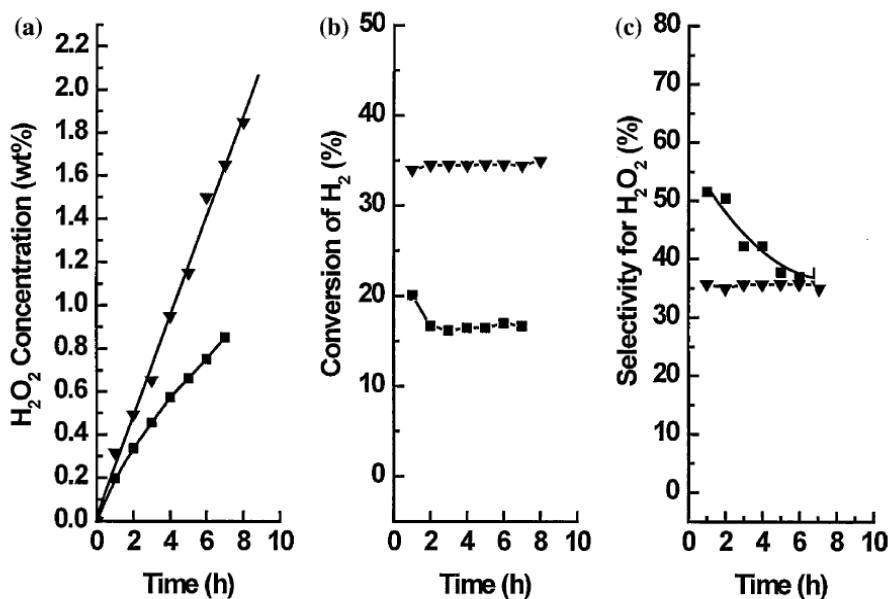
Figure 1.22: Production of H_2O_2 in ethanol (▼) and water (■) as a function of time: (a) H_2O_2 concertation, (b) conversion of H_2 and (c) selectivity of H_2O_2. **Reaction Conditions:** 50 mg 5 Wt.% Pd/SiO_2, P = 14.7 Psi, Solvent = 60 mL of 0.17 M HCl acidified $EtOH/H_2O$ O_2:H_2 4:1, T = 10 °C and Time = 1-8 h. Figure use granted in accordance with copyright by Springer Nature.[133]

Over the 8 hours, H_2 consumption was shown to have gradually increased in ethanol up to ~35%, due to the increased H_2 solubility in ethanol. While for H_2O, consumption decreased initially before plateauing out at ~15% (Figure 1.22b). Finally, regarding selectivity, when the solvent was H_2O selectivity towards H_2O_2 was initially higher than ethanol at ~50%, however over the 8 hours it gradually decreased down to ~35% (Figure 1.22c), indicating that presence of water present in the reaction does not significantly affect the behaviour of the system. These results are a clear indication that the composition of the solvent mixture has a large influence on H_2 conversion and selectivity H_2O_2, thereby influencing net production of H_2O_2.

1.12.1 Key Points.

- Methanol, when used a solvent or co-solvent and in concentrated H_2 and O_2, was shown to be the most suitable solvent, returning very high H_2O_2 yields due to having an optimal balance between high selectivity and moderate/high conversions.[131]
- The composition of the solvent mixture has a large influence on H_2 conversion and selectivity H_2O_2, thereby influencing net production of H_2O_2.[133]

1.13 The Effect Support has on the Direct Synthesis of H_2O_2.

The role of the support in a catalyst is important as it contains the ability to control the electron density and morphology of the deposited metals. Menegazzo *et. al*[134] touched on this during their research into identifying the "dream catalyst" for the direct synthesis of H_2O_2. When discussing supports they identified that carbon was an excellent support due to its hydrophobic nature and ability to stabilise oxidized active sites, allowing the protection of any synthesised H_2O_2, with the molecule being more stable at oxidized active sites and in organic solvents over water. Deliberations continued as various carbon nanostructures (activated carbon, carbon nanotubes, carbon black and mesoporous carbon) were investigated as supports for AuPd supported catalysts. The results indicated that many oxygen functional groups were paramount in the high dispersion of alloyed 2.5 wt.% Au-2.5 wt.% Pd catalysts. However, these supports didn't come without their limitations as the activated carbon suffered from mass transfer limitations, which lowered its H_2 conversion. Alongside this, the H_2O_2 synthesised by the mesoporous carbon supported catalyst was more susceptible to decomposition due to back diffusion. Even with this issue it was identified that a high O_2 content ordered mesoporous carbon supported catalyst was the most desired, due to better particle dispersion and greater Au enrichment in its smaller particles. In addition, the effect functionalization had on the activity and selectivity of a 2.5 wt.% AuPd/SBA-15 catalyst was examined. SBA-15 was used as the mesoporous silicates' properties of a huge surface area (1000 m^2/g) and large pore sizes (2-20 nm) make them ideal supports for supporting metal nanoparticles. The silica was functionalised with either SO_3H, NH_2 and SH, before introducing the metals by ion exchange. It was concluded that the inclusion of these functional groups, when compared to a non-functionalised silica support, granted greater control over the metal oxidation states. This functionalisation allowed the metals oxidation states to be held at Au^+ and Pd^{2+}, granting greater suppression towards the decomposition pathways of H_2O_2. Furthermore, the particle size distribution was reduced leading to an excellent metal particle size balance between high metal dispersion, for high activity, and less energetic sites, which prevented self-poisoning by diatomic O_2 not desorbing.

Edwards[135–139] and Ntainjua *et. al*[68,140,141] have both researched into the role the support has in achieving a catalyst with regard to achieving high activity towards H_2O_2 synthesis. The studies commenced with a 2.5 wt.% Au-2.5 wt.% Pd catalyst prepared by wet impregnation being supported upon TiO_2, Al_2O_3, Fe_2O_3, activated carbon and SiO_2. Each catalyst was then tested

for its activity for H_2O_2 synthesis. Results showed the following trend: $C > SiO_2 > CeO_2 > TiO_2$ $> MgO > Fe_2O_3 > Al_2O_3$ for H_2O_2 synthesis, which correlates with the isoelectric point of the support (Figure 1.23). This can be explained by the stability of H_2O_2 increasing with the acidity of its environment, due to the decreased rate of sequential hydrogenation, and the lower the isoelectric point (IEP) of the support the more acidic it is.
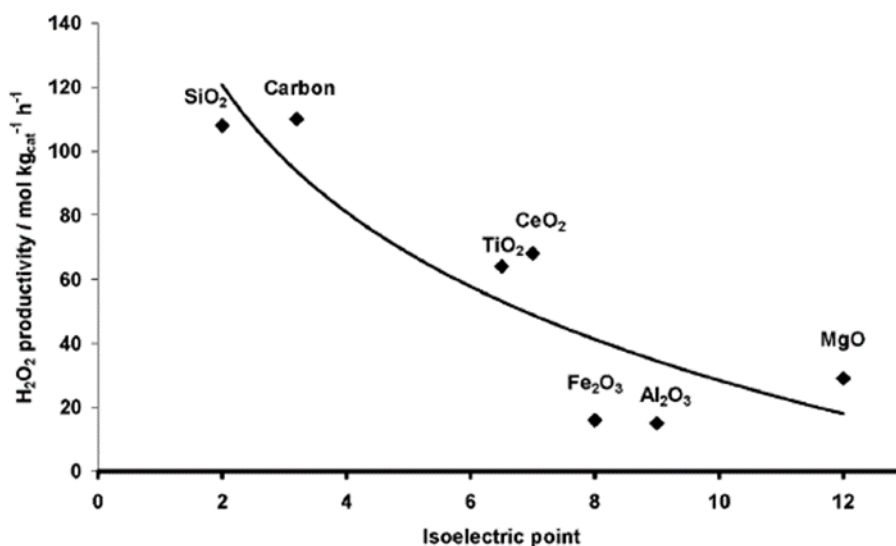
Figure 1.23: Illustrating the effect that the isoelectric point of a support has on the H_2O_2 productivity of a 2.5 wt.% Au-2.5 wt.% Pd catalyst. **Reaction Conditions:** 2 °C, 50 mg catalyst, Methanol (5.6 g) and H_2O (2.9 g) solvent, T = 0.5 h and 1200 rpm. Figure use granted in accordance with copyright by American Chemical Society.[138]

Zeolites have also been tested with Lewis *et. al*[142] using 2.5 wt.% Au-2.5 wt.% Pd/TS-1 for the direct synthesis of H_2O_2. The catalyst returned a productivity of 100 mol_{H2O2} kg_{cat}^{-1} h^{-1} and a H_2O_2 degradation of 316 mol_{H2O2} kg_{cat}^{-1} h^{-1}, which placed the support with a productivity and degradation better than of the likes of TiO_2 and SiO_2 however lower than carbon, which held a productivity of 110 mol_{H2O2} kg_{cat}^{-1} h^{-1}. This result was concluded to be due to the low isoelectric point (high acidity) of the TS-1 support, leading to high H_2O_2 selectivity. While these productivity results are not the best observed, zeolites do have some properties which encourage H_2O_2 synthesis, with this H_2O_2 being applicable to sequential reactions. Li *et. al*[143] reported using 2.5 wt.% Au-2.5 wt.% Pd/HZSM-5 for the *in-situ* oxidation of Crotylalcohol and 1-Pentene. The results showed that the H_2O_2 generated *in-situ* was able to oxidise Crotylalcohol to Crotonaldehyde, with a conversion of 81.9% over 4 hours and a selectivity of 31.5%, and 1-Pentene to 1,2-epoxypentane, with a conversion of 52.9% over 4 hours and a

selectivity of 10.5%. Once again, while these results are not optimal for the application of H_2O_2 for *in-situ* oxidation is a perceivable application.

Freakley *et. al*[144] investigated into AuPd catalysts, made by impregnation and ion exchange, and compared them with heteropolyacids precipitated with a range of cations (Cs^+, Rb^+, K^+ and Ag^+) for the direct synthesis of H_2O_2, using a batch reactor. Their research concluded that the 2.5 wt.% Au/2.5 wt.% Pd/$Rb_{2.5}H_{0.5}PW_{12}O_{40}$ catalyst, prepared by ion exchange, showed the greatest activity with a value of 696 mol_{H2O2} kg_{cat}^{-1} h^{-1}, however all the Au–Pd catalysts were shown to be more active than their analogous ion-exchanged catalysts. The Au–Pd exchanged catalysts expressed an increase in their activity towards the synthesis of H_2O_2, this increase being observed despite the observed increase in their rate of subsequent degradation, therefore indicating a very high gross synthetic activity towards H_2O_2 synthesis activity, with $Pd_{0.075}Au_{0.05}Cs_{2.5}H_{0.5}W_{12}O_{40}$ being the most active towards H_2O_2 synthesis. This result being explained by the supports loss of its crystallinity increasing H_2O_2 synthesis. In addition, the supported Au–Pd heteropolyacid catalysts showed a dramatic decrease in their rate of synthesis towards H_2O_2, with this correlating to the increase in their degradation rate. Since the Au–Pd exchanged catalyst have a much lower metal loading than the more conventional supported Au–Pd heteropolyacid catalysts it's considered that these catalysts could be a more cost-efficient alternative to synthesising H_2O_2.

Continuing the research into heteropolyacids further, Park *et. al*[145] prepared palladium-exchanged insoluble heteropolyacid ($Pd_{0.15}Cs_xH_{2.7-x}PW_{12}O_{40}$) catalysts with a variation of caesium content (x = 2.0, 2.2, 2.5, and 2.7) for the direct synthesis of H_2O_2. It was established that the $Pd_{0.15}Cs_{2.5}H_{0.2}PW_{12}O_{40}PW_{12}O_{40}$ catalyst showed the highest catalytic performance, which was concluded to be due the large surface acidity of the support. Furthermore, the yield of H_2O_2 synthesis and conversion of H_2 was shown to express volcano-shaped curve upon increasing the caesium content in the $Pd_{0.15}Cs_xH_{2.7-x}PW_{12}O_{40}$ catalyst, expressed in Figure 1.24. Finally, it was observed that the $Pd_{0.15}Cs_xH_{2.7-x}PW_{12}O_{40}$ acted as an efficient catalyst, with the heteropolyacid support serving as an alternate acid source in the direct synthesis of H_2O_2. However, the increased stability of H_2O_2 due to the increased acidity is not the only promotional effect reported, as research by Lewis *et. al*[146] discusses an additional effect in stabilising H_2O_2, when varying the amount of Cs present in the heteropolyacid support.
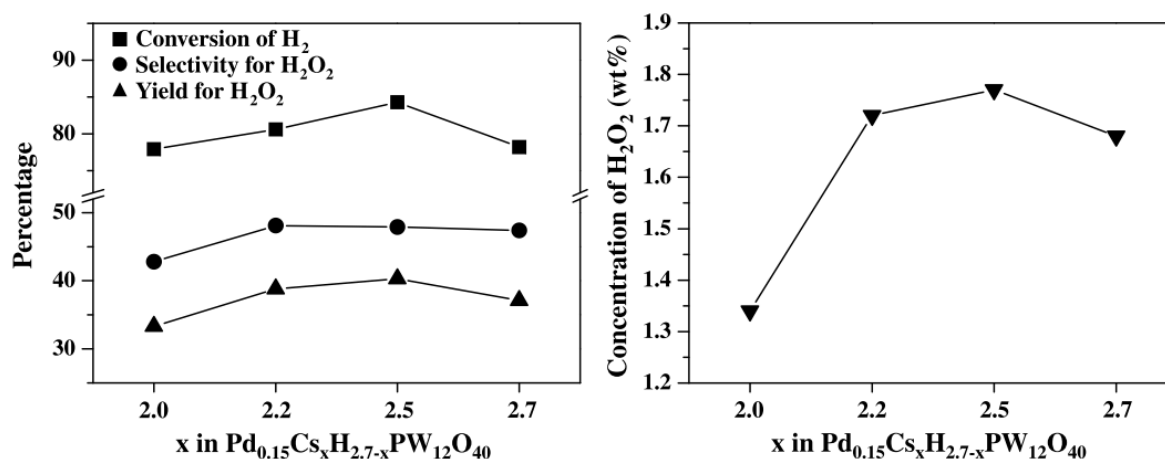
Figure 1.24: Catalytic performance of the $Pd_{0.15}Cs_xH_{2.7-x}PW_{12}O_{40}$ catalysts (x = 2.0, 2.2, 2.5, and 2.7) for the direct synthesis of H_2O_2 over a 6-hour period. **H_2O_2 Production Reaction Conditions:** 1 g $Pd_{0.15}Cs_xH_{2.7-x}PW_{12}O_{40}$, P = 147 Psi, H_2:O_2 4:10, Solvent = EtOH (80 mL), NaBr (63.2 mg) T = 27 °C, Time = 6 h and 1000 rpm. Figure use granted in accordance with copyright by Elsevier.[145]

1.13.1 Key Points.

- Carbon was an excellent support due to its hydrophobic nature and ability to stabilise oxidized active sites, leading to less decomposition of synthesised H_2O_2.[134]

- The inclusion of functional groups upon catalysts' supports grants a greater control over the metal oxidation states, allowing the metals oxidation states to be held at Au^+ and Pd^{2+} granting greater suppression towards the decomposition pathways of H_2O_2.[134]

- This IEP of a support is prevalent in the direct synthesis of H_2O_2 and can be explained by the stability of H_2O_2 increasing with the acidity of its environment, due to the decreased rate of sequential hydrogenation, and the lower the isoelectric point (IEP) of the support the more acidic it is.[135–139]

- Heteropolyacid supports have shown high catalytic performance, which was concluded to be due the large surface acidity of the support as well as an additional effect in stabilising H_2O_2, when varying the amount of Cs present in the heteropolyacid support.[145,146]

1.14 The Effect that Heat Treatment has on the Direct Synthesis of H_2O_2.

It has been observed that the effect of heat treatment is pivotal in ensuring a stable and reusable catalyst, with these factors being key in generating an economical and environmental catalyst.[103] Yet, uncalcined bimetallic catalysts have been shown to offer greater activity towards H_2O_2 synthesis and higher H_2 conversions than their heat-treated counterparts. However, while these catalysts are very active towards H_2O_2 synthesis they are intrinsically unstable, leading to the active metal components leaching from the catalyst support. Edwards *et. al*[147] researched into the effect that calcination temperature had on an acid pre-treated 2.5 wt.% Au-2.5 wt.% Pd/C catalyst, regarding its re-usability and the suppression of the H_2O_2 degradation pathway. It was observed that upon increasing the calcination temperature from 120 to 400 °C the production of H_2O_2 decreased from 212 to 160 mol_{H2O2} kg_{cat}^{-1} h^{-1}. However, the opposite was found for reusability, with the increase in calcination temperature from 120 to 400 °C leading to an improvement in the re-use activity of the catalyst from 101 mol_{H2O2} kg_{cat}^{-1} h^{-1} at 120 °C to 160 mol_{H2O2} kg_{cat}^{-1} h^{-1} for 400 °C, due to the prevention of metal leaching. In addition, it was observed that the re-use activity for the 400 °C calcined catalyst was the same as its initial activity. Regarding hydrogenation, the increase in calcination temperature has led to a complete suppression of its activity, with the 400 °C calcined catalyst having a hydrogenation activity of 0 mol_{H2O2} kg_{cat}^{-1} h^{-1}. The 2 Vol.% HNO_3 pre-treatment of the carbon support was shown to increase the activity of the catalyst when compared to a non-treated catalyst. This could be explained by a greater dispersion of the metals on the surface or the increase in the Pd/Au ratio and amount of Pd^{2+} present on the catalysts surface. The Pd/Au ratio increased even further with calcination temperature, with Pd/Au ratio increasing up to 4.2 from 2.7.

In addition, Park *et. al*[148] researched into the effect of calcination temperature by supporting Pd upon SO_3H-functionalised MCF silica, via the ion exchange method, before calcinating at a variety of temperatures (450-950 °C) and testing for the direct synthesis of H_2O_2. The experimental work established that conversion of hydrogen, selectivity for H_2O_2 and yield for H_2O_2 showed volcano-shaped curves with respect to calcination temperature of MCF silica, Figure 1.25, with the optimal calcination temperature being 750 °C. It was concluded that this result was due to the improved acid density of the catalyst at this temperature, with the catalyst calcined at 750 °C having the highest acid density value of 1.23 $\mu mol\text{-}H^+/m^2$.
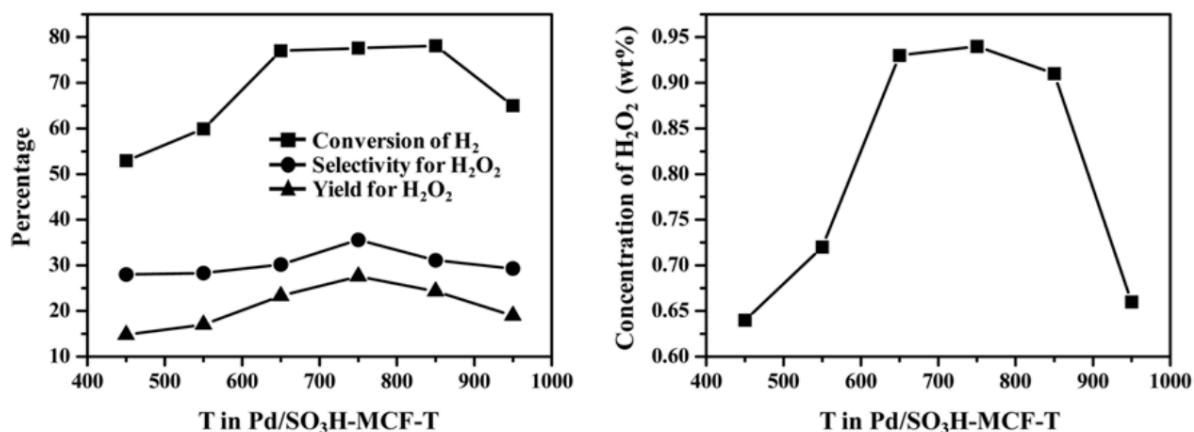
Figure 1.25: The catalytic performance of the Pd supported SO_3H-functionalised MCF silica catalyst for the direct synthesis of H_2O_2 over a 6-hour period at temperature between 450-950 °C. **H_2O_2 Production Reaction Conditions:** 1 g $Pd_{0.15}Cs_xH_{2.7-x}PW_{12}O_{40}$, P = 147 Psi, H_2:O_2 4:10, Solvent = EtOH (80 mL), NaBr (63.2 mg) T = 27 °C, Time = 6 h and 1000 rpm. Figure use granted in accordance with copyright by Springer Nature.[148]

1.14.1 Key Points.

- Upon increasing the calcination temperature from 120 to 400 °C the production of H_2O_2 decreased, yet reusability increases.[147]
- Conversion of hydrogen, selectivity for H_2O_2 and yield for H_2O_2 showed a volcano-shaped curves with respect to calcination temperature of MCF silica which was concluded to be due to the improved acid density of the catalyst up to 750 °C, with the catalyst calcined at 750 °C having the highest acid density value.[148]

1.15 The Effect of Reactor System on the Direct Synthesis of H_2O_2.

Moving towards synthesising H_2O_2 using a microreactor, Kanungo *et. al*[149] developed a method to deposit AuPd *in-situ* directly upon the walls of the microreactor. Prior to depositing the metals, polyelectrolyte multilayers (PEMs) must first be added. The PEMs are formed layer by layer using a method discovered by Decher[150] (Figure 1.26).
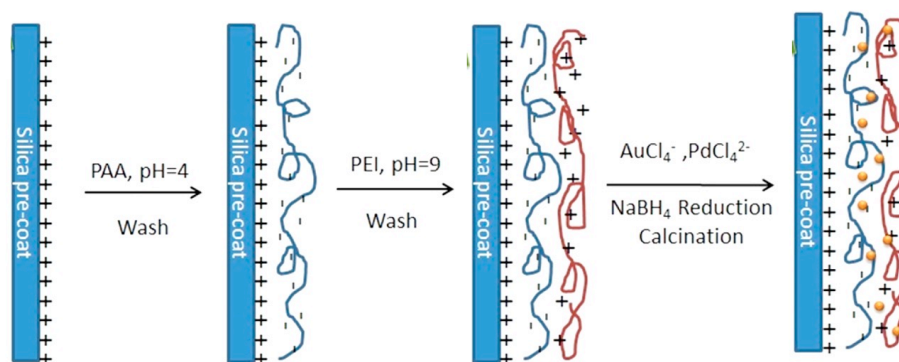
Figure 1.26: diagram demonstrating the steps towards depositing the metal upon the microreactor walls. Figure use granted in accordance with copyright by American Chemical Society.[149]

It is the porous and supramolecular structure of the PEMs that provide the binding points for the metal precursors, as well preventing aggregation and encouraging uniformity in metal particle production. The metal precursors (HAuCl$_4$ and K$_2$PdCl$_4$) are then passed through the capillary tube depositing on the surface before being calcined. TEM confirmed the deposition of metal nanoparticles on the capillary's surface, with the images confirming the deposition, identifying 0.3-1.5 nm particles on the capillary's surface. From testing for H$_2$O$_2$ production it was concluded that a 2-layer capillary was the most active for H$_2$O$_2$ synthesis due to a higher metal loading. Unfortunately, this was partnered with a loss of selectivity due to a higher site volume as well as Pd leaching, which was confirmed by inductively coupled plasma optical emission spectroscopy (ICP-OES). The 210 mol$_{H2O2}$ kg$_{cat}^{-1}$ h^{-1} produced through this capillary however was still much higher than results produced through comparable catalysts found in literature.[151,152]

The reaction conditions for the synthesis of H$_2$O$_2$ utilising a flow reactor were investigated by Freakley *et. al*[153] for a bimetallic 0.5 wt.% Au 0.5 wt.% Pd/TiO$_2$, prepared using an excess anion method previously reported by Sankar *et. al.*[112] The effect of altering gas flow rate, pressure, catalyst amount, solvent composition, solvent flow rate, temperature and H$_2$/O$_2$ ratio were all explored. The H$_2$O$_2$ concentration was shown to increase with increased gas flow up to 42 mL min^{-1}, producing 760 ppm of H$_2$O$_2$. This can be explained by increasing the amount of H$_2$ at the catalyst surface, as well removing the H$_2$ gradient previously present in the catalyst bed. Pressure also showed an increase in H$_2$O$_2$ production, this time due to the flow gases increased solubility and decreased gas bubble size, allowing greater mixing. Next, catalyst

58

amount was tested for its effect on H_2O_2 production, with amount varying from 0.05 g – 0.125 g and the gas flow adjusted to each mass to keep flow/cat mass consistent. It was shown that with increased catalyst mass, H_2O_2 production and H_2 conversion increased, indicating that production per unit mass is consistent. Solvent composition was also evaluated by varying the % MeOH in solution from 0-100%. Results returned indicating that increased MeOH % drives forwards H_2O_2 production due to MeOH's superior gas solubility compared to water. Solvent flow rate was also tested, varying between 0.2 – 1.25 mL min^{-1}. Results showed that increasing the solvents flow rate increased the moles of H_2O_2 produced up to a value of 1 mL min^{-1}. After this point production dropped off due to the residence time of the catalyst being reduced via dilution. Temperature was then studied, and it was observed that with increasing the temperature up from 2 °C to 30 °C H_2O_2 production dropped ~40%, alongside a ~60% drop in selectivity. This can be assigned to the relatively activation energies of the degradation pathways, H_2O_2 decomposition and hydrogenation, being more favourable at higher temperatures. Finally, the optimum H_2/O_2 ratio was determined to be 1, due to it being the maximum concentration of H_2 and O_2 available at which a 1:1 ratio can be achieved, given the limited gas pressures and explosive limit for hydrogen. These results can be supported by the research by Piccinini et. al[154,155] and Hutchings and co-workers,[156] who have taken a similar approaches to altering the reaction conditions towards H_2O_2 synthesis in batch using 5 wt% AuPd/TiO$_2$ catalysts in batch and have come to similar conclusions.

Research into the effect bed length has on the direct synthesis of H_2O_2 was undertaken by Sun et. al[157] by designing a polymethyl methacrylate (PMMA) microreactor. Initially, they tested the importance of catalyst bed length, questioning whether a longer bed would increase H_2O_2 yield, due to bed length correlating directly to contact time between reactants and catalyst. They tested by varying the microchannel length between 32.8 – 346 mm and testing for the concentration of H_2O_2 produced. The results returned a volcano plot trend with respect to bed length (Figure 1.27a), with a bed length of 174.2 mm producing the highest concentration of H_2O_2, with a value of ~0.055 wt.% H_2O_2.
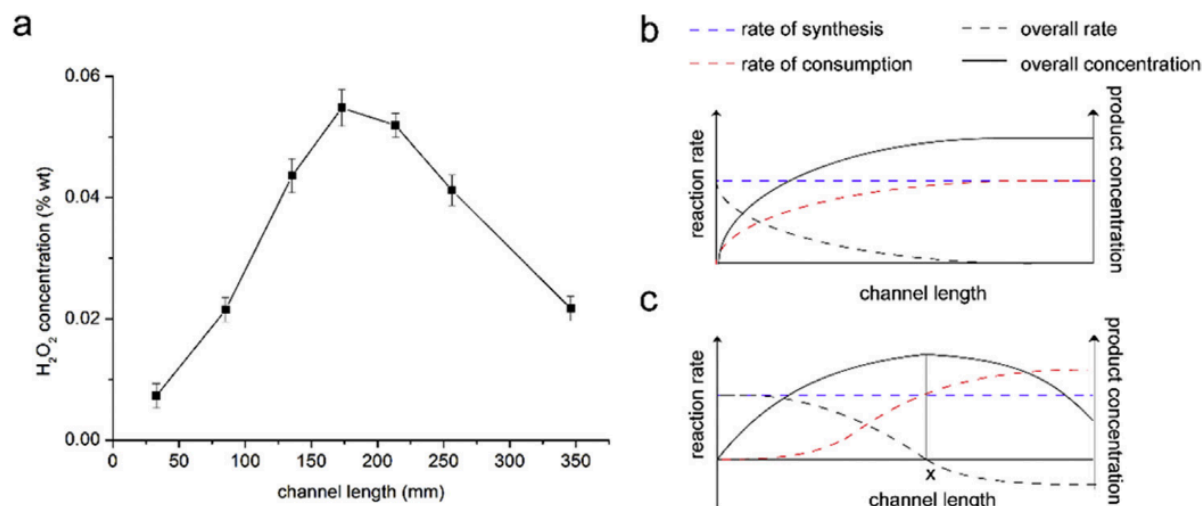
Figure 1.26: Effect of (a) channel length on product concentration (liquid flow rate 0.1 mL min^{-1}, H$_2$ flow rate 8 mL min^{-1}, O$_2$ flow rate 16 mL min^{-1}), and illustration of (b) proposed mechanisms with fast consumption and (c) slow consumption. Figure use granted in accordance with copyright by Elsevier.[157]

To comprehend the reason for this they studied into the rates of the reaction along increasing channel length (Figure 1.27b + c). In the initial stages of the reaction, the rate of H$_2$O$_2$ synthesis was higher than the rate of consumption, as H$_2$O$_2$ degradation activity is proportional to H$_2$O$_2$ concentration. Additionally, the net rate (black dash line) was also positive, leading to an increase of the accumulative concentration of H$_2$O$_2$ (black solid line). However, if both the synthesis and decomposition processes were fast and equilibrium was achieved at all time, the observed rate of H$_2$O$_2$ consumption would gradually increase alongside channel length until it reached the same value of the synthesis rate. At that time, the net rate would become zero and the H$_2$O$_2$ concentration would reach the highest value and stay constant afterwards due to equilibrium being established (Figure. 1.27b). However, a dramatic drop off in H$_2$O$_2$ concentration after it reached the peak value was observed, indicating that the previous assumption might be flawed. They reasoned that the synthesis was fast while the consumption was relatively slow, meaning there would be a delay in the change of consumption rate with H$_2$O$_2$ concentration. The length of the channel in which the consumption rate equals the synthesis rate is defined by the letter X on Figure 1.27b + c. This postponement in the change of consumption rate meant that even after X, the rate of consumption continued to increase, resulting in a negative net rate and a drop in H$_2$O$_2$ concentration.[157]

Ratchananusorn *et. al*[158] investigated the utilisation of a novel microstructured plate-type reactor and its reaction conditions for the direct synthesis of H_2O_2, using a 3 wt.% Pd/Activated carbon cloth (ACC). The reactor plate is installed in vertical position, with the inlets for gas and liquid being located at the top section. A bifurcation configuration was used for the liquid feed to improve the distribution and prevent channelling problems. However, the gas feed is passed through the cover plate against the direction of the microreactor. The microstructure section of the reactor is located below the inlet section and is made up of little triangular elements (Figure 1.28). This design for the microstructure was put in place to improve the mixing of the two phases and to generate high interfacial area.
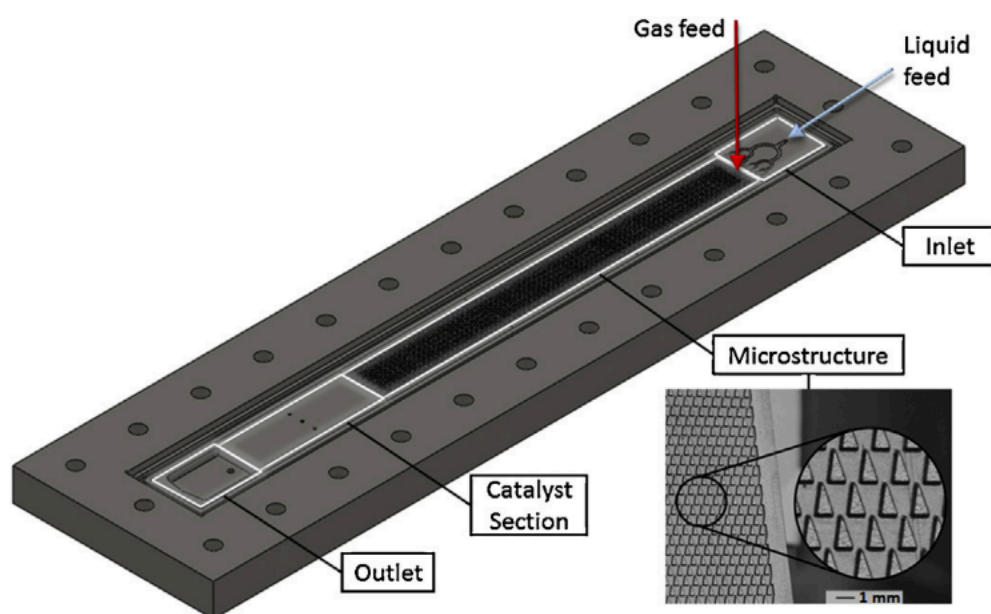
Figure 1.28: Structure of the microreactor plate used in the study by Ratchananusorn *et. al*. Figure use granted in accordance with copyright by Elsevier.[158]

In their experiments they began by varying the gas mixture, H_2/CO_2 or H_2/N_2, and the working pressure, 10 or 20 bar, for the direct synthesis of H_2O_2. The optimum results were obtained at 20 bar and with CO_2 as the inert gas, due to CO_2 increasing gas solubility and stabilising synthesised H_2O_2. Gas/liquid feed ratio was also investigated, varying between 0.75 and 2.21, while maintaining liquid flow rate constant. The results showed that increasing gas/liquid feed ratio increased the concentration of H_2O_2, due to the increase in hydrogen feed. However, there was also a decrease in selectivity, which is explained by the enhanced decomposition of H_2O_2, via the hydrogenation pathway. Following this they varied the liquid feed rate, keeping the gas/liquid ratio consistent, between $34 - 68$ mL min^{-1}. The results indicated that increasing the

flow rate increases both the concentration and selectivity of H_2O_2, which was concluded to be due to a combination of factors. The first being the improved hydrodynamical conditions in the catalyst bed, causing better surface contact and the second being faster gas-liquid mass transfer which increased the velocity of gas/liquid dispersion. These were able to occur due to the large interfacial area if the microreactor, meaning mass transfer was not a limiting factor in these experiments. The data from this research displays encouraging results that microreactor technology might offer the possibility to operate outside the operating conditions of current technologies and allow the enhancement towards H_2O_2 yield.

1.15.1 Key Points.

- It is the porous and supramolecular structure of the PEMs that provide the binding points for the metal precursors, as well preventing aggregation and encouraging uniformity in metal particle production, allowing it to become a support for catalysts.[149]

- For a flow reactor the H_2O_2 concentration was shown to increase alongside gas flow, pressure, catalyst mas, solvent flow rate and composition, yet decrease with increasing reaction temperature.[153]

- Channel length has a well-documented effect on H_2O_2 concentration, producing a volcano plot trend with respect to bed length. [157]

- Microreactor technology might offer the possibility to operate outside the operating conditions of current technologies and allow the enhancement towards H_2O_2 yield. [158]

- The gas phase direct synthesis of H_2O_2 should be possible utilising a $AuPd/TiO_2$ catalyst, a gas phase mixture of 2% H_2/Air and a gas phase reactor.[159]

1.16 Wastewater Remediation.

1.16.1 Greywater Overview.

Greywater (GW) is defined as any wastewater originating from a water stream that has not been in direct contact with faecal matter.[160] Sources of non-industrial greywater include office blocks, apartments and households, with the greywater being generated via sinks, showers, baths and washing machines. Greywater contains many hazardous bacteria that need to be removed or chemically reduced before the water can be redistributed, for use in irrigation and toilet flushing. Typical levels of all coliforms, defined as rod-shaped bacteria, in greywater

range between 1×10^2 to 1×10^7 total coliforms per 100 mL[161,162] and before redistribution the level of coliforms must be below < 1000 faecal coliforms per 100 mL of water for irrigation and 0 faecal coliforms for toilet flushing[163], which alludes to the fact that a treatment method is required. The recycling of water slowly moving towards becoming a necessity in modern day society due to constant growth in population. By the year 2050 the population is set to reach 9.8 billion and by the year 2100 this is set to reach 11.2 billion,[164] which will in turn lead to a worldwide increase in water demand. To meet these demands there are two approaches; the supplies of water can be increased to meet the demands, however these are partnered alongside large financial demands that the developing counties that require it most cannot meet. The second approach is in reducing the demand for water. This approach has a smaller financial demand and is the much more feasible of the two. By recycling water, the average household's water consumption, and in turn their demand, would reduce. This can be achieved by recycling the greywater sources and applying them to non-potable applications mentioned previously.

1.16.2 Greywater Contaminants.

Bacteria, viruses, and other contaminants can cause infection and illness when entering the human body, which can occur via contact, vector transmission, inhalation, or ingestion. The greywater re-use sources found in the household tend to be hot water systems (e.g. laundry), allowing the opportunity for pathogenic bacteria to thrive and grow[165]. Therefore, the contaminants found in greywater must be removed before the issue of human ingestion increases and the recycled greywater enters back into the household, being used in crop irrigation, laundry and/or toilet flushing.[166] To test the concentration of contaminants, present in a given wastewater sample, certain tests have been developed. The biochemical oxygen demand (BOD) is one of these tests and it measures the amount of dissolved oxygen (DO) required by aerobic organisms to break down organic material present in any given sample of water.[167] The amount of DO present in a sample can vary depending on a few conditions; temperature, increase in water temperature less O_2 can be held, salinity, the more saline the solution the less O_2 can be held, and atmospheric pressure, as pressure decreases water loses its capacity to store O_2. Another test than can be utilised is the chemical oxygen demand (COD) and it measures the amount of DO required to breakdown organic material via chemical oxidation.[167]

1.16.3 Greywater Treatments.

Research into the area of treatment and reapplication of greywater has been on record since 1974 when initial research was done into developing treatment methods utilising filtration and/or membranes alongside disinfection.[168,169] Advancements were made in the 90s when the initial treatment methods began being installed into households on a small scale[170] as well as research into utilising biological matter, such as reeds and ponds, and converting them into biological reactor.[171,172] Now well into the 21st century many different greywater treatments have been conceived and these can be divided up into separate categories. Pidou *et. al*[173] identified 5 treatment options for greywater recycling:

1. Simple Treatment
2. Physical Treatment
3. Biological Treatment
4. Extensive Treatment
5. Chemical Treatment

1.16.4 Simple Treatment.

A two-stage system which implements sedimentation, or a coarse filtration system, is defined as a simple water treatment technology. The greywater is added to the system and removes the larger solids from the water e.g. organics or solids. However, this is the only contaminants they can treat before a disinfectant, normally chlorine based, must be added to treat the microorganisms (Figure 1.29). The disinfectant, while effective, has a detrimental effect on the environment, combining with organics and inorganics present in the water forming chloride salts and organic chemicals respectively. Simple treatments are used in large quantities due to being marketed as easy to use and with low operating costs.
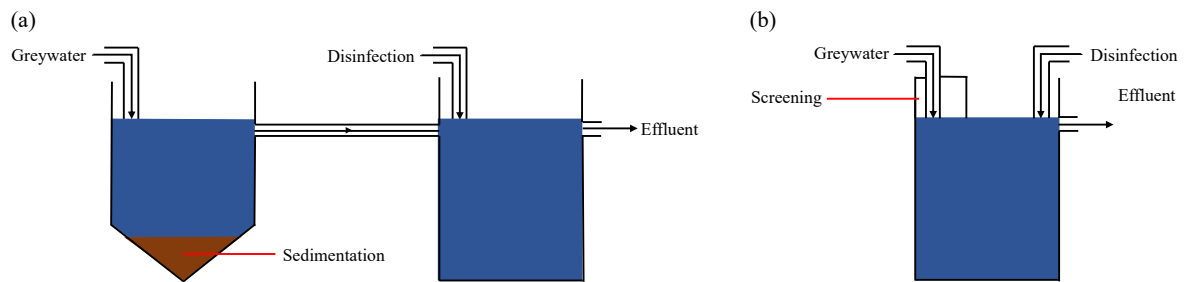
Figure 1.29: Simple treatment systems with (a) disinfection and sedimentation or (b) screening. Figure use granted in accordance with copyright by Thomas Telford.[173]

1.16.5 Physical Treatment.

Physical treatment systems can be divided into 2 types; sand filter and membrane (Figure 1.30a + b). Sand filters can be used on their own, acting as a filtration system for the greywater.[174] In a similar manner to the simple treatment system they can only provide limited treatment but become more effective when combined with a disinfectant and/or activated carbon. However, this combination does not increase the net volume of solids removed, though additional treatment using micro-organisms has been shown to drastically improve on this.[175,176]

Treatment using membranes has been shown to provide a different outcome to greywater treatment, having the ability to remove large amounts of both suspended and dissolved solids but unable to remove substantial amounts of organics. The pore size of the membranes is a very important factor in regards to the efficacy of the system, with a smaller pore size producing an improved organic pollutant removal and a greater overall treatment.[177] Membrane treatment systems are not without there issues however due to an issue identified as fouling. Fouling is the accumulation of macrorganisms, microorganisms or plant/animal life upon a wetted surface and leads to a less effective treatment, with organisms able to pass through the membrane untreated.[178] However, this issue can be combatted by pre-treating with a sand filter or screen, to remove the larger pollutants.[179]
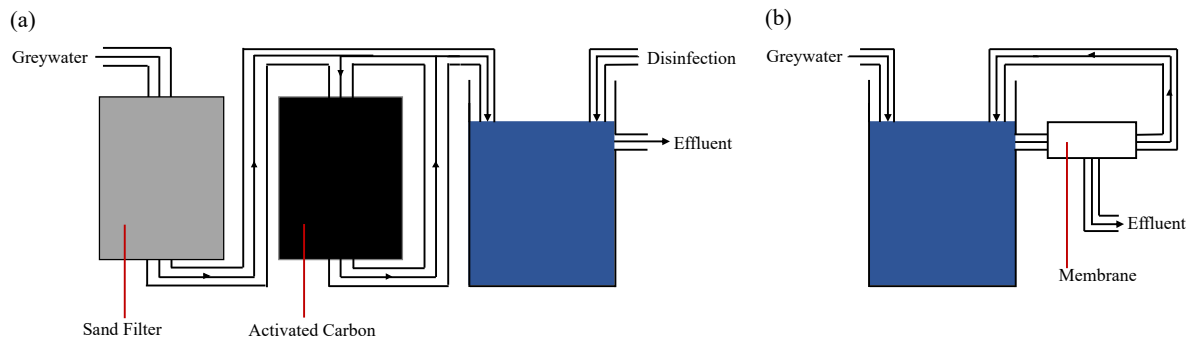
Figure 1.30: The 2 types of physical treatment; (a) sand filter and (b) membrane. Figure use granted in accordance with copyright by Thomas Telford.[173]

1.16.6 Biological Treatment.

There are many different types of biological treatment reactors e.g. membrane reactors (Figure 1.31a + b), however they are rarely used individually. The reactors tend to be grouped together into a sequential batch reactor (Figure 1.36c), beginning with a pre-treatment step of either screening and/or sedimentation, before ending with disinfection. These systems are designed for larger scale greywater recycling, being integrated into stadiums,[180] student residences,[181] and multi-storey buildings.[182]
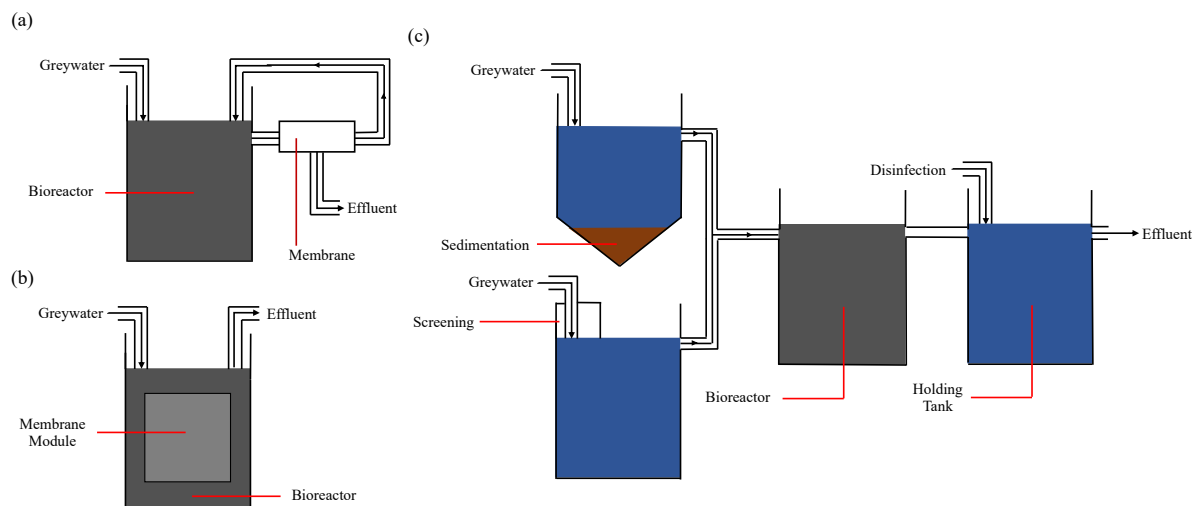
Figure 1.31: (a + b) Biological membrane reactors and a (c) sequential batch reactor. Figure use granted in accordance with copyright by Thomas Telford.[173]

The biological systems are very effective at removing organic and solid particulates in greywater with the treated water meeting the standards for re-use, independent of the combination of reactors used. Cost of function is still a factor in these reactors, with limited information available on running costs.

1.16.7 Extensive Treatment.

Extensive reactors utilise manufactured wetlands, such as reed beds and ponds, to treat greywater. Again, the wetlands are preceded by a sedimentation process to remove the larger pollutants in the greywater (Figure 1.32). The technology itself is considered inexpensive and environmentally friendly, utilising only the wetlands to treat the greywater. However, it's far from optimised as the wetland's maintenance alongside poor microorganism treatment led to other options becoming more appropriate.
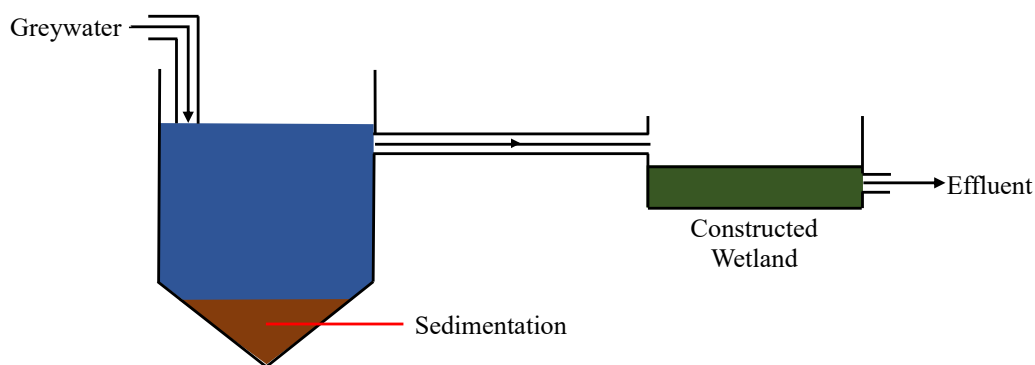
Figure 1.32: Extensive greywater treatment technology. Figure use granted in accordance with copyright by Thomas Telford.[173]

1.16.8 Chemical Treatment.

Chemical treatment refers to methods used to breakdown waste into non-toxic alternatives or to modify the chemical properties of the waste until safe e.g. neutralise pH, remove pollutants. In greywater treatment chemicals are added to remove as many/all organic/inorganic molecules and macrorganisms as possible, until pollutant levels are low enough for redistribution. The chemicals used are strong oxidants, able to oxidise other molecules/organisms. These chemicals tend to be molecules containing chlorine, ozone or H_2O_2. UV light has also been documented in its ability to oxidise microorganisms and pollutants.[183] The process of oxidation works via the oxidant producing molecules small enough to pass through the cell walls within a microorganism, while also being capable of causing irreversible damage to those cells. The

problems arise when those molecules are being occupied by other inorganic/organic pollutants that can also undergo oxidation, causing deactivation of the chemical oxidant. This addresses why screening and/or sedimentation is present in all treatment processes, removing these pollutants and increasing the chemical oxidant's potency.

1.16.8.1 Chlorine (Chlorine, Sodium hypochlorite, Chloramines) in Chemical Treatment.

The process of adding chlorine to water with the intention of it disinfecting it and eradicate contaminants is known as chlorination. Chlorine can be added either in its gaseous state (Cl_2), as sodium hypochlorite (NaOCl) or calcium hypochlorite ($CaOCl_2$) and is the most widely used chemical disinfectant, however its disinfection by-products have been linked to carcinogenic effects.[184] The hypochlorite form is the most accessible chlorine molecule due to ease of handling, storing and operation compared to the other forms.[185] The amount of chlorine required for treatment is called the "chlorine demand" and the value depends on the amount of chlorine required to treat all the impurities in the water before residual chlorine is formed. Gaseous chlorine and the hypochlorite's work by reacting with H_2O to form hypochlorous acid and subsequently the hypochlorite ion (Equations 19-22), both of which are the main disinfecting molecules.

$$H_2O + Cl_2 \longrightarrow HOCl + H^+ + Cl^- \tag{19}$$

$$H_2O + NaOCl \longrightarrow HOCl + NaOH \tag{20}$$

$$H_2O + Ca(OCl)_2 \longrightarrow 2HOCl + Ca(OH)_2 \tag{21}$$

$$HOCl \longrightarrow H^+ + OCl^- \tag{22}$$
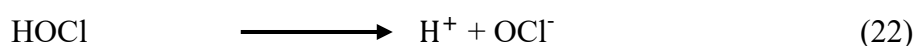
Equations 19-22: Reaction of chlorine gas, sodium and calcium hypochlorite with water. Equations reproduced in accordance with copyright by Elsevier.[186]

However, depending on the pH level of the water, the amount of each of these molecules will dominate. The optimal pH is between 6-8.5 where "free chlorine" exists, where hypochlorous acid and the hypochlorite ion are in combination. Free chlorine has a high oxidation potential so can rapidly react with any contaminants present in the water. If the pH is < 6 then hypochlorous acid dominates, which is the more effective oxidant however, dissolved gaseous chlorine will be present and the water will become extremely corrosive. If the pH is > 8.5 then hypochlorous acid levels are reduced and hypochlorite ion dominates, which is less microbicidal and will reduce disinfection by up to 90% compared to free chlorine.[187] Both of

these conditions have worse oxidation potential than free chlorine and leaves the water untreated. Chlorine can also react with ammonia, which can be present in wastewater, and form chloramines, instead of free chlorine, which have a lower oxidation potential. In addition, chlorine can be deactivated by reacting with organic material present in the water instead of reacting with the microorganisms, so wastewater must be filtered prior to treatment to increase chlorination's efficacy. However, gaseous chlorine is not without its issues. It's a toxic respiratory irritant therefore exposure for longer than an hour can cause significant respiratory affects.[188] It is highly reactive with certain reactants including acetylene, hydrogen, fluorine and ammonia, which can lead to explosions. Due to all these properties chlorine gas is limited to the amount that can be stored at a single location, which has led to wastewater treatment plants looking towards alternatives.[189]

1.16.8.2 Ultraviolet Radiation in Chemical Treatment.

UV radiation is a known effective disinfectant being able to treat bacteria, viruses, and protozoans, unlike chlorine. UV radiation can be separated into three wavelength zones: UV-A, UV-B and UV-C and it's UV-C that can be utilised for wastewater treatment, due to its wavelength range. Nucleic acids have an adsorption range between 240-280 nm and if this value is reached the DNA inside the microorganisms will be altered and reproduction will be suspended[190]. The UV-C radiation wavelength range is between 10-400 nm, so can provide the wavelength required to treat the microorganisms. Hydroxyl radicals can also be generated as a consequence of the UV radiation, via the homolysis of H_2O (Equation 23).[191]

$$H_2O \xrightarrow{h\nu} OH\cdot + H\cdot \qquad (23)$$
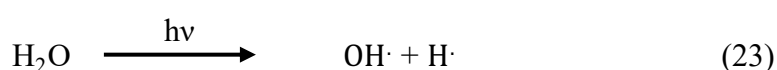
Equations 23: homolysis of H_2O. Equation reproduced in accordance with copyright by Elsevier.[191]

For treatment, a low-pressure Hg lamp is used as it emits a wavelength of 254 nm. The lamp is shone onto the wastewater and the radiation is absorbed by the water and the DNA inside the pathogen, generating peroxyl radicals and deactivating microorganisms respectively. The extent of the treatment depends on the initial bacterial concentration, contact time, intensity of the UV light, and quantity of organic/inorganic pollutants. If the contact time, or intensity of light is too low not all the bacteria will be treated and any remaining bacteria can repair the UV-induced damage, reactivating the previously deactivated bacteria. This can also be caused

by using a high initial bacterial concentration, as the radiation, in combination with peroxyl radicals, may not be able to deactivate all the bacteria. In addition, if there is a large presence of organic pollutants these could decrease the efficacy of the treatment by shielding/absorbing the UV radiation from the microorganisms, therefore filtration/sedimentation prior to treatment is advised. UV radiation alone is not enough to completely treat the wastewater and further treatment from additional chemical treatments e.g. chlorination is typically required.

1.16.8.3 Ozone in Chemical Treatment.

Ozone is an inorganic molecule with the chemical formula O_3. It is an allotropic form of oxygen containing 3 atoms of oxygen per molecule compared to the standard form of oxygen, dioxygen (O_2), which contains two. O_3 is generated by the subsequent splitting and recombination of O_2. In nature this occurs utilising ultraviolet radiation to split O_2 into two oxygen atoms ($2O$). This is then followed by each of those oxygen atoms combining with another O_2 to form O_3. Synthetically O_3 can also be generated using a method known as the corona discharge method[192]. This is achieved by passing a high voltage current across an oxygen containing gas stream, usually air, however pure oxygen can replace air to increase the efficiency. The energy generated from the current then mimics that of UV radiation and in a similar manner split the dioxygen molecule into two oxygen atoms which then combine with O_2 to form ozone.

Ozone is also the strongest non-halide chemical disinfectant as when added to H_2O the molecule facilitates the formation of $OH^\bullet$ radicals, which are well documented in their biocidal nature and will treat the contaminants, turning them into inorganic substances e.g. H_2O, CO_2 (Equations 24-28). O_3 destroys bacteria by attacking the glycoproteins and glycolipids inside the cell membrane resulting in a rupturing of the cell membrane. In addition, O_3 also has the capabilities to incapacitate certain enzymes by attack their sulfhydryl groups resulting in a loss of normal cellular enzymatic activity. Finally, O_3 also attacks purine and pyridine bases held inside DNA, resulting in catastrophic damage, this antimicrobial activity is not just for bacteria but includes mold, viruses and protozoa.[193]

$$O_3 + H_2O_2 \longrightarrow OH^{\cdot} + O_2 + HO_2^{\cdot} \tag{24}$$

$$O_3 + OH^{\cdot} \longrightarrow HO_2^{\cdot} + O_2 \tag{25}$$

$$O_3 + HO_2^{\cdot} \longrightarrow OH^{\cdot} + 2O_2 \tag{26}$$

$$OH^{\cdot} + HO_2^{\cdot} \longrightarrow H_2O + O_2 \tag{27}$$

$$2OH^{\cdot} \longrightarrow H_2O \tag{28}$$
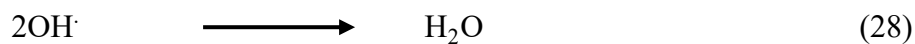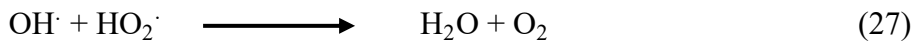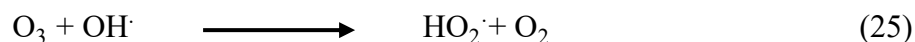
Equations 24-28: O_3 and H_2O_2 radical formation and deactivation process. Equations reproduced in accordance with copyright by Elsevier.[183]

In comparison, all the non-oxidising disinfectants e.g. chlorine must be transported across the cells membrane before being able to inflict irreparable damage, causing a less effective treatment. The treatment itself is not without its faults as the $OH^{\cdot}$ radicals have very short lifetime meaning contact time between radical and contaminant is key. As discussed with both UV and chlorine, organic contaminants present in the water can react with the ozone itself, vastly reducing the efficacy of ozone by chemical deactivation. The organics can be filtered out prior to treatment using sedimentation/filtration however, this is joined with additional complexity and cost, both of which should be avoided.

1.16.8.4 H_2O_2 in Chemical Treatment.

H_2O_2 is a chemical oxidant that has seen its application grow in the treatment of wastewater due to the increased demand for water removed of toxic chemical residues[194,195]. Previously, H_2O_2 was only seen as an additive to chemical treatments, being in combination with other chemical oxidants such as UV and O_3,[183] as well as being used in sterilization process due to its low sporicidal activity.[196,197] However, it has now been identified as a stand-alone oxidant, due to the drive to find environmentally friendly, non-toxic, yet potent biocides. The advantage of H_2O_2, when compared to the other chemical oxidants, is its high redox potential and oxidative properties (Table 6)[198], leading to a vast production of reactive oxygen species (ROS) which are very active for oxidation and theorised to be capable of cell deactivation. In addition, the common chemical oxidants e.g. chlorine, NaOCl and ozone release toxic by-products following there degradation, yet the only by-products of H_2O_2 application as an oxidant are H_2O and O_2, both of which are notably non-toxic and environmentally friendly.[199]

Table 6: Standard reduction potentials at 25°C. Table reproduced in accordance with copyright by Colby.edu.[198]

Half Reaction	E° (V)
$Cl_{2(g)} + 2e^- \rightarrow 2Cl^-_{(aq)}$	+1.359
$HClO_{(aq)} + H^+_{(aq)} + e^- \rightarrow Cl_{2(g)} + H_2O$	+1.630
$ClO^-_{(aq)} + H_2O_{(l)} + 2e^- \rightarrow Cl^-_{(aq)} + 2OH^-$	+0.890
$H_2O_{2\,(aq)} + 2H^+_{(aq)} + 2e^- \rightarrow 2H_2O_{(l)}$	+1.776
$HO_2^-_{(aq)} + H_2O_{(l)} + 2e^- \rightarrow 3OH^-_{(aq)}$	+0.880
$O_{3(g)} + 2H^+_{(aq)} + 2e^- \rightarrow O_{2(g)} + H_2O_{(l)}$	+2.07

Ronen *et. al*[200] researched into the disinfection of greywater using a stabilised H_2O_2-based compound (HPP) and compared it to chlorination, the efficacy of the HPP for a small-scale GW treatment system was also evaluated. Raw GW was extracted from two small scale greywater sources in Israel and treated with either chlorine or HPP at varying concentrations. The GW contained many different contaminants, with each one responding differently to the respective treatments. To inactivate 99% of all faecal coliforms, 125 mg L^{-1} of HPP was required, alongside a contact time of 35 mins, whereas only 10 mg L^{-1} and a contact time of 12 mins was needed for chlorine. Somatic coliphages, a virus that is ineffective against *E. coli*, responded in a similar way for the chlorine treatment, however a longer contact time of 56 minutes was needed for the HPP. Treatment of the F$^+$ bacteriophage, a virus which infects and replicates inside bacteria, was not effective for either treatment, suggesting a more effective alternative disinfectant is required. Both disinfectants were cost analysed for areas that produce 5 m^3 per day of GW, with the results suggesting a negligible difference between the two treatments. This result favours the use of HPP moving forward due to the production of disinfection by-products for chlorine in high organic effluents, which HPP does not.

The current biocide for the inhibition of the cells contained within wastewater is still disputed. It is hypothesised that the apparent H_2O_2 biocidal efficacy is down to its capacity to generate, the more oxidative, ROS e.g. OH$^\bullet$, which have the capacity to initiate oxidation and cause irreversible damage to the DNA and RNA inside a cell[201]. Furthermore, although there is little evidence into the biocidal activity of HOO$^\bullet$/O$_2$, it is reasonable to assume they have reasonable capacity for bacterial remediation.[199] Before the radicals can take effect however, the H_2O_2 must diffuse through the cell membrane to access the DNA present inside the cell. Aquaporins, a well-known diffusion facilitator, can allow solutes into a cell. Yet, before this can occur the

solute must align with specific criteria for diffusion by being a non-charged molecule with negligible polarity and a size of less than 0.3 nm.[202] Fortunately, this is where H_2O_2 has an advantage over other chemical oxidants, with the molecule fitting the profile for diffusion into the cell with a size of between 0.25–0.28 nm and almost the same dipole moment and capacity to form hydrogen bonds as a molecule which is readily diffused through aquaporins, H_2O. All this combined gives H_2O_2 the capability to effortlessly diffusion inside a cell and initiate cell deactivation.

1.17 Aims and Objectives.

The aim of this research is to develop and optimise heterogenous catalysts, using wet co-impregnation methods, to produce H_2O_2 and reactive oxygen radical species (ROS) for application in water remediation in batch and flow regimes. The generation of such oxidative species from molecular H_2 and O_2 has the potential to offer an economical replacement for traditional disinfection technologies such as chlorination, while also avoiding the chemical resides that are generated through the application of such compounds.

The aims of this thesis are outlined below:

1.   **Investigate the Efficacy of a Catalytic Approach to Water Remediation.**

This will be achieved using AuPd supported catalysts, previously reported to be highly active in the formation of H_2O_2 from molecular H_2 and O_2. In particular, a focus will be placed on the *in-situ* generation of oxidative species (H_2O_2 and ROS) for the remediation of biological and chemical contaminants commonly found in grey-water. The catalytic approach will be standardised against two traditional oxidants used in water disinfection, namely pre-formed, commercially available H_2O_2 and NaOCl.

2.   **Develop Novel Materials for the Direct Synthesis of H_2O_2.**

The replacement of Au with alternative, readily available transition metals will be investigated in order to improve catalytic activity while minimising material cost. The optimised catalyst should be stable in regard to activity and metal loading, as many heavy metals can lead to adverse health effects in humans and aquatic life. With an aim to investigate the efficacy of such materials for the remediation of contaminated water streams, catalytic performance will be evaluated under conditions optimal for H_2O_2 production and those more likely to be adopted for industrial application.

1.18 References.

1   J. Wisniak, *Educ. Química*, 2010, **21**, 60–69.

2   J. J. Berzilius, *Edinburgh New Philos.*, 1836, **21**, 223.

3   H. Toulhoat, *Encycl. Mater. Sci. Technol.*, 2010, 1–7.

4   A. Mcnaught and A. Wilkinson, *Compendium of chemical terminology*, 1997, vol. 68.

5   Chemistry Libretexts, Catalysis, https://chem.libretexts.org/Bookshelves/General_Chemistry/Map%3A_A_Molecular_ Approach_(Tro)/14%3A_Chemical_Kinetics/14.7%3A_Catalysis, (accessed 25 September 2019).

6   C. Mateo, J. M. Palomo, G. Fernandez-Lorente, J. M. Guisan and R. Fernandez-Lafuente, *Enzyme Microb. Technol.*, 2007, **40**, 1451–1463.

7   C. Mateo, O. Abian, R. Fernandez-Lafuente and J. M. Guisan, *Enzyme Microb. Technol.*, 2000, **26**, 509–515.

8   S. C. Tsang, C. H. Yu, X. Gao and K. Tam, *J. Phys. Chem. B*, 2006, **110**, 16914–16922.

9   J. M. Bolivar, L. Wilson, S. A. Ferrarotti, R. Fernandez-Lafuente, J. M. Guisan and C. Mateo, *Biomacromolecules*, 2006, **7**, 669–673.

10   G. B. Antonio Blanco, *Medcial Biochemistry*, 2017,Ch. 8,153–175.

11   S. J. Freakley, S. Kochius, J. van Marwijk, C. Fenner, R. J. Lewis, K. Baldenius, S. S. Marais, D. J. Opperman, S. T. L. Harrison, M. Alcalde, M. S. Smit and G. J. Hutchings, *Nat. Commun.*,2019, **10**, 1-8.

12   T. Tan, J. Lu, K. Nie, L. Deng and F. Wang, *Biotechnol. Adv.*, 2010, **28**, 628–634.

13   K. Hellmuth and J. M. van den Brink, *Microbial production of enzymes used in food applications*, Woodhead Publishing Limited, 2013, Ch. 11, 262-287.

14   A. C. Flores-Gallegos, M. Delgado-García, J. A. Ascacio-Valdés, S. Villareal-Morales, M. R. Michel-Michel, C. N. Aguilar-González and R. Rodríguez-Herrera, *Hydrolases of halophilic origin with importance for the food industry*, Elsevier Inc., 2018, Ch. 13, 197-219.

15   K. Kakaei, M. D. Esrafili and A. Ehsani, *Interface Sci. Technol.*, 2019, **27**, 1–21.

16   B. R. Jagirdar, *Resonance*, 1999, **4**, 63–81.

17   S. Bettuzzi, *Adv. Cancer Res.*, 2009, **104**, 1–8.

18   J. M. Modak, *Resonance*, 2002, **7**, 69–77.

19   US Pat., 4369144, 1983 .

20   D. B. Carlisle, *Proc. R. Soc. London. Ser. B. Biol. Sci.*, 1968, **171**, 31–42.

21	P. Anastas and N. Eghbali, *Chem. Soc. Rev.*, 2010, **39**, 301–312.

22	M. Campanati, G. Fornasari and A. Vaccari, *Catal. Today*, 2003, **77**, 299–314.

23	G. Ertl, H. Knözinger, F. Schüth and J. Weitkamp, *Handbook of Heterogenous Catalysis*, 2008, **1**, 49.

24	G. Shaw, PhD Thesis, Cardiff University, 2013.

25	B. G. Rao, D. Mukherjee and B. M. Reddy, *Nanostructures for novel therapy,* Elsevier Inc., 2017, Ch. 1, 8.

26	D. Bradley, R. C. Mehrotra, I. Rothwell and A. Singh, *Alkoxo and Aryloxo Derivatives of Metals*, 2001, Ch. 2, 3-181.

27	N. Y. Turova, E. P. Turevskaya, V. G. Kessler and M. I. Yanovskaya, *The Chemistry Of Metal Alkoxides*, 2002, Ch. 1, 11-30.

28	 R. L. Bickerdike, A. R. G. Brown, G. Hughes and H. Ranson ,*Proc. Fifth Cod. Carbon*, 1962, **1**, 575-583.

29	US Pat., 3160517, 1964.

30	M.-B. Coltelli and A. Lazzeri, *Chemical vapour infiltration of composites and their applications*, CRC Press., 2019, 363-390.

31	M. Haruta, *Catal. Today*, 1997, **36**, 153–166.

32	M. Sankar, Q. He, M. Morad, J. Pritchard, S. J. Freakley, J. K. Edwards, S. H. Taylor, D. J. Morgan, A. F. Carley, D. W. Knight, C. J. Kiely and G. J. Hutchings, *ACS Nano*, 2012, **6**, 6600–6613.

33	P. Zhao, N. Li and D. Astruc, *Coord. Chem. Rev.*, 2013, **257**, 638–665.

34	F. Porta, L. Prati, M. Rossi, S. Coluccia and G. Martra, *Catal. Today*, 2000, **61**, 165–172.

35	A. Villa, D. Wang, G. M. Veith, F. Vindigni and L. Prati, *Catal. Sci. Technol.*, 2013, **3**, 3036–3041.

36	T. Athar, *Emerging Nanotechnologies for Manufacturing*, Elsevier Inc., Second Edi., 2014, Ch. 17, 444-538.

37	R. Kumar, H. Mahalingam and K. K. Tiwari, *APCBEE Procedia*, 2014, **9**, 181–186.

38	S. A. Kondrat, P. J. Smith, P. P. Wells, P. A. Chater, J. H. Carter, D. J. Morgan, E. M. Fiordaliso, J. B. Wagner, T. E. Davies, L. Lu, J. K. Bartley, S. H. Taylor, M. S. Spencer, C. J. Kiely, G. J. Kelly, C. W. Park, M. J. Rosseinsky and G. J. Hutchings, *Nature*, 2016, **531**, 83–87.

39	J. Hu, Y. Song, J. Huang *et.al., Chemistry - A European Journal,* 2017, **44**, 10632-10637.

40   P. Gao, F. Li, F. Xiao, N. Zhao, N. Sun, W. Wei, L. Zhong and Y. Sun, *Catal. Sci. Technol.*, 2012, **2**, 1447–1454.

41   C. Perego and P. Villa, *Catal. Today*, 1997, **34**, 281–305.

42   P. A. Giguère, J. Chem. Phys., 1950, **18**, 88.

43   Eric V. Anslyn and Dennis A. Dougherty, Modern Physical Organic Chemistry, 2005,

44   K. Pulidindi and H. Pandey, *Hydrogen Peroxide Market Size By End-User (Paper & Pulp, Chemical, Waste Water Treatment, Mining), Industry Analysis Report, Regional Outlook, Application Growth Potential, Price Trends, Competitive Market Share & Forecast, 2016 – 2024*, https://www.gminsights.com/industry-analysis/hydrogen-peroxide-market, (Accessed Septemeber 2019).

45   C. Samanta, *Appl. Catal. A Gen.*, 2008, **350**, 133–149.

46   G. Blanco-Brieva, M. C. Capel-Sanchez, M. P. De Frutos, A. Padilla-Polo, J. M. Campos-Martin and J. L. G. Fierro, *Ind. Eng. Chem. Res.*, 2008, **47**, 8011–8015.

47   R. J. Lewis and G. J. Hutchings, *ChemCatChem*, 2019, **11**, 298–308.

48   J. M. Campos-Martin, G. Blanco-Brieva and J. L. G. Fierro, *Angew. Chemie Int. Ed.*, 2006, **45**, 6962–6984.

49   L. J. Thenard, *Ann. Chim. Phys.*, 1818, **8**, 306.

50   H. Meidinger, *Justus Liebigs Annalen der Chemie*, 1853, **88**, 57-81.

51   W. Manchot, *Leibigs Ann. Chim*, 1901, **314**, 377.

52   US Pat.,US2215883A, 1940.

53   X. Jia, F. Sun, Y. Fei, M. Jin, F. Zhang, W. Xu, N. Shi and Z. Lv, *Process Saf. Environ. Prot.*, 2018, **119**, 218–222.

54   Q. Chen, *Chem. Eng. Process. Process Intensif.*, 2008, **47**, 787–792.

55   EU Pat., 0351772A2, 1889.

56   S. Ranganathan and V. Sieber, *Catalysts*, 2018, **8**, 1-22.

57   S. C. Perry, D. Pangotra, L. Vieira, L. I. Csepei, V. Sieber, L. Wang, C. Ponce de León and F. C. Walsh, *Nat. Rev. Chem.*, 2019, **3**, 442–458.

58   M. Traube, *Dtsch. Chem. Ges*, 1887, **20**, 3345–3351.

59   US Pat., US1138520A, 1914.

60   J. K. Edwards, S. J. Freakley, R. J. Lewis, J. C. Pritchard and G. J. Hutchings, *Catal. Today*, 2015, **248**, 3–9.

61   J. K. Edwards, B. Solsona, E. N. N, A. F. Carley, A. a Herzing, C. J. Kiely and G. J. Hutchings, *Science*, 2009, **323**, 1037–1041.

62   N. M. Wilson and D. W. Flaherty, *J. Am. Chem. Soc.*, 2016, **138**, 574–586.

63   T. A. Pospelova and N. I. Kobozev, *Zh. Fiz. Khim*, 1961, **35**, 535–542.

64   T. A. Pospelova and N. I. Kobozev, *Zh. Fiz. Khim*, 1961, **35**, 1192–1197.

65   T. A. Pospelova, N. I. Kobozev and E. N. Ermin, *Zh. Fiz. Khim*, 1961, **35**, 298–305.

66   V. R. Choudhary and C. Samanta, *J. Catal.*, 2006, **238**, 28–38.

67   D. P. Dissanayake and J. H. Lunsford, *J. Catal.*, 2003, **214**, 113–120.

68   E. Ntainjua N., J. K. Edwards, A. F. Carley, J. A. Lopez-Sanchez, J. A. Moulijn, A. A. Herzing, C. J. Kiely and G. J. Hutchings, *Green Chem.*, 2008, **10**, 1162–1169.

69   D. W. Flaherty, *ACS Catal.*, 2018, **8**, 1520–1527.

70   J. Li, A. Staykov, T. Ishihara and K. Yoshizawa, *J. Phys. Chem. C*, 2011, **115**, 7392–7398.

71   A. Staykov, T. Kamachi, T. Ishihara and K. Yoshizawa, *J. Phys. Chem. C*, 2008, **112**, 19501–19505.

72   D. P. Dissanayake and J. H. Lunsford, *J. Catal.*, 2002, **206**, 173–176.

73   Q. Liu, K. K. Gath, J. C. Bauer, R. E. Schaak and J. H. Lunsford, *Catal. Letters*, 2009, **132**, 342–348.

74   V. R. Choudhary, A. G. Gaikwad and S. D. Sansare, *Catal. Letters*, 2002, **83**, 235–239.

75   V. R. Choudhary, C. Samanta and T. V. Choudhary, *Appl. Catal. A Gen.*, 2006, **308**, 128–133.

76   P. Tian, L. Ouyang, X. Xu, C. Ao, X. Xu, R. Si, X. Shen, M. Lin, J. Xu and Y. F. Han, *J. Catal.*, 2017, **349**, 30–40.

77   L. Ouyang, P. F. Tian, G. J. Da, X. C. Xu, C. Ao, T. Y. Chen, R. Si, J. Xu and Y. F. Han, *J. Catal.*, 2015, **321**, 70–80.

78   V. R. Choudhary, C. Samanta and P. Jana, *Appl. Catal. A Gen.*, 2007, **317**, 234–243.

79   V. R. Choudhary, C. Samanta and A. G. Gaikwad, *Chem. Commun.*, 2004, **10**, 2054–2055.

80   Y. F. Han and J. H. Lunsford, *J. Catal.*, 2005, **230**, 313–316.

81   Q. Liu and J. H. Lunsford, *Appl. Catal. A Gen.*, 2006, **314**, 94–100.

82   Q. Liu and J. H. Lunsford, *J. Catal.*, 2006, **239**, 237–243.

83   V. R. Choudhary and A. G. Gaikwad, *Chem. Eng.*, 2003, **80**, 27–32.

84   C. Samanta and V. R. Choudhary, *Appl. Catal. A Gen.*, 2007, **330**, 23–32.

85   P. Biasi, N. Gemo, J. R. Hernández Carucci, K. Eränen, P. Canu and T. O. Salmi, *Ind. Eng. Chem. Res.*, 2012, **51**, 8903–8912.

86   A. Bernardini, N. Gemo, P. Biasi, P. Canu, J. P. Mikkola, T. Salmi and R. Lanza,

Catal. Today, 2015, **256**, 294–301.

87   S. Park, J. H. Choi, T. J. Kim, Y. M. Chung, S. H. Oh and I. K. Song, *Catal. Today*, 2012, **185**, 162–167.

88   G. C. Bond, P. A. Sermon, G. Webb, D. A. Buchanan and P. B. Wells, *J. Chem. Soc. Chem. Commun.*, 1973, **13**, 444–445.

89   M. Haruta, T. Kobayashi, H. Sano and N. Yamada, *Chem. Lett.*, 1987, **16**, 405–408.

90   G. J. Hutchings, *J. Catal.*, 1985, **96**, 292–295.

91   A. S. K. Hashmi, *Gold Bull.*, 2004, **37**, 51–65.

92   F. Gasparrini, M. Giovannoli, D. Misiti, G. Natile, L. Maresca and G. Palmieri, *J. Am. Chem. Soc.*, 1993, **115**, 4401–4402.

93   F. Gasparrini, M. Giovannoli, D. Misiti, G. Natile and G. Palmieri, *J. Org. Chem.*, 1990, **55**, 1323–1328.

94   F. Gasparrini, M. Giovannoli, D. Misiti, G. Natile and G. Palmieri, *Tetrahedron*, 1984, **40**, 165–170.

95   F. Gasparrini, M. Giovannoli, D. Misiti, G. Natile and G. Palmieri, *Tetrahedron*, 1983, **39**, 3181–3184.

96   Y. Ito, M. Sawamura and T. Hayashi, *J. Am. Chem. Soc.*, 1986, **108**, 6405–6406.

97   M. Haruta, S. Tsubota, T. Kobayashi, H. Kageyama, M. J. Genet and B. Delmon, *J. Catal.*, 1993, **144**, 175–192.

98   A. S. K. Hashmi and G. J. Hutchings, *Angew. Chem. Int. Ed.,* 2006, **47**,7896–7936.

99   C. Della Pina, E. Falletta, L. Prati and M. Rossi, *Chem. Soc. Rev.*, 2008, **37**, 2077–2095.

100   A. K. Sinha, S. Seelan, S. Tsubota and M. Haruta, *Angew. Chemie - Int. Ed.*, 2004, **43**, 1546–1548.

101   C. Wei and C. J. Li, *J. Am. Chem. Soc.*, 2003, **125**, 9584–9585.

102   P. Landon, P. J. Collier, A. J. Papworth, C. J. Kiely and G. J. Hutchings, *Chem. Commun.*, 2002, **18**, 2058–2059.

103   P. Landon, P. J. Collier, A. F. Carley, D. Chadwick, A. J. Papworth, A. Burrows, C. J. Kiely and G. J. Hutchings, *Phys. Chem. Chem. Phys.*, 2003, **5**, 1917–1923.

104   M. Okumura, Y. Kitagawa, K. Yamagcuhi, T. Akita, S. Tsubota and M. Haruta, *Chem. Lett.*, 2003, **32**, 822–823.

105   T. Ishihara, Y. Ohura, S. Yoshida, Y. Hata, H. Nishiguchi and Y. Takita, *Appl. Catal. A Gen.*, 2005, **291**, 215–221.

106   J. K. Edwards, B. Solsona, P. Landon, A. F. Carley, A. Herzing, M. Watanabe, C. J.

Kiely and G. J. Hutchings, *J. Mater. Chem.*, 2005, **15**, 4595–4600.

107 F. Gao and D. W. Goodman, *Chem. Soc. Rev.*, 2012, **41**, 8009–8020.

108 C. H. Hyung, S. H. Gyeong, H. Jonghee, W. N. Suk and H. L. Tae, *J. Phys. Chem. C*, 2009, **113**, 12943–12945.

109 J. A. Lopez-Sanchez, N. Dimitratos, P. Miedziak, E. Ntainjua, J. K. Edwards, D. Morgan, A. F. Carley, R. Tiruvalam, C. J. Kiely and G. J. Hutchings, *Phys. Chem. Chem. Phys.*, 2008, **10**, 1921–1930.

110 J. K. Edwards, A. F. Carley, A. A. Herzing, C. J. Kiely and G. J. Hutchings, *Faraday Discuss.*, 2008, **138**, 225–239.

111 J. Pritchard, L. Kesavan, M. Piccinini, Q. He, R. Tiruvalam, N. Dimitratos, J. A. Lopez-Sanchez, A. F. Carley, J. K. Edwards, C. J. Kiely and G. J. Hutchings, *Langmuir*, 2010, **26**, 16568–16577.

112 M. Sankar, Q. He, M. Morad, J. Pritchard, S. J. Freakley, J. K. Edwards, S. H. Taylor, D. J. Morgan, A. F. Carley, D. W. Knight, C. J. Kiely and G. J. Hutchings, *ACS Nano*, 2012, **6**, 6600–6613.

113 J. C. Pritchard, Q. He, E. N. Ntainjua, M. Piccinini, J. K. Edwards, A. A. Herzing, A. F. Carley, J. A. Moulijn, C. J. Kiely and G. J. Hutchings, *Green Chem.*, 2010, **12**, 915–921.

114 A. Villa, S. J. Freakley, M. Schiavoni, J. K. Edwards, C. Hammond, G. M. Veith, W. Wang, D. Wang, L. Prati, N. Dimitratos and G. J. Hutchings, *Catal. Sci. Technol.*, 2016, **6**, 694–697.

115 J. Li, T. Ishihara and K. Yoshizawa, *J. Phys. Chem. C*, 2011, **115**, 25359–25367.

116 J. K. Edwards, N. N. Edwin, A. F. Carley, A. A. Herzing, C. J. Kiely and G. J. Hutchings, *Angew. Chemie - Int. Ed.*, 2009, **48**, 8512–8515.

117 J. K. Edwards, S. F. Parker, J. Pritchard, M. Piccinini, S. J. Freakley, Q. He, A. F. Carley, C. J. Kiely and G. J. Hutchings, *Catal. Sci. Technol.*, 2013, **3**, 812–818.

118 E. Ntainjua N., M. Piccinini, J. C. Pritchard, J. K. Edwards, A. F. Carley, J. A. Moulijn and G. J. Hutchings, *ChemSusChem*, 2009, 2, 575–580.

119 S. J. Freakley, Q. He, J. H. Harrhy, L. Liu, D. A. Crole, D. J. Morgan, E. N. Ntainjua, J. K. Edwards, A. F. Carley, A. Y. Borisevich, C. J. Kiely and G. J. Hutchings, *Science.*, 2016, **351**, 965–968.

120 Z. Khan, N. F. Dummer and J. K. Edwards, Phil.Trans.R.Soc., 2017, **2110**, 1-12.

121 J. Gu, S. Wang, Z. He, Y. Han and J. Zhang, *Catal. Sci. Technol.*, 2016, **6**, 809–817.

122 D. J. Childers, N. M. Schweitzer, S. M. K. Shahari, R. M. Rioux, J. T. Miller and R. J.

Meyer, *J. Catal.*, 2014, **318**, 75–84.

123   S. Wang, K. Gao, W. Li and J. Zhang, *Appl. Catal. A Gen.*, 2017, **531**, 89–95.

124   S. Wang, R. J. Lewis, D. E. Doronkin, D. J. Morgan, J.-D. Grunwaldt, G. J. Hutchings and S. Behrens, *Catal. Sci. Technol.*, 2020, **10**, 1925–1932.

125   S. Maity and M. Eswaramoorthy, *J. Mater. Chem. A*, 2016, **4**, 3233–3237.

126   K. S. Krishna, C. S. S. Sandeep, R. Philip and M. Eswaramoorthy, *ACS Nano*, 2010, **4**, 2681–2688.

127   S. Chinta and J. H. Lunsford, *J. Catal.*, 2004, **225**, 249–255.

128   E. N. Ntainjua, S. J. Freakley and G. J. Hutchings, *Top. Catal.*, 2012, **55**, 718–722.

129   J. K. Edwards, J. Pritchard, L. Lu, M. Piccinini, G. Shaw, A. F. Carley, D. J. Morgan, C. J. Kiely and G. J. Hutchings, *Angew. Chemie - Int. Ed.*, 2014, **53**, 2381–2384.

130   A. Santos, R. J. Lewis, G. Malta, A. G. R. Howe, D. J. Morgan, E. Hampton, P. Gaskin and G. J. Hutchings, *Ind. Eng. Chem. Res.*, 2019, **58**, 12623–12631.

131   V. Paunovic, V. V. Ordomsky, V. L. Sushkevich, J. C. Schouten and T. A. Nijhuis, *ChemCatChem*, 2015, **7**, 1161–1176.

132   J. H. Lunsford, *J. Catal.*, 2003, **216**, 455–460.

133   Y. F. Han and J. H. Lunsford, *Catal. Letters*, 2005, **99**, 13–19.

134   F. Menegazzo, M. Signoretto, E. Ghedini and G. Strukul, *Catalysts*, 2019, **9**, 1-32.

135   B. E. Solsona, J. K. Edwards, P. Landon, A. F. Carley, A. Herzing, C. J. Kiely and G. J. Hutchings, *Chem. Mater.*, 2006, **18**, 2689–2695.

136   J. K. Edwards, A. Thomas, B. E. Solsona, P. Landon, A. F. Carley and G. J. Hutchings, *Catal. Today*, 2007, **122**, 397–402.

137   J. K. Edwards, B. Solsona, P. Landon, A. F. Carley, A. Herzing, M. Watanabe, C. J. Kiely and G. J. Hutchings, *J. Mater. Chem.*, 2005, **15**, 4595–4600.

138   J. K. Edwards, S. J. Freakley, A. F. Carley, C. J. Kiely and G. J. Hutchings, *Acc. Chem. Res.*, 2014, 47, 845–854.

139   J. K. Edwards, A. F. Carley, A. A. Herzing, C. J. Kiely and G. J. Hutchings, *Faraday Discuss.*, 2008, **138**, 225–239.

140   E. N. Ntainjua, M. Piccinini, J. C. Pritchard, J. K. Edwards, A. F. Carley, C. J. Kiely and G. J. Hutchings, *Catal. Today*, 2011, **178**, 47–50.

141   E. N. Ntainjua, M. Piccinini, S. J. Freakley, J. C. Pritchard, J. K. Edwards, A. F. Carley and G. J. Hutchings, *Green Chem.*, 2012, **14**, 170–181.

142   R. J. Lewis, K. Ueura, Y. Fukuta, S. J. Freakley, L. Kang, R. Wang, Q. He, J. K. Edwards, D. J. Morgan, Y. Yamamoto and G. J. Hutchings, *ChemCatChem*, 2019, **11**,

1673–1680.

143   G. Li, J. Edwards, A. F. Carley and G. J. Hutchings, *Catal. Commun.*, 2007, **8**, 247–250.

144   S. J. Freakley, R. J. Lewis, D. J. Morgan, J. K. Edwards and G. J. Hutchings, *Catal. Today*, 2015, **248**, 10–17.

145   S. Park, S. H. Lee, S. H. Song, D. R. Park, S. H. Baeck, T. J. Kim, Y. M. Chung, S. H. Oh and I. K. Song, *Catal. Commun.*, 2009, **10**, 391–394.

146   R. J. Lewis, J. K. Edwards, S. J. Freakley and G. J. Hutchings, *Ind. Eng. Chem. Res.*, 2017, **56**, 13287–13293.

147   J. K. Edwards, J. Pritchard, M. Piccinini, G. Shaw, Q. He, A. F. Carley, C. J. Kiely and G. J. Hutchings, *J. Catal.*, 2012, **292**, 227–238.

148   S. Park, T. J. Kim, Y. M. Chung, S. H. Oh and I. K. Song, *Korean J. Chem. Eng.*, 2011, **28**, 1359–1363.

149   S. Kanungo, V. Paunovic, J. C. Schouten and M. F. Neira D'Angelo, *Nano Lett.*, 2017, **17**, 6481–6486.

150   G. Decher, *Science.*, 1997, **277**, 1232–1237.

151   J. K. Edwards and G. J. Hutchings, *Angew. Chemie - Int. Ed.*, 2008, **47**, 9192–9198.

152   J. K. Edwards, A. Thomas, A. F. Carley, A. A. Herzing, C. J. Kiely and G. J. Hutchings, *Green Chem.*, 2008, **10**, 388–394.

153   S. J. Freakley, M. Piccinini, J. K. Edwards, E. N. Ntainjua, J. A. Moulijn and G. J. Hutchings, *ACS Catal.*, 2013, **3**, 487–501.

154   M. Piccinini, E. Ntainjua N., J. K. Edwards, A. F. Carley, J. A. Moulijn and G. J. Hutchings, *Phys. Chem. Chem. Phys.*, 2010, **12**, 2488–2492.

155   M. Piccinini, J. K. Edwards, J. A. Moulijn and G. J. Hutchings, *Catal. Sci. Technol.*, 2012, **2**, 1908–1913.

156   D. A. Crole, S. J. Freakley, J. K. Edwards and G. J. Hutchings, *Proc. R. Soc. A Math. Phys. Eng. Sci.*, 2016, **472**, 1-9.

157   B. Sun, H. Zhu, W. Liang, X. Zhang, J. Feng and W. Xu, *Int. J. Hydrogen Energy*, 2019, **44**, 19547–19554.

158   W. Ratchananusorn, D. Gudarzi and I. Turunen, *Chem. Eng. Process. Process Intensif.*, 2014, **84**, 24–30.

159   A. Akram, S. J. Freakley, C. Reece, M. Piccinini, G. Shaw, J. K. Edwards, F. Desmedt, P. Miquel, E. Seuna, D. J. Willock, J. A. Moulijn and G. J. Hutchings, *Chem. Sci.*, 2016, **7**, 5833–5837.

160   B. Jefferson, A. Palmer, P. Jeffrey, R. Stuetz and S. Judd, *Water Sci. Technol.*, 2004, **50**, 157–164.

161   O. R. Al-Jayyousi, *Desalination*, 2003, **156**, 181–192.

162   D. Christova-Boal, R. E. Eden and S. McFarlane, *Desalination*, 1996, **106**, 391–397.

163   E. Eriksson, K. Auffarth, M. Henze and A. Ledin, *Urban Water*, 2002, **4**, 85–104.

164   World population projected to reach 9.8 billion in 2050, and 11.2 billion in 2100, https://www.un.org/development/desa/en/news/population/world-population-prospects-2017.html, (accessed 25 September 2019).

165   J. Ottosson, PhD Thesis, KTH Royal Instituate Technology, 2003.

166   J. H. Harrhy, PhD Thesis, Cardiff Univeristy, 2017.

167   Main Difference Between BOD and COD, https://pediaa.com/difference-between-bod-and-cod/#:~:text=The%20main%20difference%20between%20BOD,total%20organic%20matter%20in%20water., (accessed Septemober 2019).

168   J. H. T. Winneberger, *Maual of Greywater Treatment Practice,* 1974.

169   Us Pat., NASA-TN-D-7600, 1974

170   D. Brewer, R. Brown and G. Stanfield, *Rainwater and Greywater In Buildings: Prohect Report and Case Studies*, BSRIA, Berkshire, 2001.

171   M. Andersen, G. H. Kristensen, M. Brynjolf and H. Grüttner, *Water Sci. Technol.*, 2002, **46**, 67–76.

172   F. Günther, *Ecol. Eng.*, 2000, **15**, 139–146.

173   M. Pidou, F. A. Mamon, T. Stephenson, B. Jefferson and P. Jeffrey, *Proc. Inst. Civ. Eng. Eng. Sustain.*, 2007, **160**, 119–131.

174   G. Smethurst, *Basic Water Treatment,* Third Ed., Ch. 9, 2017.

175   W. D. Hypes, C. E. Batten and J. R. Wilkins, *Processing of Combined Domestic Bath and Laundry Waste Waters for Reuse As Commode Flushing Water*, 1975, vol. 4.

176   S. A. Prathapar, M. Ahmed, S. Al Adawi and S. Al Sidiari, *Int. J. Environ. Stud.*, 2006, **63**, 283–292.

177   G. Ramon, M. Green, R. Semiat and C. Dosoretz, *Desalination*, 2004, **170**, 241–250.

178   L. D. Nghiem, N. Oschmann and A. I. Schäfer, *Desalination*, 2006, **187**, 283–290.

179   M. Pidou, F. Memon, T. Stephenson, B. Jefferson, P. Jeffery, *Engineering Sustainability*, 2007, **160**, 119-131.

180   K. Schaefer, K. Exall and J. Marsalek, *Water Quality Research Journal,* 2004, 1, 1-12..

181   E. Friedler, R. Kovalio and N. I. Galil, *Water Sci. Technol.*, 2005, **51**, 187–194.

182   N. E, *Urban Water*, 2000, **1**, 10.

183   N. Hassanshahi and A. Karimi-Jashni, *Ecotoxicol. Environ. Saf.*, 2018, **161**, 683–690.

184   M. J. Nieuwenhuijsen, M. B. Toledano, N. E. Eaton, J. Fawell and P. Elliott, *Occup. Environ. Med.*, 2000, **57**, 73–85.

185   T. Clasen and P. Edmondson, *Int. J. Hyg. Environ. Health*, 2006, **209**, 173–181.

186   R. Singh, *Hybrid Membr. Syst. Water Purif.*, 2005, Ch. 2, 57–130.

187   L. McKeen, *The Effect of Sterilization on Plastics and Elastomers: Fourth Edition*, 2018.

188   T. Zellner and F. Eyer, *Toxicol. Lett.*, 2020, **320**, 73–79.

189   D. L. Sedlak and U. Von Gunten, 2011, **331**, 42–44.

190   W. A. M. Hijnen, E. F. Beerendonk and G. J. Medema, *Water Res.*, 2006, **40**, 3–22.

191   K. Zoschke, H. Börnick and E. Worch, *Water Res.*, 2014, **52**, 131–145.

192   J. S. Chang, P. A. Lawless and T. Yamamoto, *IEEE Trans. Plasma Sci.*, 1991, **19**, 1152–1166.

193   A. Megahed, B. Aldridge and J. Lowe, *PLoS One*, 2018, **13**, 1–22.

194   C. Xia, Y. Xia, P. Zhu, L. Fan and H. Wang, *Science*, 2019, **366**, 226–231.

195   Y. Xie, *Disinfection Byproducts in Drinking Water: Formation, Analysis and Control*, Taylor & Francis, 2003.

196   M. J. Leggett, J. Spencer Schwarz, P. A. Burke, G. McDonnell, S. P. Denyer and J. Y. Maillard, *Appl. Environ. Microbiol.*, 2016, **82**, 1035–1039.

197   M. Finnegan, E. Linley, S. P. Denyer, G. McDonnell, C. Simons and J. Y. Maillard, *J. Antimicrob. Chemother.*, 2010, **65**, 2108–2115.

198   Colby.edu, https://www.colby.edu/chemistry/CH142/CH142A/StandardReductionPotentials.pdf, (Accessed September 2019).

199   E. Linley, S. P. Denyer, G. McDonnell, C. Simons and J. Y. Maillard, *J. Antimicrob. Chemother.*, 2012, **67**, 1589–1596.

200   Z. Ronen, A. Guerrero and A. Gross, *Chemosphere*, 2010, **78**, 61–65.

201   B. J. Juven and M. D. Pierson, *J. Food Prot.*, 1996, **59**, 1233–1241.

202   G. P. Bienert, J. K. Schjoerring and T. P. Jahn, *Biochim. Biophys. Acta - Biomembr.*, 2006, **1758**, 994–1003.

2 Experimental.

2.1 Materials Used.

The following list contains all the chemicals, materials, and bacteria used during experimentation in this thesis:

- $HAuCl_4.3H_2O$ (99.99% trace metals basis, 30 wt.% dil. HCl, Strem Chemicals)
- $PdCl_2$ (Reagent Plus®, 99.9% trace metals basis, Sigma Aldrich)
- $FeCl_3$ (99.99% trace metals basis, Sigma Aldrich)
- $CoCl_2.6H_2O$ (98% trace metals basis, Sigma Aldrich)
- $NiCl_2.6H_2O$ (99.99% trace metals basis, Sigma Aldrich)
- $CuCl_2.2H_2O$ (99+% trace metals basis, Fisher Scientific)
- $PtCl_2$ (99.99% trace metals basis, Sigma Aldrich)
- $ZnCl_2$ (98+% trace metals basis, Alfa Aesar)
- $InCl_2$ (99.9% trace metals basis, Sigma Aldrich
- TiO_2 (p25, Rutile: Anatase 85:15, 99.9% trace metals basis, 20 nm, Degussa)
- CeO_2 (Sigma Aldrich)
- ZrO_2 (99% trace metals basis, Sigma Aldrich)
- SiO_2 (99.9+% trace metals basis, granular, Sigma Aldrich)
- Al_2O_3 (y-phase, Alfa Aesar)
- Nb_2O_5 (Sigma Aldrich)
- Carbon (ROX 0.8, powdered, Cabot)
- MeOH (HPLC grade, Sigma Aldrich)
- H_2O (HPLC grade, Sigma Aldrich)
- H_2O_2 (50 wt.%, stabilised, Sigma Aldrich)
- $Ce(SO_4)_2$ (Sigma Aldrich)
- $C_{36}H_{24}FeN_6O_4S_6$ (0.025 M, Sigma Aldrich)
- Silicon Carbide (46 grit, Alfa Aesar)
- *Escherichia Coli* (JM109)
- Tryptic Soy Broth (Oxoid)
- Tryptic Soy Agar (Oxoid)
- Metronidazole (Alfa Aesar)

2.2   Catalyst Preparation.

2.2.1   AuPd Supported Catalyst by Excess Chlorine Wet Co-Impregnation

The procedure to generate 2 g of 0.5 wt.% Au-0.5 wt.% Pd/TiO$_2$ catalyst by excess chlorine wet co-impregnation was taken from research by Sankar *et al*[1]. HAuCl$_4$.3H$_2$O was used as a gold precursor and was dissolved in deionized water to form a solution with a gold concentration of 12.25 mg/mL. The PdCl$_2$ salt was dissolved in a 0.58 M aqueous HCl solution (conc HCl, diluted using the requisite amount of deionized water) with gentle warming and vigorous stirring to form a solution with a Pd concentration of 6 mg/mL. PdCl$_2$ (0.833mL, 6 mg mL^{-1}) and HAuCl$_4$.3H$_2$O (1.224 mL, 12.25 mg mL^{-1}) were charged into a clean 50 mL round-bottom flask fitted with a magnetic stirrer bar. The volume of the solution was adjusted to 16 mL using deionized water. The flask was then immersed into an oil bath sitting on a magnetic stirrer hot plate. The solution was stirred (1000 rpm) and the temperature of the oil bath was raised from room temperature to 60 °C. At 60 °C, TiO$_2$ (1.98 g, P25) was added slowly over a period of 10 min with constant stirring. The resulting slurry was stirred at 60 °C for a further 15 min; following this, the temperature was raised to 95 °C for 16 h to allow for complete evaporation of water. The resulting solid was ground prior to heat treatment in a reductive atmosphere (flowing 5% H$_2$/Ar, 400 °C, 4 h, 10 °C min^{-1}).

2.3   Testing of Catalyst.

2.3.1   Direct Synthesis of H$_2$O$_2$ – Batch Reactor.

Hydrogen peroxide synthesis was evaluated using a Parr Instruments stainless steel autoclave with a nominal volume of 100 mL and a maximum working pressure of 2030 psi. The autoclave contains an overhead mechanical stirrer (0-2000 rpm) and has provisions for measurement of the autoclaves temperature and pressure included. To maintain the desired temperature a cooling jacket is used and for gas insertion 2 lines containing the pre-mixed gas cylinders (5% H$_2$/CO$_2$ and 25% O$_2$/CO$_2$) are connected. The procedure for the direct synthesis was derived from previous literature in the area[2]. A schematic of the batch reactor is shown in Figure 2.1.
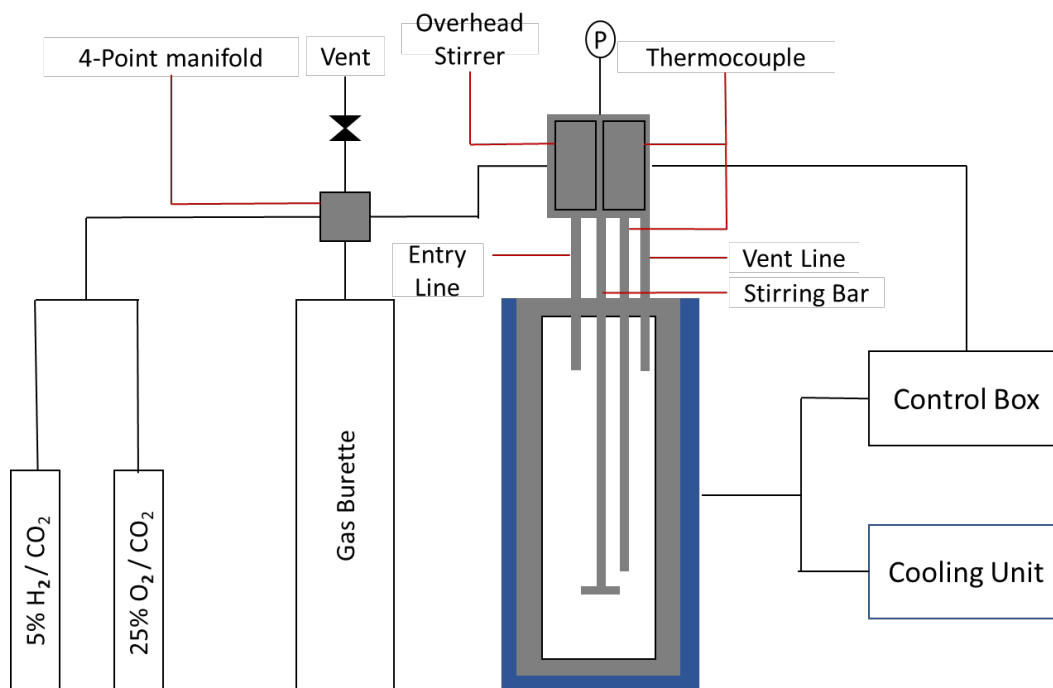
Figure 2.1: Schematic of the batch reactor used for direct synthesis and degradation of H_2O_2.

2.3.2   Ideal direct H_2O_2 Synthesis Conditions in a Batch Reactor.

A typical synthesis involves charging the autoclave with catalyst (0.01 g), solvent (5.6 g CH_3OH and 2.9 g H_2O) and purging three times with 5% H_2/CO_2 (100 psi) before filling to 580 psi with 5% H_2/CO_2 (420 psi) and 25% O_2/CO_2 (160 psi), to give a $H_2:O_2$ ratio of 1:2. The reaction mixture was then cooled to the desired temperature (2 °C), before stirring commenced (1200 rpm) and the reaction time of 30 minutes began. H_2O_2 yield was then determined by titering aliquots of the final, filtered, reaction solution with acidified $Ce(SO_4)_2$ solution (ca.8x10^{-3} M) and using ferroin as an indicator, with $Ce(SO_4)_2$ being standardised against $(NH_4)_2Fe(SO_4)_2.6H_2O$. Catalyst productivities are reported as $mol_{H2O2} \, kg_{cat}^{-1} \, h^{-1}$, with error bars being assigned based on standard deviation of 3 repeat experiments.

2.3.3   Ideal H_2O_2 Degradation Conditions in a Batch Reactor.

To test for H_2O_2 degradation the autoclave was charged with catalyst (0.01 g), a reactant solution containing 4 wt.% H_2O_2 (5.6 g CH_3OH, 2.22 g H_2O and 0.68 g 50 wt.% H_2O_2) and was purged three times with 5% H_2/CO_2 (100 psi) before filling to 420 psi with 5% H_2/CO_2. The reaction mixture was then cooled to the desired temperature (2 °C), before stirring commenced (1200 rpm) and the reaction time of 30 minutes began. H_2O_2 yield was then

determined by titering aliquots of the initial and final, filtered, reaction solution with acidified $Ce(SO_4)_2$ solution (ca.8x10^{-3} M) and using ferroin as an indicator, with $Ce(SO_4)_2$ being standardised against $(NH_4)_2Fe(SO_4)_2.6H_2O$. The degradation activity is reported as mol_{H2O2} kg_{cat}^{-1} h^{-1}, with error bars being assigned based on standard deviation of 3 repeat experiments.

2.3.4 Non-Ideal Direct H_2O_2 Synthesis Conditions in a Batch Reactor.

A typical synthesis involves charging the autoclave with catalyst (0.01 g), solvent (8.5 g H_2O) and purging three times with 5% H_2/N_2 (100 psi) before filling to 580 psi with 5% H_2/N_2 (420 psi) and 25% O_2/N_2 (160 psi), to give a $H_2:O_2$ ratio of 1:2. The reaction mixture was then heated to the desired temperature (30 °C), before stirring commenced (1200 rpm) and the reaction time of 30 minutes began. H_2O_2 yield was then determined by titering aliquots of the final, filtered, reaction solution with acidified $Ce(SO_4)_2$ solution (ca.8x10^{-3} M) and using ferroin as an indicator, with $Ce(SO_4)_2$ being standardised against $(NH_4)_2Fe(SO_4)_2.6H_2O$. Catalyst productivities are reported as mol_{H2O2} kg_{cat}^{-1} h^{-1}, with error bars being assigned based on standard deviation of 3 repeat experiments.

2.3.5 Non-Ideal H_2O_2 Degradation Conditions in a Batch Reactor.

To test for H_2O_2 degradation the autoclave was charged with catalyst (0.01 g), a reactant solution containing 4 wt.% H_2O_2 (7.82 g H_2O and 0.68 g 50 wt.% H_2O_2) and was purged three times with 5% H_2/N_2 (100 psi) before filling to 420 psi with 5% H_2/N_2. The reaction mixture was then heated to the desired temperature (30 °C), before stirring commenced (1200 rpm) and the reaction time of 30 minutes began. H_2O_2 yield was then determined by titering aliquots of the initial and final, filtered, reaction solution with acidified $Ce(SO_4)_2$ solution (ca.8x10^{-3} M) and using ferroin as an indicator, with $Ce(SO_4)_2$ being standardised against $(NH_4)_2Fe(SO_4)_2.6H_2O$. The degradation activity is reported as mol_{H2O2} kg_{cat}^{-1} h^{-1}, with error bars being assigned based on standard deviation of 3 repeat experiments.

2.3.6 Calculating Productivity and Degradation.

Productivity and degradation are used to compare between catalysts, with an acidified $Ce(SO_4)_2$ solution (ca.8x10^{-3} M) and ferroin indicator being implemented to give a titre which can then be manipulated to produce a productivity/degradation value. The equations used to calculate these values can be found below:

Initially, the volume of $Ce(SO_4)_2$ solution used to titrate the entire 8.5 g of reaction solution is calculated:

$$\text{Volume of } Ce(SO_4)_2 \text{ solution used to titrate against the entire 8.5 g of reaction solution} = \frac{\text{Titre x 8.5}}{\text{Catalyst Mass}} \quad (1)$$

The calculated volume of $Ce(SO_4)_2$ solution is then converted to moles:

$$\text{Moles of } Ce(SO_4)_2 = \frac{\text{volume of } Ce(SO_4)_2 \text{ x concentration of } Ce(SO_4)_2}{1000} \quad (2)$$

From the redox reaction the stoichiometric ratio between $Ce(SO_4)_2$ and H_2O_2 can be determined:

$$H_2O_2 + 2Ce(SO_4)_2 \longrightarrow Ce_2(SO_4)_3 + H_2SO_4 + O_2 \quad (3)$$

The moles of H_2O_2 present in the reaction solution can then be calculated:

$$\text{Moles of } H_2O_2 = \frac{\text{Moles of } Ce(SO_4)_2}{2} \quad (4)$$

Finally, productivity is calculated:

$$\text{Productivity} = \frac{\text{Moles of } H_2O_2}{\text{mass of catalyst x reaction time}} \quad (5)$$

To calculate degradation, the productivity of the reaction solution is calculated prior to the reaction starting, as well as after. The difference in these two values is the degradation value.

2.3.7   Worked Example for Calculating Productivity and Degradation.

- Catalyst mass used was 0.5059 g and the titration value returned as 6.35 cm^3
- Values were substituted into Equation 1 as follows to calculate the vol of $Ce(SO_4)_2$ required to titrate against total reaction solution
- (6.35 x 8.5)/0.5059 = 106.69
- This value was then substituted into Equation 2 to calculate the moles of $Ce(SO_4)_2$
- (106.69 x 0.008)/1000 = 0.00085
- Using Equation 3 this value was then divided by 2 to calculate the moles of H_2O_2
- 0.00085/2 = 0.000425
- This value was then used to calculate the productivity value using Equation 5
- 0.000425/(0.00001 x 0.5) = 85

2.4   Direct Synthesis of H_2O_2 – Flow Reactor.

The synthesis of H_2O_2 was also performed using a continuous flow microreactor. Swagelok 316L 1/8-inch tubing was used to generate the lines, with 316L 1/4-inch tubing being used for the catalyst beds. An Agilent HPLC pump was used to pump the mobile phase and a Swagelok 150 mL gas-liquid separator (GLS) was attached at the end of the line for sample collection. A Brooks gas flow controller was used to regulate gas flow and a Swagelok back pressure regulator was used to set the overall pressure. To monitor the pressure during reactions a Swagelok pressure gauge was added prior and post catalyst bed and to maintain temperature a water bath was used, with the lines and catalyst bed being submerged (Figure 2.2)
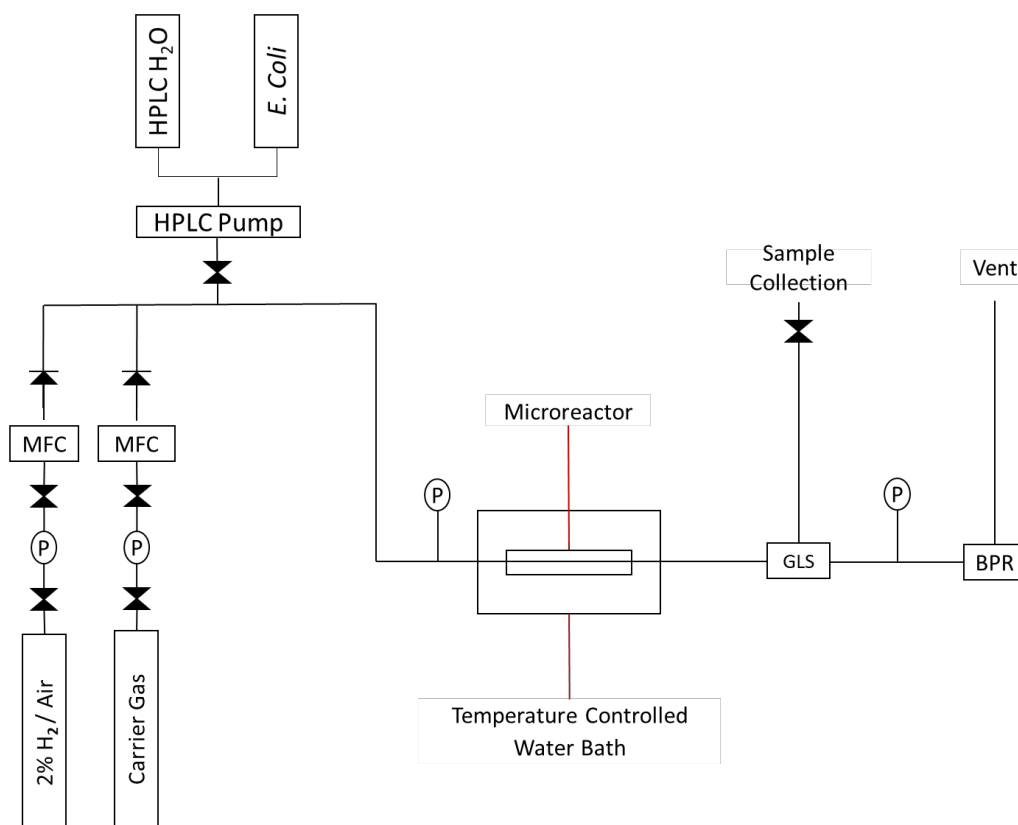
Figure 2.2: Schematic of the flow reactor used for the direct synthesis of H_2O_2.

2.4.1 Direct Synthesis of H_2O_2 in a Flow Reactor.

A synthesis reaction began with packing the union prior to the bed with quartz wool and then 120 mg of catalyst, pelleted under 10 bars of pressure with a diameter of 425 – 350 microns, was added alongside 3.3 g of silicon carbide (SiC). The bed was then attached to the lines and submerged into a water bath set to 2 °C and pressurised to 175 psi. Once pressurised the gas flow rate was set to 42 mL min^{-1} and the HPLC pump began pumping the solvent at 0.2 mL min^{-1}. The reaction conditions and methodology for this synthesis of H_2O_2 in a continuous flow using a microreactor were modelled on work previously done by Freakley *et al*[3]. Error bars presented in data are assigned based on standard deviation of 3 repeat experiments.

2.4.2 Calculating Productivity and Degradation.

Productivity was calculated in ppm and used to compare between catalysts. An acidified $Ce(SO_4)_2$ solution (ca.8×10^{-4} M) and ferroin indicator were implemented to give a titre which can then be manipulated to produce a productivity value. The equations used to calculate these values can be found below:

Initially, the volume of $Ce(SO_4)_2$ solution used to titrate the entire 8.5 g of reaction solution is calculated:

$$\text{Volume of } Ce(SO_4)_2 \text{ solution used to titrate against the entire reaction solution} = \frac{\text{Titre x (Sample)}}{\frac{Sample\ Mass\ -\ Acid}{Sample\ Mass}}$$

The calculated volume of $Ce(SO_4)_2$ solution is then converted to moles:

$$\text{Moles of } Ce(SO_4)_2 = \frac{\text{volume of } Ce(SO_4)_2 \text{ x concentration of } Ce(SO_4)_2}{1000} \qquad (2)$$

From the redox reaction the stoichiometric ratio between $Ce(SO_4)_2$ and H_2O_2 can be determined:

$$H_2O_2 \ + \ 2Ce(SO_4)_2 \longrightarrow Ce_2(SO_4)_3 + H_2SO_4 + O_2 \qquad (3)$$

The moles of H_2O_2 present in the reaction solution can then be calculated:

$$\text{Moles of } H_2O_2 = \frac{\text{Moles of } Ce(SO_4)_2}{2} \qquad (4)$$

The Weight percentage (wt.%) of H_2O_2 produced during the reaction can then be concluded:

$$\text{wt.\% of } H_2O_2 = \left(\frac{\text{Moles of } H_2O_2 \text{ x Mr of } H_2O_2}{\text{sample mass}} \right) \text{x } 100 \qquad (6)$$

Finally, weight percentage is converted to ppm:

$$H_2O_2 \text{ produced in ppm} = \text{wt.\% of } H_2O_2 \text{ x } 10000 \qquad (7)$$

To calculate degradation, the H_2O_2 concentration of the reaction solution is calculated prior to the reaction starting, as well as after. The difference in these two values is the degradation value.

2.4.3 Worked Example for Calculating Productivity and Degradation

- Sample mass used was 6 mL, volume of acid was 1 mL and the titration value returned as 11.55 cm^3

- Values were substituted into Equation 1 as follows to calculate the vol of $Ce(SO_4)_2$ required to titrate against total reaction solution

- 11.55 x 6/(6-1/6) = 83.2

- This value was then substituted into Equation 2 to calculate the moles of $Ce(SO_4)_2$

- (1.6 x 0.0008)/1000 = 0.000071

- Using Equation 3 this value was then divided by 2 to calculate the moles of H_2O_2

- 0.0000014/2 = 0.0000355

- This value was then used to calculate the wt.% of H2O2 value using Equation 6

- ((0.0000355 x 34.04)/6) x 100 = 0.02

- This value was then used to calculate ppm using Equation 7

- 0.02 x 10000 = 200

2.5 Oxidative Degradation of *E. coli.*

2.5.1 *In-Situ* Oxidative Degradation of *E. coli* with H_2O_2.

The *in-situ* oxidative degradation of *E. coli* with H_2O_2 was performed using the same continuous flow microreactor as used for the direct synthesis experiments. The conditions were the same as for a direct synthesis reaction, however the solvent (H_2O (HPLC grade)) was swapped for a solution of *E. coli* (JM109) suspended in H_2O. A reaction began with the generation of the bacterial solution, preparation of the bacterial solution was achieved by the following procedure:

To make the bacterial solution, a single colony of *E. Coli* (JM109) was transferred to tryptic soya broth (TSB) growth medium (20 mL) and incubated at 37 °C for 16 h. This culture was then centrifuged (1500 g, 10 minutes, 23 °C) and the supernatant TSB was decanted off. The bacteria were then re-dispersed into sterile H_2O (20 mL) and vortexed until complete re-

dispersion was achieved. 6 mL of this solution was then diluted into 24 mL of sterile H_2O to provide the subsequent reaction solution. To understand the extent of the *E. coli* treatment for each individual catalyst the drop plate (Figure 2.3) and spread plate (Figure 2.4) methods were used:
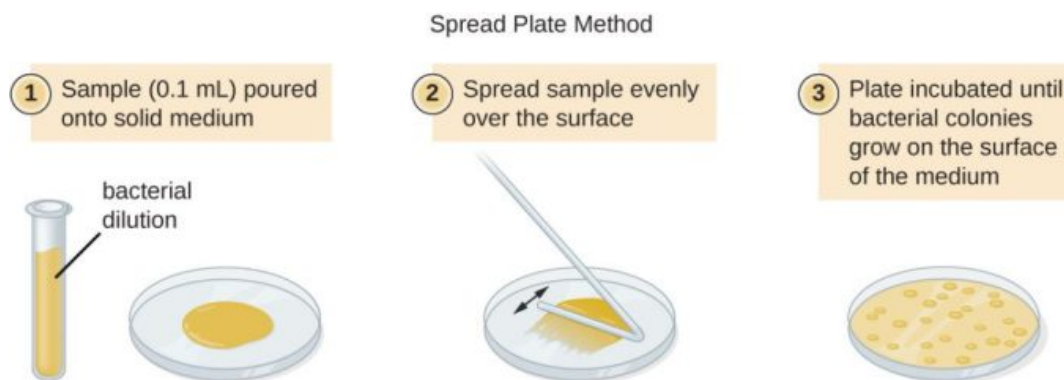
Figure 2.3: Diagram showing the dilution and plating procedures for the drop plate method for bacterial solutions. Figure use granted in accordance with copyright by Alfred B. Cunningham, John E. Lennox and Rockford J. Ross [4]

The drop plate method was implemented using tryptic soya agar (TSA) plates containing 2% w/v agar. The pre and post treatment samples of the reaction solution were plated directly following $1–10^7$-fold dilutions and 3 x 10 μl aliquots of each of these dilutions were added to each plate before being incubated at 37 °C for 16 h. The colonies were then counted on all plates that gave growth and an averaged count from the 3 aliquots plated was taken and cell counts were expressed as colony forming units per millilitre of sample (CFU mL^{-1}).
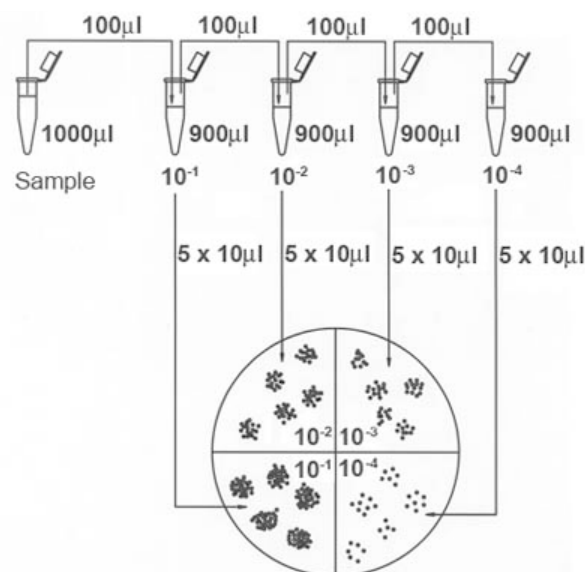
Figure 2.4: Diagram showing the plating procedures for the spread plate method for bacteria solutions. Figure use granted in accordance with copyright by microbeonline.[5]

The spread plate method was used to confirm large logarithmic kills. 1 mL of the neat post treated solution is plated on tryptic soya agar (TSA) plates and incubated at 37 °C for 16 h. The colonies, or absence of, on the plate were counted to confirm if the catalyst treated the entire bacterial solution.

2.5.2 *Ex-Situ* Oxidative Degradation of *E. coli* with H_2O_2.

The *ex-situ* oxidative degradation tests with H_2O_2 were performed in a similar manner to the *in-situ* tests; however, a few minor adjustments were made. To be able to introduce the chosen concentration of stabilised H_2O_2 through the flow reactor, alongside the model greywater solution, a second HPLC pump was added to allow for this. In addition, a second binding point for the additional HPLC pump was added prior to the bed to allow the H_2O_2 to be co-fed correctly. The stock concentrations of H_2O_2 were made 10x more concentrated as required, as the flow rates of greywater solution: H_2O_2 were 0.18 mL min^{-1}: 0.02 mL min^{-1} in turn diluting the H_2O_2 10-fold during flow leading to the required concentration. The drop count method was implemented to comprehend the effects of *ex-situ* H_2O_2 on the degradation of *E. coli* and for certain experiments the flow gas was switched out for synthetic air. Error bars presented in data are assigned based on standard deviation of 3 repeat experiments.

2.5.3 *Ex-Situ* Oxidative Degradation of *E. coli* with NaOCl.

The *ex-situ* oxidative degradation tests with chlorine were performed in a similar manner to the *ex-situ* oxidative degradation of *E. coli* with H_2O_2, the only difference being that sodium hypochlorite (NaOCl) was co-fed through the second HPLC pump instead of stabilised H_2O_2. Error bars presented in data are assigned based on standard deviation of 3 repeat experiments.

2.6 Oxidative Degradation of Metronidazole.

2.6.1 *In-Situ* Oxidative Degradation of Metronidazole in a Batch Reactor.

A typical synthesis involves charging the autoclave with catalyst (0.01 g), solvent (8.5 g of 50 ppm metronidazole in H_2O) and purging three times with 5% H_2/N_2 (100 psi) before filling to 580 psi with 5% H_2/N_2 (420 psi) and 25% O_2/N_2 (160 psi), to give a H_2:O_2 ratio of 1:2. The reaction mixture was then heated to the desired temperature (30 °C), before stirring commenced (1200 rpm) and the reaction time of 2 hours began. The metronidazole concentration was determined by submitting to a HPLC and calculating peak area at 340 nm. H_2O_2 yield was then determined by titering aliquots of the final, filtered, reaction solution with acidified $Ce(SO_4)_2$ solution (ca.8×10^{-3} M) and using ferroin as an indicator, with $Ce(SO_4)_2$ being standardised against $(NH_4)_2Fe(SO_4)_2.6H_2O$. Catalyst productivities are reported as $mol_{H2O2} \, kg_{cat}^{-1} \, h^{-1}$, with error bars presented in data are assigned based on standard deviation of 3 repeat experiments.

2.6.2 Re-use of Catalyst for the *In-Situ* Oxidative Degradation of Metronidazole in a Batch Reactor.

An identical procedure to the one above (Section 6.1) was done for the 2 hour *in-situ* oxidative degradation of metronidazole. The catalyst was then filtered, washed with de-ionised water to remove any organic matter, and stored in a vacuum oven for 16 hours at 30 °C, before testing again following the procedure as discussed above for the initial synthesis reaction. Error bars presented in data are assigned based on standard deviation of 3 repeat experiments.

2.6.3 Gas Replacement Experiments for the *In-Situ* Oxidative Degradation of Metronidazole in a Batch Reactor.

An identical procedure to the one outlined above (Section 6.1) for the *in-situ* oxidative degradation of metronidazole was followed for a reaction time of 2 h. After this, stirring was stopped and the reactant gas mixture was vented prior to replacement with the standard pressures of 5% H_2/N_2 (420 psi) and 25% O_2/N_2 (160 psi). The reaction mixture was then stirred (1200 rpm) for a further 2 h two more time. To collect these series of data points it should be noted that individual experiments were carried out and the reactant mixture was not sampled on-line.[6]

2.6.4 Hot Filtration Experiments for the *In-Situ* Oxidative Degradation of Metronidazole in a Batch Reactor.

An identical procedure to that outlined above (Section 6.1) for the *in-situ* oxidative degradation of metronidazole was followed for a reaction time of 1 h. Following this, the stirring was stopped, and the reactant gas mixture vented prior to the removal of the solid catalyst via filtration. The post-reaction solution was returned to the reactor to identify the contribution of leached species to the observed activity, with both steps of the reaction conducted at a temperature of 30 °C.[6]

2.7 Characterisation.

2.7.1 X-ray Photoelectron Spectroscopy (XPS).

X-ray Photoelectron Spectroscopy (XPS) is a technique used to analyse the surface chemistry of a material. The spectra are obtained by irradiating the sample with X-rays and counting the kinetic energy and electrons ejected from the sample. This enables the understanding of the materials' elemental composition and empirical formula, as well as the chemical and electronic states of the elements contained within.

2.7.1.1 Background.

Upon irradiating an atom with x-rays, the atom can absorb an x-ray photon and eject a core or valence electron. The atom then releases kinetic energy equivalent to the energy needed to eject the electron. This energy can be expressed using the photoelectric effect equation (Equation 8). and all this can be collected and labelled under the photoelectric effect.

$$E_K = hv - \phi \qquad (8)$$

Equation 8: photoelectric equation, E_K = maximum kinetic energy of the emitted electron, h = Planck's constant, v = frequency of incident light (Hz) and ϕ = energy needed to eject photoelectron (J).

For XPS the x-ray beam can only penetrate up to 10 nm, allowing only the surface atoms of a sample to be analysed.[7] The measuring of the emission energy released allows the structure and composition of the materials surfaced to be determined. This is achieved due to the binding energy of an electron being dependent the orbital it was situated in, the element it was emitted from and the chemical environment surrounding the atom, (Figure 2.5).
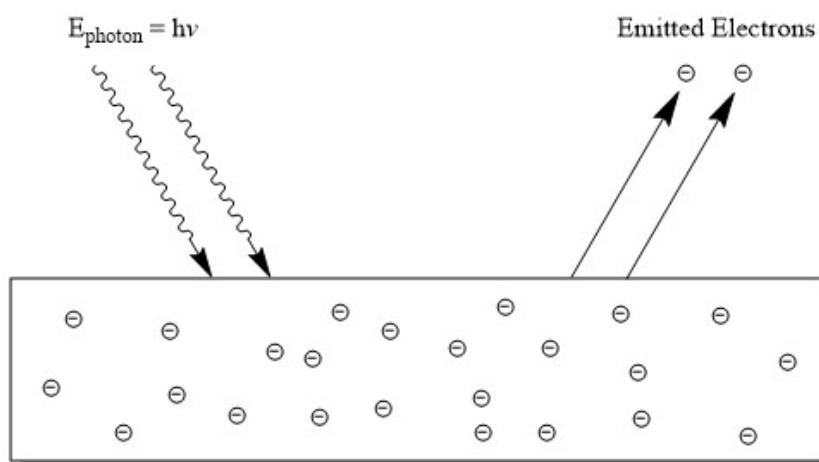
Figure 2.5: Photoelectric process for XPS surface analysis. Figure reproduced in accordance with copyright as image is in the public domain.

A spectrometer is attached to collect the emitted electrons, while calculating and assigning each one their kinetic energy. This generates a spectrum for the samples surface as each electron emitted has a different kinetic energy due to the reasons mentioned previously. These differences allow the surface to be characterised, with each peak being describing each electrons environment.

2.7.1.2   Procedure.

XPS analysis was carried out by Dr. David Morgan using a Kratos Axis Ultra DLD spectrometer. Samples were mounted using double-sided adhesive tape while monochromatic Al Kα radiation was used for all the measurements. An analyser pass energy of 160 eV was used for survey scans, and 40 eV was employed for more detailed regional scans. XPS spectra were calibrated to the Ti $2p_{3/2}$ peak for the TiO_2 support taken to be 458.5 eV which was measured on a blank P25 TiO_2 sample. The C(1s) energy for this blank sample was found to be 284.8 eV, typically of our calibration energy. Pd^0 and Pd^{2+} binding energies were assigned based on this initial calibration and those of bulk metal and oxide references and confirmed by the characteristic asymmetric and gaussian-like line shapes characteristic of the bulk materials. Au binding energies are assigned similarly, with bulk Au having a binding energy of 83.9 eV, however this has been shown to be lower on TiO_2 if there is significant charge transfer from the support or low coordination, spherical Au nanoparticles. The intensities of the Au $4f$ and Pd $3d$ features were used to derive the Au/Pd surface composition ratios.

2.7.2   Inductively Coupled Plasma Mass Spectroscopy (ICP-MS).

Inductively Coupled Plasma Mass Spectroscopy (ICP-MS) is an instrumental analytical technique which uses a high temperature ionisation source partnered alongside a mass spectrometer. It uses the ionisation source to break down liquid samples down to their elements and then convert those elements to ions ready for detection by the spectrometer. The spectrometer can detect a large proportion of the periodic table and can detect a range of concentrations from mg L^{-1} to ng L^{-1}.

2.7.2.1 Background.

The ionisation source, inductively coupled plasma (ICP), is ideal for mass spectroscopy, being able to ionise >90% of all the elements. The ICP ionisation source is formed from concentric quartz tubes surrounded by a copper induction coil. Plasmas are generated by partnering argon gas, in a continuous flow, with a radio frequency (RF) generator at oscillating frequencies. Upon introducing argon gas, this combination eventually ionises part of the argon supply causing production of cations and electrons which accelerate towards the RF generator.[8] This causes further ionisation with these cations and electrons reacting with the rest of the argon supply, creating higher temperatures until the plasma reaches equilibrium where the temperature is maintained at 6000 °C. The liquid samples are introduced to the plasma using a nebulizer in combination with a spray chamber. The nebulizer utilises supersonic expansion of gas to turn the liquid into a fine mist, while the spray chamber removes any droplets that would be too large for analysis by the plasma. Upon introduction to the plasma the samples absorb the ICP's energy until emitting an electron, becoming ionised. This electron is then passed towards the interface. The gas is passed through a skimmer cone which cools the gas and allows it to then enter the depressurising chamber, in which further cooling occurs. A second skimmer cone is used to take a fraction of the sample gas and pass it into a second chamber containing the mass spectrometer (MS), therefore preparing the sample gas to enter at the correct temperature and pressure. Prior to entering the MS, the gas passes through a charged metallic cylinder, known as an ion lens. This is required as nearly all ions generated via the plasma are positive and will therefore repel each other, these lenses prevent the splitting of the beam. The ions then enter the MS, which implements a quadrupole to sperate each ion identified by its m/z. As well as identifying the quantity of the ion present in the sample via the intensity of the ions peak. An electron multiplier device is implemented as the detector and generates a measurable signal pulse via the impact of an ion. The ions arrive at the detector and are reflected by a series of a dynodes which emit electrons upon impact. It is these emitted electrons which produce the measured ion count for each element in the sample, a structure of this setup can be observed in Figure 2.6.
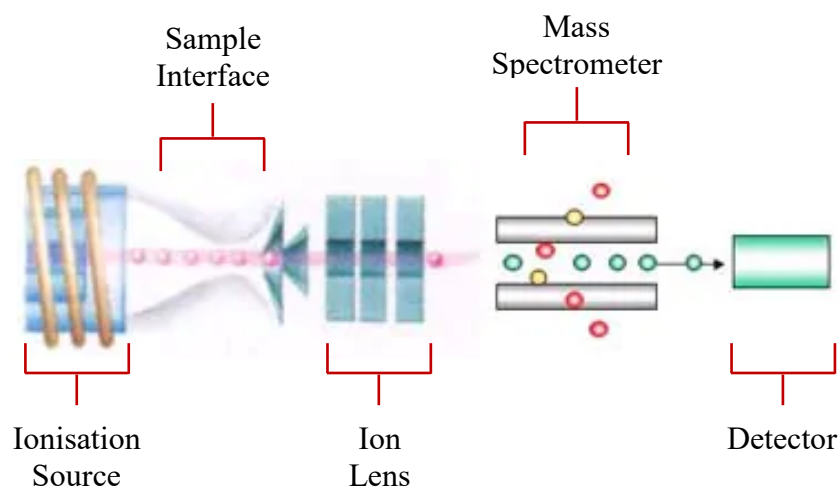
Figure 2.6: Structure of an ICP Mass Spectrometer. Figure use granted in accordance with copyright by Hitachi High-Tech Corporation.[9]

2.7.2.2   Procedure.

All ICP-MS analysis was undertaken by Simon Waller using an Agilent 7900 ICP-MS equipped with an I-AS autosampler. All the samples were diluted by a factor of ten using HPLC grade H_2O (1% HNO_3 and 0.5% HCl matrix). All calibrants were matrix matched and measured against a five-point calibration using certified reference materials purchased from Perkin Elmer and certified internal standards acquired from Agilent. The detection limits for Au and Pd were reported as 0.0192 and 0.048 μg l^{-1}, respectively.

2.7.3   Scanning Transmission Electron Microscopy (STEM).

Scanning Transmission Electron Microscopy (STEM) is a microscopic imaging technique that utilises a high energy electron beam to gain an image of a sample. The electrons, after interacting with the sample, are scattered at large angles, and detected using a high angular dark field (HAADF) detector. It is the interaction between the electrons in the beam and the particles on the surface of the sample that allows surface features such as particle size, distribution, and morphology to be determined.

2.7.3.1 Background.

To generate the high energy beam of electrons an illumination source is required, this is achieved using a cathode. A filament, usually a hairpin-shaped tungsten wire, is used as the source of electrons. The filament is surrounded by a negative current, known as a cathode cap. This allows any electrons generated when a small current is applied to the filament to be stored ready for use. An anode is then located below and is electronically grounded. This generates a positive attraction for the electrons which pass through an aperture between the cathode cap and the anode. Condenser lenses are then used to gather and focus the electrons to the area of interest, before the sample is inserted into the objective lenses to allow imagery. Further lenses, intermediate and projector, are added to further magnify the incoming image produced from the objective lenses. This is achieved by catching any transmitted or diffracted electrons post sample, before projecting these towards producing the final image.[10] High angle annular dark-field (HAADF) imaging captures these electrons by using detectors set at a great angle, as shown below in Figure 2.7. These electrons when captured from elements with greater atomic numbers undergo enhanced high angle scattering, with HAADF signal approximately proportional to $Z^{3/2}$, where Z is the atomic number of a given element which has caused the scattering. This technique allows for images with very good contrast by atomic number, with the atoms with a higher atomic number having a brighter signal, with the resulting images also referred to as 'Z-contrast' images.[11]
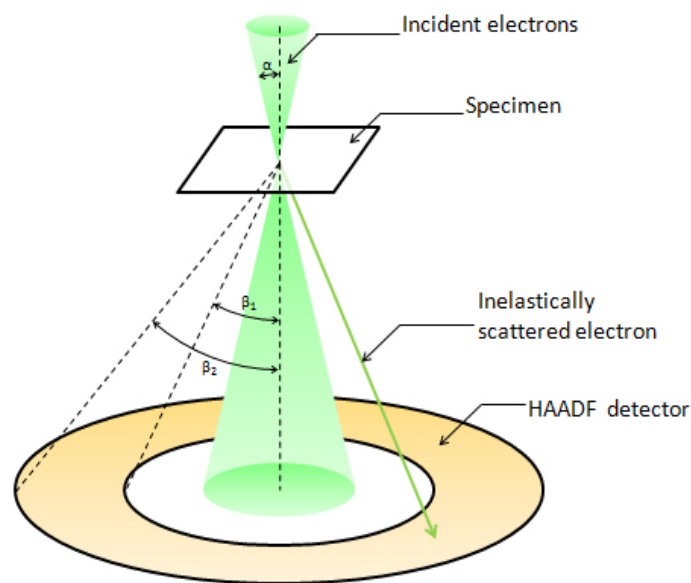
Figure 2.7: Diagram showing how the inelastically scattered electrons are detected using HAADF-STEM. Figure use granted in accordance with copyright by JEOL Ltd.[12]

2.7.3.2   Procedure.

STEM analysis was undertaken by Dr. Thomas Davies using the JEM-2100 electron microscope. Samples for examination were prepared by dry dispersing the catalyst powder onto a holey carbon film supported by a 300-mesh copper TEM grid. Bright field (BF) and high angle annular dark field (HAADF) STEM images were taken using the 200 kV microscope. Particle size distribution analysis was performed from analysis of the HAADF electron micrographs using ImageJ, with energy dispersive spectroscopy also achieved using the microscopes JEOL Centurio silicon drift detector.

2.7.4   Electron Paramagnetic Resonance (EPR).

Electron paramagnetic resonance spectroscopy is an analytical technique applied to the study and interpretation of chemical substances with unpaired electrons. This is achieved by placing the unpaired electron in an applied magnetic field and measuring the energy difference between the two states of the electron.

2.7.4.1   Background.

The application of EPR spectroscopy is dependent on the interaction of the magnetic dipole moment of an unpaired electron alongside that of an applied magnetic field.[13] This interaction, known as the Zeeman interaction, splits the electron into its respective spin energy levels, shown in Figure 2.8. Furthermore, if the energy of the applied magnetic field aligns with the energy gap between the respective spin energy levels this allows transitions between the states, which then leads to an EPR signal as shown at the bottom of Figure 2.8. There are two approaches to take to achieve the appropriate energy for transitions to take place, the first being the varying the frequency of the electromagnetic resonance, however this is less likely to be done. The second approach and the more readily done is changing the magnitude of the magnetic field while keeping the frequency constant.
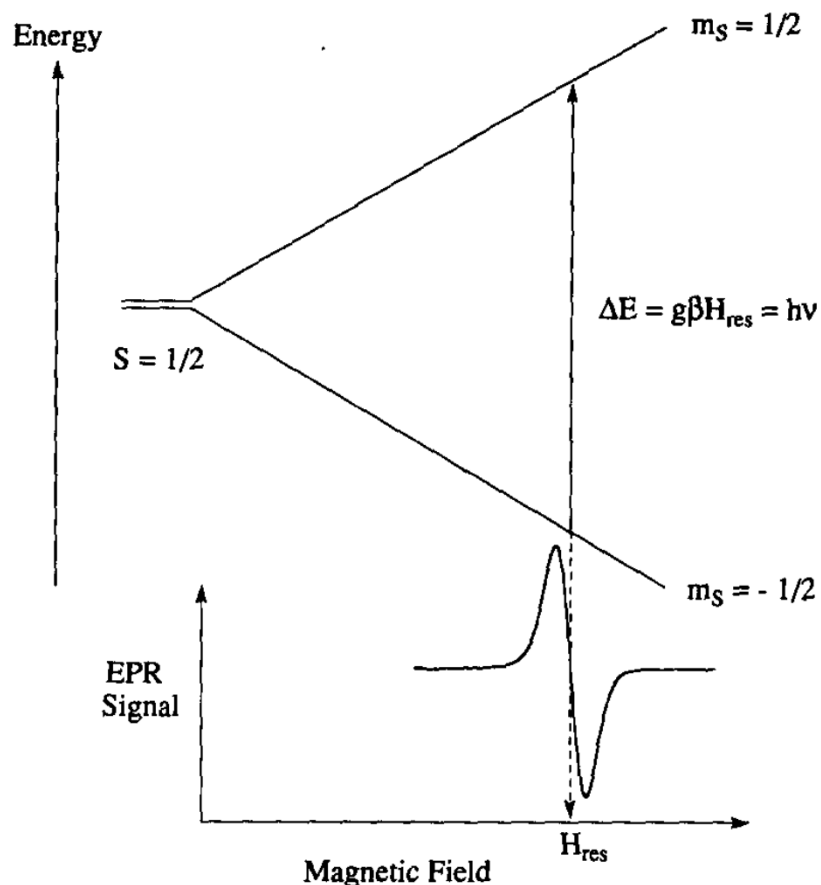
Figure 2.8: Schematic illustration of the splitting of the electron spin states by a magnetic field for the case when S = ½. When the splitting of the states, AE, equals the energy of the electromagnetic radiation, hv, an EPR signal is observed. The graph at bottom shows the EPR signal from a light-induced chlorophyll radical in photosystem II. Figure use granted in accordance with copyright by Elsevier.[13]

To gain a spectrum from the chemical being analysed the sample itself is first holstered in the sample cavity. Once holstered the chemical is then hit with a microwave radiation generated from a microwave source, most used sources are either a klystron or a magnetron. The microwave radiation alongside the correct magnetic field, generated by the electromagnet (Figure 2.9) then triggers the change in the unpaired electrons spin state allowing the sample to then produces a signal. Additionally, a modulation input is added which applies an additional oscillating magnetic field to the external magnetic field and allows only the detection of the peaks at the same frequency, in turn reducing the amount of background noise picked up by the EPR's detector or phase sensitive detector.
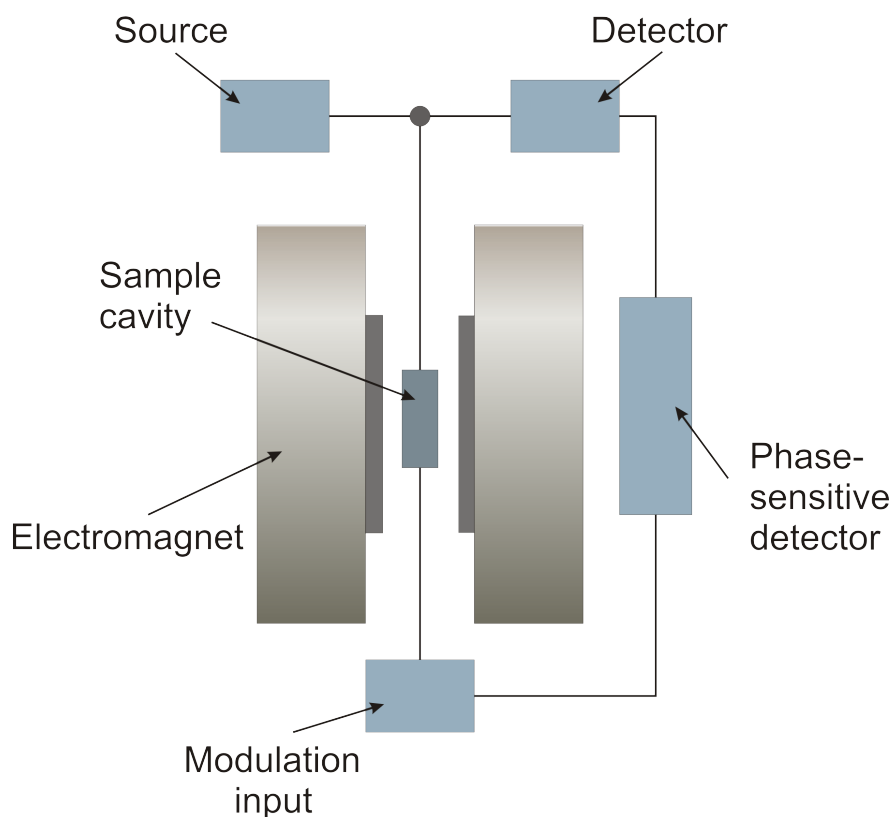
Figure 2.9: Schematic diagram of the electron paramagnetic resonance (EPR) system. Figure use granted in accordance with copyright by The University of Texas at Austin.[14]

2.7.4.2   Procedure.

The X-band CW-EPR spectra was recorded by Andrea Folli on a Bruker EMX Micro spectrometer equipped with a Bruker ER4123-D dielectric resonator, operating at room temperature. Before each measurement, samples coming from the flow reactor were deoxygenated for 20 min under N_2 flow and transferred into a Q-band EPR tube (1.6 mm outer diameter, 1.1 mm inner diameter suprasil tube, product number: WG-222T-RB Wilmad Labglass). Experimental spectra were simulated using the EasySpin package[15] operating within the Mathworks Matlab environment.

2.7.5   High Performance Liquid Chromatography (HPLC).

High performance liquid chromatography (HPLC) is a column chromatography method that passes a mobile phase (solvent), containing the injected analyte, through a column containing the stationary phase at high pressures. The HPLC then allows the compounds inside of the injected analyte to be separated and subsequently analysed via their capacity to interact with the column or the mobile phase.

2.7.5.1 Background.

A HPLC system is used to sperate chemical compounds on either their respective polarity, electrical charge or molecular size, each of which an HPLC can be tuned towards.[16] To separate via polarity the HPLC's solvent, mobile phase due to its moving through the system, and column, stationary phase as it does not move, can be adjusted either by making the HPLC column and mobile phase more/less polar to the analyte meaning the sample will take more/less time to pass thought the column dependent on the polarity of the analyte and its interaction with both phases respectively. However, when separating via electrical charge a different approach is taken. With polarity like is attracted like and opposites oppose each other, however for electrical charge this is the opposite. The stationary phase in the column is either cationic or anionic in nature and these attract analytes anionic and cationic nature respectively meaning it takes a longer time for them to pass through the column due to the attraction. Finally for separation based off size this is achieved by generating a stationary phase that has been synthesized with pore sizes that permit a certain range of analytes of interest to pass or be excluded through the bed allowing separation based off their ability to pass through these respective pore sizes.

Any model HPLC system (Figure 2.10) is made up of many different parts each with their own respective task to allow for the final chromatogram to be produced. A HPLC system is made up of a solvent reservoir, which contains the mobile phases that will be used for analysis, an HPLC pump, which passes the solvent through the system at a predetermined flow rate, an injector, that introduces the sample to the system alongside the mobile phase, an HPLC column, which contains the packing material to allow for the respective separation decided and finally a detector, which allows the user to see the separation of the respective elutes from the column in graphical form.[17]
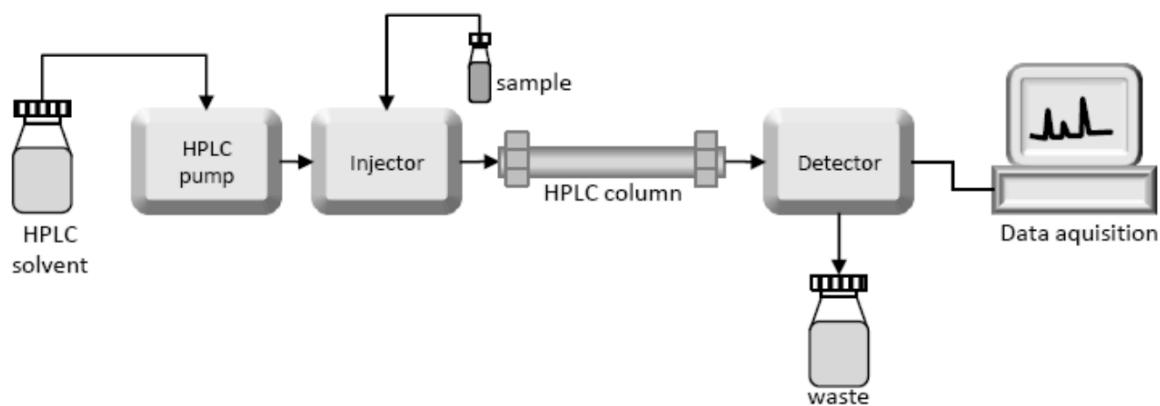
Figure 2.10: Schematic diagram of the High-Performance Liquid Chromatography (HPLC) system. Figure use granted in accordance with copyright by IntechOpen.[18]

2.7.5.2 Procedure.

Metronidazole analysis was carried out using an Agilent 1260 Infinity HPLC equipped with an ultraviolet detector and a reverse phase C18 column (250 mm x 4.6 mm)[19] at 30 °C. The sample mixture is filtered through a PTFE syringe filter prior to a 5 μL injection. The mobile phase used was an isocratic mixture of water: acetonitrile in a 70:30 ratio with a flow rate of 0.250 mL min^{-1}. The post reaction solution detection peak at 340 nm was compared to an initial reactant detection peak and a calibration curve (Figure 2.11) to allow the calculation of reactant loss and concentration.
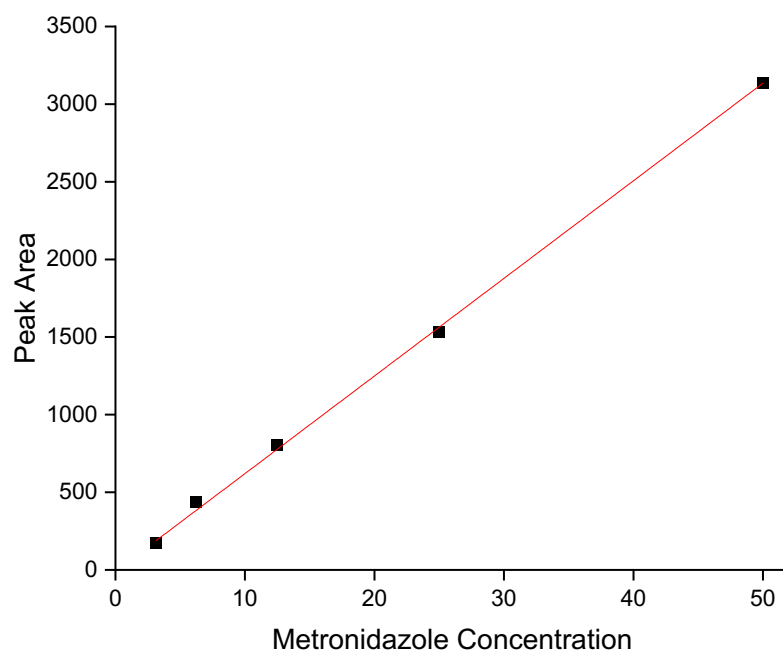
Figure 2.11: Calibration curve for metronidazole by HPLC-UV.

2.7.6 Proton Nuclear Magnetic Resonance Spectroscopy (^{1}H NMR).

^{1}H NMR spectroscopy is a technique which implements nuclear magnetic resonance alongside ^{1}H nuclei present within molecules found within a chosen analyte.[20] Thus allowing the user to determine what these molecules are within the analyte, when comparing to a ^{1}H NMR spectral library.

2.7.6.1 Background.

Quantum mechanical studies into the physical properties of atoms and subatomic particles has alluded to the fact that these particles spin upon their own axes. This means that for ^{1}H the nucleus of the atom contains an overall spin, however assigning this spin a net value comes with some rules, expressed below;[21]

1. If the number of neutrons and the number of protons is both even, then the nucleus has no spin.
2. If the number of neutrons plus the number of protons is odd, then the nucleus has a half-integer spin (i.e., 1/2, 3/2, 5/2).
3. If the number of neutrons and the number of protons is both odd, then the nucleus has an integer spin (i.e., 1, 2, 3).

The overall spin of the nuclei, I, is vital as quantum mechanics has conclude that a nucleus with spin I will have $2I + 1$ possible spin orientations. Therefore for ^{1}H, with a spin of ½, there are 2 possible orientations. However, when there is no applied magnetic field, these orientations are of equal energy and therefore cannot be separated and quantified, nonetheless as soon as an induced external magnetic field is applied these energy levels split, with each given a magnetic quantum number, m. In addition, before the magnetic quantum number of a nuclei can be deduced one of the conditions of quantum mechanics is that only one of the three cartesian components of I can be specified, with this being the z-axis, I_z. Therefore, in the case of ^{1}H, with respect to the z-axis, the 2 values for m are $+$ ½ and $-$ ½.[21]

When $I \neq 0$, a magnetic moment will be present, which will give rise to a small magnetic field. The magnitude of the nuclear magnetic moment (μ_z) of a nucleus with respect to its relative spin angular momentum (I_z) is quantified by the gyromagnetic ratio (γ) (equation 9).[21]

$$\mu_z = \gamma I_z = \gamma hm \qquad (9)$$

Following the introduction of an applied magnetic field, the orientation of the nuclear magnetic moment (μ_z) is determined. The lowest energy state is achieved when the μ_z is aligned with the applied magnetic field and the higher energy state when the μ_z is opposed (Figure 2.12). In accordance with the Boltzmann distribution, at equilibrium, the bulk magnetisation is in the lower energy state meaning it contains slightly more nuclei than the higher energy state. It is possible to excite these nuclei into the higher states via electromagnetic radiation of a frequency that correlates to the difference in energy between the corresponding energy levels. The NMR will then subsequently perturb the bulk magnetisation allowing relaxation back to the equilibrium.
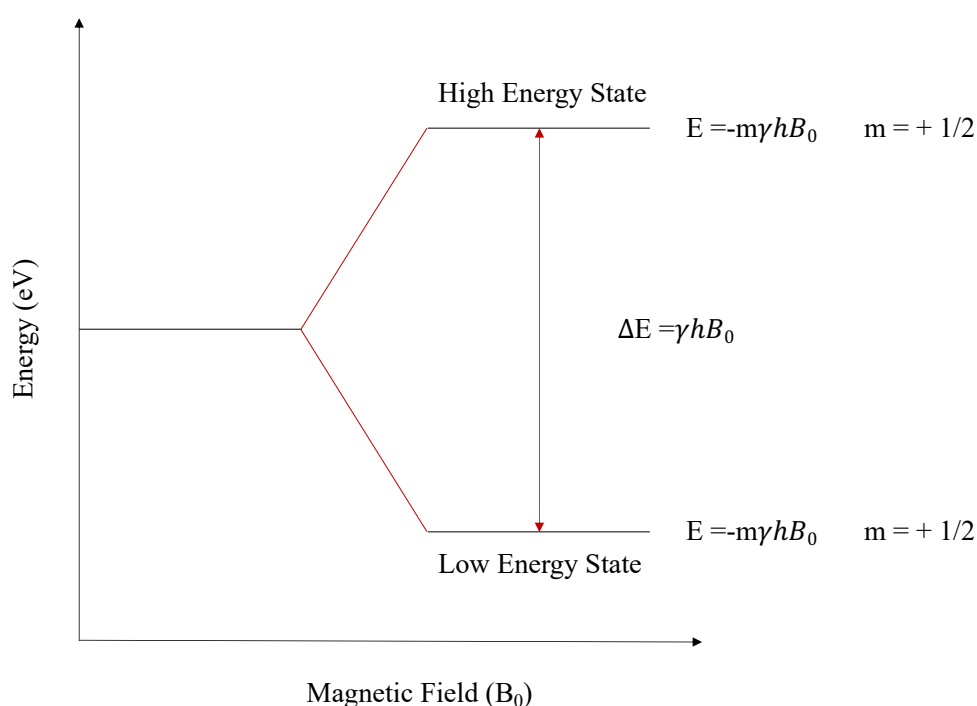
Figure 2.12: Splitting of the degenerate nuclear energy states under an applied magnetic field. Figure reproduced in accordance with copyright as image is in the public domain.

2.7.6.2 Procedure.

All ^{1}H NMR spectra were recorded on a Bruker Avance 500 MHz spectrometer. Chemical shifts are expressed as parts per million (ppm, δ) with $CDCl_3$ (7.26 ppm) being utilised as the internal standard throughout.

2.7.7 Brunauer-Emmett-Teller (BET) Surface Area Measurements.

BET surface area measurements utilises the continuous flow/suspension of an inert gas over a solid sample to calculate the analytes specific surface area via the adsorption of the gas to the surface of the analyte.[22]

2.7.7.1 Background.

The application of BET is commonly used for the quantification of the surface area of a given finely ground/porous solid analyte. In a typical BET surface area measurement, a known amount (~100 mg) of catalyst is saturated with a recorded amount of nitrogen and leads to the formation of a bond between the nitrogen available in the system and the available surface sites present on the analyte. To calculate the surface area a modification to the Langmuir adsorption model is used and is shown below:

$$\frac{p}{v(p_0-p)} = \frac{(c-1)p}{v_m c p_0} + \frac{1}{V_m c} \tag{10}$$

V_m = Volume of gas required to form a monolayer

v = Voume of gas adsorbed at the relative pressure p/p_0

p = Equilibrium pressure

p_0 = Saturation pressure

c = BET constant where:

$$c = exp\left(\frac{E_1 - E_L}{RT}\right) \tag{11}$$

E_1 = heat of adsorption for one monolayer

E_L = heat of liquefaction

R = Molar Gas constant

T = Temperature

Using equation 10 + 11, $p/v(p_0 - p)$ can be plotted against p/p_0 which leads to a straight-line graph, for which $1/v_m c$ correlates to the intercept and $(c - 1)/V_m c$ correlates to the gradient, with all this data making the determination of the analytes surface area possible.

2.7.7.2 Procedure.

BET surface area measurements were undertaken using a Quantachrome Nova 2200 using a 5-point N_2 adsorption method. Prior to this analysis the solid samples are degassed at 250 °C for 2 hours under vacuum.

2.7.8 Powder X-Ray Diffraction (XRD)

Powder X-ray diffraction is a bulk characterisation technique used to probe the crystal structure of given samples. An X-ray beam is utilised and when it hits the crystalline structure it causes incident X-rays to be diffracted. The angles and intensities of the incident beams can then be utilised to allow the crystal structure of the sample to be concluded.

2.7.8.1 Background

The X-rays required for the diffraction are formed by bombarding a metal target, usually Cu or Mo, with a high energy electron emitted. Collision of the incident electrons with the metal target produces a broad range of X-rays from the K-shell (1s) of the target atoms. X-rays are emitted and the resultant vacancies are filled with electrons from the L (2p) or M (3p) levels which have superimposed onto it characteristic narrow energies known as K_α and K_β. The X-rays are passed through a monochromator to produce an X-ray beam of a very narrow range of wavelengths. This X-ray can then interact with the atomic planes of the sample and subsequently scatter, which can result in a constructive interference (reflection). With reference to Figure 2.13, a reflection occurs when the spacing between lattice planes (d) is equal to an integer number of wavelengths or when $AB + BC = 2d\sin\theta = n\lambda$.[23]
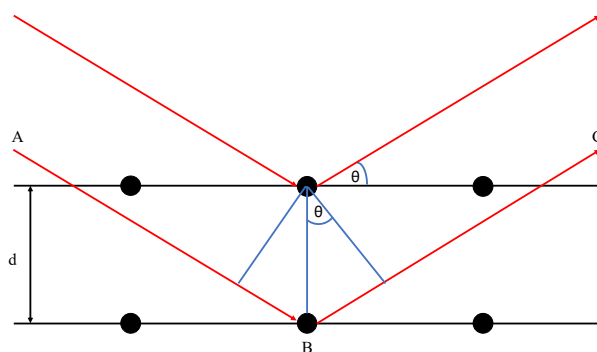
Figure 2.13: Schematic of X-ray diffraction from lattice planes in a crystalline material. θ = incident angle, normal to the plane and d = lattice spacing. Figure reproduced in accordance with copyright as image is in the public domain.

When using powder XRD, the powder sampled have an infinite number of randomly orientated crystallites. The X-ray source utilised is stationary and the detector moves around the sample to detect the angle (2θ) at which reflections occur. The lattice spacing (d) can then be calculated using Bragg's Law:[23]

$$n\lambda = 2d\sin\theta \qquad (12)$$

n = integer

λ = X-ray wavelength

d = lattice spacing

θ = angle of incident X-ray beam, normal to the plane

For small crystallites, such as those regularly found in supported metal catalysts, line broadening in the diffraction pattern can occur because of partial destructive interference. The shape of the detected reflections can therefore give information regarding the size of crystallites. The size of a crystalline particle can be estimated from the Scherrer equation.[23]

$$n = \frac{k\lambda}{\beta\cos\theta} \qquad (13)$$

τ = mean crystallite size

k = form factor

λ = X-ray wavelength

β = full width half maximum of the reflection peak

θ = diffraction angle.

2.7.8.2   Procedure

Bulk structure of the crystalline materials was investigated using a (θ-θ) PANalytical X'pert Pro powder diffractometer using a Cu Kα radiation source, operating at 40 KeV and 40mA. The analysis was carried out using a 40-minute run with a back filled sample, between 2θ values of 10 – 80°. Phase identification was carried out using the International Centre for Diffraction Data (ICDD).
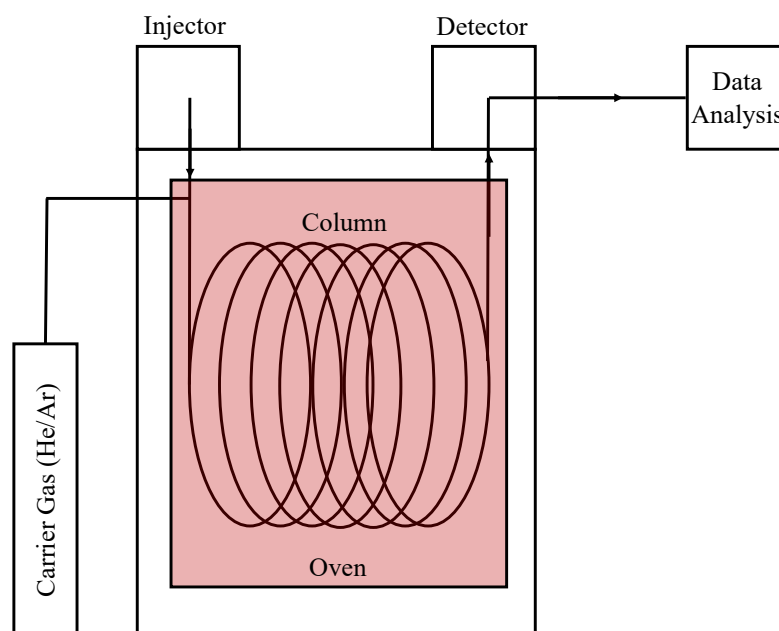
2.7.9 Gas Chromatography (GC)

Gas chromatography is an analytical technique used to separate and confirm the presence of analytes in a gas sample and calculate their quantities. The analytes are injected and carried through a heated column, coated with the stationary phase, using a mobile phase, and subsequently separated based on their ability to interfere with the stationary phase. The analytes are then detected, and a signal is released which can be quantified.

2.7.9.1 Background

Gas chromatography commences with the injection of a vaporised liquid or gaseous compound into a chromatographic column by an injector block. The sample is then eluted towards the column via the flowing mobile phase, which is an inert gas either He or N_2. The sample then reaches the column, with this stage being where the analytes in the sample begin to sperate. There are two types of chromatographic column: packed or capillary style. A packed column usually consists of a 2-4 mm internal diameter glass, quartz or stainless-steel tube filled with an inert stationary support material; while a capillary column has an internal diameter of less than 1 mm and consists of either an inert support and adsorbed stationary phase or just stationary phase liquid coated directly onto the walls of column. The stationary phase held within these columns are either an adsorbent or a high boiling point liquid on an inert material, with the most commonly used supports being diatomaceous earth, silica gel or alumina. The column is housed in a temperature regulated oven (Figure 2.14), which can either be held at a constant temperature or programmed for a ramped increase through analysis to affect the rate of elution of analytes. The analytes rate of elution can also depend on their interaction with the stationary phase, if the analytes are attracted to the stationary phase they take longer to elute and if they repel the stationary phase, they take less time. The analytes are then detected. There are many detectors available to monitor the carrier gas as it emerges from the column and act in response to changes in the gas composition as analytes are eluted. The most commonly used detector is the Flame Ionisation Detector (FID). This detector mixes the effluent gas, that previously passed through the column, with H_2 and air and burns it using a small metal jet. Pyrolysis of the organic compounds produces ions and electrons which are attracted to a cathode situated above the flame burner tip, over which a large electrical potential is applied. The movement of the electrons and ions to the cathode produce a current which is measured and recorded. A Thermal conductivity detector (TCD) is another common detector used in gas chromatography. This detector works using the principle of the relative charge in the thermal conductivity of the gas passing across the detector filament, as the analytes elute from the

column. Heat is lost continuously from the filament through the carrier gas to the wall of the detector. Through measuring the current required to maintain the temperature of the filament as the analytes pass over the filament a chromatographic signal is produced.[24]

Figure 2.14: Schematic of a gas chromatograph. Figure reproduced in accordance with copyright as image is in the public domain.

2.7.9.2   Procedure

A Varian 3800 gas chromatogram (GC), a CP-wax 52 CB column, which was held at 30°C to separate the analytes, and a thermal conductivity detector (TCD) were used to analyse the gas mixtures from the direct synthesis of H_2O_2 and metronidazole degradation experiments. This technique was used to calculate H_2 conversion and H_2O_2 selectivity of given reactions. To calculate these the peaks of the analytes were integrated and the H_2: CO_2 or H_2: N_2 ratio of a blank reaction, absence of catalyst, was compared to a catalysed reaction allowing H_2 conversion to be calculated. From this value the H_2O_2 selectivity can be calculated by factoring in the moles of H_2O_2 synthesised, determined by titration, in the direct synthesis reaction/metronidazole degradation and therefore producing a value for the hydrogen selectivity towards synthesised H_2O_2. Each sample was analysed for 22 min, which is sufficient to allow for all gasses under analysis to pass through the column, the retention times for the gasses analysed are shown in Table 2.1.

Table 2.1: Retention time for gases analysed for the direct synthesis of H_2O_2 and degradation of metronidazole.

Gas	Retention time (mins)
H_2	1.76
N_2	2.32
O_2	2.45
CO_2	9.94

2.8 References.

1   M. Morad, M. Sankar, E. Cao, E. Nowicka, T. E. Davies, P. J. Miedziak, D. J. Morgan, D. W. Knight, D. Bethell, A. Gavriilidis and G. J. Hutchings, *Catal. Sci. Technol.*, 2014, **4**, 3120–3128.

2   R. J. Lewis, K. Ueura, Y. Fukuta, S. J. Freakley, L. Kang, R. Wang, Q. He, J. K. Edwards, D. J. Morgan, Y. Yamamoto and G. J. Hutchings, *ChemCatChem*, 2019, **11**, 1673–1680.

3   S. J. Freakley, M. Piccinini, J. K. Edwards, E. N. Ntainjua, J. A. Moulijn and G. J. Hutchings, *ACS Catal.*, 2013, **3**, 487–501.

4   A. B. Cunningham, J. E. Lennox and R. J. Ross, Biofilms: The Hypertextbook, https://www.cs.montana.edu/webworks/projects/stevesbook/index.html, (accessed September 2020).

5   N. Rijal, Spread Plate Technique Principle, Procedure and Results - Microbeonline, https://microbeonline.com/spread-plate-technique-principle-procedure-results/, (accessed September 2020).

6   A. Santos, R. Lewis, D. J. Morgan, T. Davies, E. Hampton, P. Gaskin and G. Hutchings, *Catal. Sci. Technol.*, 2021, **11**, 7866-7874.

7   J. B. Gilbert, M. F. Rubner and R. E. Cohen, *Proc. Natl. Acad. Sci. U. S. A.*, 2013, **110**, 6651–6656.

8   F. R. Abou-Shakra, *Handb. Anal. Sep.*, 2003, **4**, 351–371.

9   Principle of ICP Mass Spectrometry (ICP-MS), https://www.hitachi-hightech.com/global/products/science/tech/ana/icp/descriptions/icp-ms.html, (accessed September 2020).

10   D. B. Williams and B. C. Carter, *Transmission Electron Microscopy*, 2009, Ch. 1, 3-22.

11   J. Y. Zhang, J. Hwang, B. J. Isaac and S. Stemmer, *Sci. Rep.*, 2015, **5**, 1–10.

12   HAADF, https://www.jeol.co.jp/en/words/emterms/search_result.html?keyword=HAADF-STEM, (accessed September 2020).

13   G. W. Brudvig, *Methods Enzymol.*, 1995, **246**, 536–554.

14   What is EPR?, https://sites.cns.utexas.edu/epr_facility/what-epr, (accessed September 2020).

15   S. Stoll and A. Schweiger, *J. Magn. Reson.*, 2006, **178**, 42–55.

16   HPLC Seperation Modes, https://www.waters.com/waters/en_US/HPLC-Separation-

Modes/nav.htm?cid=10049076&locale=en_US, (accessed September 2020).

17   How Does High Performance Liquid Chromatography Work?, https://www.waters.com/waters/en_US/How-Does-High-Performance-Liquid-Chromatography-Work%3F/nav.htm?cid=10049055&locale=en_US, (accessed September 2020).

18   S. Czaplicki, *Column Chromatography., 2013, Ch. 4, 99-123.*

19   J. Chen, X. Qiu, Z. Fang, M. Yang, T. Pokeung, F. Gu, W. Cheng and B. Lan, *Chem. Eng. J.*, 2012, **181**–**182**, 113–119.

20   R. W. Silverstein and G. C. Bassler, *J. Med. Chem.*, 1963, **6**, 826–827.

21   P. Atkins and J. De Paula, *Oxford Univeristy Press*, 2014, **10**, 876.

22   A. M. Kalijadis, M. M. Vukčević, Z. M. Jovanović, Z. V. Laušević and M. D. Laušević, *J. Serbian Chem. Soc.*, 2011, **76**, 757–768.

23   J. M. Thomas and W. J. Thomas, *Principles and practice of heterogeneous catalysis*, John Wiley & Sons, 2nd edn., 2014.

24   G. Schwedt, *Essential Guide To Analytical Chemistry*, Wiley and Sons, 1997.

3 The Application of *In-situ* Generated H_2O_2 for the Treatment of *E. coli.*

3.1 Introduction.

The treatment of greywater (GW) using H_2O_2 is an area of water treatment that has slowly become of greater interest due to the benign nature of H_2O_2, with H_2O the only product of its application and the high oxidative potential of H_2O_2, second only to O_2. It has been eluded to that with the appropriate treatment and the right system the treatment of greywater could become an on-site enterprise.[1] It is theorised that the greywater produced in all offices and residential properties, through showers, baths, sinks and washing machines, could be stored at location, treated *in-situ* with H_2O_2 and recycled, before being reapplied into on-site applications, including toilet flushing, garden irrigation and washing machines.[2,3] With this system in place, there could be a great reduction in the water consumption of the average household, and in turn the global water demand over the general population, and with an ever-increasing population set to reach 11.2 billion by 2100[4] this is an issue that will only become more pressing in the coming decades.

There are many current methods used for the treatment of greywater with each one expressing varying degrees of success when it comes to the removal of water impurities and contaminants, as discussed in Chapter 1.16. The simpler wastewater treatment systems including sedimentation, membranes, sand, and biological filters are limited in their ability to treat greywater, having the capacity to only remove the larger solids. However, the application of chemical oxidants, including O_3, UV and the chlorine variants, have all been shown to be much more effective as a treatment method.[5,6] Yet, even these don't come without their pitfalls, with the use of chlorine producing a large amount of hazardous waste, O_3 being largely toxic even in very small doses and finally the large economical expense that comes with implementing a UV disinfectant system.

The direct synthesis of H_2O_2 offers a much more efficient treatment for greywater. Potentially offering the high disinfecting efficiency of the other chemical oxidants, however this time without the hazardous waste and high economical expenses the other treatment systems bring. H_2O_2 provides an excellent alternative to the other oxidants by producing the oxidative species in the form of $OH^{\bullet}$ radicals, which in the human body are naturally occurring species with the

capacity to denature cells if hydroxyl radical accumulation is not controlled by breaking down nucleic acids, carbonylates proteins, and peroxidases lipids.[7] Therefore, if these same radicals are generate in a large enough quantity they could infiltrate, react and denature the microorganisms and organics found in greywater.

The production of a household GW treatment system requires the ability to separate GW from other household waste streams, a filter to remove any large organic substrates and finally a storage tank to hold the filtered and treated greywater. A potential household greywater treatment can be observed in Figure 3.1.[8] The schematic shows that the water taken from the acceptable greywater sources from a household, including baths, sinks, showers and washing machines, are all extracted and filtered. Upon being filtered, the water is then held in a storage tank before being fed through a reactor system. It is at this point in which a reactor system would be implemented that can generate the *in-situ* H_2O_2, and the subsequent radicals, required for the treatment and subsequent reapplication of the sterile greywater.
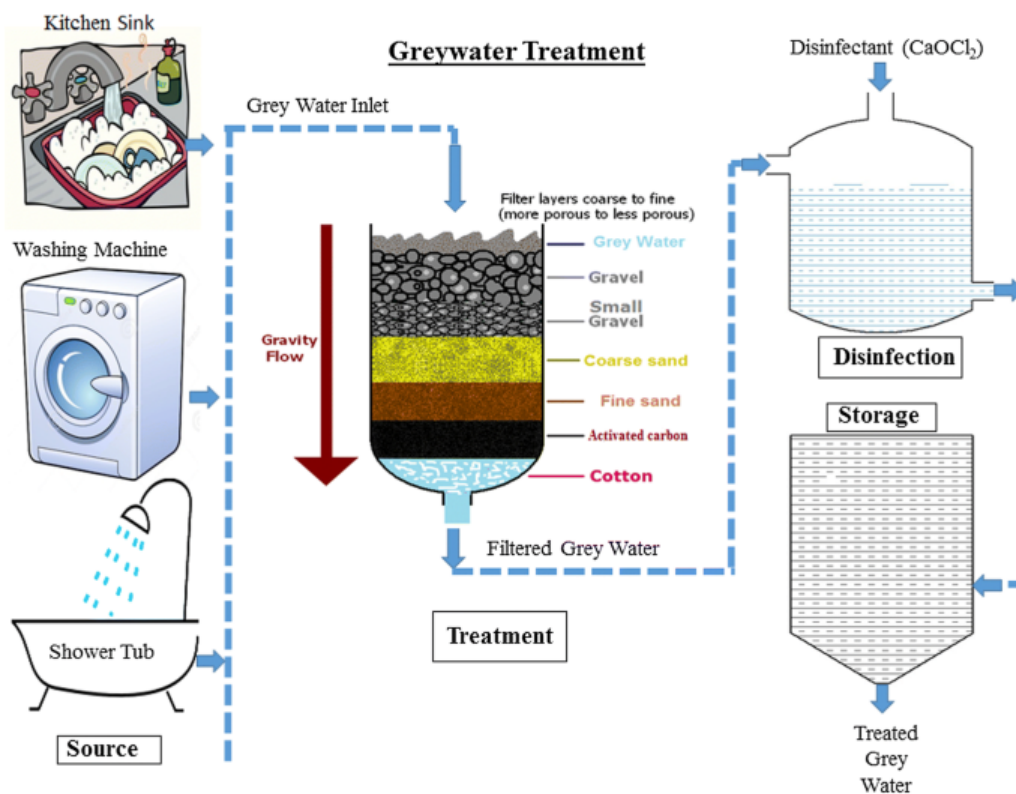
Figure 3.1: Schematic of a potential household greywater regeneration system. Figure use granted in accordance with copyright by Springer Nature.[8]

When looking towards producing a catalyst and reactor system that can generate the *in-situ* H_2O_2 required for the treatment of GW, different approaches can be taken. Many studies have

been undertaken in the development of a heterogenous catalyst with high activity towards the direct synthesis of H_2O_2, predominately based on the initial patent from Henkel and Weber[9] and the studies utilising Pd from Pospelova.[10–12] This work was then continued further, by developing a bimetallic catalyst than included Au, which aided in increasing selectivity towards H_2O_2 as well as supressing the documented high degradation values previously expressed using monometallic Pd. In addition, additives have also been included into a catalyst, or the reaction medium, to further improve its performance, in the form of halides and acids.[14] However, this would be counter intuitive, due to adding the chemicals we are trying to replace/remove during greywater treatment. Furthermore, the effect that elemental composition of a AuPd catalyst has on its ability to synthesise H_2O_2 has been studied with H_2O_2 productivity increasing alongside increasing Pd content, up to 0.5 wt.% Pd where H_2O_2 productivity plateaus out.[15]

In an attempt to develop a catalyst with improved catalytic activity and selectivity towards the direct synthesis of H_2O_2, a 1 wt.% AuPd/TiO$_2$ catalyst, made using a excess chlorine wet co-impregnation technique,[16] is studied[15,17]. The Au:Pd ratio of the 1 wt.% AuPd/TiO$_2$ was altered and its effect on the catalysts ability to synthesise H_2O_2 and subsequently degrade H_2O_2 under standard reaction conditions outlined in Chapter 2.3.1 were studied. Upon optimising the catalyst, it was then carried over to a continuous flow reactor and used to assess the biocidal activity of any *in-situ* generated H_2O_2, testing it on *E. coli,* implemented as a model wastewater microorganism contaminant. The efficacy of the *in-situ* generated H_2O_2 is then compared alongside sodium hypochlorite and commercially available H_2O_2, which were both implemented *in-situ*.

3.2   Results.

3.2.1   The Effect of Pd Content for the Direct Synthesis and Degradation of H_2O_2 in a Batch Regime.

The following H_2O_2 synthesis and degradation tests were carried out according to the procedures discussed in Chapter 2.3.2 and 2.3.3. Blank degradation reactions in the absence of a catalyst, were ran periodically to comprehend if the reactor contamination was contributing to H_2O_2 degradation. If any contamination was detected the reactor underwent substantial cleaning with aqua-regia followed by thorough cleaning with water. A subsequent blank

reaction was then carried out to confirm the removal of contaminates. Initial testing was undertaken in a batch reactor (Schematic in Chapter 2.3.1) to understand the effect that Pd weight loading had on the direct synthesis and degradation of H_2O_2. It can be observed in Figure 3.2 that there is no/minimal formation or degradation of H_2O_2 in the absence of the 1 wt.% AuPd catalyst, with the reactor only producing 2 $mol_{H2O2}\ kg_{cat}^{-1}\ h^{-1}$ and degrading 1 $mol_{H2O2}\ kg_{cat}^{-1}\ h^{-1}$, which is within experimental error. The effect of Pd content on the rate of H_2O_2 synthesis is also shown in Table 3.1.
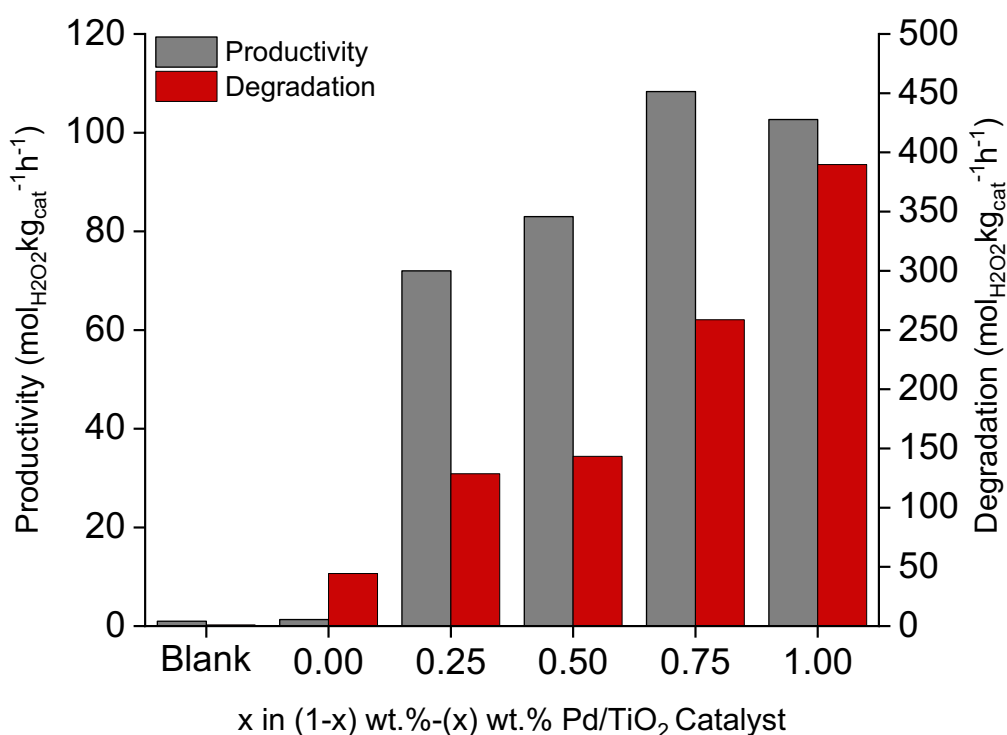
Figure 3.2: The effect of Pd content on the direct synthesis and degradation of H_2O_2 in a batch reactor. **H_2O_2 direct synthesis reaction conditions:** Catalyst (0.01 g), H_2O (2.9 g), MeOH (5.6 g), 5% H_2/CO_2 (420 psi), 25% O_2/CO_2 (160 psi), 0.5 h, 2 °C, 1200 rpm. **H_2O_2 degradation reaction conditions:** Catalyst (0.01 g), H_2O_2 (50 wt.% 0.68 g) H_2O (2.22 g), MeOH (5.6 g), 5% H_2/CO_2 (420 psi), 0.5 h, 2 °C, 1200 rpm.

Table 3.1: The effect of Pd content on the rate of H_2O_2 synthesis in a batch reactor.

Catalyst	Rate of Reaction $(mol_{H2O2}mmol_{metal}^{-1}h^{-1})$
1 wt.% Au/TiO$_2$	31
0.75 wt.% Au-0.25 wt.% Pd/TiO$_2$	1160
0.5 wt.% Au-0.5 wt.% Pd/TiO$_2$	1230
0.25 wt.% Au-0.75 wt.% Pd/TiO$_2$	1340
1 wt.% Pd/TiO$_2$	924

H_2O_2 direct synthesis reaction conditions: Catalyst (0.01 g), H_2O (2.9 g), MeOH (5.6 g), 5% H_2/CO_2 (420 psi), 25% O_2/CO_2 (160 psi), 0.5 h, 2 °C, 1200 rpm. Rate of reaction calculated using a theoretical metal loading and minimal number of active sites.

The various Pd weight loaded catalysts, ranging from 0-1%, were then introduced to the batch reactor and each tested three times to test reproducibility. It should be noted that these catalysts are made based on a weight basis. As a result of the variation in the atomic masses of Au and Pd the ratio of Au: Pd on a molar basis will vary from the wt.%. This can be explained further with the results in Table 3.1, in which the three bimetallic catalysts have a similar rate of reaction yet have a more varied H_2O_2 productivity value. The results in Figure 3.2 show that the catalysts that don't contain any Pd show minimal activity towards both the synthesis and degradation of H_2O_2, returning values of 1 mol_{H2O2} kg_{cat}^{-1} h^{-1} and 44 mol_{H2O2} kg_{cat}^{-1} h^{-1} for synthesis and degradation respectively. However, when the catalyst contains 1 wt.% Pd a much more active catalyst is observed, with both the synthesis and degradation of H_2O_2 returning values of 103 mol_{H2O2} kg_{cat}^{-1} h^{-1} and 390 mol_{H2O2} kg_{cat}^{-1} h^{-1}. These results are expected as monometallic Pd-catalysts are well known for their high activity towards both the synthesis and degradation of H_2O_2,[18] while Au is known to be very poor[13] but when alloyed with Pd can result in suppressing its degradation activity, improving catalytic selectivity.[19]

With regards to the overall trend that, increasing the Pd content of the 1 wt.% supported catalyst has on activity towards the synthesis of H_2O_2, the results seen in Figure 3.2 follows a similar trend to that reported by Santos *et. al,*[15] under identical conditions. The study reports that with

increasing Pd content the degradation activity increases, peaking at 1 wt.% Pd, however regarding the production of H_2O_2 the results don't correlate. In my results, synthesis of H_2O_2 increases up to a peak value of 110 $mol_{H2O2}\ kg_{cat}^{-1}\ h^{-1}$ for the 0.25 wt.% Au-0.75 wt.% Pd/TiO$_2$ catalyst before plateauing out, with research conducted by Pritchard *et. al*[20] coming to similar conclusion that the 1:1 Au:Pd ratio doesn't always correlate to the most productive catalyst. Yet, for Santos *et. al*[15] their results indicated that the 0.5 wt.% Au-0.5 wt.% Pd/TiO$_2$ was the optimum catalyst with a value of ~90 $mol_{H2O2}\ kg_{cat}^{-1}\ h^{-1}$, before once again plateauing out. However, it is apparent that the combination of Au and Pd is paramount in the generation of a highly efficient catalyst with all 3 of the catalyst having the best ratio of synthesis: degradation for H_2O_2. While my results may not align exactly with Santos *et. al*[15] it is clear that 0.5 wt.% Au-0.5 wt.% Pd/TiO$_2$ is the optimum catalyst for the synthesis of H_2O_2, having the best balance between a high activity and a suppressed degradation. The data for H_2 conversion however shows a different trend.
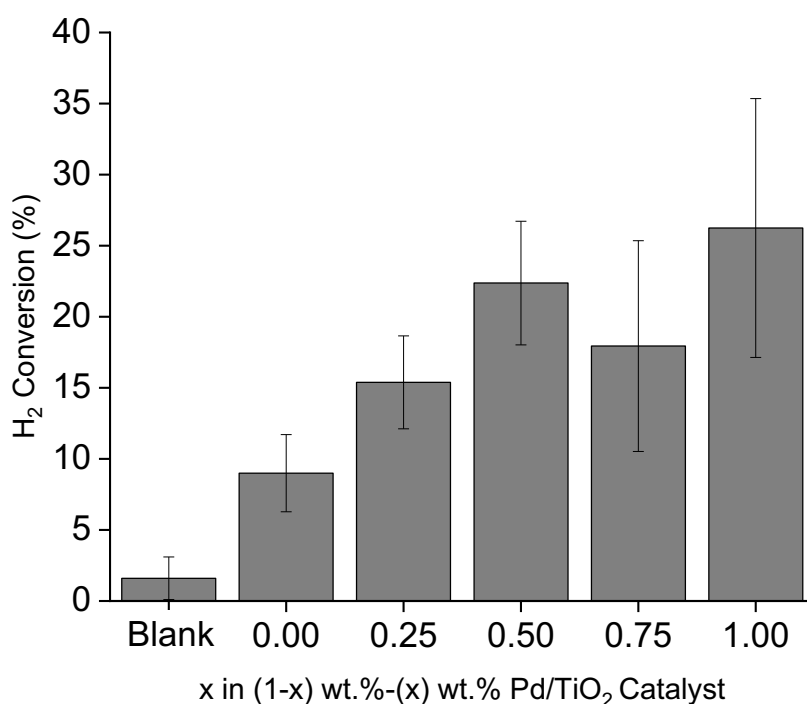
Figure 3.3: The effect of Pd content on the conversion of H_2 during the direct synthesis of H_2O_2 in a batch reactor. **H_2O_2 direct synthesis reaction conditions:** Catalyst (0.125 g), H_2O (2.9 g), MeOH (5.6 g), 5% H_2/CO_2 (420 psi), 25% O_2/CO_2 (160 psi), 0.5 h, 2 °C, 1200 rpm.

This data corresponds to an overall increase in H_2 conversion when increasing the Pd content in a 1 wt.% AuPd/TiO$_2$ catalyst (Figure 3.3). The initial peak in H_2 conversion is justified by

the increasing Pd content present in the catalyst which in turn reduces the amount of Au present in the system, both of which increase H_2 conversion. As Au, while being the most selective metal towards H_2O_2, is very poor towards the synthesis of H_2O_2.[21] While Pd is different, being very active towards both the synthesis and subsequent degradation of H_2O_2.[22] The further increase in H_2 conversion for the 1 wt.% Pd/TiO$_2$ could be due to the complete removal of Au from the catalyst allowing Pd present in the catalyst to demonstrate its poor selectivity, with high rates of H_2O_2 degradation, through hydrogenation and decomposition pathways,[15] leading to the degradation of any H_2O_2 present in the reactor and in turn the high H_2 conversion displayed (Figure 3.3).

It has been documented that AuPd catalysts prepared via an impregnation procedure and exposed to reductive heat treatments result in the formation of random alloy metal nanoparticles, with a a tight particle size distribution, typically in the range of 2-5 nm observed.[16] Analysis of the supported AuPd catalysts by X-ray diffraction (Figure 3.4) and high-angle annular dark-field scanning transmission electron microscopy (HAADF-STEM) (Figure 3.6 (ci)) of the as-prepared powdered catalysts are in keeping with these previous observations. From the powder X-ray diffractogram of the 1 wt.% Pd/TiO$_2$, 1 wt.% AuPd/TiO$_2$ and 0.5 wt.% Au-0.5 wt.% Pd/TiO$_2$ catalysts no information was able to be provided around the extent of the alloying, with this being due to the small particles size that results from the route to catalyst synthesis.[16] However, further analysis by HAADF-STEM of the 0.5 wt.% Au-0.5 wt.% Pd/TiO$_2$ catalysts (Figure 3.6c i-ii) confirms random alloy metal nanoparticles by having two different brightnesses present in the image, indicating the two different atomic masses of Au and Pd.
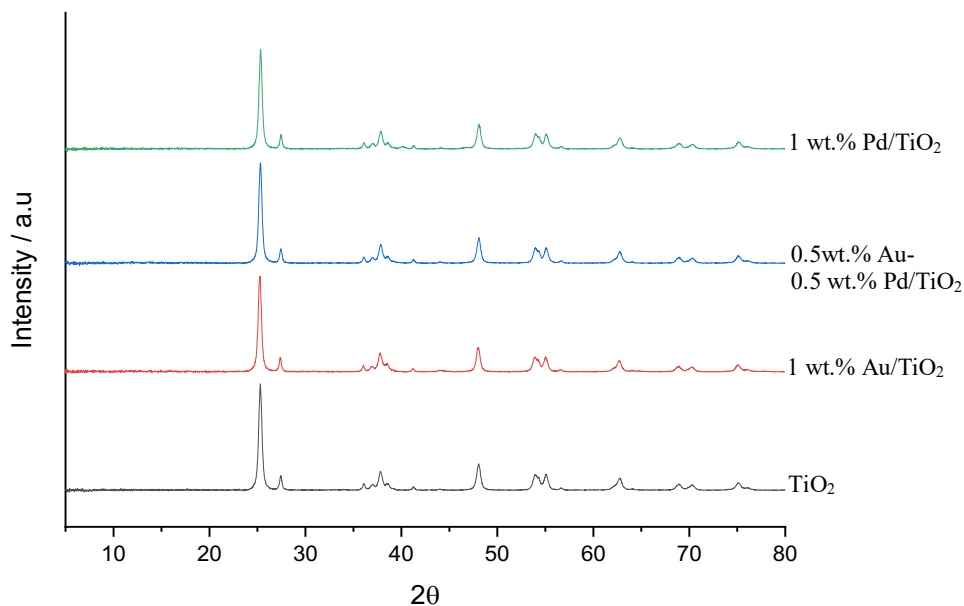
Figure 3.4: Powder X-ray diffractograms of as-prepared powdered 1 wt.% AuPd/TiO$_2$ catalysts with varying Au:Pd ratio, prepared by excess chlorine wet co-impregnation, reduced at 400 °C, 4 h, 5% H$_2$/Ar, ramp rate = 10 °C min^{-1}. Figure use granted in accordance with copyright by Springer Nature.[23]

3.2.2   Effect of Pelleting Pressure on the Direct Synthesis of H$_2$O$_2$ in a Batch Regime.

Before testing can be commenced in a continuous flow reactor, the catalysts must first be pelleted. To test the effect of pelleting parameters, 3 batches of 0.5 wt.% Au-0.5 wt.% Pd/TiO$_2$ were pressed for varying lengths of time (10 s – 5 min) and pressures (3 –10 Tonnes (t)) to determine the effect on catalyst performance. The results of this study are reported in Figure 3.5. When comparing the powdered and pelleted catalysts, there is minimal difference in net H$_2$O$_2$ synthesis activity, while the rate of H$_2$O$_2$ degradation was found to increase following pelleting. This could be explained by the fact a limited amount of particle agglomeration takes place due to the pelleting process, with mean particle size increasing from 2.9 nm in the powdered catalyst to 4.5 nm in the pelleted analogue (histograms in Figure 3.6 (a,b) HAADF-STEM images Figure 3.6 (c (ii-iv)). With studies by Tian *et. al*[24] highlighing the increased rate of H$_2$O$_2$ degraation over larger nanoparticles.   Increasing pressing pressure from 3-10 t was found to lead to an increase in productivity, which could be explained by the potential increased mean strength and density of the pellets with pressure. This in turn could allow for a better

diffusion of the gas and liquid reactants with the catalyst bed. Finally, the effect of pressing duration was found to be negligible, with the variation in H_2O_2 synthesis between samples pressed for differing periods of time found to be within experimental error.
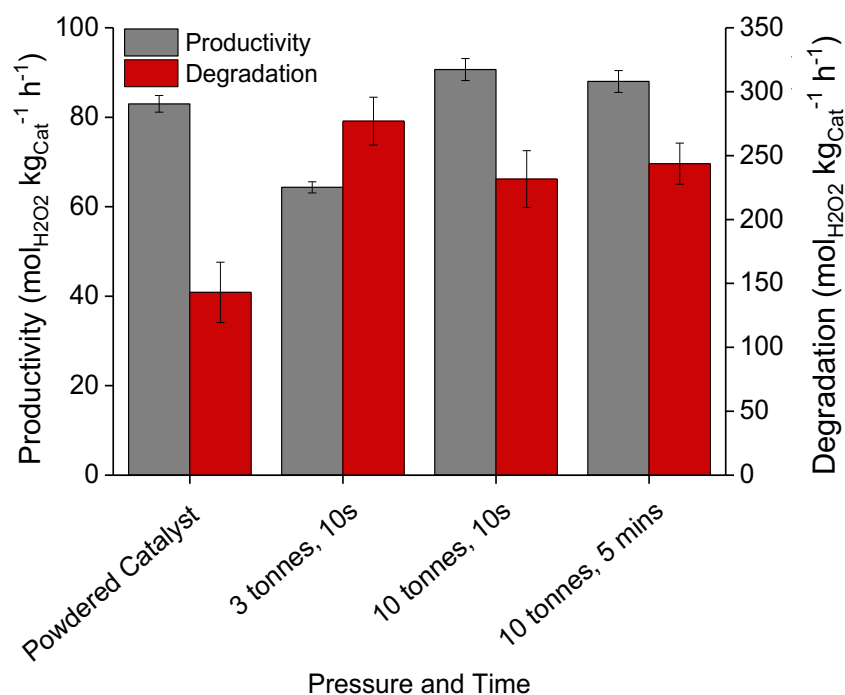
Figure 3.5: Effect of pelleting pressure and time on the direct synthesis and degradation of H_2O_2. **H_2O_2 direct synthesis reaction conditions:** Catalyst (0.125 g), H_2O (2.9 g), MeOH (5.6 g), 5% H_2/CO_2 (420 psi), 25% O_2/CO_2 (160 psi), 0.5 h, 2 °C, 1200 rpm. **H_2O_2 degradation reaction conditions:** Catalyst (0.01 g), H_2O_2 (50 wt.% 0.68 g) H_2O (2.22 g), MeOH (5.6 g), 5% H_2/CO_2 (420 psi), 0.5 h, 2 °C, 1200 rpm.
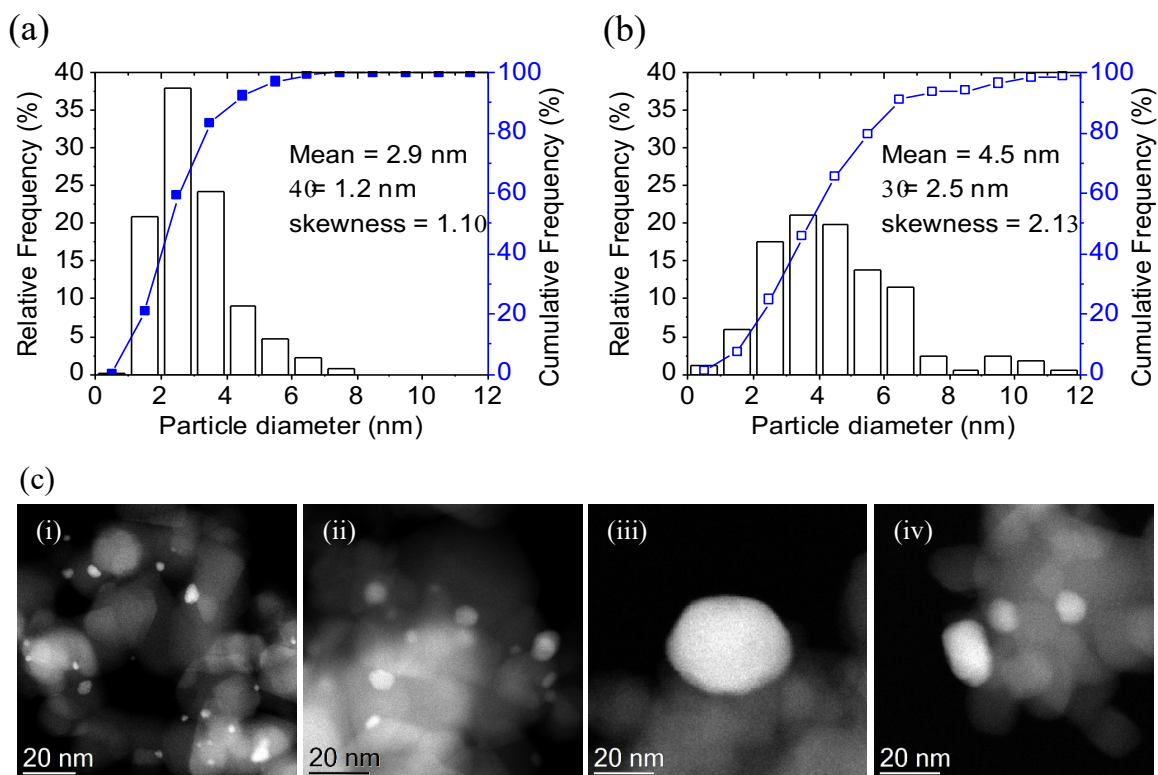
Figure 3.6: Particle size histograms for (a) as prepared powdered 0.5 wt.% Au-0.5 wt.% Pd/TiO$_2$ catalyst and (b) pelleted analogue, (c) Representative STEM-HAADF images of selected catalysts: (i) As prepared powdered 0.5 wt.% Au-0.5 wt.% Pd/TiO$_2$ catalyst; (ii) Pelleted 0.5 wt.% Au-0.5 wt.% Pd/TiO$_2$ catalyst; (iii) Pelleted 1 wt.% Au/TiO$_2$ catalyst; (iv) Pelleted 1 wt.% Pd/TiO$_2$ catalyst. Figure use granted in accordance with copyright by Springer Nature.[23]

3.3 The Direct Synthesis of H$_2$O$_2$ in a Flow Regime.

Upon confirmation that the many variants of the 1 wt.% AuPd/TiO$_2$ catalyst have the capacity to generate substantial amount of H$_2$O$_2$, these catalysts where then tested for their ability to synthesise H$_2$O$_2$ in a continuous flow reactor. Previous work by Freakley *et. al*[26] has shown that using a continuous flow reactor and under the optimal conditions, 10 bar pressure, 42 mL min^{-1} 2% H$_2$/air, 0.2 mL min^{-1} methanol, 120 mg catalyst and 2 °C, it is possible to produce 1000 ppm of H$_2$O$_2$. However, these concentrations were only achieved when methanol was used as a co-solvent, due to its high dissolution of H$_2$ compared to water only, and reaction gases were diluted with carbon dioxide (CO$_2$), with CO$_2$ increasing H$_2$ solubility alongside forming carbonic acid (HCO$_3^-$) making the solution acidic, the preferential storage conditions for H$_2$O$_2$.[27] A study by Crole *et. al*[28] in a batch regime indicated that the degradation of H$_2$O$_2$

is substantially higher in a H_2O only solvent than in a H_2O (34%)/MeOH (66%) solvent mixture, due to the points mentioned above for CO_2. Nonetheless, a decrease in H_2O_2 hydrogenation was observed when they moved to an H_2O only solvent which was attributed to the reduced solubility of H_2 in H_2O relative to methanol. For this study the intended application of the continuous flow reactor is for the treatment of greywater, rather than the production of H_2O_2, and if the system was to utilise the same pressurised cylinders, as those used by Freakley *et. al*[26], containing CO_2, this would become extremely expensive, likely prohibiting the large scale application of the *in-situ* approach to water treatment. Such problems are because eliminating CO_2 from the gas feed will promote the degradation of H_2O_2 and the formation of H_2O due to the reduced stability of H_2O_2 in methanol, which would enable the formation of the OH radicals required for biocidal activity. To resolve potential issues associated with cost 2% H_2/air is used within this study, this gaseous mixture can mimic that of a real-life application while also ensuring that the mixture of H_2 and O_2 is maintained below the explosive limit. This 2% H_2/air and H_2O system also allows the acquisition of the direct synthesis gases, H_2, via H_2O electrolysis, and O_2, from the air, while removing the issue of CO_2. Finally, silicon carbide (SiC) has been added to the catalyst bed to prevent pressure build ups in the flow reactor system brought upon by the compacting of the pelleted catalyst preventing gas flow.

Initial testing in the flow regime was undertaken to comprehend the effect that Pd weight loading, in a 1 wt.% catalyst supported on TiO_2, has on the direct synthesis of H_2O_2 and to make note of any variations between the testing in a batch regime. Figure 3.7 and Table 3.2 shows the results from this testing.
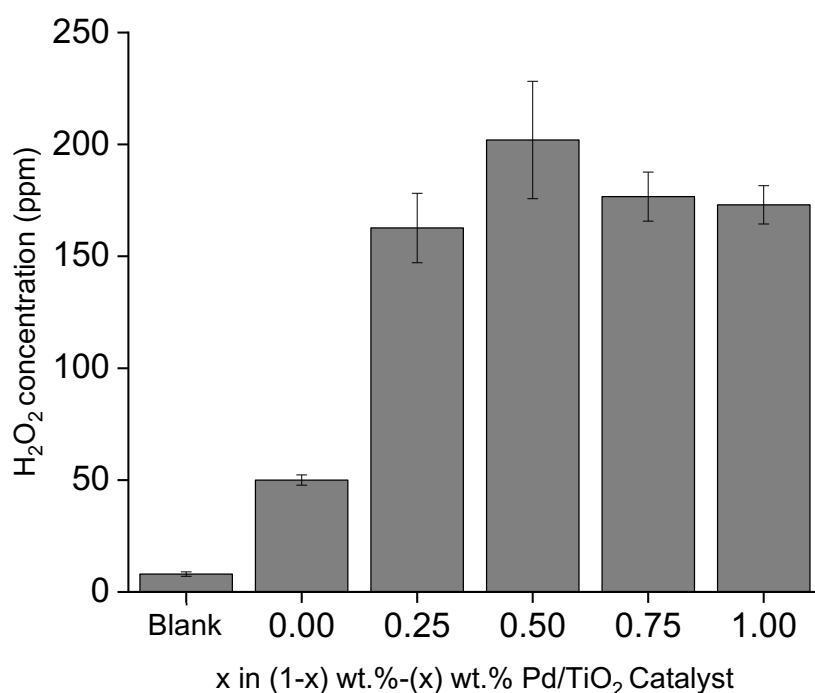
Figure 3.7: The effect of Pd content on the direct synthesis of H_2O_2 in a flow reactor. **Reaction conditions:** Pelleted catalyst (0.125 g), silicon carbide (3.30 g), 42 mL min^{-1}, 2% H_2/air, 0.2 mL min^{-1} HPLC water, residence time 30 s, 0.5 h, 2 °C.

Table 3.2: The effect of Pd content on the rate of H_2O_2 synthesis in a flow reactor.

Catalyst	Rate of Reaction ($mol_{H2O2}mmol_{metal}^{-1}h^{-1}$)
1 wt.% Au/TiO$_2$	0.4
0.75 wt.% Au-0.25 wt.% Pd/TiO$_2$	5.6
0.5 wt.% Au-0.5 wt.% Pd/TiO$_2$	7.1
0.25 wt.% Au-0.75 wt.% Pd/TiO$_2$	4.1
1 wt.% Pd/TiO$_2$	5.2

Reaction conditions: Pelleted catalyst (0.125 g), silicon carbide (3.30 g), 42 mL min^{-1}, 2% H_2/air, 0.2 mL min^{-1} HPLC water, residence time 30 s, 0.5 h, 2 °C. Rate of reaction calculated using a theoretical metal loading and minimal number of active sites.

An initial blank direct synthesis reaction was undertaken prior to testing the catalysts using 3.3 g of SiC and no catalyst, with the same flow rate for 2% H_2/air and HPLC water as the synthesis reaction, 42 mL min^{-1} and 0.2 mL min^{-1} respectively. This was done to confirm that the reactor itself is not making substantial amounts of H_2O_2. The results indicated that 15 ppm of H_2O_2 is produced without the presence of a catalyst which is an inconsequential amount. Following this, the many variants of the 1 wt.% AuPd/TiO$_2$ catalyst were then introduced to the flow reactor, revealing a different outcome to the results from the batch reactor (Figure 3.2), with the 0.5 wt.% Au-0.5 wt.% Pd/TiO$_2$ catalyst now producing the most H_2O_2 with a value of 202 ppm, which is ~50 ppm more than that reported by Freakley $et.$ al[26] using the same reaction conditions. However, this result is not unexpected as the 0.5 wt.% Au-0.5 wt.% Pd/TiO$_2$ catalyst in batch had the optimal balance between H_2O_2 synthesised and H_2O_2 degraded.

The rate of reaction towards H_2O_2 offers further support for the 0.5 wt.% Au-0.5 wt.% Pd/TiO$_2$ catalyst, with the results in Table 3.2 showing an optimal rate of reaction of 7.1 mmol$_{H2O2}$mmol$_{metal}$$^{-1}$h^{-1} tailing off to 0.4 mmol$_{H2O2}$mmol$_{metal}$$^{-1}$h^{-1} for the 1 wt.% AuPd/TiO$_2$ due to the limited production of H_2O_2 and low mmol of metal on the catalyst surface, due to Au's high atomic mass. The data in Figure 3.7 expresses that upon increasing Pd content from 0 to 0.5 wt.% an increase in the amount H_2O_2 produced is observed. This can be explained by the poor ability of Au to synthesise H_2O_2[13] and the incremental increase in the amount of Pd present in the catalyst, a well-documented metal for the synthesis of H_2O_2.[18] However, when increasing the wt.% of Pd content from 0.5 to 1 wt.% the opposite is observed with a drop in the production of H_2O_2, predominately due to the reduction of Au content in the catalyst leading to an increased formation of Pd ensembles,[29] leading to an increase in the previously supressed H_2O_2 degradation. Evaluating the powdered catalysts atomic surface ratios by X-ray photoelectroon spectrscopy (XPS) (Figure 3.8, Table 3.3) reveals that the introduction of Au significantly modifies the Pd-oxidation state, with the proportion of Pd^{2+} in the optimal 0.5 wt.% Au-0.5 wt.% Pd/TiO$_2$ catalyst greatly increased compared to the Pd-only analogue, with this further affirmating that the presence of domains of mixed Pd oxidation state aids in improving the catalytic performance towards H_2O_2[30,31] with the 0.5 wt.% Au-0.5 wt.% Pd/TiO$_2$ catalyst synthesising the largest amount of H_2O_2.

Table 3.3. Surface atomic composition of 1 wt.% AuPd/TiO$_2$ catalysts as determined via XPS, using Pd (3d) and Au (4f) regions. Table use granted in accordance with copyright by Springer Nature.[23]

Entry	Catalyst	Pd: Au	Pd^{2+}: Pd^0	Reduction in bacterial viability/log$_{10}$
1	1 wt.% Au/TiO$_2$ (powder)	-	-	-
2	1 wt.% Au/TiO$_2$ (pellet)	-	-	1.6
3	0.75 wt.% Au-0.25 wt.% Pd/TiO$_2$ (powder)	7.0	1.3	-
4	0.75 wt.% Au-0.25 wt.% Pd/TiO$_2$ (pellet)	7.0	1.5	2.4
5	0.5 wt.% Au-0.5 wt.% Pd/TiO$_2$ (powder)	4.22	0.52	-
6	0.5 wt.% Au-0.5 wt.% Pd/TiO$_2$ (pellet)	4.78	0.54	8.1
7	0.25 wt.% Au-0.75 wt.% Pd/TiO$_2$ (powder)	19.5	0.50	-
8	0.25 wt.% Au-0.75 wt.% Pd/TiO$_2$ (pellet)	19.5	0.40	4.1
9	1wt.% Pd/TiO$_2$ (powder)	-	All Pd^0	-
10	1 wt.% Pd/TiO$_2$ (pellet)	-	0.11	2.6

Reaction conditions: 0.5 wt.% Au-0.5 wt.% Pd/TiO$_2$ (0.125 g), Silicon Carbide (3.30 g), 42 mL min^{-1} Gas, 0.2 mL min^{-1} bacterial solution, residence time 30 s, 0.5 h, 2 °C.
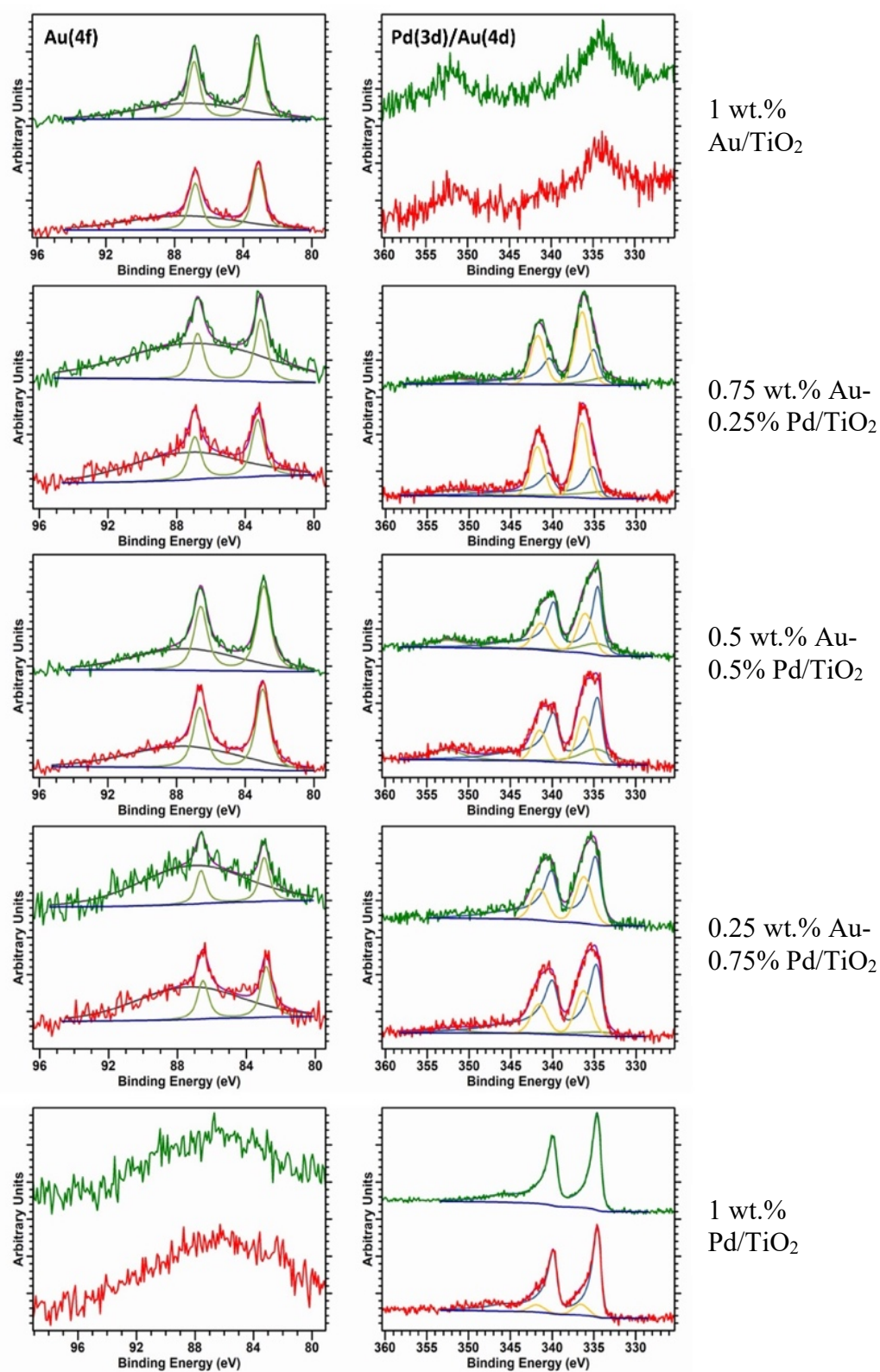
Figure 3.8: Surface atomic compositions of powdered (red) and pelleted (green) catalysts as determined by XPS using Au 4*f* (left column) and Pd 3*d*/Au 4*d* (right column) regions. Au^0 (olive), Pd^0 (blue), Pd^{2+} (yellow), loss of structure and Pd 4s (black). a.u., arbitrary units. Figure use granted in accordance with copyright by Springer Nature.[23]

3.4 The Effect of Removing Catalyst on the *In-Situ* Reduction of *E. coli* in a Flow Regime.

The use of *E. coli* as a model bacterium for wastewater treatment systems is well documented in literature,[32–34] with the simplicity and affordability of its microbiological protocol for culturing being one of the contributing factors. In addition, it is a highly prevalent contaminant found in greywater given that *E. coli* is found most commonly in faecal contaminants which can be found in both laundry and bathroom waste, which make up 50-80% of all greywater production.[35] These points make this bacterium the perfect simulant for continuous testing of model greywater. The reactions were carried out using laboratory grown *E. coli*, as outlined in Chapter 2.5.1, of known concentrations. An initial cell density of 10^8 CFU mL^{-1} was chosen and was cultured following the procedure set out in the experimental Chapter above. Now that the flow reactor can generate ~200 ppm of H_2O_2 it is desirable to test the biocidal activity of this towards our model greywater contaminant, *E. coli*. However, before testing the different variations of the 1 wt.% catalyst it is important to first confirm that it is the catalyst that is responsible for activating the H_2O_2 synthesis gases which aid in the formation of the required ROS for effective biocidal activity. To simulate this, a set of experiments were undertaken in which different flow gas atmospheres were used while keeping all other reaction conditions the same to test their capacity to reduce the concentrations of *E. coli*.

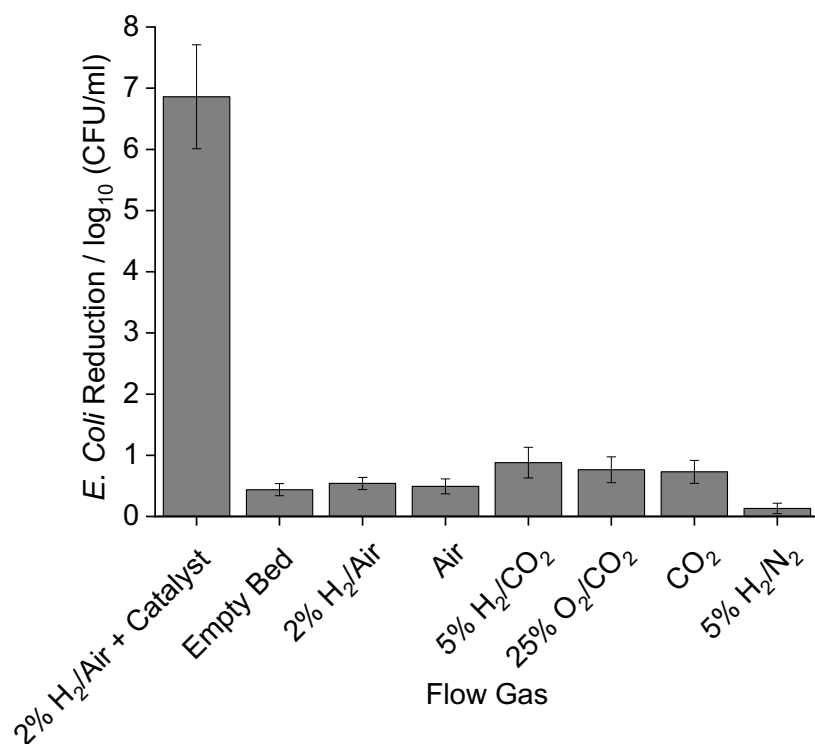**Figure 3.9:** *E. coli* reduction under different gas atmospheres in the absence of a catalyst. **Reaction conditions:** 0.5 wt.% Au-0.5 wt.% Pd/TiO$_2$ (0.125 g), Silicon Carbide (3.30 g), 42 mL min^{-1} Gas, 0.2 mL min^{-1} bacterial solution, residence time 30 s, 0.5 h, 2 °C.

The data expressed in Figure 3.9 indicates the need for the 0.5 wt.% Au-0.5 wt.% Pd/TiO$_2$ catalyst to allow the removal of *E. coli*. The absence of both the catalyst and the H$_2$O$_2$ synthesis gases from the flow reactor expresses no noticeable difference in the biocidal activity of the system, with all gas atmospheres registering no logarithmic reduction greater than 0.9 log$_{10}$. This illustrates that both the presence of the 0.5 wt.% Au-0.5 wt.% Pd/TiO$_2$ catalyst and the H$_2$O$_2$ synthesis gases are required to enable an 8 log$_{10}$ reduction towards *E. coli.*

3.5   The Effect of Gas Atmosphere on the *In-Situ* Reduction of *E. coli* in a Flow Regime.

Following the identification that the presence of a catalyst is required for the effective treatment of *E. coli*, the 0.5 wt.% Au-0.5 wt.% Pd/TiO$_2$ was then used again this time to study the effect that the different gas atmospheres used above have on the biocidal activity of the catalyst. The aim of this study is to comprehend the effect that removing both the H$_2$O$_2$ synthesis gases (H$_2$ + O$_2$) from the flow stream have on the biocidal activity of the aforementioned catalyst.
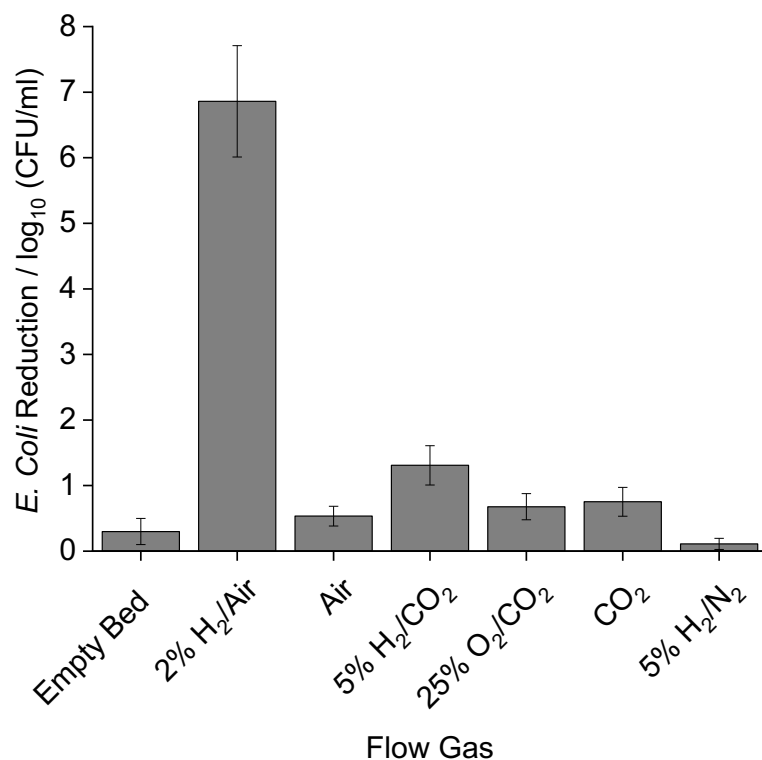
Figure 3.10: *E. coli* reduction under different gas atmospheres and with a catalyst. **Reaction conditions:** 0.5 wt.% Au-0.5 wt.% Pd/TiO$_2$ (0.125 g), Silicon Carbide (3.30 g), 42 mL min^{-1} Gas, 0.2 mL min^{-1} bacterial solution, residence time 30 s, 0.5 h, 2 °C.

The data shows that by removing H$_2$ and O$_2$ from the gas stream has a drastic effect on the biocidal activity of the 0.5 wt.% Au-0.5 wt.% Pd/TiO$_2$ catalyst. As can be seen (Figure 3.10) when either H$_2$ or O$_2$ are absent from the gas stream the maximum logarithmic reduction of *E. coli* seen is 1.2 log$_{10}$. Demonstrating the bactericidal activity of ROS generated through combination of H$_2$ and O$_2$ over the AuPd catalyst. Interestingly, varying the diluent is seen to influence bactericidal activity, with the use of 5% H$_2$/CO$_2$ offering nearly 4x times the activity of the analogous N$_2$ diluted gas feed. This is perhaps unsurprising given the formation of carbonic acid *in-situ*, resulting from the solvation of CO$_2$. Indeed, Edwards *et. al.*[36] have previously reported that the presence of CO$_2$, (under batch conditions, similar to those utilised in Chapter 3.2.1) decreases solution pH to a value of 4, with this acidity likely the cause for the greater bactericidal activity.

3.6 Stabilised H_2O_2 for the *In-Situ* Reduction of *E. coli* in a Flow Regime.

Upon concluding that both a catalyst and the H_2O_2 synthesis gases are required to both synthesise H_2O_2 and remove high concentrations of *E. coli* this catalytic system was then compared with the direct addition of commercial, pre-formed H_2O_2. Commercial H_2O_2 is currently being used to remove pollutants from wastewater making it an excellent comparison for our system. However, the common issues with regards to commercial H_2O_2 is the underlying costs and safety. For the process of synthesising H_2O_2 to be economically viable it must be made at a centralized site, yet this then leads for the need to transport to the sites of requirement which adds an additional cost and energy to the process.[27] Furthermore, the instability of H_2O_2, due to its rapid decomposition to H_2O in the presence of weak bases or at mild temperatures requires the use of stabilizing agents, often acidic stabilizers such as; acetic acid, peracetic acid. However, the use of such stabilizing agents often leads to reactor corrosion as well increased costs associated with their down-stream removal.[22] All of these points lead to the large cost associated with using commercial H_2O_2, yet if H_2O_2 was to be synthesised on site using water and a hydrogen source this would remove the requirement for any of the above and therefore their associated cost. As discussed in Chapter 3.3, the 0.5 wt.% Au-0.5 wt.% Pd/TiO_2 catalyst can produce upwards of 200 ppm, with this synthesis mechanism also having the capacity to reduce 8 $\log_{10}$ of *E. coli*. For this study, concentrations between 5-10000 ppm were trailed, with the solutions being prepared by dissolving the required amount of commercial H_2O_2 in HPLC grade H_2O before then passing the solutions through the reactor parallel with the *E. coli* solution utilising a second HPLC pump.
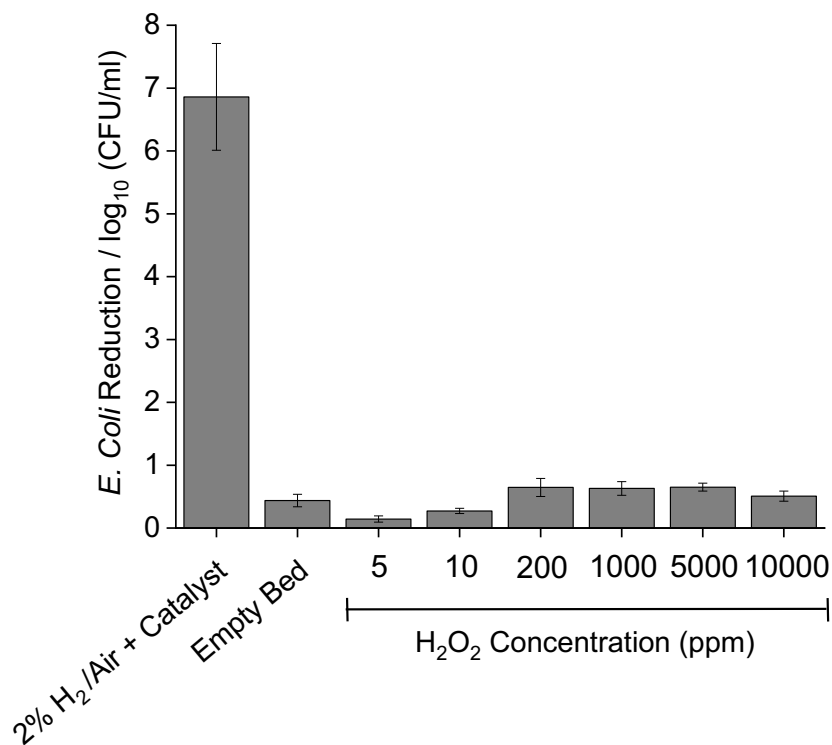
**Figure 3.11:** The effect of increasing stabilised H_2O_2 concentration on the reduction of *E. coli* without a catalyst and in air. **Reaction conditions:** 0.5 wt.% Au-0.5 wt.% Pd/TiO$_2$ (0.125 g), Silicon Carbide (3.30 g), 42 mL min^{-1} air, 0.18 mL min^{-1} bacterial solution, 0.02 mL min^{-1} H_2O_2 solution, 0.5 h, 2 °C.

This data in Figure 3.11 highlights the efficiency of the *in-situ* generated H_2O_2, with it being clear that the catalytic system is far more active than the equivalent concentrations of preformed, commercial H_2O_2. These results indicate that it is not just the concentration of H_2O_2 that leads to an increased reduction in the *E. coli* levels, with even the highest concentration of commercial H_2O_2 (10000 ppm) still producing a < 1 log$_{10}$ reduction. These diminished logarithmic reductions at the varying H_2O_2 concentrations can be concluded to be due to a poor contact time of H_2O_2 against the *E. coli,* with the CDC identifying that 15 minutes of exposure time is required for 6000 ppm of H_2O_2 to produce a 8 log$_{10}$ reduction of *E. coli.*[37] Therefore, the concentrations of H_2O_2 utilised in this study are both not high enough and/or not in contact with *E. coli* for enough time, with the flow reactor having a contact time in the seconds.

Following the study of various concentrations of commercial, stabilized H_2O_2 it was important to understand the effect that any potential stabilizers contained within the H_2O_2 solution may have on preventing the biocidal activity of the oxidant. To determine this, H_2O_2 was generated in a batch reactor and was suspended in a solution of *E. coli* prior to introduction to the reactor. In a similar manner commercial, stabilized H_2O_2 was also evaluated. These comparatively similar results using the *ex-situ* synthesised and commercial H_2O_2 indicate that the lack of activity in the latter cannot be ascribed to the presence of stabilising agents present in H_2O_2 (Figure 3.12).
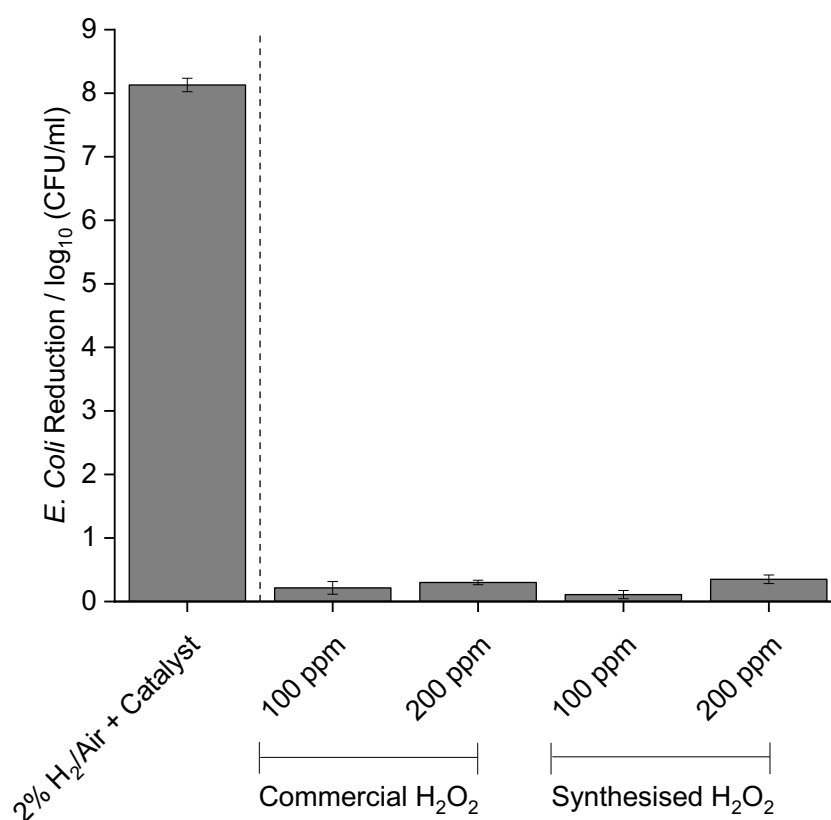
Figure 3.12: A comparison of commercial, stabilised H_2O_2 against synthesised H_2O_2 on the reduction of *E. coli*, biocidal activity after a 1-minute contact time for the H_2O_2 testing and 30 seconds for the flow test. **Reaction conditions:** 0.5 wt.% Au-0.5 wt.% Pd/TiO$_2$ (0.125 g), Silicon Carbide (3.30 g), 42 mL min^{-1} air, 0.2 mL min^{-1} bacterial solution, residence time 30 s, 0.5 h, 2 °C.

This study showed neither commercial H_2O_2 or synthesised H_2O_2 can reduce substantial amounts of *E. coli*, with the concentrations of 100 and 200 ppm of both H_2O_2 solutions unable to reduce anything greater then 0.5 log$_{10}$ of *E. coli*. This data indicates that the stabilizers

present in the commercial H_2O_2 are not the reason for the limited reduction observed in Figure 3.11 + 3.12 but rather the aforementioned points of limited biocidal activity at the residence times/concentrations utilised. Furthermore, these results further support the suggestion that it is the ROS, formed prior to the direct synthesis of the *in-situ* H_2O_2, that leads to the enhanced biocidal activity, with the more of this un-stabilised H_2O_2 produced leading to the formation of more ROS.

3.7 The Direct Synthesis of H₂O₂ and *In-Situ* Reduction of *E. coli* in a Flow Regime.

The experiments utilising *E. coli* continued by introducing the various 1 wt.% AuPd catalysts, varying the Pd content from 0-1%, to the continuous flow reactor and testing their ability to reduce *E. coli* levels in model greywater via the *in-situ* combination of H_2 and O_2, residual H_2O_2 was also determined via titration (outlined in Chapter 2.4.3).
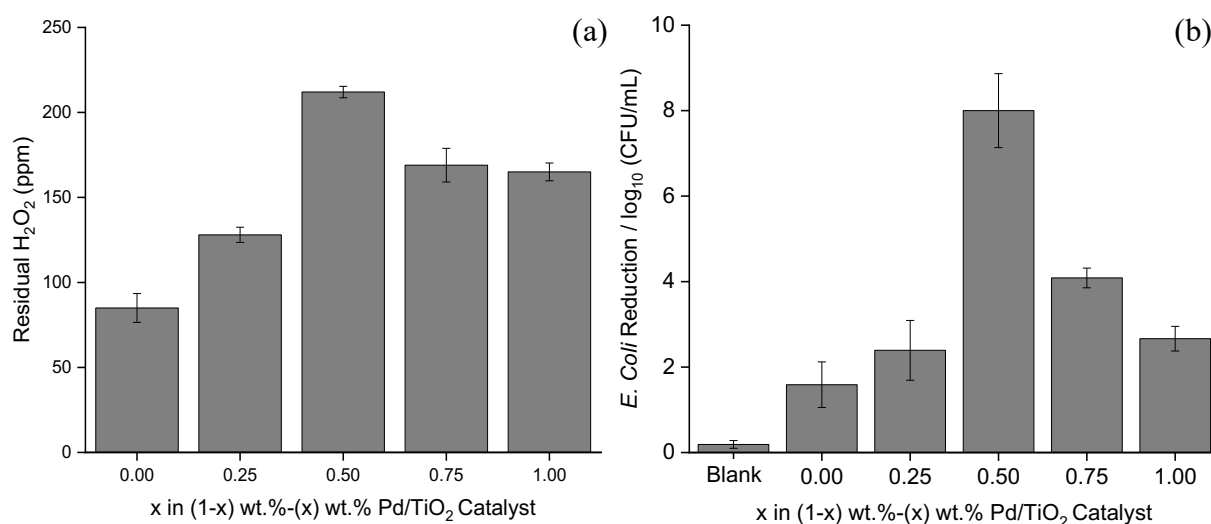
Figure 3.13: The effect of Pd content on (a) the *in-situ* reduction of *E. coli* and (b) determination of residual H_2O_2. **Reaction conditions:** Pelleted Catalyst (0.125 g), Silicon Carbide (3.30 g), 42 mL min^{-1} 2% H_2/air, 0.2 mL min^{-1} bacterial solution, residence time 30 s, 0.5 h, 2 °C.

Table 3.4: The effect of Pd content on the rate of *E. coli* reduction and the rate of residual H_2O_2 production

Catalyst	Rate of Reaction $(mol_{H2O2}mmol_{metal}^{-1}h^{-1})$	Rate of *E.coli* conversion $(CFUmL^{-1}$ (converted) $mmol_{metal}^{-1}h^{-1})$
1 wt.% Au/TiO$_2$	0.4	287
0.75 wt.% Au-0.25 wt.% Pd/TiO$_2$	5.3	201
0.5 wt.% Au-0.5 wt.% Pd/TiO$_2$	7.1	201
0.25 wt.% Au-0.75 wt.% Pd/TiO$_2$	3.6	245
1 wt.% Pd/TiO$_2$	5.1	170

Reaction conditions: Pelleted Catalyst (0.125 g), Silicon Carbide (3.30 g), 42 mL min^{-1} 2% H_2/air, 0.2 mL min^{-1} bacterial solution, residence time 30 s, 0.5 h, 2 °C. Rate of reaction calculated using a theoretical metal loading and minimal number of active sites.

Upon collecting the results, when the *E. coli* solution is passed through the flow reactor, under the H_2O_2 synthesis conditions, each of the various 1 wt.% AuPd/TiO$_2$ experience different success extents of bactericidal activity (Figure 3.13a). A similar trend to that observed in Figure 3.7 can be observed in Figure 3.12b, with the amount of residual H_2O_2 synthesised in the flow reactor correlating with Pd content. When the same solutions are tested for the reduction of *E. coli* the trend presented differs. The 0.5 wt.% Au-0.5 wt.% Pd/TiO$_2$ catalyst is seen to offer optimal bactericidal activity (8.1 log_{10}) and rate of reaction for H_2O_2 synthesis (7.1). Either side of this Au:Pd ratio there is a drastic reduction in the catalyst's ability to act as a biocide, with results plateauing out to a 2 log_{10} reduction for the catalyst's respective monometallics. However, when comparing the rate of *E. coli* conversion, the 1 wt.% Au/TiO$_2$ catalyst is shown to be optimal, with this being assigned to the larger atomic mass of Au compared to Pd leading to a low metal loading for the amount of *E. coli* converted.

This data illustrates that the elimination of bacteria, although assisted by the *in-situ* generated H_2O_2, does not depend on it, with a higher H_2O_2 production not leading to a higher logarithmic reduction. This is despite the bi-metallic AuPd, and Pd-only catalysts producing similar concentrations of residual H_2O_2 concentrations (163-202 ppm) and further demonstrates that the enhanced reduction in CFU observed over the 0.5 wt.% Au-0.5 wt.% Pd/TiO$_2$ catalyst is not simply related to H_2O_2 production. The corresponding apparent turnover frequencies (TOFs) based on mmol of metal further highlights the stark differences in bactericidal efficacy (Table 3.5), with the activity of the 0.5 wt.% Au-0.5 wt.% Pd/TiO$_2$ catalyst (1.89 x10^{11}

$CFU_{reduction}$ h^{-1} mmol$_{metal}^{-1}$) greatly exceeding that determined for the alternative formulations. Furthermore, the H_2O_2 present in reactor effluent with (Figure 3.13b) and without *E. coli* (Figure 3.7) was comparable, cementing that the biocidal activity is independent from the generation or consumption of H_2O_2 by the catalyst. In addition, the concentration of residual H_2O_2 is comparable to the allowable limits of H_2O_2 within drinking water recommended by the US Environmental Protection Agency[38], therefore the ability of low levels of residual H_2O_2 to prolong the potable lifetime of the treated water is a promising decontamination technique.

Table 3.5: Summary of catalytic testing results for the direct synthesis of H_2O_2 and *E. coli* remediation. Figure use granted in accordance with copyright by Springer Nature.[23]

Catalyst	H_2O_2 (ppm)	Apparent reaction rate at 30 min (mmol$_{H2O2}$ mmol$_{metal}^{-1}$h^{-1})	Reduction in bacterial viability (log$_{10}$)	Apparent reaction rate at 30 min (CFU$_{reduction}$h^{-1}mmol$_{metal}^{-1}$)
1 wt.% Au/TiO$_2$	132	7.33	1.6	4.6×10^{10}
0.75 wt.% Au-0.25 wt.% Pd/TiO$_2$	163	7.47	2.4	8.04×10^{10}
0.5 wt.% Au-0.5 wt.% Pd/TiO$_2$	202	7.69	8.1	1.89×10^{11}
0.25 wt.%Au-0.75 wt.% Pd/TiO$_2$	178	6.21	4.1	3.86×10^{10}
1 wt.% Pd/TiO$_2$	173	5.37	2.6	2.79×10^{9}

Reaction conditions: Pelleted Catalyst (0.125 g), Silicon Carbide (3.30 g), 42 mL min^{-1} 2% H_2/air, 0.2 mL min^{-1} bacterial solution, residence time 30 s, 0.5 h, 2 °C.

3.8 Monometallic and Physical Mixtures for the Direct Synthesis of H_2O_2 and *In-situ* Reduction of *E. coli* in a Batch and Flow Regime.

Upon identifying that the inclusion of Au into a 1 wt.% Pd catalyst can increase both the amount of H_2O_2 synthesised and the biocidal activity of the catalyst, it was important to identify the reason. To do so the bimetallic 0.5 wt.% Au-0.5 wt.% Pd/TiO$_2$ catalyst was tested alongside a physical mixture of this catalyst as well as the respective monometallics, 0.5 wt.% Pd/TiO$_2$, 0.5 wt.% Au/TiO$_2$. The results of this testing can be seen in Figure 3.14 and Table 3.6.
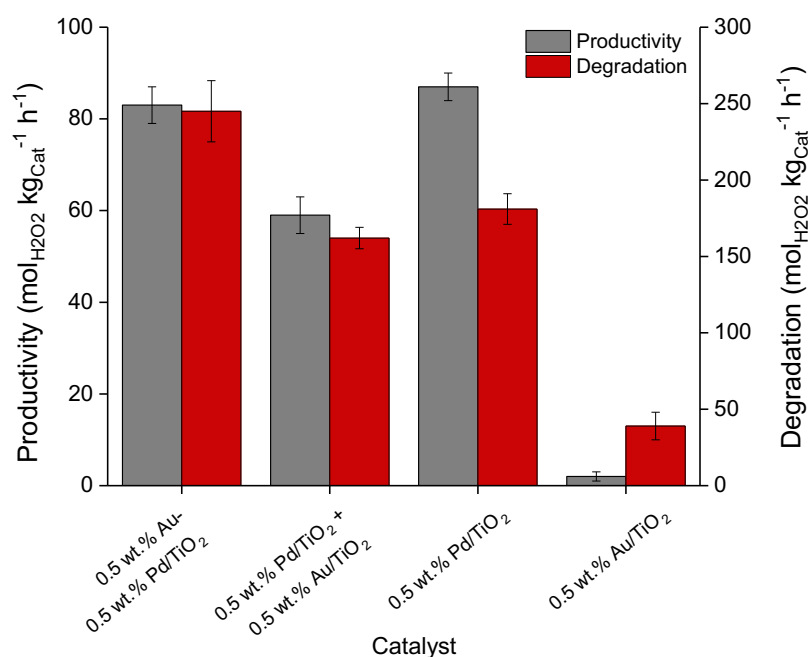
Figure 3.14: Comparing 0.5 wt.% Au/TiO₂, 0.5 wt.% Pd/TiO₂, a physical mixture of a 0.5 wt.% Au/TiO₂ + 0.5 wt.% Pd/TiO₂ to 0.5 wt.%Au-0.5 wt.% Pd/TiO₂ for the direct synthesis and degradation of H_2O_2. **H_2O_2 direct synthesis reaction conditions:** Catalyst (0.01 g), H_2O (2.9 g), MeOH (5.6 g), 5% H_2/CO_2 (420 psi), 25% O_2/CO_2 (160 psi), 0.5 h, 2 °C, 1200 rpm. **H_2O_2 degradation reaction conditions:** Catalyst (0.01 g), H_2O_2 (50 wt.% 0.68 g) H_2O (2.22 g), MeOH (5.6 g), 5% H_2/CO_2 (420 psi), 0.5 h, 2 °C, 1200 rpm.

Table 3.6: Comparing 0.5 wt.% Au/TiO₂, 0.5 wt.% Pd/TiO₂, a physical mixture of a 0.5 wt.% Au/TiO₂ + 0.5 wt.% Pd/TiO₂ to 0.5 wt.%Au-0.5 wt.% Pd/TiO₂ for the rate of H_2O_2 synthesis.

Catalyst	Rate of Reaction $(mol_{H2O2} mmol_{metal}^{-1} h^{-1})$
0.5 wt.% Au-0.5 wt.% Pd/TiO₂	1230
0.5 wt.% Au/TiO₂ + 0.5 wt.% Pd/TiO₂	745
0.5 wt.% Pd/TiO₂	2000
0.5 wt.% Au/TiO₂	117

H_2O_2 direct synthesis reaction conditions: Catalyst (0.01 g), H_2O (2.9 g), MeOH (5.6 g), 5% H_2/CO_2 (420 psi), 25% O_2/CO_2 (160 psi), 0.5 h, 2 °C, 1200 rpm. Rate of reaction calculated using a theoretical metal loading and minimal number of active sites.

The bimetallic 0.5 wt.% Au-0.5 wt.% Pd/TiO$_2$ catalyst is shown to have a similar productivity to the monometallic 0.5 wt.% Pd/TiO$_2$, however a higher degradation (Figure 3.14). However, when comparing the rate of reaction the 0.5 wt.% Pd/TiO$_2$ catalyst has a greater rate of 2000 mol$_{H2O2}$mmol$_{metal}$$^{-1}$h^{-1}. This can be concluded to be due to the lower total metal loading of the catalyst leading to a greater dispersion of the Pd upon the support surface, consequently leading to the formation of smaller Pd nanoparticles which are shown to increase H$_2$O$_2$ selectivity.[24] Furthermore, the rate of reaction for the 0.5 wt.% Pd/TiO$_2$ is much higher than that of the 0.5 wt.% Au-0.5 wt.% Pd/TiO$_2$ catalyst, due to the lower metal loading of the catalyst. For the physical mixture 0.5 wt.% Au/TiO$_2$ + 0.5 wt.% Pd/TiO$_2$ catalyst a reduction in H$_2$O$_2$ synthesis and degradation is observed, this can be explained by the 0.5 wt.% Au/TiO$_2$ catalyst acting as diluent in the catalytic mixture, due to its poor productivity and degradation towards H$_2$O$_2$ (documented in Figure 3.13), reducing the amount of 0.5 wt.% Pd/TiO$_2$ present and subsequently reducing the activity of the catalyst towards H$_2$O$_2$.

Once the many variants of the 1 wt.% AuPd/TiO$_2$ catalyst had been tested for their capacity to generate substantial amounts of H$_2$O$_2$ in. a batch reactor, these catalysts where then tested for their ability to synthesise H$_2$O$_2$ in a continuous flow reactor. The bimetallic 0.5 wt.% Au-0.5 wt.% Pd/TiO$_2$ was the first catalyst to be tested, being reintroduced into the flow reactor. Following this the 0.5 wt.% Pd/TiO$_2$, 0.5 wt.% Au/TiO$_2$ and a physical mixture of the 0.5 wt.% Pd/TiO$_2$ and 0.5 wt.% Au/TiO$_2$ catalysts were each added to the flow reactor individually and tested for the direct synthesis of H$_2$O$_2$, to allow for comparison. The rate of reaction towards H$_2$O$_2$ synthesis is also shown in Table 3.7.

Figure 3.15: Comparing 0.5 wt.% Au/TiO_2, 0.5 wt.% Pd/TiO_2 and a physical mixture of a 0.5 wt.% Au/TiO_2 + 0.5 wt.% Pd/TiO_2 to 0.5 wt.% Au-0.5 wt.% Pd/TiO_2 for (a) the direct synthesis of H_2O_2 and (b) the *in-situ* reduction of *E. coli*. **Reaction conditions (Synthesis):** Pelleted Catalyst (0.125 g), Silicon carbide (3.30 g), 42 mL min^{-1} 2% H_2/air, 0.2 mL min^{-1} HPLC water, 0.5 h, residence time 30 s, 2 °C. **Reaction conditions (E. coli Treatment):** Pelleted Catalyst (0.125 g), Silicon Carbide (3.30 g), 42 mL min^{-1} 2% H_2/air, 0.2 mL min^{-1} bacterial solution, residence time 30 s, 0.5 h, 2 °C.

Table 3.7: Comparing 0.5 wt.% Au/TiO$_2$, 0.5 wt.% Pd/TiO$_2$ and a physical mixture of a 0.5 wt.% Au/TiO$_2$ + 0.5 wt.% Pd/TiO$_2$ to 0.5 wt.% Au-0.5 wt.% Pd/TiO$_2$ for the rate of H$_2$O$_2$ production and the rate of *E. coli* reduction.

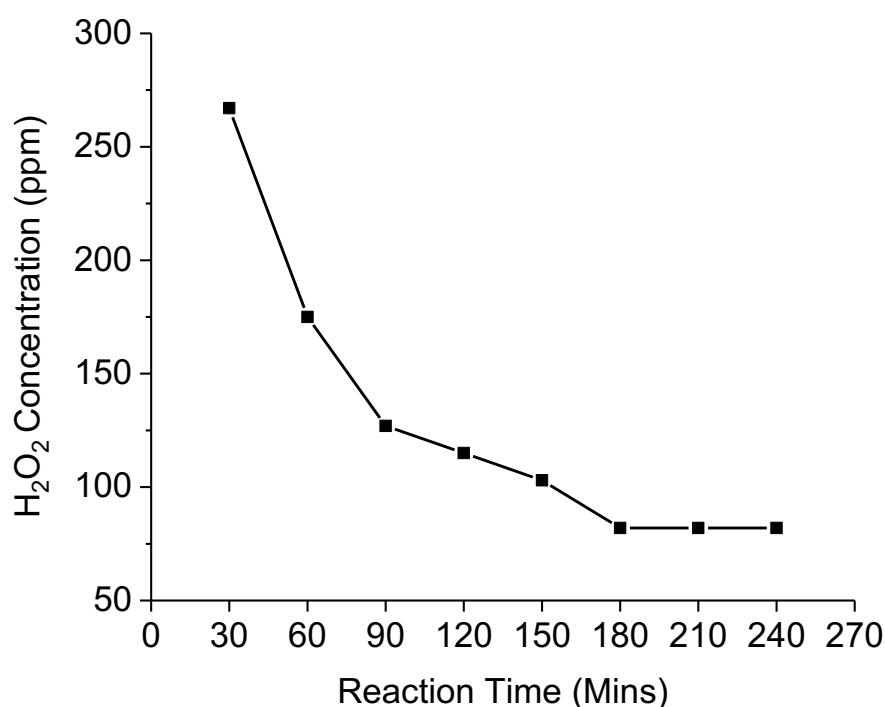| Catalyst	Rate of Reaction (mol$_{H2O2}$mmol$_{metal}$$^{-1}$h^{-1})	Rate of *E.coli* conversion (CFUmL^{-1} (converted) mmol$_{metal}$$^{-1}$h^{-1})
0.5 wt.% Au-0.5 wt.% Pd/TiO$_2$	7.1	221
0.5 wt.% Au/TiO$_2$ + 0.5 wt.% Pd/TiO$_2$	9.1	220
0.5 wt.% Pd/TiO$_2$	15.1	340
0.5 wt.% Au/TiO$_2$	0.1	609

Reaction conditions (Synthesis): Pelleted Catalyst (0.125 g), Silicon carbide (3.30 g), 42 mL min^{-1} 2% H$_2$/air, 0.2 mL min^{-1} HPLC water, 0.5 h, residence time 30 s, 2 °C. **Reaction conditions (E. coli Treatment):** Pelleted Catalyst (0.125 g), Silicon Carbide (3.30 g), 42 mL min^{-1} 2% H$_2$/air, 0.2 mL min^{-1} bacterial solution, residence time 30 s, 0.5 h, 2 °C. Rate of reaction calculated using a theoretical metal loading and minimal number of active sites.

Figure 3.15a demonstrates that the 0.5 wt.% Pd/TiO$_2$ has the greatest capacity to synthesise H$_2$O$_2$, producing 373 mol$_{H2O2}$ kg$_{cat}$$^{-1}$ h^{-1}, even greater than the 1 wt.% Pd/TiO$_2$ catalyst (Figure 3.7). Furthermore, it has a higher rate of reaction for the synthesis of $_{H2O2}$ when compared to the other catalysts in Table 3.7, with a value of 15.1 mol$_{H2O2}$mmol$_{metal}$$^{-1}$h^{-1}. This can be concluded to be due to the lower amount of Pd allowing a greater dispersion upon the TiO$_2$, in turn producing a smaller Pd nanoparticle which has been shown to be more active for the production of H$_2$O$_2$ while subsequently reducing its degradation activity.[24,39] It can also be shown that the physical mixture 0.5 wt.% Au/TiO$_2$ + 0.5 wt.% Pd/TiO$_2$ catalyst also produces more H$_2$O$_2$ than the bimetallic 0.5 wt.% Au-0.5 wt.% Pd/TiO$_2$ catalyst, with this observed activity can be assigned to the aforementioned enhanced activity of the 0.5 wt.% Pd/TiO$_2$ catalyst. For the reduction of *E. coli,* the bimetallic 0.5 wt.% Au-0.5 wt.% Pd/TiO$_2$ catalyst has the most biocidal activity producing a 6.8 log$_{10}$ reduction, more than either the physical mixture or the respective 0.5 wt.% monometallics catalysts (Figure 3.15b). This enhanced biocidal activity can be hypothesised to be because the inclusion of Au improves the ability of the catalyst to desorb the reactive species generated from the catalyst surface in the form of free radicals on route to the synthesis of H$_2$O$_2$, however this is yet to be confirmed. For the rate of *E. coli* conversion however, the 0.5 wt.% Au/TiO$_2$ is shown to be the best with a rate of 609

$CFUmL^{-1}$(converted)$mmol_{metal}^{-1}h^{-1}$, with this being due to the high atomic mass of Au leading to a lower loading of metal on the catalyst for the rate of *E. coli* converted.

3.9 The Effect that Time-on-line Activity has on the Direct Synthesis of H_2O_2 and *In-situ* Reduction of *E. coli* in a Flow Regime.

Upon concluding that the 0.5 wt.% Au-0.5 wt.% Pd/TiO$_2$ is the most active catalyst for both the synthesis of H_2O_2 and the degradation of *E. coli* over a 30-minute timeframe, being able to reproducibly produce an 8-log reduction in *E. coli*, it then needed to be seen if it could produce this same result over an extended period. The same catalyst when tested by Sankar *et. al* [40] under batch conditions was seen to be stable upon re-use, with no loss in H_2O_2 synthesis activity (99 mol_{H2O2} kg_{cat}^{-1} h^{-1}). Therefore, indicating that this same catalyst should hold its ability to synthesise H_2O_2 concentrations of approximately 200 ppm over a similar time frame. To test this theory the bimetallic 0.5 wt.% Au-0.5 wt.% Pd/TiO$_2$ catalyst was reintroduced to the flow reactor under the same flow reactor conditions previously used, however the catalyst is now tested over a 4-hour time frame for its ability to synthesise H_2O_2 with reaction solutions sampled every 30 minutes.

Figure 3.16: Productivity of a 0.5 wt.% Au-0.5 wt.% Pd/TiO$_2$ catalyst towards the direct synthesis of H_2O_2 over 4 hours. **Reaction conditions:** Pelleted Catalyst (0.125 g), Silicon carbide (3.30 g), 42 mL min^{-1} 2% H$_2$/air, 0.2 mL min^{-1} HPLC water, residence time 30 s, 0.5 h, 2 °C.

The results differ from what is expected following the works of Sankar *et. al*[40] as the concentration of H_2O_2 is shown to drastically decrease by more than 50% after the first 90 minutes of testing, before gradually dropping off furthermore and plateauing out at 82 ppm after 3 hours (Figure 3.16). These results indicate the activity of the catalyst is lost over time; however, it cannot be due to limited reactants as fresh water and gas are cycled through the reaction constantly. Furthermore, it cannot be due to leaching of the precious metals as it has been concluded by ICP analysis of the reaction mixture that there is no presence of Au or Pd, over the time frame studied (Table 3.8).

Table 3.8: Leaching of Au and Pd in 0.5 wt.% Au-0.5 wt.% Pd/TiO_2 catalyst, during the H_2O_2 synthesis reaction as a function of reaction time.

Time	Pd Leached (%)	Pd Leached (ppb)	Au Leached (%)	Au Leached (ppb)
30	0	0	0	0
60	0	0	0	0
90	0	0	0	0
120	0	0	0	0
150	0	0	0	0
180	0	0	0	0
210	0	0	0	0
240	0	0	0	0

Reaction conditions: Pelleted Catalyst (0.125 g), Silicon carbide (3.30 g), 42 mL min^{-1} 2% H_2/air, 0.2 mL min^{-1} HPLC water, residence time 30 s, 0.5 h, 2 °C.

Therefore, it can be suggested that the reason for the observed deactivation is due to a change in the state of the active sites on the surface of the catalyst, most probably due to a loss of available active surface area via a change in the state of the active sites themselves with the state of the Pd changing from a mixture of Pd and PdO prior to testing to a PdO dominant surface post-reaction, preventing further H_2O_2 production.

Catalytic bactericidal activity was also determined (Figure 3.17) in a similar manner to that used to measure H_2O_2 synthesis activity (Figure 3.16). To further test the catalyst the HPLC water was swapped for the model greywater solution once again and this was passed through the flow reactor over a 4.5-hour time frame to see if a correlation was observed for the catalysts

ability to act as a biocide over the prolonged time frame, given the information now understood. Once again reaction solutions were removed every 30 minutes and this time plated using the methodology discussed in Chapter 2.5.1.

Figure 3.17: The logarithmic reduction of E. coli over 4.5 hours using a 0.5 wt.% Au-0.5 wt.% Pd/TiO$_2$. **Reaction conditions:** Pelleted Catalyst (0.125 g), Silicon Carbide (3.30 g), 42 mL min^{-1} 2% H$_2$/air, 0.2 mL min^{-1} bacterial solution, residence time 30 s, 0.5 h, 2 °C.

Table 3.9: The effect of time on the rate of H$_2$O$_2$ production and the rate of *E. coli* reduction.

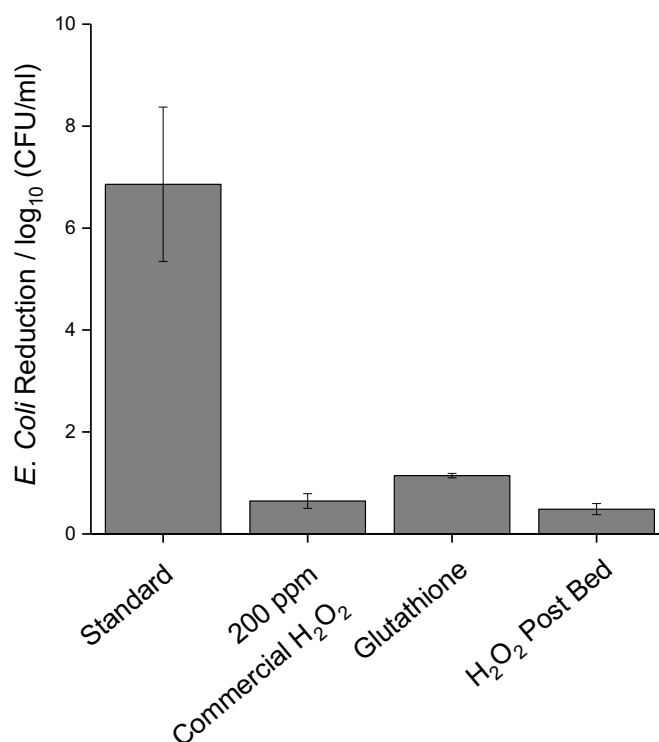| Time (minutes)	Rate of Reaction $(mol_{H2O2}mmol_{metal}^{-1}h^{-1})$	Rate of *E.coli* conversion $(CFUmL^{-1}$ (converted) $mmol_{metal}^{-1}h^{-1})$
30	8.6	221
60	3.1	111
90	1.8	74
120	1.1	55
150	0.7	44
180	0.5	36
210	0.4	30
240	0.3	26
270	0.2	23

Reaction conditions: Pelleted Catalyst (0.125 g), Silicon Carbide (3.30 g), 42 mL min^{-1} 2% H$_2$/air, 0.2 mL min^{-1} bacterial solution, residence time 30 s, 0.5 h, 2 °C. Rate of reaction calculated using a theoretical metal loading and minimal number of active sites.

As seen in Figure 3.17 and Table 3.9, a similar trend to that observed in Figure 3.16 is expressed. The data in Figure 3.17 and Table 3.9 shows that once again after 30 minutes an 8 log reduction returns, however over the first 90-minutes of the reaction, where the amount of *in-situ* and rate of H_2O_2 produced drops $> 50\%$, the logarithmic reduction of the bacterial solution also drops to 2 log_{10}, with the rate of *E. coli* reduction also falling below 2 with a value of 1.8. This drop in the reduction of *E. coli* continues further over the subsequent 3 hours, finally plateauing to a reduction of 1.3 log, which correlates well with the decrease in H_2O_2 produced. These results support the assumption that it is the ROS generated during the direct synthesis of H_2O_2 that are responsible for the reduction of *E. coli*. Therefore, any loss in ROS generation will have a substantial effect on *E. coli* remediation (as observed by the ~3 log_{10} reduction observed upon re-use). The potential loss of surface chloride from the catalyst could be responsible for the observed decrease in catalyst performance. Brehm *et. al*[41] have recently demonstrated by XPS analysis that this is a major concern with catalysts prepared by the excess-chloride co-impregnation procedure. The role of Cl in promoting catalytic performance is well known[14] and as such it is reasonable to conclude that the lack of stability of the materials studied within this work can be attributed to the loss of surface chloride, with no significant loss of active metals observed via ICP-MS analysis of post reaction solutions. There is also the possibility that organic debris generated in the initial 30-minute reaction may lead to catalyst deactivation. To study if this is the possible cause for the observed loss of activity the catalyst could be recovered and calcined at relatively mild temperatures, to remove any of this potential biological matter. If a reactivation of the catalyst is observed this could be concluded as a possibly reason for the documented deactivation. While the biological debris theory has not been tested within this work the proposal that the ROS are responsible for the observed oxidative degradation activity is discussed below.

3.10 Mechanism for the *In-situ* Reduction of *E. coli* in a Flow Regime.

While it is apparent that ROS species aligned with H_2O_2 production via the 1 wt.% AuPd/TiO$_2$ catalysts are responsible for the biocidal activity observed, the mechanism behind how this is achieved is unknown. It is hypothesised that it is the radicals generated in the synthesis (H$^{\bullet}$ + OOH$^{\bullet}$) of H_2O_2 that are responsible for the observed biocidal activity and not the degradation (OH$^{\bullet}$) of H_2O_2 as confirmed by the limited reduction of *E. coli* using commercial H_2O_2. To support this hypothesis glutathione, a well-documented radical scavenger for OOH$^{\bullet}$ and OH$^{\bullet}$,[42,43] was added to the bacterial suspensions to confirm that the radicals are responsible for

the observed biocidal activity. To further support his theory, 200 ppm of *in-situ* generated H_2O_2 from the flow reactor was added post catalyst bed to support the idea that it is the short-lived radicals generated at the surface of the catalyst that are responsible.

Figure 3.18: Reactions to understand the role radicals play in the reduction of *E. coli*. **Reaction conditions: (standard Treatment)** 0.5 wt.% Au-0.5 wt.% Pd/TiO$_2$ (0.125 g), Silicon Carbide (3.30 g), 42 mL min^{-1} H$_2$/air, 0.2 mL min^{-1} bacterial solution, residence time 30 s, 0.5 h, 2 °C. **(Glutathione Treatment)** Glutathione (0.045 g), 0.5 wt.% Au-0.5 wt.% Pd/TiO$_2$ (0.125 g), Silicon Carbide (3.30 g), 42 mL min^{-1} H$_2$/air, 0.2 mL min^{-1} bacterial solution, residence time 30 s, 0.5 h, 2 °C. **(H$_2$O$_2$ Post Bed):** 0.5 wt.% Au-0.5 wt.% Pd/TiO$_2$ (0.125 g), Silicon Carbide (3.30 g), 42 mL min^{-1} H$_2$/air, 0.2 mL min^{-1} HPLC water, bacterial solution (6 mL), residence time 30 s, 0.5 h, 2 °C. Figure use granted in accordance with copyright by Springer Nature.[23]

The data in Figure 3.18 indicates that the short-lived OOH$^{\bullet}$ and OH$^{\bullet}$ radicals generated through the synthesis and/or degradation of H_2O_2 are responsible for the biocidal activity observed for the degradation of *E. coli*. Upon the addition of glutathione, the bactericidal activity dropped to < 1 log$_{10}$ indicating that the radicals have been removed from the reaction solution upon creation and are unable to react and degrade the *E. coli*. In addition to this, a similar < 1 log$_{10}$

reduction was observed when the 200 ppm of *in-situ* H_2O_2 was added post-bed, further supporting the assumption that *E. coli* must be passed over the catalyst bed and in proximity of the short-lived radicals that are generated on the catalysts surface and further indicating the *in-situ* H_2O_2 itself has minimal biocidal activity. The bactericidal efficacy observed near the catalyst bed suggests that reactive species generated over the catalyst are far more effective than the generation of ROS through subsequent H_2O_2 decomposition.

Now that it is affirmed that the radicals are responsible for the observed biocidal activity the next step is to confirm which radicals are responsible. The mechanism for the direct synthesis and degradation of H_2O_2 has been confirmed by Wilson *et. al*[18] and they eluded that three radicals can be generated during of these reactions, these being H•, OOH• and OH•. To comprehend if any of the oxygen-centred radicals are responsible for the reduction of the bacterial concentration spin trapping EPR experiments were ran by Andrea Folli using 5,5-dimethyl-1-pyrroline N-oxide (DMPO) and various gas atmospheres to trap either OOH• and/or OH•.

Figure 3.19(a-b): Identification of key reactive oxygen species responsible for the treatment of greywater pathogens. Experimental (black) and simulated (red) X-band CW-EPR spectra of DMPO radical adducts formed in aqueous solutions passed through the catalyst bed in the flow reactor with different fresh catalysts and different gas feedstocks: (i-vii) 0.5 wt.% Au-0.5 wt.% Pd/TiO₂ catalyst, with (i) 10 bar 5% H₂/N₂; (ii) 200 ppm of synthesised H₂O₂, 10 bar 5% H₂/N₂; (iii) 10 bar 2% H₂/air; (iv) 200 ppm of synthesised H₂O₂ solution, 10 bar air; (v) 200 ppm of commercial H₂O₂, 10 bar air; (vi) 10 bar 5% H₂/N₂ + 5 mM of glutathione; (vii) 10 bar 2% H₂/air + 5 mM of glutathione. (viii-ix) 1 wt.% Pd/TiO₂ catalyst, with (viii) 10 bar 5% H₂/N₂;

(ix) 10 bar 2% H_2/air. (x-xi) 1 wt.% Au/TiO_2 catalyst, with (x) 10 bar 5% H_2/N_2; (xi) 10 bar 2% H_2/air. Spectra (i-xi) were recorded at 25 °C; 5.02 10^4 receiver gain; 100 kHz modulation frequency; 1.5 Gauss modulation amplitude; 6.48 mW microwave power. ^{14}N and ^1H hyperfine couplings are also reported. Spectra i, ii and vi are indicative of a H$^{•}$ trapped by DMPO forming a DMPO-H adduct, characterised by g_{iso} = 2.0057; $a_{iso}(^{14}N)$ = 1.64 mT (x1) and $a_{iso}(^1H)$ = 2.25 mT (x2). Spectra iii, iv, v and xi are indicative of ROS radicals trapped by DMPO forming a DMPO-OH adduct, characterised by g_{iso} = 2.0057; $a_{iso}(^{14}N)$ = 1.48 mT (x1) and $a_{iso}(^1H)$ = 1.48 mT (x1). The presence of DMPO-OH adduct is an indication of the presence of both HO$^{•}$ and HOO$^{•}$, given that the DMPO-OOH adduct has a half-life of 1-4 min (i.e. much shorter than the time passed between sample collection from the reactor and EPR analysis) and decays (given an excess of DMPO) into DMPO-OH.[44,45] Figure use granted in accordance with copyright by Springer Nature.[23]

Figure 3.19a (i-v) show spin trapping EPR experiments using 5,5-dimethyl-1-pyrroline N-oxide (DMPO) and various gas atmospheres. Using 5% H_2/N_2 flow (absence of O_2-derived intermediates), trapping of H$^{•}$ in the reaction solution was observed proving homolytic H_2 cleavage occurs on the catalyst surface and radical diffusion into the surrounding solution (Figure 3.19a (i)). Furthermore, when H_2 and H_2O_2 was fed into the reactor, no radical ROS were detected and only H$^{•}$ was observed (Figure 3.19a(ii)), suggesting that H_2 cleavage is not initiating the production of O-centred radicals from H_2O_2. It is reasonable to suggest that any H_2 activation would lead to reaction with adsorbed O_2 species when both reaction gases are present. No signal associated with H$^{•}$ in solution was detected if both H_2 and O_2 were used (Figure 3.19a (iii)). When H_2O_2, commercial or synthesised, is fed through the reactor limited radical ROS are detected under a pressure of 10 bar, consistent with the limited biocidal activity observed when H_2O_2 is used as a disinfectant (Figure 3.19a (iv-v)). The EPR spin trapping experiments show that, as previously suggested by Li *et. al*[46], that surface bound intermediates can desorb from the catalyst surface as radicals in the case of reaction with H_2 and O_2, and H_2O_2 passing through the catalyst bed but not in the case of H_2 and preformed H_2O_2. When H_2O_2 is synthesised *in-situ*, this will enrich the aqueous solution of newly formed H_2O_2 with a broadband of O-centred radicals available to attack bacterial cells; highly oxidative, short lived and short-range HO$^{•}$ plus longer-range HOO$^{•}/O_2^{•-}$ (Figure 3.19a(iii)). Double integration from spin trapping EPR in conjunction with the calibration curve (based on the calibration in Supplementary Figure 3.27 + 3.28) suggested a concentration of trapped O-centred radicals (in the form of DMPO-OH adduct) equal to 0.66 ± 0.04 μM. When feeding *ex-situ* synthesised

H_2O_2, with or without stabilisers at 200 ppm, the amount of trapped O-centred radicals was quantified between 0.13 ± 0.04 μM and 0.18 ± 0.04 μM corresponding to 22–27% of the amount measured when feeding the reactor with H_2 and O_2. It is important to stress that these concentrations are not the total amount of O-centred radicals released into solution by the Au-Pd catalyst. These are only representative of the number of radicals trapped in the form of the DMPO-OH adduct at the time of measurements (and before the adduct further reacts via side-reactions). Nevertheless, these changes in relative concentrations of the DMPO–OH adduct do follow the changes of total O-centred radicals released by the catalyst. Concentrations in the range of 0.13 to 0.66 μM appear to be much smaller than the concentration of DMPO spin trap added to the water feeding the reactor (8.8 mM). Furthermore, when using a 5% H_2/N_2 gas feed, resulting in the absence of O_2-derived intermediates, the concentration of trapped H$^\bullet$ was 7.8 ± 0.5 μM (based on the calibration in Supplementary Figure 3.27 + 3.28) which, although still much smaller than the concentration of spin trap used, is an order of magnitude larger than the concentration of trapped HO$^\bullet$ and HOO$^\bullet$. These results would suggest that most of the proton-mediated electron transfer events leading to the formation of H_2O_2 are indeed surface reactions with H_2O_2 being the main product being desorbed from the catalyst surface, however the AuPd catalysts are also capable of injecting into solution O-based radicals (HO$^\bullet$/HOO$^\bullet$/$O_2^{\bullet-}$) which can directly attack bacteria as well as sustain further radical formation through reaction with H_2O_2.

Furthermore, no free radical injection into solution is observed with Pd only catalysts (Figure 3.19b(viii-ix)), despite forming H_2O_2. However, a detectable amount of radical ROS is observed with Au only catalysts (Figure 3.19b(xi)). This new observation indicates that the presence of Au is necessary for desorbing reactive species from the catalyst surface in the form of free radicals. This knowledge unearthed by these spin trapping EPR experiments prompts the possibility that the radical ROS released into solution, in conjunction with H_2O_2, can have applications in water disinfection.

The extensive reduction in *E. coli* observed can be associated with fast and extensive loss of membrane function, bacterial homeostasis and the release of intracellular components, driven by HO$^\bullet$ as the primary oxidant species.[47] Lipids and proteins composing the bacterial membrane have been proven to be vulnerable to reactions with HO$^\bullet$ via H abstraction besides other oxidation pathways.[48] At the same time, $O_2^{\bullet-}$ and H_2O_2 are only moderately reactive when

compared to HO$^{•}$[47] and, although they have been associated with internal damage[49] their action would be a much lengthier process regulated by diffusion and mass transport through the membrane and within the cytoplasmatic medium. Therefore, given that i) bactericidal efficacy is likely to result from damage to cellular membranes, rather than to DNA (as indicated by the short reaction time required); ii) *E. coli* expresses the enzymes superoxide dismutase (SOD) and catalase, devoted to inhibiting damage from superoxide and H_2O_2 respectively, but there is no enzymatic mechanism to eliminate HO$^{•}$;[50] and that iii) the reaction kinetics of O-centred radicals in solution (Chapter 1, Figure 1.8) show that conversion of HOO$^{•}$/O$_2$$^{•-}$ into HO$^{•}$ cannot happen; it would appear that the high bactericidal efficacy observed is largely driven by HO$^{•}$ directly formed over the catalyst. Although more work needs to be done to further understand speciation of the radicals in solution and their direct vs. indirect effect on bacterial deactivation, the linear correlation existing between total radical ROS concentration and log kill (Figure 3.20), confirms the enhanced bactericidal effect of using H_2 and O_2 when compared to preformed H_2O_2. This is further corroborated by the near total reduction in bactericidal activity in the presence of glutathione (5 mM), a quencher of HO$^{•}$ (Figure 3.18) with bactericidal activity decreasing to levels equivalent to thar observed when using preformed H_2O_2 (Figure 3.11).
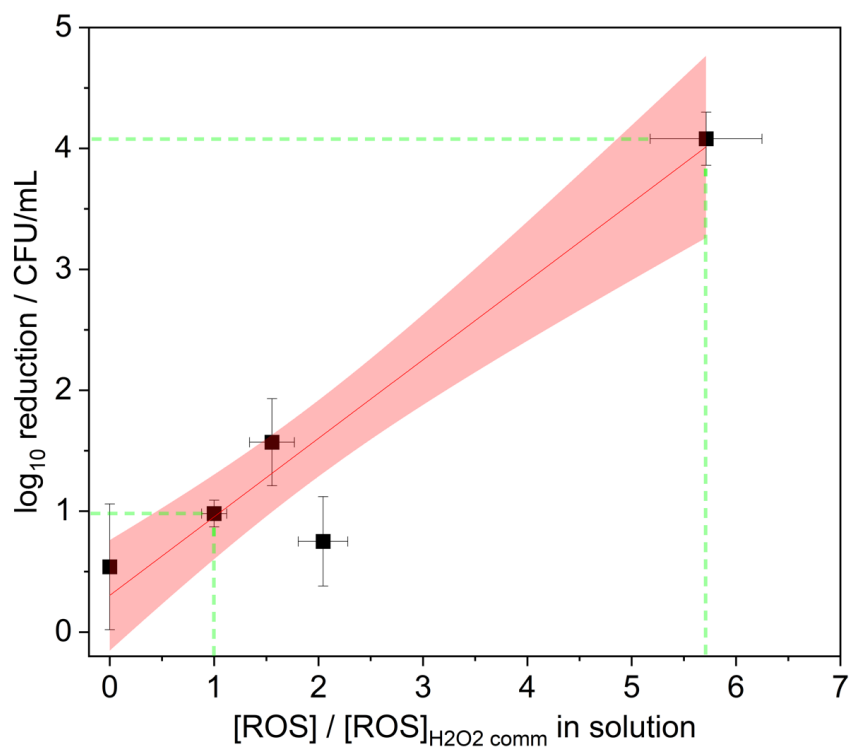
Figure 3.20: Correlation analysis between reduction in bacterial viability ($\log_{10}$) after a single pass through the reactor system and relative (to commercial H_2O_2 and air with fresh 0.5 wt.% Au-0.5 wt.% Pd/TiO_2) amount of ROS radicals; the shaded area represents the 90 % confidence band. Data points are relative to the EPR spectra where either H_2 and air or H_2O_2 and air mixtures were used. Figure use granted in accordance with copyright by Springer Nature.[23]

3.11 The Application of NaOCl for the *In-situ* Reduction of *E. coli* in a Flow Regime.

3.11.1 The Effect the Absence of Catalyst has on the Ability of NaOCl to Reduce the Concentration of *E. coli.*

Once the biocidal activity of the *in-situ* H_2O_2 was affirmed for the removal of high levels of *E. coli,* this system was then compared with a current industrial greywater disinfectant, sodium hypochlorite (NaOCl).[51] To assess the viability of non-catalytic disinfection regimes NaOCl, an active chlorine solution, was fed into the continuous flow reactor in the absence of a catalyst (Figure 3.21). For this study, concentrations between 5-10000 ppm were trialled, with studies showing concentrations between 0.2-5 ppm are capable of treating greywater.[52] The various concentrations were made by dissolving the required amount of commercial NaOCl in HPLC grade H_2O before then passing the solutions through the reactor parallel with the *E. coli* solution utilising a second HPLC pump.
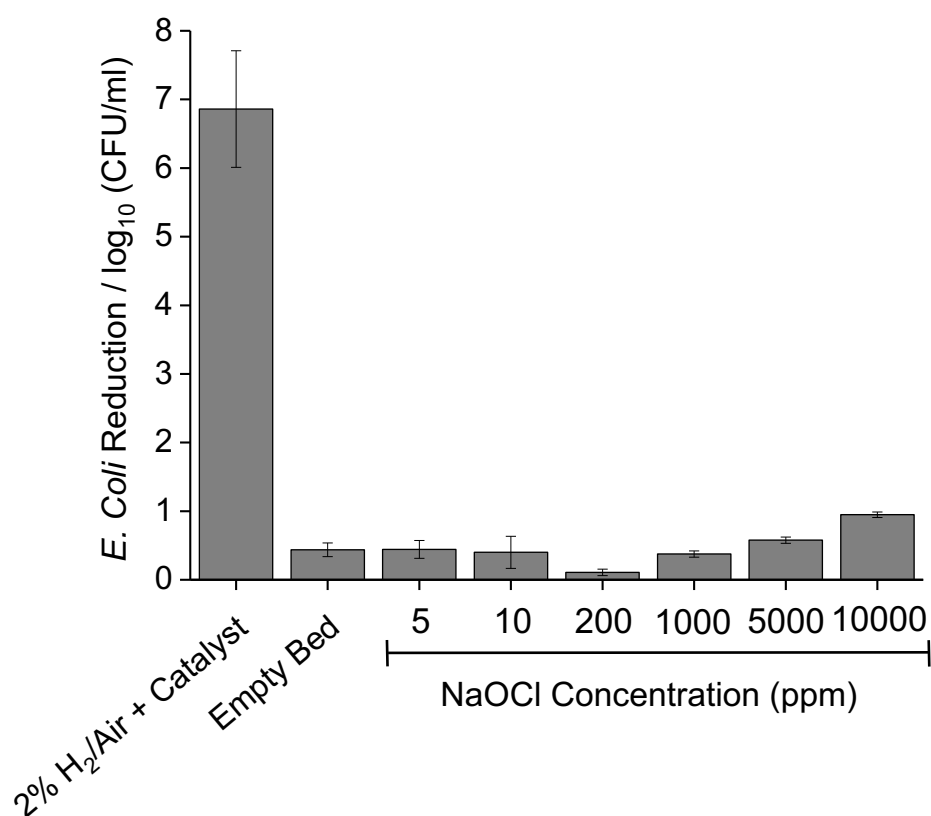
Figure 3.21: The effect of increasing chlorine concentration on the reduction of *E. coli* without a catalyst and in 2% H$_2$/air. **Reaction conditions:** Silicon Carbide (3.30 g), 42 mL min^{-1}, 2% H$_2$/air, 0.18 mL min^{-1} bacterial solution, 0.02 mL min^{-1} sodium hypochlorite solution, 0.5 h, 2 °C.

The results in Figure 3.21 indicate that under the optimal flow conditions, all chlorine concentrations failed to register a significant reduction in *E. coli*. At the lower concentrations the low residence times lead to a reduced biocidal activity consistent with the research conducted by Mazzola *et. al*,[53] which reported that for chlorine derived disinfectants to be highly efficient against *E. coli* they must be subjected to a 35 minute exposure time at a relatively low concentration (0.5 ppm) for a 6 log$_{10}$ reduction. They arrived at this assumption by assigning a numerical value known as the D-value, which is defined as the exposure time required to cause a 1 log$_{10}$ or 90% reduction of a given pollutant, to each disinfectant. Their study concluded that the D value for 500 ppm of NaOCl towards *E. coli* is 6.1 minutes, therefore indicating for the NaOCl to have a substantial biocidal activity a longer contact time than is currently available in the continuous flow reactor (30 seconds)[23] is required for an adequate disinfection of *E. coli* using the chlorine-based disinfectant. In addition, at the higher

NaOCl concentrations the increased alkalinity of the solution has a negative effect on the efficacy of NaOCl as a biocide. This effect is due to the control pH has on chlorines potency as a disinfectant (Figure 3.22). The pH of the treatment solution is of great importance to the relative proportions of either hypochlorous acid or hypochlorite ions present in solution. At the lower hypochlorous acid concentrations the proportion of hypochlorous acid present in solution is virtually 100%, however upon increasing the concentration the pH increases > 7 hypochlorous acid no longer dominates and hypochlorite ion now becomes the dominating species. This drastically reduces the biocidal efficacy of the NaOCl, due to hypochlorous ion being 80x less effect as a biocide when compared to hypochlorous acid.[54] Thus explaining the comparatively poor biocidal activity of the varying NaOCl concentrations when compared to our *in-situ* generated H_2O_2 system.
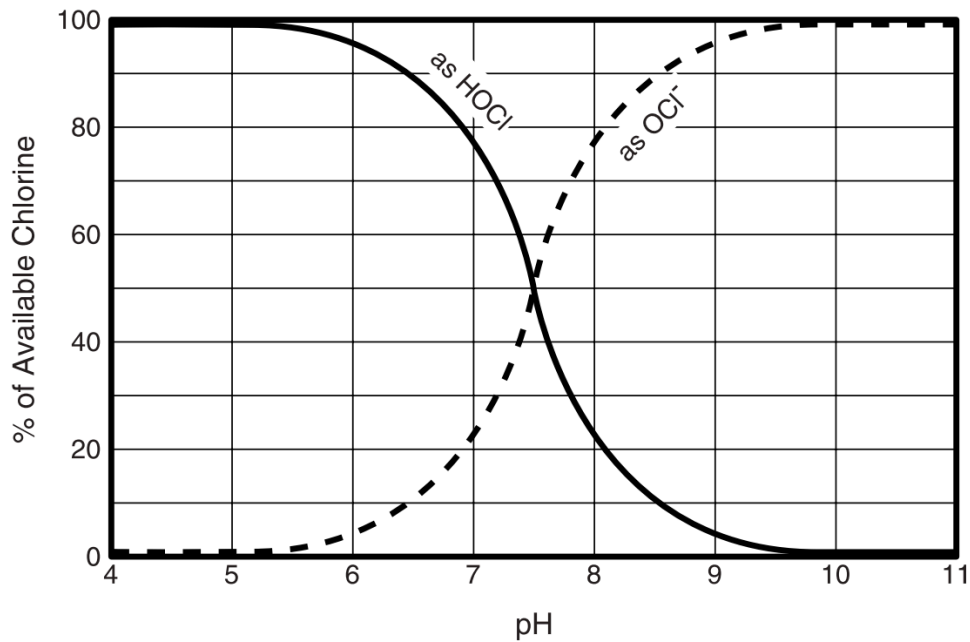
Figure 3.22: Relationship between HOCl and OCl⁻ at various pH values. Figure use granted in accordance with copyright as image right are in the public domain.

3.11.2 The Effect the Absence of H$_2$ has on the Ability of NaOCl to Reduce the Concentration of *E. coli.*

Continuing this study, the same concentrations of the NaOCl were passed through the continuous flow reactor, however this time the 0.5 wt.% Au-0.5 wt.% Pd/TiO$_2$ catalyst was included into the reactor bed to comprehend if the catalyst had any effect on the observed low levels of *E. coli* reduction.
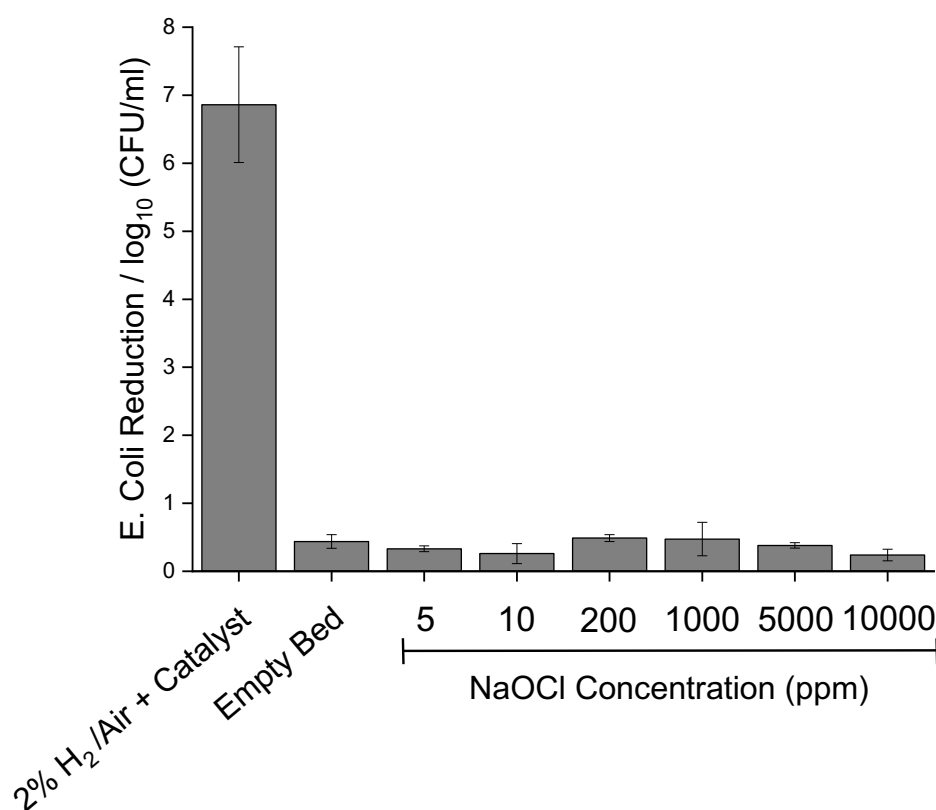
Figure 3.23: The effect of increasing chlorine concentration on the reduction of *E. coli* with a catalyst and in air. **Reaction conditions:** 0.5 wt.% Au-0.5 wt.% Pd/TiO$_2$ (0.125 g), Silicon Carbide (3.30 g), 42 mL min^{-1} air, 0.18 mL min^{-1} bacterial solution, 0.02 mL min^{-1} sodium hypochlorite solution, residence time 30 s, 0.5 h, 2 °C.

The findings observed in Figure 3.23 further illustrate the enhanced efficacy of *in-situ* generated H$_2$O$_2$ when compared to NaOCl, with the biocidal activity of the *in-situ* H$_2$O$_2$ being several orders of magnitude more effective for the removal of *E. coli* with or without the presence of a catalyst. The results show a similarly low *E. coli* reduction across all the concent-

rations of NaOCl used (10000-5 ppm), producing a reduction of < 1log$_{10}$ with the inclusion a cat. This indicates that the inclusion of a catalyst into the continuous flow reactor has no effect on the biocidal activity of NaOCl towards the eradication of *E. coli*.

3.11.3 The Effect the Absence of a Catalyst and H$_2$ has on the Ability of NaOCl to Reduce the Concentration of *E. coli.*

Whilst it has been shown so far that NaOCl in the flow reactor is ineffective for the eradication of *E. coli* from the model greywater solution, all the parameters have not been experimented with. One necessary parameter is the inclusion of H$_2$ in the gas stream, which aids in the formation of the required ROS associated with biocidal activity, however the effect of H$_2$ on the efficiency of NaOCl remains untested. To simulate this, a set of experiments were undertaken in which the same NaOCl concentrations used in the previous experiments were tested for their capacity to incapacitate *E. coli*, however this time the gas feed stream contained only air.
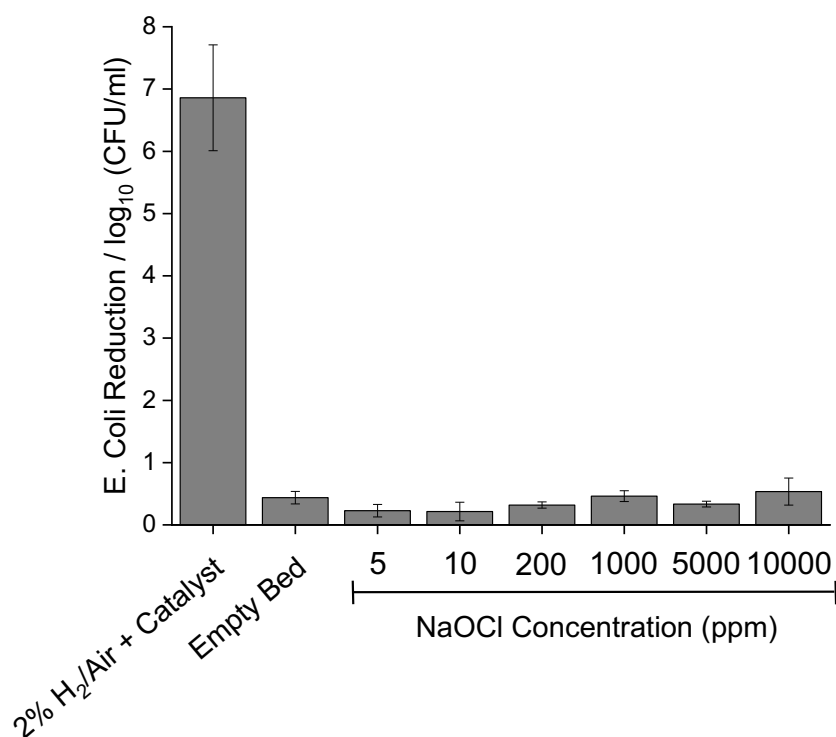

Figure 3.24: The effect of increasing chlorine concentration on the reduction of *E. coli* without a catalyst and in air. **Reaction conditions:** Silicon Carbide (3.30 g), 42 mL min^{-1} air, 0.18 mL min^{-1} bacterial solution, 0.02 mL min^{-1} sodium hypochlorite solution, 0.5 h, 2 °C.

Once again, the data expressed in Figure 3.24 further affirms the superiority of *in-situ* generated H_2O_2 for the removal of *E. coli* when compared to NaOCl. The absence of both the catalyst from the reactor bed and H_2 from the gas feed expresses no noticeable difference in the biocidal activity of NaOCl towards *E. coli*, with all tested concentrations of NaOCl (10000-5 ppm) once again recording a reduction in the levels of *E. coli* of < 1 $\log_{10}$. This illustrates that both of these parameters have no effect on the ability of NaOCl to treat *E. coli* when passed *in-situ* through the continuous flow reactor.

3.12 The Effect of Model Inorganic and Organic Contaminants have on the Synthesis of H_2O_2.

While the *in-situ* radicals generated towards the synthesis of H_2O_2 have a capacity to treat *E. coli* it is unclear if additional pollutants that may be present in greywater will influence the catalyst's ability for this. To examine this, 3 model organic species; 2-methylisoborneol (MIB), geosmin, a bicyclic terpene, and glucose were introduced to a batch reactor, at varying concentrations, and the concentration of H_2O_2 produced by the catalyst was collected. While H_2O_2 production and E. coli reduction have been proven to not show a direct correlation, this test allows the closest comparison possible given it's the ROS generated on route to H_2O_2 that are responsible for its observed biocidal activity.
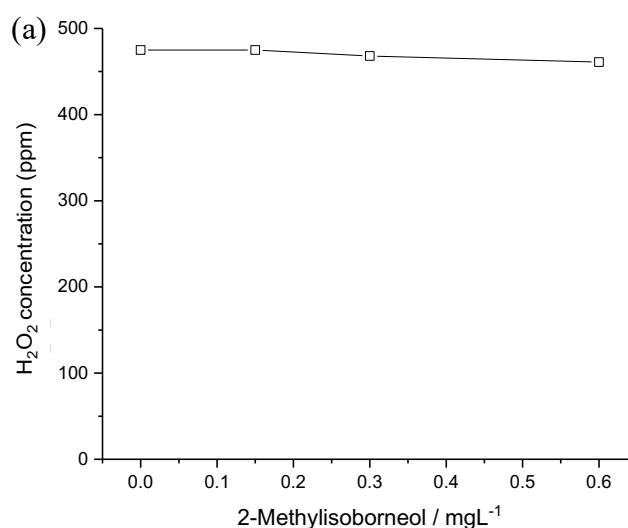
Figure 3.25 (a): The effect of 2-methylisoborneol on the activity of 2.5% Au-2.5% Pd/TiO$_2$ towards H_2O_2 synthesis, under batch conditions. **H_2O_2 direct synthesis reaction conditions:** Catalyst (0.01 g), H_2O (2.9 g), MeOH (5.6 g), 5% H_2/CO_2 (420 psi), 25% O_2/CO_2 (160 psi), 0.5 h, 30 °C, 1200 rpm. Figure use granted in accordance with copyright by Springer Nature.[23]
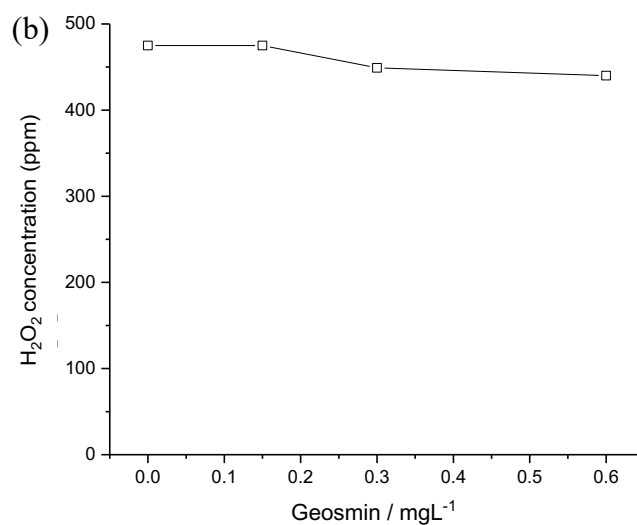
Figure 3.25 (b): The effect of geosmin on the activity of 2.5% Au-2.5% Pd/TiO$_2$ towards H$_2$O$_2$ synthesis, under batch conditions. **H$_2$O$_2$ direct synthesis reaction conditions:** Catalyst (0.01 g), H$_2$O (2.9 g), MeOH (5.6 g), 5% H$_2$/CO$_2$ (420 psi), 25% O$_2$/CO$_2$ (160 psi), 0.5 h, 30 °C, 1200 rpm. Figure use granted in accordance with copyright by Springer Nature.[23]
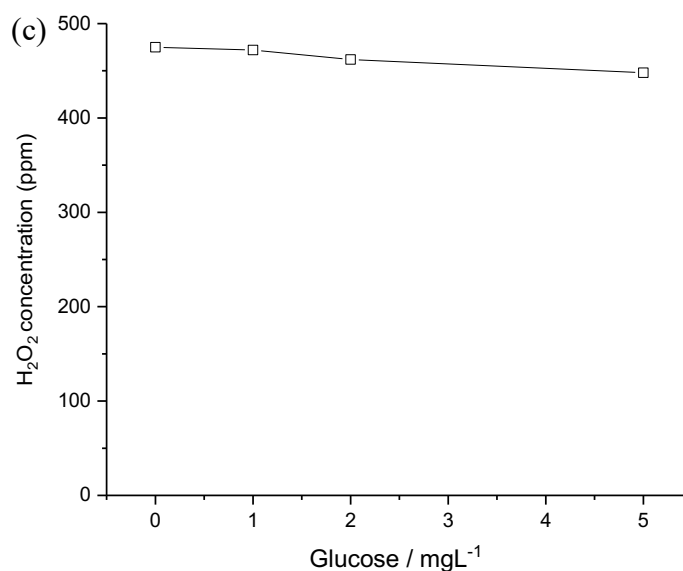
Figure 3.25 (c): The effect of glucose on the activity of 2.5% Au-2.5% Pd/TiO$_2$ towards H$_2$O$_2$ synthesis, under batch conditions. **H$_2$O$_2$ direct synthesis reaction conditions:** Catalyst (0.01

g), H$_2$O (2.9 g), MeOH (5.6 g), 5% H$_2$/CO$_2$ (420 psi), 25% O$_2$/CO$_2$ (160 psi), 0.5 h, 30 °C, 1200 rpm. Figure use granted in accordance with copyright by Springer Nature.[23]

The results established a limited deleterious effect of the model organic species; 2-methylisoborneol, geosmin and glucose, with all three compounds resulting in negligible effects on the catalytic activity towards H$_2$O$_2$ formation (Figure 3.25 a-c), even when increasing the concentration of MIB and geosmin up to 0.6 mg L^{-1} and glucose to 5 mg L^{-1} no more than a ~5% drop in H$_2$O$_2$ formation was displayed.

Additionally, given that underlying geology and local environment can result in appreciable variation in the degree of water quality, including 'hardness' and the concentration of inorganic salt impurities further work was undertaken by Crole *et.al*[55] in which the effect of a range of common ions on catalytic activity towards H$_2$O$_2$ synthesis was investigated. The studies were also undertaken in a batch reactor, utilising a well-studied AuPd catalyst, where under extended contact time the possible influence of common ions could be more easily discerned. It was understood that the addition of common ions such as Na$^+$, Ca^{2+}, Mg^{2+}, Fe^{2+}, CO$_3^{2-}$, NO$_3^-$, PO$_4^{3-}$ and SO$_4^{2-}$ had no significant effect on H$_2$O$_2$ synthesis activity. Perhaps unsurprisingly, given the ability of halide ions to inhibit H$_2$O$_2$ degradation pathways the presence of Cl$^-$ resulted in an appreciable increase in net H$_2$O$_2$ concentration. These discoveries in which the insignificant effect that model inorganic and organic contaminants has on the synthesis of H$_2$O$_2$ further support that this work into the application of *in-situ* generated H$_2$O$_2$ for the treatment of greywater is showing exceptional promise.

3.13 Conclusions.

In this Chapter, it has been shown that a variety of 1 wt.% AuPd/TiO$_2$ catalyst, prepared by excess chlorine wet co-impregnation, have the capacity to synthesise H$_2$O$_2$, with varying degrees of success, in both a batch and flow reactor. Furthermore, it has been concluded that the combination of a continuous flow reactor system and a 0.5 wt.% Au-0.5 wt.% Pd/TiO$_2$ catalyst can lead to the promotion of the release of highly reactive ROS, as identified by EPR analysis, into solution, which have high efficacy in water disinfection.

While in the presence of a 2% H$_2$/air mixture and a 0.5 wt.% Au-0.5 wt.% Pd/TiO$_2$ catalyst this study has shown that a reduction culminating to 8.1 log$_{10}$ in viable bacteria is the optimal catalyst in this study, better than the comparable physical mixture and different 1 wt.%

AuPd/TiO$_2$ catalyst (Table 3.10), representing a 99.999999% reduction in CFU with a 30 s contact time through the packed bed. This is comparable to the bactericidal efficacy reported for a range of alternative approaches, including photocatalytic and photo-Fenton technologies (Table 3.10). However, these routes typically require extended reaction times (on the order of hours) or require the presence of a secondary disinfectant such as ClO$_2$ or preformed H$_2$O$_2$, with the latter generating radical species, responsible for disinfection. While these routes are effective, they do not overcome the health concerns associated with the application of Cl-based disinfectants or preformed H$_2$O$_2$ and the need for continual illumination of the catalyst surface likely precludes this approach from widescale application. By comparison, the rapid generation of ROS from in situ generated H$_2$O$_2$ is far simpler and would not require significant redesign of reactor technology.

Table 3.10: Comparison of bactericidal efficacy using a range of non-traditional processes.[23] Table use granted in accordance with copyright by Springer Nature.[23]

Catalytic System	Initial Conc. of E. *coli* /CFUml^{-1}	Conversion/ %	Method	Time / h	Reference
TiO$_2$/cellulose	6.5 x 10^4	100	Photocatalytic	0.5	[56]
TiO$_2$/PS		94.0	Photocatalytic	0.75	[57]
Fe/TiO$_2$	1x10^5	99.99	Photocatalytic	24	[58]
Non-catalytic (UV+ClO$_2$)	3.57x10^4	99.9	Photocatalytic	24	[59]
Ag/TiO$_2$ +UV H$_2$O$_2$	1x10^8	100	Photocatalytic	0.033	[60]
Non-catalytic (UV/TiO$_2$/H$_2$O$_2$)	8.75x10^4	100	Photocatalytic	0.33	[61]
Fe$_3$O$_4$-SiO$_2$-TiO$_2$	2.4x10^7	98.0	Adsorbent	1.67	[62]
Cu$_2$O/TiO2-NTs	1.86x10^8	99.8	Photocatalytic	7	[63]
Ag/ceramic	1x10^7	99.99999	Flow -Filtration	0.33ml/min	[64]
Ag/ceramic	7 x 10^9 (MPN)/100ml	100	Flow -Filtration	1.5	[65]
CuO-ZnO/ eggshell membrane	1x10^8	Not provided	Adsorption / metal leaching	24	[66]
MoS$_2$ co-catalytic Fe^{2+} / H$_2$O$_2$	1x10^6	100	Fenton	0.5	[67]
Ni-Sb-SnO$_2$	1x10^8	100	Electrocatalytic	0.13	[68]
g-C$_3$N$_4$/m-Bi$_2$O$_4$	1x10^6	100	Photocatalytic	1.5	[69]
B-BiOBr	1x10^7	100	Photocatalytic	0.5	[70]
Ni$_2$P/g-C$_3$N$_4$	1x10^7	100	Photocatalytic	4	[71]
Fe / H$_2$O$_2$ / UV	1.5x10^8	100	Photo-Fenton	3	[72]
TiO$_2$	1x10^8	100	Photocatalytic	3	[73]
FeSO$_4$ / H$_2$O$_2$	1x10^8	100	Photo-Fenton	4	[73]
Fe$_2$O$_3$-AgBr /H$_2$O$_2$	1x10^7	100	Photocatalytic	1	[74]
FeSO$_4$ / H$_2$O$_2$	1x10^6	100	Ultrasound coupled Photo-Fenton	4	[75]
Fe-MABs / H$_2$O$_2$	1x10^7	100	Photo-Fenton	1	[76]

Sample		%	Method		
1 wt.% Au/TiO$_2$ +H$_2$ + O$_2$	1x10^8	95	Heterogeneous Catalysis	0.0083	N/A
0.75 wt.% Au-0.25 wt.% Pd/TiO$_2$ +H$_2$ + O$_2$	1x10^7	99	Heterogeneous Catalysis	0.0083	N/A
0.5 wt.% Au-0.5 wt.% Pd/TiO$_2$ +H$_2$ + O$_2$	1x10^8	99.999999	Heterogeneous Catalysis	0.0083	N/A
0.25 wt.% Au-0.75 wt.% Pd/TiO$_2$ +H$_2$ + O$_2$	4x10^7	99	Heterogeneous Catalysis	0.0083	N/A
1 wt.% Pd/TiO$_2$ +H$_2$ + O$_2$	3x10^7	99	Heterogeneous Catalysis	0.0083	N/A
0.5 wt.% Pd/TiO$_2$ +0.5 wt.% Au/TiO$_2$ H$_2$ + O$_2$	3x10^7	99.9	Heterogeneous Catalysis	0.0083	N/A
0.5 wt.% Pd/TiO$_2$ H$_2$ + O$_2$	2x10^7	99.9	Heterogeneous Catalysis	0.0083	N/A
0.5 wt.% Au/TiO$_2$ H$_2$ + O$_2$	5x10^7	95	Heterogeneous Catalysis		

The bactericidal activity results combined with EPR data (Figure 3.13a and 3.19) shows that a high radical flux in solution is achieved by the bimetallic 0.5 wt.% Au-0.5 wt.% Pd/TiO$_2$ catalyst, however this catalyst is only stable on stream for a 30-minute period before a gradual loss in activity is observed, plateauing out at 60 ppm after a 4-hour period. With this loss in activity also correlating to the catalytic systems ability to degrade the *E. coli* solution, experiencing a similar drop in their biocidal activity. Furthermore, when comparing this bactericidal activity to the monometallic Au and Pd analogues a much larger activity is documented, due to the drop in radical flux present in solution (Figure 3.26). As shown, Pd can catalyse direct formation of H$_2$O$_2$, however the reactive intermediates of the direct synthesis of H$_2$O$_2$ remain on the surface not allowing the generation of the radical flux necessary to achieve high bactericidal efficacy (Figure 3.19b(viii-ix)). On the contrary Au alone has very low activity towards H$_2$O$_2$ production, hence the number of radical species that it is able to generate is low. However, Au facilitates the diffusion into solution (from the catalyst surface) of the reactive intermediates of the direct synthesis of H$_2$O$_2$ in the form of free radicals (Figure 3.19b(xi)). As a result, it is clear that Pd is needed for the generation of a high amount of ROS whilst Au ensures that they are released into solution where they can be used to kill pathogens, enhancing the disinfection mechanism provided by H$_2$O$_2$.
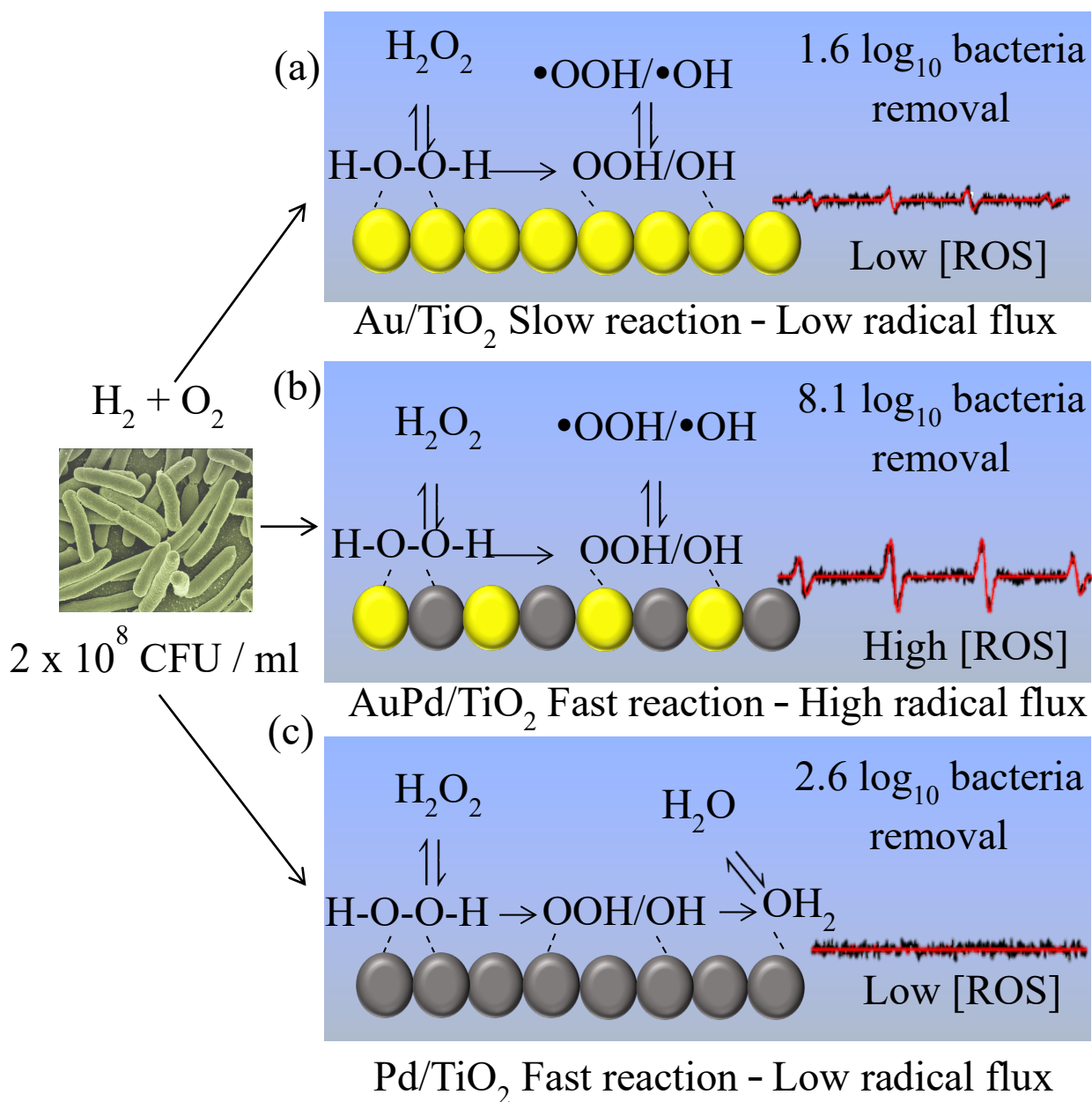
Figure 3.26. Proposed reaction scheme for the *in-situ* remediation of *E. coli*. K12 JM109 by reactive oxygen species over supported (a) Au, (b) AuPd and (c) Pd catalysts, summarising our observations of catalytic performance towards the direct synthesis of H_2O_2 (Figure 3.7) and O-centred radical speciation during the bacteria remediation studies as evidenced by EPR analysis (Figure 3.19).Figure use granted in accordance with copyright by Springer Nature.[23]

When comparing the different types of biocides, under the optimised working conditions, the *in-situ* approach is far more effective than equivalent concentrations of preformed, commercial H_2O_2 and the industrial standard, sodium hypochlorite. The results suggest that $H^{\bullet}$ are not directly involved in the bactericidal activity under the conditions where a high bacterial kill is

observed. Indeed, the low bactericidal activity observed (i.e., < 1 $\log_{10}$ reduction) under 5% H_2/N_2 alone also confirms that H$^\bullet$ are not involved in the killing of the bacteria. EPR spectra with the addition of 5 mM glutathione (Figure 3.19b(vi-vii)) demonstrated that under 5% H_2/N_2, H$^\bullet$ could be detected in solution whereas under H_2 and O_2 mixtures no ROS were detected, supporting the hypothesis that H$^\bullet$ are not responsible for microbicidal activity and that glutathione removed the ROS from solution correlating with the low bactericidal activity.

It was proposed that the difference in radical flux and hence the dramatically increased bactericidal ability of the H_2 and O_2 mixtures in the presence of the AuPd catalyst depends on the initiation steps of the radical flux. In the case of H_2 and O_2, the presence of H$^\bullet$ from homolytic H_2 dissociation initiates the reaction cascade by turning adsorbed O_2 into HO$^\bullet$/HOO$^\bullet$ which either irreciprocally damage the bacterial cells or propagate the radical chain with contribution from synthesised H_2O_2 to support the radical flux away from the catalyst surface. In the case of preformed H_2O_2, the initiation can only occur by cleaving the O-O bond which is known to be kinetically slower when compared to O-O bond cleavage in HOO$^\bullet$, and therefore the radical flux when using preformed H_2O_2 is significantly hindered, as proved by our EPR studies.

This documented significant enhancement in the bactericidal and virucidal activities achieved when reacting H_2 and O_2 rather than using commercial H_2O_2 or chlorination shows the potential of revolutionising water disinfection technologies, i.e., a novel process where, besides the catalyst, inputs of contaminated water and electricity are the only requirements to attain disinfection. Crucially, this process presents the opportunity for rapid disinfection of water at contact times for which conventional biocidal methods are ineffective.

3.14 Future Work.

Given additional time and resources I would have pursued the following issues further:

1. Comprehend how the different processes H_2O_2 reactions (formation, degradation, hydrogenation, and formation) interact together to affect the generation of ROS. Need to think about maximum flux not a concentration.

2. Building on the previous point try to devise a more accurate method to allow for the detection of all the ROS generated during the process of synthesising H_2O_2. Possibly investigate into the use of UV fluorescence for the detection of ROS.[77]

3. Look into developing a way in which ROS can be monitored in a non-invasive way. Current use of monitoring, radical traps, can interfere with the reaction.

4. Research into developing a method in which an accurate link can be made between H_2O_2, $^{\bullet}OH$, $OOH^{\bullet}$, and pathogen kill.

5. Run EPR experiments on the low pathogen reduction experiments to comprehend what is responsible. Quantify if the low pathogen reduction is due to a reduction in the quantity of ROS available or is it due to the chlorine removing from the surface of the catalyst and entering the liquid stream.

6. Research further into the preventing the pathogens being treated using the *in-situ* H_2O_2, and ROS from developing resistance to this treatment.
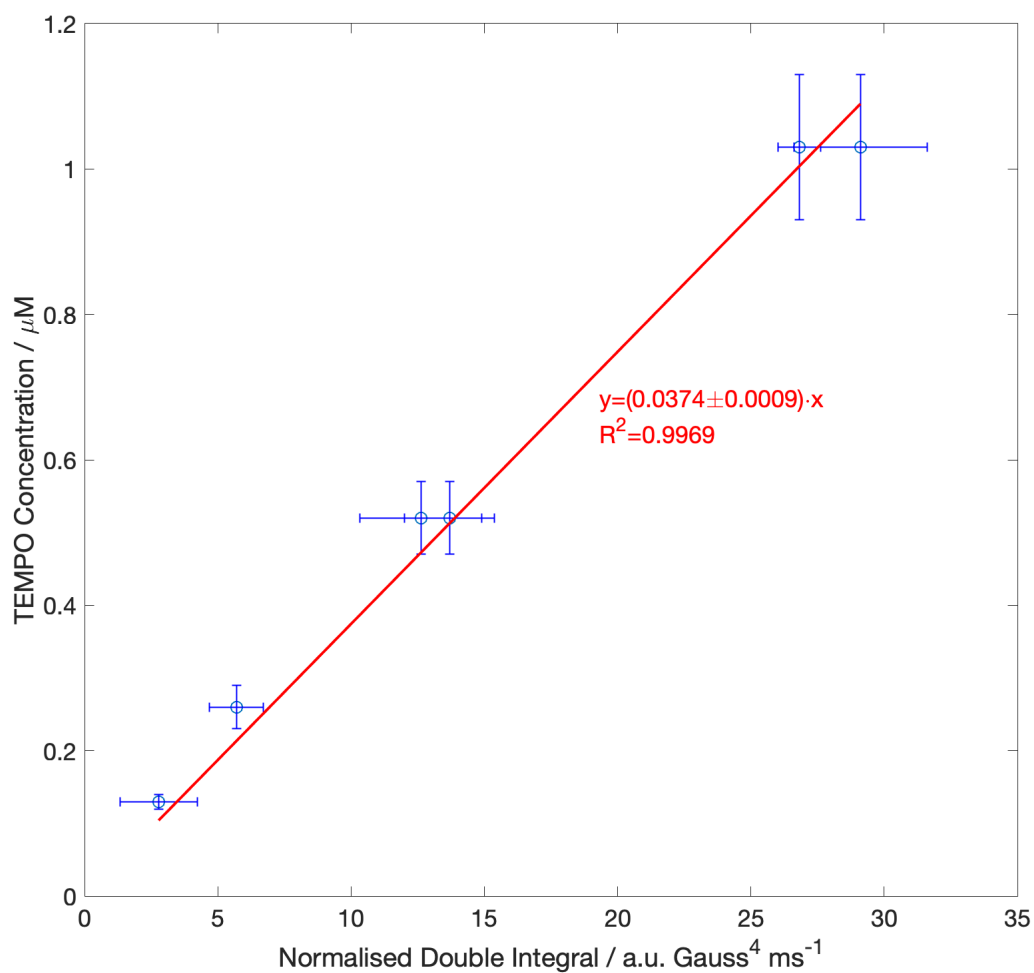
Figure 3.27: 0.1 mM – 1.0 mM calibration curve for the analysis of DMPO radical adducts using EPR. Figure use granted in accordance with copyright by Springer Nature.[23]
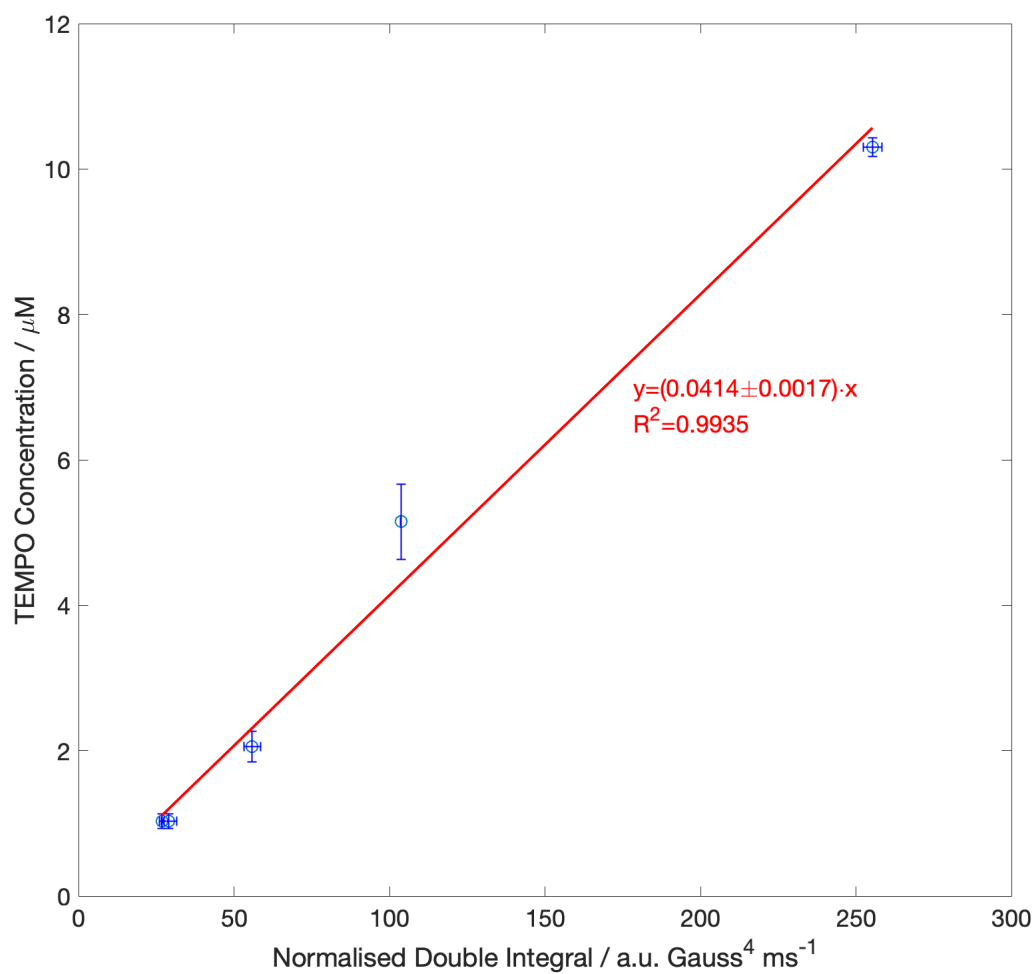
Figure 3.28: 1.0 mM – 10 mM calibration curve for the analysis of DMPO radical adducts using EPR. Figure use granted in accordance with copyright by Springer Nature.[23]

3.16 References.

1   G. Blanco-Brieva, M. C. Capel-Sanchez, M. P. De Frutos, A. Padilla-Polo, J. M. Campos-Martin and J. L. G. Fierro, *Ind. Eng. Chem. Res.*, 2008, **47**, 8011–8015.

2   E. Friedler and Y. Alfiya, *Water Sci. Technol.*, 2010, **62**, 2357–2363.

3   S. Zadeh, D. Lombardi, D. Hunt and C. Rogers, 2019, 1021.

4   World population projected to reach 9.8 billion in 2050, and 11.2 billion in 2100, https://www.un.org/development/desa/en/news/population/world-population-prospects-2017.html, (accessed 25 September 2019).

5   N. Hassanshahi and A. Karimi-Jashni, *Ecotoxicol. Environ. Saf.*, 2018, **161**, 683–690.

6   M. Pidou, F. A. Memon, T. Stephenson, B. Jefferson and P. Jeffery, *Eng. Sustain.*, 2007, **160**, 119–131.

7   X. Zhao and K. Drlica, *Curr. Opin. Microbiol.*, 2014, **21**, 1–6.

8   D. R. Samayamanthula, C. Sabarathinam and H. Bhandary, *Appl. Water Sci.*, 2019, **9**, 1–12.

9   US Pat., US1138520A, 1914.

10   T. A. Pospelova and N. I. Kobozev, *Zh. Fiz. Khim*, 1961, **35**, 1192–1197.

11   T. A. Pospelova, N. I. Kobozev and E. N. Ermin, *Zh. Fiz. Khim*, 1961, **35**, 298–305.

12   T. A. Pospelova and N. I. Kobozev, *Zh. Fiz. Khim*, 1961, **35**, 535–542.

13   P. Landon, P. J. Collier, A. F. Carley, D. Chadwick, A. J. Papworth, A. Burrows, C. J. Kiely and G. J. Hutchings, *Phys. Chem. Chem. Phys.*, 2003, **5**, 1917–1923.

14   E. Ntainjua N., M. Piccinini, J. C. Pritchard, J. K. Edwards, A. F. Carley, J. A. Moulijn and G. J. Hutchings, *ChemSusChem*, 2009, **2**, 575–580.

15   A. Santos, R. J. Lewis, G. Malta, A. G. R. Howe, D. J. Morgan, E. Hampton, P. Gaskin and G. J. Hutchings, *Ind. Eng. Chem. Res.*, 2019, **58**, 12623–12631.

16   M. Sankar, Q. He, M. Morad, J. Pritchard, S. J. Freakley, J. K. Edwards, S. H. Taylor, D. J. Morgan, A. F. Carley, D. W. Knight, C. J. Kiely and G. J. Hutchings, *ACS Nano*, 2012, **6**, 6600–6613.

17   D. A. Crole, R. Underhill, J. K. Edwards, G. Shaw, S. J. Freakley, G. J. Hutchings and R. J. Lewis, *Philos. Trans. R. Soc. A Math. Phys. Eng. Sci.*, 2020, 378, 1-11.

18   N. M. Wilson and D. W. Flaherty, *J. Am. Chem. Soc.*, 2016, **138**, 574–586.

19   N. M. Wilson, P. Priyadarshini, S. Kunz and D. W. Flaherty, *J. Catal.*, 2018, **357**, 163–175.

20   J. Pritchard, M. Piccinini, R. Tiruvalam, Q. He, N. Dimitratos, J. A. Lopez-Sanchez,

D. J. Morgan, A. F. Carley, J. K. Edwards, C. J. Kiely and G. J. Hutchings, *Catal. Sci. Technol.*, 2013, **3**, 308–317.

21   F. Menegazzo, M. Signoretto, E. Ghedini and G. Strukul, *Catalysts*, 2019, **9**, 1-32.

22   R. J. Lewis and G. J. Hutchings, *ChemCatChem*, 2019, **11**, 298–308.

23   T. Richards, J. H. Harrhy, R. J. Lewis, A. G. R. Howe, G. M. Suldecki, A. Folli, D. J. Morgan, T. E. Davies, E. J. Loveridge, D. A. Crole, J. K. Edwards, P. Gaskin, C. J. Kiely, Q. He, D. M. Murphy, J. Y. Maillard, S. J. Freakley and G. J. Hutchings, *Nat. Catal.*, **4**, 575-585.

24   P. Tian, L. Ouyang, X. Xu, C. Ao, X. Xu, R. Si, X. Shen, M. Lin, J. Xu and Y. F. Han, *J. Catal.*, 2017, **349**, 30–40.

25   Y. Li, J. Zhao, L. Chang and Department, *Preperations Catal. V*, 1991, **63**, 145–153.

26   S. J. Freakley, M. Piccinini, J. K. Edwards, E. N. Ntainjua, J. A. Moulijn and G. J. Hutchings, *ACS Catal.*, 2013, **3**, 487–501.

27   S. Ranganathan and V. Sieber, *Catalysts*, 2018, **8**, 1-22.

28   D. A. Crole, S. J. Freakley, J. K. Edwards and G. J. Hutchings, *Proc. R. Soc. A Math. Phys. Eng. Sci.*, 2016, **472**, 1-9.

29   F. Gao and D. W. Goodman, *Chem. Soc. Rev.*, 2012, **41**, 8009–8020.

30   L. Ouyang, P. F. Tian, G. J. Da, X. C. Xu, C. Ao, T. Y. Chen, R. Si, J. Xu and Y. F. Han, *J. Catal.*, 2015, **321**, 70–80.

31   X. Gong, R. J. Lewis, S. Zhou, D. J. Morgan, T. E. Davies, X. Liu, C. J. Kiely, B. Zong and G. J. Hutchings, *Catal. Sci. Technol.*, 2020, **10**, 4635–4644.

32   J. Koivunen and H. Heinonen-Tanski, *Water Res.*, 2005, **39**, 1519–1526.

33   L. Restaino, E. W. Frampton, J. B. Hemphill and P. Palnikar, *Appl. Environ. Microbiol.*, 1995, **61**, 3471–3475.

34   P. A. Christensen, T. P. Curtis, T. A. Egerton, S. A. M. Kosa and J. R. Tinlin, *Appl. Catal. B Environ.*, 2003, **41**, 371–386.

35   O. R. Al-Jayyousi, *Desalination*, 2003, **156**, 181–192.

36   J. K. Edwards, A. Thomas, A. F. Carley, A. A. Herzing, C. J. Kiely and G. J. Hutchings, *Green Chem.*, 2008, **10**, 388–394.

37   W. A. Rutala, D. J. Weber and HICPAC, *Guideline for Disinfection and sterilization in Healthcare Facilities,* 2008, Univeristy of North Carolina Health Care System and School of Medicine, Chapel Hill, 2019.

38   T. Clark, B. Dean and S. Watkins, *Avian Adivce*, 2009, 11, 1-5.

39   N. Gemo, S. Sterchele, P. Biasi, P. Centomo, P. Canu, M. Zecca, A. Shchukarev, K.

Kordás, T. O. Salmi and J. P. Mikkola, *Catal. Sci. Technol.*, 2015, **5**, 3545–3555.

40 M. Sankar, Q. He, M. Morad, J. Pritchard, S. J. Freakley, J. K. Edwards, S. H. Taylor, D. J. Morgan, A. F. Carley, D. W. Knight, C. J. Kiely and G. J. Hutchings, *ACS Nano*, 2012, **6**, 6600–6613.

41 J. Brehm, R. J. Lewis, D. J. Morgan, T. E. Davies and G. J. Hutchings, *Catal. Letters*, 2021, **152**, 254-262.

42 A. Galano and J. R. Alvarez-Idaboy, *RSC Adv.*, 2011, **1**, 1763–1771.

43 F. Ahmadinejad, S. G. Møller, M. Hashemzadeh-Chaleshtori, G. Bidkhori and M. S. Jami, *Antioxidants*, 2017, **6**, 1–15.

44 E. Finkelstein, G. M. Rosen and E. J. Rauckman, *Arch. Biochem. Biophys.*, 1980, **200**, 1–16.

45 E. L. I. D. Finkelstein, R. G. Surgery, O. D. M. Rosen, R. Durham and N. Carolina, *Mol. Pharmacol.*, 1982, **21**, 262–265.

46 J. Li, T. Ishihara and K. Yoshizawa, *J. Phys. Chem. C*, 2011, **115**, 25359–25367.

47 M. Cho, H. Chung, W. Choi and J. Yoon, *Water Res.*, 2004, **38**, 1069–1077.

48 P. Lukes, E. Dolezalova, I. Sisrova and M. Clupek, *Plasma Sources Sci. Technol.*, 2014, 13, 1-25.

49 K. Keyer and J. A. Imlay, *Proc. Natl. Acad. Sci. U. S. A.*, 1996, **93**, 13635–13640.

50 E. Pinto, T. C. S. Sigaud-Kutner, M. A. S. Leitão, O. K. Okamoto, D. Morse and P. Colepicolo, *J. Phycol.*, 2003, **39**, 1008–1018.

51 G. P. Winward, PhD Thesis, Cranfield Univeristy, 2007.

52 D. S. Lantagne, *J. / Am. Water Work. Assoc.*, 2008, **100**, 106-119.

53 P. Gava Mazzola, T. C. Vessoni Penna and A. M. Alzira, *BMC Infect. Dis.*, 2003, **3**, 1–10.

54 P. Telford, *Hydroinstruments*, 2018, **1**, 8.

55 D. A. Crole, PhD Thesis, Cardiff University, 2017.

56 N. De Vietro, A. Tursi, A. Beneduci, F. Chidichimo, A. Milella, F. Fracassi, E. Chatzisymeon and G. Chidichimo, *Photochem. Photobiol. Sci.*, 2019, **18**, 2248–2258.

57 S. Varnagiris, M. Urbonavicius, S. Sakalauskaite, R. Daugelavicius, L. Pranevicius, M. Lelis and D. Milcius, *Sci. Total Environ.*, 2020, **720**, 1-10.

58 Y. Zhao, G. Huang, C. An, J. Huang, X. Xin, X. Chen, Y. Hong and P. Song, *J. Water Process Eng.*, 2020, **33**, 101013.

59 H. M. Murphy, S. J. Payne and G. A. Gagnon, *Water Res.*, 2008, **42**, 2083–2092.

60 S. Sontakke, J. Modak and G. Madras, *Appl. Catal. B Environ.*, 2011, **106**, 453–459.

61   A. Paleologou, H. Marakas, N. P. Xekoukoulotakis, A. Moya, Y. Vergara, N. Kalogerakis, P. Gikas and D. Mantzavinos, *Catal. Today*, 2007, **129**, 136–142.

62   N. Esfandiari, M. Kashefi, S. Afsharnezhad and M. Mirjalili, *Mater. Chem. Phys.*, 2020, **244**, 122633.

63   M. Abidi, A. Hajjaji, A. Bouzaza, K. Trablesi, H. Makhlouf, S. Rtimi, A. A. Assadi and B. Bessais, *J. Photochem. Photobiol. A Chem.*, 2020, **400**, 1-12.

64   D. Van Halem, S. G. J. Heijman, A. I. A. Soppe, J. C. Van Dijk and G. L. Amy, *Water Sci. Technol. Water Supply*, 2007, **7**, 9–17.

65   V. A. Oyanedel-Craver and J. A. Smith, *Environ. Sci. Technol.*, 2008, **42**, 927–933.

66   X. He, D. P. Yang, X. Zhang, M. Liu, Z. Kang, C. Lin, N. Jia and R. Luque, *Chem. Eng. J.*, 2019, **369**, 621–633.

67   J. Liu, C. Dong, Y. Deng, J. Ji, S. Bao, C. Chen, B. Shen, J. Zhang and M. Xing, *Water Res.*, 2018, **145**, 312–320.

68   S. Y. Yang, D. Kim and H. Park, *Environ. Sci. Technol.*, 2014, **48**, 2877–2884.

69   D. Xia, W. Wang, R. Yin, Z. Jiang, T. An, G. Li, H. Zhao and P. K. Wong, *Appl. Catal. B Environ.*, 2017, **214**, 23–33.

70   D. Wu, S. Yue, W. Wang, T. An, G. Li, H. Y. Yip, H. Zhao and P. K. Wong, *Appl. Catal. B Environ.*, 2016, **192**, 35–45.

71   W. Wang, T. An, G. Li, D. Xia, H. Zhao, J. C. Yu and P. K. Wong, *Appl. Catal. B Environ.*, 2017, **217**, 570–580.

72   D. Spuhler, J. Andrés Rengifo-Herrera and C. Pulgarin, *Appl. Catal. B Environ.*, 2010, **96**, 126–141.

73   C. Ruales-Lonfat, N. Benítez, A. Sienkiewicz and C. Pulgarín, *Appl. Catal. B Environ.*, 2014, **160–161**, 286–297.

74   T. W. Ng, L. Zhang, J. Liu, G. Huang, W. Wang and P. K. Wong, *Water Res.*, 2016, **90**, 111–118.

75   S. Giannakis, S. Papoutsakis, E. Darakas, A. Escalas-Cañellas, C. Pétrier and C. Pulgarin, *Ultrason. Sonochem.*, 2015, **22**, 515–526.

76   S. Barreca, J. J. Velez Colmenares, A. Pace, S. Orecchio and C. Pulgarin, *J. Environ. Chem. Eng.*, 2015, **3**, 317–324.

77   X. Chen, X. Tian, I. Shin and J. Yoon, *Chem. Soc. Rev.*, 2011, **40**, 4783–4804.

4 Effect of Reaction Variables on the Conversion of Metronidazole via *In-situ* H₂O₂ Synthesis.

4.1 Introduction.

The composition of greywater can include a vast range of components; however, most commonly mimics the lifestyle of a given area. The chemicals chosen for household laundry, cleaning, and bathing as well as the composition of chemicals used by local industry will vary the collection of contaminants present.[1] Furthermore, the quantity of the pollutants will differ dependent on how densely populated the chosen area is and if there is an agricultural presence adding to potential livestock effluent and further contaminates. Generally, greywater is predominately made up of easily biodegradable organic contaminants such as nutrients (nitrates and phosphorus), xenobiotic organic compounds (XOC's),[2] and biological microbes (faecal coliforms and salmonella). However, with populations growing, in addition to medicinal developments, more complex pollutants are composing greywater including pharmaceuticals products, aerosols,[3] toxic heavy metals,[4,5] and health and beauty products.[3]

The presence of antibiotics as a wastewater, greywater and eco-system contaminant has been a known commodity for as many as 40 years however, the use of catalyst and compounds to eradicate the pollutant has only started gaining attention in the past 20 years.[6] The severity of antibiotic contamination within water supplies has been undermined due to a combination of their continuous use in the modern day lifestyle and the fact that antibiotics have only recently been assigned as a pollutant. Both points have led to a build-up of antibiotic concentrations in aqueous environments over time. This growing application of antibiotics for both human and animals eventually leads to their introduction into wastewater effluents from municipal treatments plants,[7] hospital effluents[8] and livestock activities.[9] Metronidazole, a common antibiotic primarily used in the treatment of anaerobic protozoan and bacterial infections, has been found to be one of the most prominent antibiotics found in wastewater from hospital effluent,[10] as shown in Table 4.1.[11] As such it is important to remove metronidazole and other antibiotics from waste streams prior to discharge into water bodies as this can lead to antibiotic resistance.

Table 4.1: Concentrations (µg/L) of studied antibiotics in wastewater of a rural hospital in Vietnam. Table use granted in accordance with copyright by MDPI.[11]

Month	MET *		SUL		TRI *		CEF		CIP *		OFL *		SPI *	
	WBT	WAT	WBT	WAT	WBT	WAT	WBT	WAT	WBT	WAT	WBT	WAT	WBT	WAT
January	0.1	0.1	1.9	1.9	3.7	0.7	-	-	18.0	9.8	3.1	0.8	2.0	0.5
February	-	-	0.4	0.2	1.2	0.1	-	-	26.0	6.4	1.2	1.1	0.4	-
March	0.2	-	2.7	2.9	4.3	0.5	11.0	5.0	56.4	39.5	-	-	0.7	0.4
April	0.2	0.2	12.2	3.7	15.5	0.8	2.8	2.6	66.0	16.2	9.4	2.0	0.8	0.2
May	0.2	-	3.2	3.8	3.0	0.5	-	-	7.9	5.6	7.1	-	0.5	0.4
June	1.2	-	1.2	4.5	1.4	0.7	-	-	17.4	11.0	-	-	0.9	0.3
July	2.1	0.2	3.7	3.4	1.8	0.5	-	-	16.1	13.9	2.0	-	4.3	2.2
August	-	-	23.5	20.3	5.7	4.3	-	-	26.3	19.5	3.1	2.0	-	-
September	19.9	16.4	17.2	11.0	2.8	0.9	-	-	79.9	48.1	5.3	4.6	8.4	1.2
October	-	-	25.5	11.2	19.1	5.0	-	-	71.5	16.3	5.2	-	2.9	0.6
November	6.3	-	17.5	8.3	10.9	2.7	-	-	87.3	53.3	9.7	7.4	-	-
December	1.0	-	9.1	5.4	22.4	1.1	-	-	41.3	18.7	9.7	7.1	-	-
Total	31.3	16.9	118.0	76.5	91.8	17.9	13.8	7.6	514.0	258.2	55.7	25.1	20.9	5.8
Mean	2.6	1.4	9.8	6.4	7.7	1.5	1.2	0.6	42.8	21.5	4.6	2.1	1.7	0.5
Average Difference		46.0%		35.2%		80.5%		45.0%		49.8%		54.9%		72.3%

WBT: Wastewater before treatment; WAT: Wastewater after treatment; "-": Below Limit of Detection; * Differences between mean values of antibiotic concentrations before and after wastewater treatment are significant (p values are presented below with antibiotic names); MET: Metronidazole (p = 0.01); SUL: Sulfamethoxazole (p = 0.06); TRI: Trimethoprim (p = 0.002); CEF: Ceftazidime (p = 0.16); CIP: Ciprofloxacin (p = 0.002); OFL: Ofloxacin (p = 0.003); SPI: Spiramycin (p = 0.004).

The ability of metronidazole to treat bacterial infection leads to its application towards the treatment of both humans and animals, increasing its capacity to enter waste streams.[12] In addition, there have been concerns regarding the side effects of the drug entering waste streams, with the molecule and its metabolites found to possess a collection of mutagenic, toxic and carcinogenic properties towards a select few animal species.[10] With this discovery it is paramount that metronidazole concentrations in water effluents are reduced to the upmost amount as not to enter the human body, which could lead to antibiotic resistance[13] and cell mutation, of livestock, with the EU and US banning the use of any metronidazole containing livestock for consumption.[10]

Following this, it is key to understand the mechanism by which it is possible to denature metronidazole and prevent it from influencing aquatic environments and human life. The use of reactive oxygen species (ROS) to denature greywater contaminates is well documented following research by Koivunen *et. al*[14] and a review by Marquez *et. al*[15] which both indicated that ROS can be used to degrade *E. Coli* alongside alternative organic matter and pesticides respectively. Furthermore, research has shown that advanced oxidation processes have shown

promise for the degradation of such pollutant.[16–18] These processes theoretically could completely oxidise the antibiotic, following sequential oxidation reactions, to form CO_2, H_2O, and inorganic ions,[15] which can be easily filtered out of solution meaning no further treatment would be required. Antibiotics have shown susceptibility to ROS generated during advanced oxidation processes,[6] showing susceptibility to ROS catalysed degradation via a UV and UV/H_2O_2 process.[19] Additionally, a study undertaken by Ammar *et. al*[20] into the ability of sunlight, via a photo-Fenton process, when used in conjunction with H_2O_2 to degrade metronidazole, hypothesised a mechanism. As shown in Figure 4.1, and supported by further research,[21–23] the application of peroxy radicals to metronidazole has shown the potential to completely denature the molecule, while breaking open the key nitroimidazole ring responsible for the mutagenic capacity of the molecule. Furthermore, metronidazole has been shown to be degraded by ROS, generated via photocatalysis,[16] electrochemical oxidation,[22] and photo-Fenton's pathways.[18]
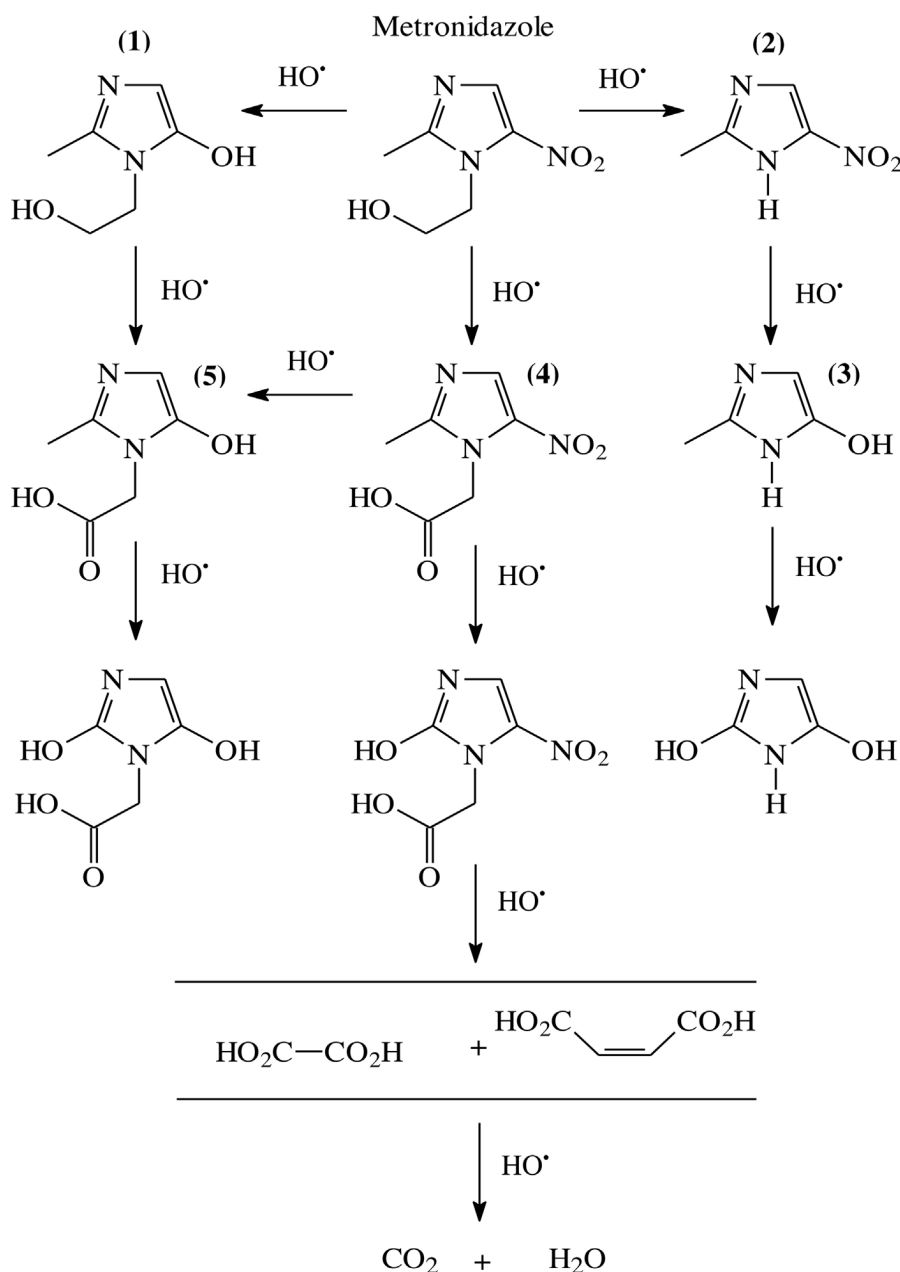
Figure 4.1: Proposed degradation pathway of metronidazole via hydroxyl radicals. Figure use granted in accordance with copyright by Elsevier.[20]

Additionally, Chen *et. al*[24] have shown that it is also plausible to degrade metronidazole via an hydrogenation reduction pathway utilising nanoscale zero-valent iron (NZVI). Therefore, the potential hydrogenation of the metronidazole molecule must be considered when testing commences, with the possibility of hydrogenation of the metronidazole molecules nitro group and/or its C=C and C=N functionalities (Figure 4.2).
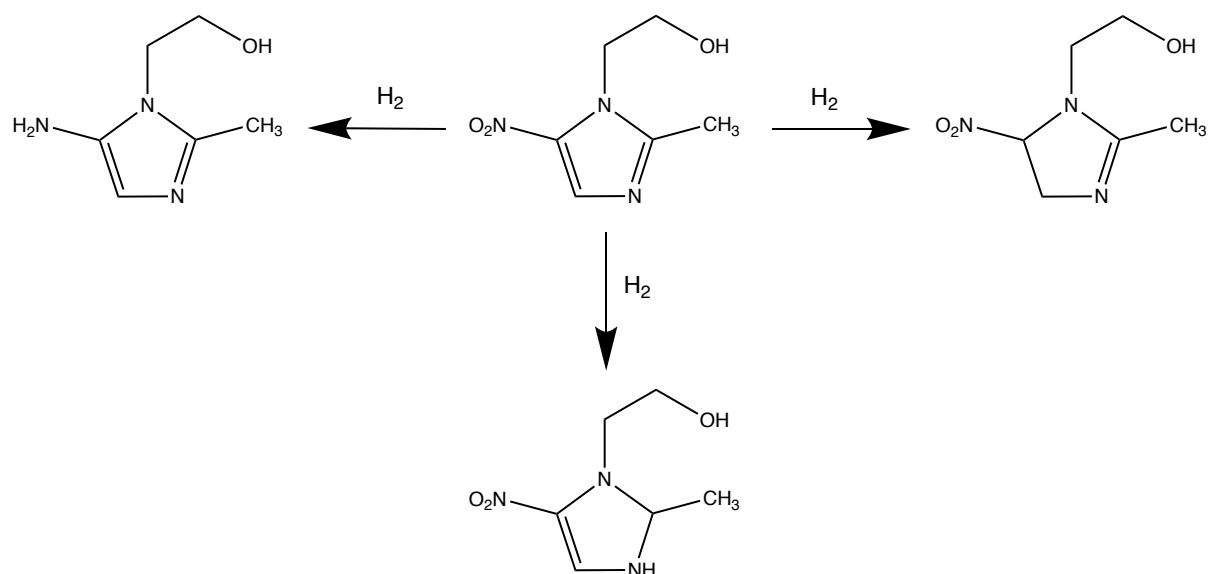
Figure 4.2: Proposed reaction pathways for the hydrogenation of metronidazole.

Therefore, following on from the investigation in Chapter 3, in which the ability of the 1 wt.% AuPd/TiO$_2$ catalysts to produce ROS and the ability of such species to denature *E. coli* was identified. Metronidazole was subsequently chosen to determine if a similar approach could be utilised to degrade chemical pollutants.

4.2 The Effect of Reaction Variables on the Synthesis of H$_2$O$_2$.

Initial experimentation was conducted to transition towards reaction conditions that would be used for the treatment of greywater. Previous research has shown that in a batch reactor a 0.5 wt.% Au-0.5 wt.% Pd/TiO$_2$ catalyst has the capability to generate 82 mol$_{H2O2}$ kg$_{cat}^{-1}$ h^{-1} of H$_2$O$_2$. However, these batch reactor experiments were conducted at 2 °C, with methanol and using CO$_2$ diluted gases, all of which would be impractical for the real-world application of the treatment of greywater. This is because greywater is predominately kept at temperatures between 18-35 °C, due to the warm water originating from personal hygiene and cooking activities.[1] Additionally, methanol will not be added to the greywater solution due to the toxicity if ingested in addition to the increased cost associated with removing the co-solvent from the treatment samples[25] and finally CO$_2$ diluent gases would not be used once again due to the increased cost of using it as a gas diluent will likely prevent its use on an industrial scale.[25]. As such, it is first important to determine the effect of reaction conditions on catalytic performance to H$_2$O$_2$ synthesis. Using the 0.5 wt.% Au-0.5 wt.% Pd/TiO$_2$ catalyst reaction

parameters were transitioned away from those previously established for optimal H_2O_2 production to those likely to be utilised for real-world application. The results for the transitioning of these reaction conditions are shown below in Figure 4.3 and Table 4.2.
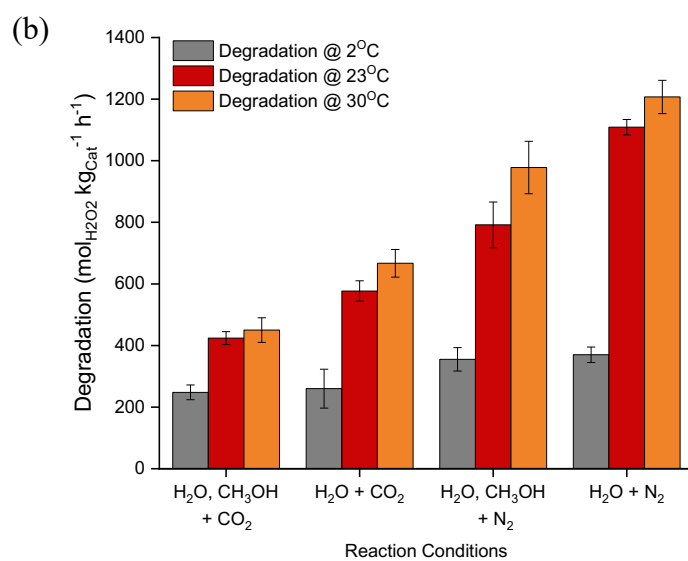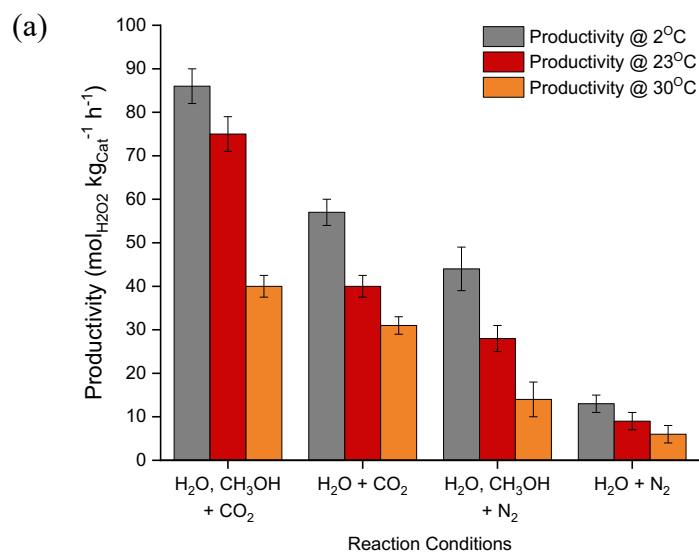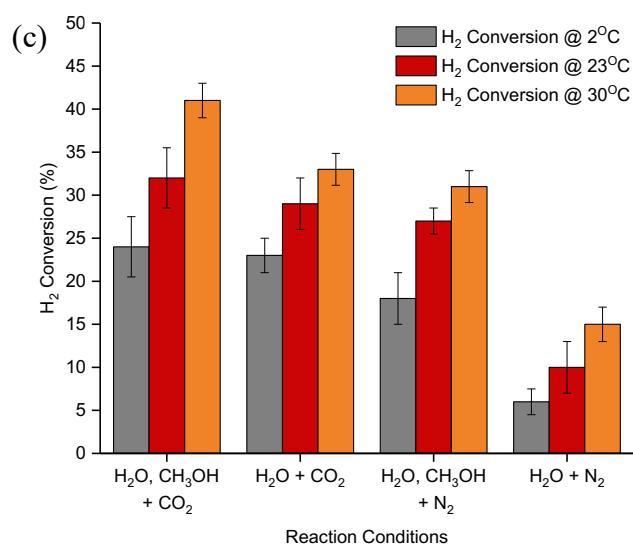
Figure 4.3 (a-c): The effect of gas mixture, solvent, and temperature on the productivity (a), degradation (b) and H_2 conversion (c) towards the direct synthesis of H_2O_2 in the presence of a 0.5 wt.% Au-0.5 wt.% Pd/TiO_2 catalyst. **H_2O_2 direct synthesis reaction conditions (CO_2):** Catalyst (0.01 g), H_2O (2.9 g), MeOH (5.6 g), 5% H_2/CO_2 (420 psi), 25% O_2/CO_2 (160 psi), 0.5 h, 2 °C, 1200 rpm. **H_2O_2 degradation reaction conditions (CO_2):** Catalyst (0.01 g), H_2O_2 (50 wt.% 0.68 g), H_2O (7.82 g), 5% H_2/CO_2 (420 psi), 0.5 h, 2 °C, 1200 rpm. **H_2O_2 direct synthesis reaction conditions (N_2):** Catalyst (0.01 g), H_2O (8.5 g), 5% H_2/N_2 (420 psi), 25% O_2/N_2 (160 psi), 0.5 h, 30 °C, 1200 rpm. **H_2O_2 degradation reaction conditions (N_2)** Catalyst (0.01 g), H_2O_2 (50 wt.% 0.68 g), H_2O (7.82 g), 5% H_2/N_2 (420 psi), 0.5 h, 30 °C, 1200 rpm.

Table 4.2: The effect of gas mixture, solvent, and temperature has on the H_2O_2 selectivity towards the direct synthesis of H_2O_2 in the presence of a 0.5 wt.% Au-0.5 wt.% Pd/TiO$_2$ catalyst.

Reaction Conditions	H_2O_2 Selectivity at 2°C (%)	H_2O_2 Selectivity at 23°C (%)	H_2O_2 Selectivity at 30°C (%)
H_2O, CH_3OH + CO_2	54	23	8
H_2O + CO_2	33	13	6
H_2O, CH_3OH + N_2	21	11	5
H_2O + N_2	7	3	2

H_2O_2 direct synthesis reaction conditions (CO$_2$): Catalyst (0.01 g), H_2O (2.9 g), MeOH (5.6 g), 5% H_2/CO$_2$ (420 psi), 25% O_2/CO$_2$ (160 psi), 0.5 h, 2 °C, 1200 rpm. **H_2O_2 degradation reaction conditions (CO$_2$):** Catalyst (0.01 g), H_2O_2 (50 wt.% 0.68 g), H_2O (7.82 g), 5% H_2/CO$_2$ (420 psi), 0.5 h, 2 °C, 1200 rpm. **H_2O_2 direct synthesis reaction conditions (N$_2$):** Catalyst (0.01 g), H_2O (8.5 g), 5% H_2/N$_2$ (420 psi), 25% O_2/N$_2$ (160 psi), 0.5 h, 30 °C, 1200 rpm. **H_2O_2 degradation reaction conditions (N$_2$)** Catalyst (0.01 g), H_2O_2 (50 wt.% 0.68 g), H_2O (7.82 g), 5% H_2/N$_2$ (420 psi), 0.5 h, 30 °C, 1200 rpm.

It was observed that increasing reaction temperature from 2 °C towards 30 °C led to a decrease in net H_2O_2 production, while increasing both H_2 conversion and H_2O_2 degradation (Figure 4.3 a-c). This was to be expected given the low stability of H_2O_2 at mild temperatures[25] and the fact that sub-ambient temperatures are well documented to promote H_2O_2 stability through the inhibition of both the decomposition and hydrogenation pathways.[26] As such it is possible to correlate the reduction in the observed H_2O_2 synthesis rate and increased degradation rate to reaction temperature. However, this may not be desired if the aforementioned hydrogenation of metronidazole is the dominant pathway towards its degradation.

The effect of changing the gas mixture diluent from CO_2 to N_2 showed a similar effect to that observed with increasing reaction temperature, once again decreasing H_2O_2 production and increasing H_2O_2 degradation. This can be explained by the ability of CO_2 to form carbonic acid *in-situ* by dissolving in the solvent at elevated pressure, in turn lowering the pH of the reaction solution and increasing H_2O_2 production by making the solvent acidic and suppressing the subsequent decomposition reaction.[27] However, H_2 conversion reduced upon replacing CO_2 for N_2. The decrease in H_2O_2 production and the increase in H_2O_2 degradation (Figure 4.3a + b),

can be assigned to a decrease in H_2 solubility that is documented in reactions without both CO_2 and methanol.[28] Similarly it is possible to attribute the decrease of H_2 conversion in methanol to the ability of CO_2 to promote H_2 solubility (Figure 4.3c). Finally, methanol was removed from the solvent mixture, and this was met with an increase in H_2O_2 production and a decrease in both H_2O_2 degradation and H_2 conversion. This result is related to a decrease in H_2 solubility when methanol/water solvent mixture is replaced with a water-only solvent mixture,[29] which leads to a reduction in H_2O_2 formation and an increase towards H_2O_2 degradation.[30]

4.3 The Effect of AuPd Alloying on the Direct Synthesis of H_2O_2.

Subsequently the possible synergistic effects that may result from the alloying Au with Pd was investigated, under non-idealised reaction conditions and is shown in Figure 4.4.
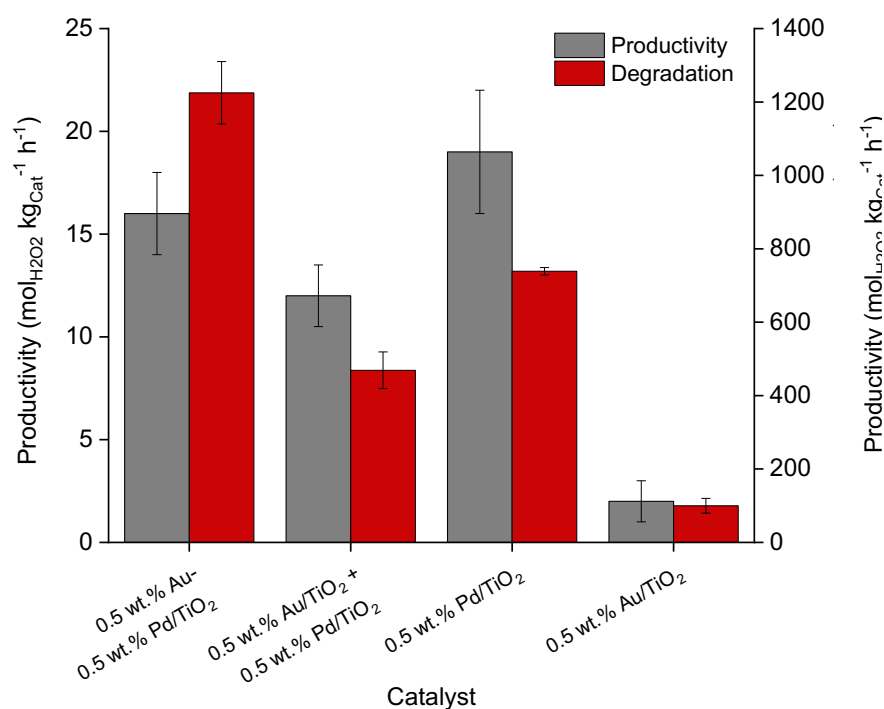
Figure 4.4: The effect of metal alloying on the catalytic activity towards H_2O_2 synthesis and its subsequent degradation under non-idealised reaction conditions. **H_2O_2 direct synthesis reaction conditions (N_2):** Catalyst (0.01 g), H_2O (8.5 g), 5% H_2/N_2 (420 psi), 25% O_2/N_2 (160 psi), 0.5 h, 30 °C, 1200 rpm. **H_2O_2 degradation reaction conditions (N_2)** Catalyst (0.01 g), H_2O_2 (50 wt.% 0.68 g), H_2O (7.82 g), 5% H_2/N_2 (420 psi), 0.5 h, 30 °C, 1200 rpm.

181

Table 4.3: Comparison of the monometallics, the alloyed catalyst and a physical mixture on the productivity, H_2O_2 wt.%, degradation and H_2 conversion towards the direct synthesis of H_2O_2 in the presence of a 0.5 wt.% Au-0.5 wt.% Pd/TiO$_2$ catalyst

Catalyst	H_2O_2 Productivity $(mol_{H2O2}\ kg_{cat}^{-1}\ h^{-1})$	H_2O_2 (Wt. %)	H_2 Conversion (%)	H_2O_2 Degradation $(mol_{H2O2}\ kg_{cat}^{-1}\ h^{-1})$
0.5 wt.% Au-0.5 wt.% Pd/TiO$_2$	16	0.03	17	1230
0.5 wt.% Au + 0.5 wt.% Pd/TiO$_2$	12	0.02	25	469
0.5 wt.% Pd/TiO$_2$	18	0.04	33	739
0.5 wt.% Au /TiO$_2$	2	0.004	3	100

H_2O_2 direct synthesis reaction conditions (N_2): Catalyst (0.01 g), H_2O (8.5 g), 5% H_2/N_2 (420 psi), 25% O_2/N_2 (160 psi), 0.5 h, 30 °C, 1200 rpm. **H_2O_2 degradation reaction conditions (N_2)** Catalyst (0.01 g), H_2O_2 (50 wt.% 0.68 g), H_2O (7.82 g), 5% H_2/N_2 (420 psi), 0.5 h, 30 °C, 1200 rpm.

The monometallic 0.5 wt.% Pd/TiO$_2$ catalyst was shown to have a comparable activity towards the synthesis of H_2O_2, (18 $mol_{H2O2}\ kg_{cat}^{-1}\ h^{-1}$), as the bimetallic 0.5 wt.% Au-0.5 wt.% Pd/TiO$_2$ catalyst (16 $mol_{H2O2}\ kg_{cat}^{-1}\ h^{-1}$). In addition, the 0.5 wt.% Pd/TiO$_2$ catalyst also has a lower degradation activity of 739 $mol_{H2O2}\ kg_{cat}^{-1}\ h^{-1}$ (Figure 4.4) than the bimetallic 0.5 wt.% Au-0.5 wt.% Pd/TiO$_2$ catalyst (1230 $mol_{H2O2}\ kg_{cat}^{-1}\ h^{-1}$). This can be attributed to the same reasons discussed in Chapter 3.8, where the lower total metal loading of the catalyst leads to a greater dispersion of the Pd upon the support surface, consequently leading to the formation of smaller Pd nanoparticles which are known to offer increased H_2O_2 selectivity (Table 4.3).[31] Furthermore, a physical mixture of the 0.5 wt.% Au TiO$_2$ + 0.5 wt.% Pd/TiO$_2$ catalysts has a lower H_2O_2 synthesis and degradation activity when compared to the bimetallic catalyst, with this being explained because only the Pd catalyst is active towards the synthesis of H_2O_2 and half the amount of this catalyst is present in the reactor (Figure 4.4).

4.4 The Effect of AuPd Alloying on the Conversion of Metronidazole in a Batch Regime.

Even though it can be concluded that the 0.5 wt.% Pd/TiO$_2$ catalyst has the greatest propensity to synthesise H$_2$O$_2$ while minimising its degradation, it was concluded in Chapter 3.10 that H$_2$O$_2$ is not a key species that is used to oxidise the *E. coli* but rather the OOH$^•$/OH$^•$ radicals generated on the way to synthesising H$_2$O$_2$, which has been shown to be promoted by Au incorporation into Pd surfaces.[32] Therefore, to confirm which pathway the degradation of metronidazole occurs by, the various catalysts were then tested for their ability to degrade 50 ppm of metronidazole under greywater treatment conditions, as outlined in Chapter 2.6.1, (Figure 4.5).
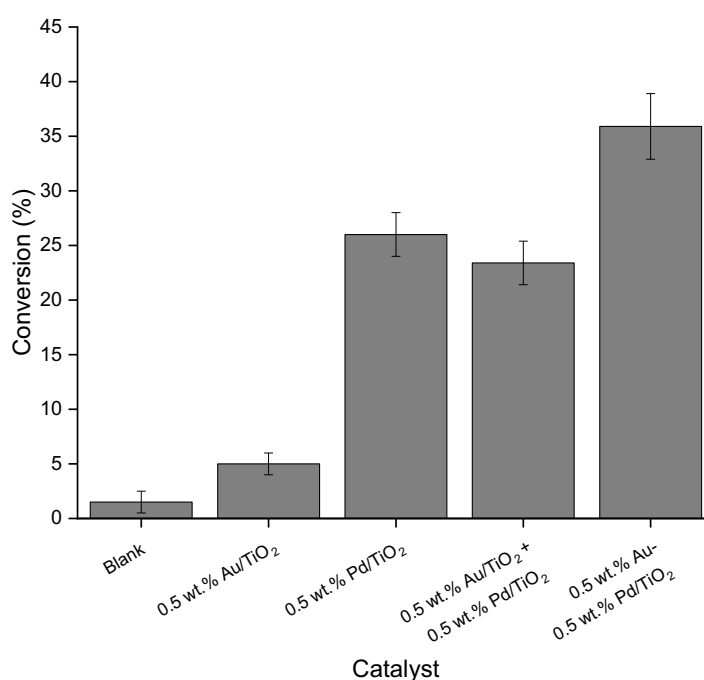
Figure 4.5: The effect of metal alloying on the catalytic activity towards the conversion of metronidazole under non-idealised reaction conditions. **Metronidazole conversion reaction conditions (N$_2$):** Catalyst (0.01 g), metronidazole (8.5 g, 50 ppm), 5% H$_2$/N$_2$ (420 psi), 25% O$_2$/N$_2$ (160 psi), 0.5 h, 30 °C, 1200 rpm. **Blank reaction conditions:** metronidazole (8.5 g, 50 ppm), 5% H$_2$/N$_2$ (420 psi), 25% O$_2$/N$_2$ (160 psi), 0.5 h, 30 °C, 1200 rpm. The mmol$_{metro}$: mmol$_{metal}$ for 10 mg of catalyst and 50 ppm of metronidazole is 3.45.

Table 4.4: The effect of metal alloying on the conversion of metronidazole, H_2O_2 concentration and H_2 conversion, in the presence of a 0.5 wt.% Au-0.5 wt.% Pd/TiO_2 catalyst.
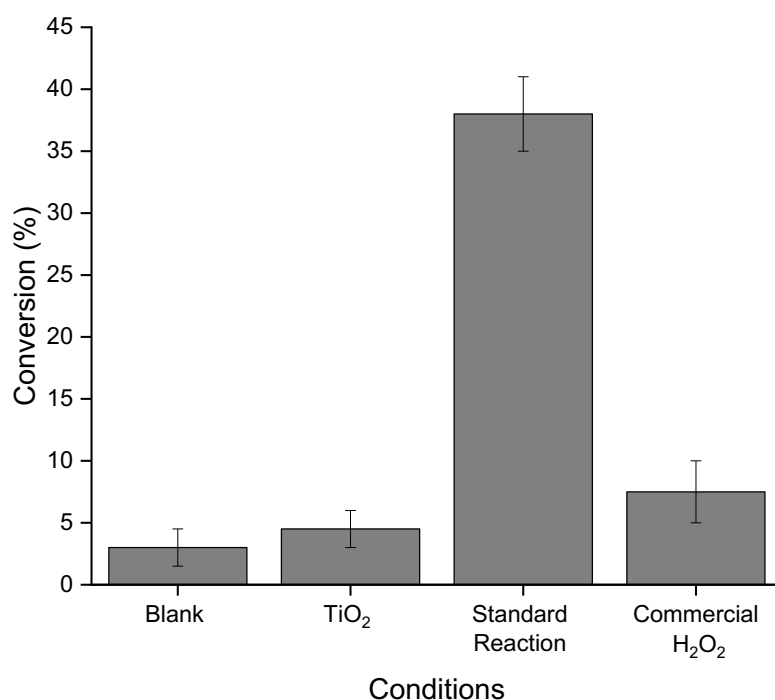
Catalyst	Metronidazole Conversion (%)	H_2O_2 Concentration (ppm)	H_2O_2 (Wt. %)	H_2 Conversion (%)
0.5 wt.% Au-0.5 wt.% Pd/TiO_2	23	320	0.032	20
0.5 wt.% Au + 0.5 wt.% Pd/TiO_2	13	190	0.019	30
0.5 wt.% Pd/TiO_2	15	370	0.037	37
0.5 wt.% Au /TiO_2	3	49	0.0049	6

Metronidazole conversion reaction conditions (N_2): Catalyst (0.01 g), metronidazole (8.5 g, 50 ppm), 5% H_2/N_2 (420 psi), 25% O_2/N_2 (160 psi), 0.5 h, 30 °C, 1200 rpm.

These results demonstrate the greater propensity for the 0.5 wt.% Au-0.5 wt.% Pd/TiO_2 catalyst to convert metronidazole (23%), compared to either the Au or Pd-only monometallics or a physical mixture thereof (Table 4.4). This data is currently providing evidence that it is the oxidation pathway that is the dominant pathway towards the degradation of metronidazole. The greater activity of the 0.5 wt.% Au-0.5 wt.% Pd/TiO_2 catalyst compared to the Pd-only analogue for metronidazole degradation is counter to that previously observed for H_2O_2 synthesis (Figure 4.5) which may indicate that, as with *E. coli* remediation, H_2O_2 is not a key species responsible for metronidazole conversion, but rather, in a similar manner to that outlined in Chapter 3, it is the radicals generated during the formation of H_2O_2 that is used to oxidise metronidazole molecule.[32]

4.5 The Effect of Stabilised, Commercial H_2O_2 on the Conversion of Metronidazole in a Batch Regime.

Upon concluding in the previous sections that the 0.5 wt.% Au-0.5 wt.% Pd/TiO_2 catalyst can generate *in-situ* H_2O_2 that then converts metronidazole it is important to confirm that this in fact the case. Following this, TiO_2 alone was tested to confirm that the conversion observed is not just from absorption of the antibiotic onto the catalyst supports surface. Furthermore, commercial, pre-formed, H_2O_2, of the same concentration as that generated over the 0.5 wt.% Au-0.5 wt.% Pd/TiO_2 catalyst, was tested to compare if one of the current methods for antibiotic conversion is more effective than this *in-situ* H_2O_2 generation reactor. The results of this testing are shown below in Figure 4.6.

Figure 4.6: The comparison of TiO_2 and stabilised and commercial H_2O_2 against the 0.5 wt.% Au-0.5 wt.% Pd/TiO_2 catalyst for the conversion of metronidazole. **Blank reaction conditions:** metronidazole (8.5 g, 50 ppm), 5% H_2/N_2 (420 psi), 25% O_2/N_2 (160 psi), 2 h, 30 °C, 1200 rpm. **Metronidazole conversion reaction conditions (N_2):** Catalyst (0.01 g), metronidazole (8.5 g, 50 ppm), 5% H_2/N_2 (420 psi), 25% O_2/N_2 (160 psi), 2 h, 30 °C, 1200 rpm **Metronidazole conversion with TiO_2 reaction conditions (N_2):** TiO_2 (0.01 g), H_2O_2 (0.2448 g), metronidazole (8.5 g, 50 ppm), 100% N_2 (560 psi), 2 h, 30 °C, 1200 rpm. **Metronidazole conversion with commercial H_2O_2 reaction conditions (N_2):** Catalyst (0.01 g), H_2O_2 (0.2448 g), metronidazole (8.5 g, 50 ppm), 100% N_2 (560 psi), 2 h, 30 °C, 1200 rpm. The $mmol_{metro}$: $mmol_{metal}$ for 10 mg of catalyst and 50 ppm of metronidazole is 3.45.

The data in Figure 4.6 indicates that a reaction blank and unsupported TiO_2 have minimal capacity for degrading metronidazole, or the more likely outcome absorbing metronidazole. This result allows the removal of either of these as a potential reason for any future conversion of metronidazole when a catalyst is involved. Furthermore, the data clearly highlights the ability of the *in-situ* generated H_2O_2 to convert metronidazole, while the activity of commercial H_2O_2 was found to be limited, achieving only 8% conversion. However, the observed conversion in the presence of commercial H_2O_2 does indicate that oxidation of metronidazole

through H_2O_2 is possible but is not the dominant route. This result is as expected as previous work into the conversion of metronidazole by Shemer *et. al*[33] has shown promise in using H_2O_2 in combination with UV, Fe^{2+} or UV + Fe^{2+} to generate the $OH^\bullet$ required for the oxidation of metronidazole. Therefore, this limited conversion of metronidazole is expected indicates that while conversion of metronidazole is possible through this method, our method by with H_2O_2 and its ROS are generated *in-situ* is more efficient. However, testing of the effect that the stabilizers may have on the ability of commercial H_2O_2 to degrade antibiotic would need to be studied to confirm this.

4.6   The Effect of Catalyst Re-use on the Conversion of Metronidazole in a Batch Regime.

Building on the data shown in Chapter 3 Section 9, the production of H_2O_2 using the 0.5 wt.% Au-0.5 wt.% Pd/TiO$_2$ catalyst in a flow regime was shown to rapidly reduce after 30 minutes H_2O_2 synthesis reaction, before plateauing at a value of 78 ppm. Following this result, it was important to determine what specifically is the issue as to not see this issue persist further towards the oxidation of metronidazole, as well as any future biocide testing. To do this the effect catalyst re-use has on the conversion of metronidazole was tested by doing a standard 30-minute metronidazole conversion reaction before filtering the reaction solution and drying the subsequent recovered catalyst for 16 hours at 30 °C under vacuum before testing again for a standard 30-minute reaction. The results of which can be found below in Table 4.5.

Table 4.5: The reusability of the 0.5 wt.% Au-0.5 wt.% Pd/TiO$_2$ catalyst towards the conversion of metronidazole.

Reaction number	Metronidazole Conversion (%)	H_2O_2 Productivity (ppm)	H_2O_2 (Wt. %)	H_2 Conversion (%)
1	38	330	0.033	17
2	7	78	0.0078	7

Metronidazole conversion reaction conditions (N_2): Catalyst (0.01 g), metronidazole (8.5 g, 50 ppm), 5% H_2/N_2 (420 psi), 25% O_2/N_2 (160 psi), 2 h, 30 °C, 1200 rpm. The $mmol_{metro}$: $mmol_{metal}$ for 10 mg of catalyst and 50 ppm of metronidazole is 3.45.

Upon re-introducing the catalyst into the batch reactor and using again for a second metronidazole conversion reaction there is a large decrease in the capacity of the catalyst to degrade metronidazole (Table 4.5). This decrease could be assigned to a reduction in H_2 conversion, which will in turn lead to a reduction of H_2O_2 produced, given that less H_2 is being utilised by the catalyst for H_2O_2 production. Additionally, the chlorine could be being removed from the surface of the catalyst after the initial reaction and following washing, as documented by Brehm et. al.[34] This removal of the chlorine could remove the promotional effect that chlorine has on allowing the dispersion of the highly active, for H_2O_2 synthesis, and stable supported Au and Pd nanoparticles.

4.7   The Contribution of Homogenous Catalysis for the Conversion of Metronidazole in a Batch Regime.

Further investigation into the catalyst was conducted in which a 1-hour standard reaction was carried out before removing the catalyst via filtration and re-running the reaction mixture for another 1-hour reaction to determine the contribution of the leached, homogeneous species, if any. The results of this hot-filtration reaction are tabulated below (Table 4.6).

Table 4.6: The activity of homogenous metal species on the conversion of metronidazole.

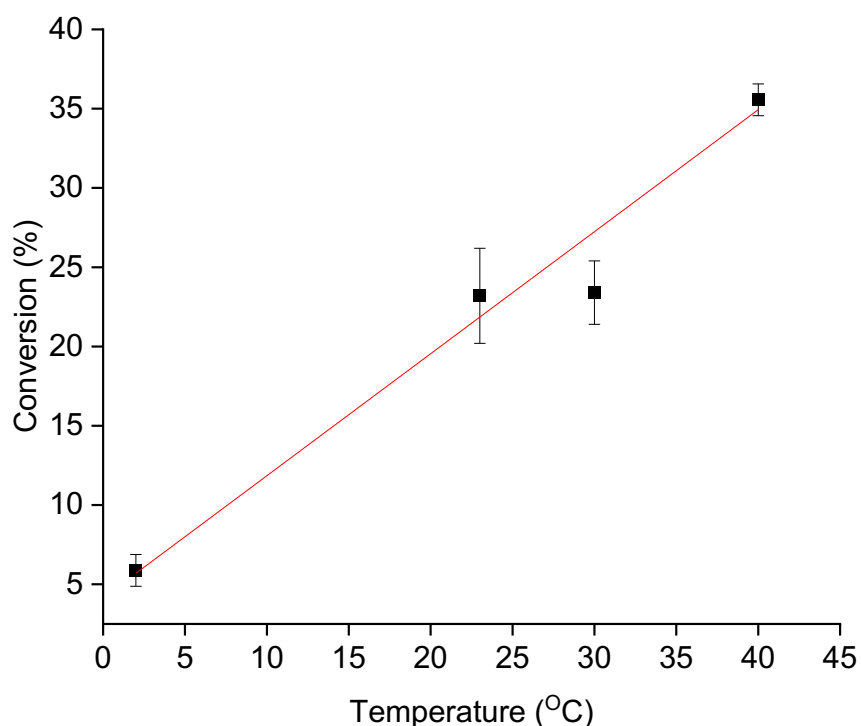| Catalyst	Metronidazole Conversion (%)	H_2O_2 Productivity (ppm)	H_2O_2 (wt.%)	H_2 Conversion (%)
0.5 wt.% Au-0.5 wt.% Pd/TiO$_2$	27	330	0.033	9
Homogenous Mixture	27	150	0.015	3

Metronidazole conversion reaction conditions (N_2): Catalyst (0.01 g), metronidazole (8.5 g, 50 ppm), 5% H_2/N_2 (420 psi), 25% O_2/N_2 (160 psi), 2 h, 30 °C, 1200 rpm. The $mmol_{metro}$: $mmol_{metal}$ for 10 mg of catalyst and 50 ppm of metronidazole is 3.45.

The results indicate that upon removing the catalyst after an hour and continuing the reaction for a further 1 h there is no further increase in the conversion of metronidazole. The data shows that any Pd or Au that has leached from the initial 1-hour reaction is converting the H_2O_2 generated to H_2O, perhaps by hydrogenation given the H_2 converted during the second hour of the reaction. However, this H_2 conversion could occur through H_2O_2 production. This data

further indicates that H_2O_2 alone does offer activity towards the conversion of metronidazole, however that not enough H_2O_2, if any, is being made in the homogenous reaction mixture to degrade a measurable amount of metronidazole.

4.8 The Effect of Temperature on the Conversion of Metronidazole in a Batch Regime.

Succeeding the comparison of a heterogenous catalyst and a homogenous reaction mixture, the effect reaction temperature has on the ability of the catalysts to convert 50 ppm of metronidazole was then pursued. Reaction temperatures between 2-40 °C, testing from the optimal temperature for H_2O_2 synthesis (2 °C) and the upper limits of greywater treatment (40 °C). Results are reported below in Figure 4.7 and Table 4.7.

Figure 4.7: The effect temperature has on the conversion of metronidazole in the presence of a 0.5 wt.% Au-0.5 wt.% Pd/TiO$_2$ catalyst. **Metronidazole conversion reaction conditions (N$_2$):** Catalyst (0.01 g), metronidazole (8.5 g, 50 ppm), 5% H$_2$/N$_2$ (420 psi), 25% O$_2$/N$_2$ (160 psi), 0.5 h, 30 °C, 1200 rpm. The mmol$_{metro}$: mmol$_{metal}$ for 10 mg of catalyst and 50 ppm of metronidazole is 3.45.

Table 4.7: The effect temperature has on the conversion of metronidazole, H_2O_2 concentration and H_2 conversion, in the presence of a 0.5 wt.% Au-0.5 wt.% Pd/TiO$_2$ catalyst.

| Temperature (°C)	Metronidazole Conversion (%)	H_2O_2 Concentration (ppm)	H_2 Conversion (%)
40	36	240	20
30	23	330	15
23	23	320	10
2	6	440	6

Metronidazole conversion reaction conditions (N_2): Catalyst (0.01 g), metronidazole (8.5 g, 50 ppm), 5% H_2/N_2 (420 psi), 25% O_2/N_2 (160 psi), 0.5 h, 30 °C, 1200 rpm. The mmol$_{metro}$: mmol$_{metal}$ for 10 mg of catalyst and 50 ppm of metronidazole is 3.45.

The results show that an increase in reaction temperature from 2–40 °C results in an increase in metronidazole conversion up from 6–36% (Figure 4.7) and a concurrent increase in H_2 conversion, from 6–20% (Table 4.7). Although H_2 solubility is not a factor in water at different temperatures,[35] the documented increase in H_2 conversion could be associated with the increase in reaction temperature resulting in a decrease in H_2O_2 selectivity and a push towards H_2O_2 hydrogenation.[36] This increase in temperature leads to an increase in the kinetic favourability to synthesise H_2O_2 and its intermediates. However, this also leads to an ever bigger increase towards the degradation of H_2O_2, forming H_2O,[27,37] with the possibility that some of the radicals generated during these reactions could be used for the degradation of metronidazole.

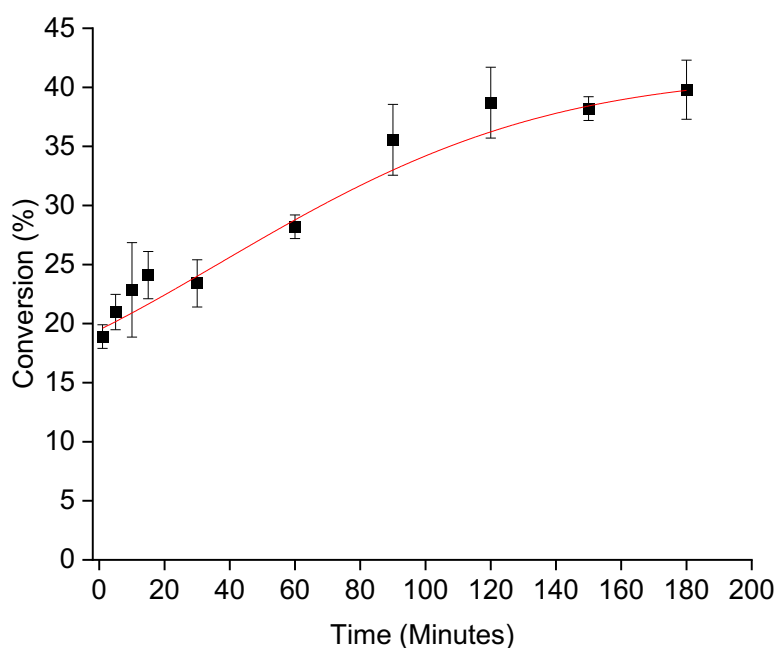## 4.9 The Effect of Reaction Time on the Conversion of Metronidazole in a Batch Regime.

The effect of reaction on the conversion of metronidazole was investigated next. Research by Piccinini *et. al*[38] studied the effect that time has on the production of a 1 wt.% AuPd/TiO$_2$ catalyst over a 120-minute reaction time (Figure 4.8). The result concluded that as time increases so does the amount of H_2O_2 present in the reaction vessel. However, given the first order dependence of H_2O_2 degradation on H_2O_2 concentration, catalytic selectivity was found to decrease at extended reaction times. Within this study, time was varied from 1 – 180 minutes to comprehend the efficacy and stability of the AuPd catalyst during H_2O_2 production (Table 4.8), metronidazole conversion (Figure 4.9), with catalyst stability during metronidazole conversion reported in Table 4.9.
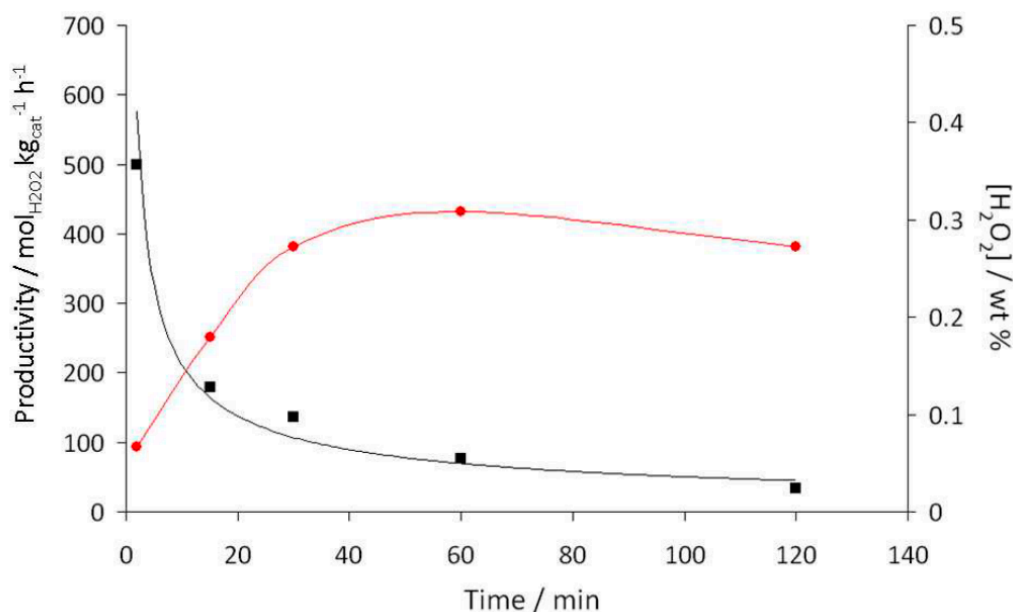
Figure 4.8: The influence of reaction time on the productivity (■) and wt.% (●)of H_2O_2 as produced by Marco Piccinini. **H_2O_2 direct synthesis reaction conditions (CO_2):** Catalyst (0.01 g), 5% H_2 /CO_2 (420 psi), 25% O_2/CO_2 (160 psi), 0.5 h, 2 °C, 1200 rpm. Figure use granted in accordance with copyright as Figure is public domain.[38]

Figure 4.8: The effect time has on the conversion of metronidazole in the presence of a 0.5 wt.% Au-0.5 wt.% Pd/TiO_2 catalyst. **Metronidazole conversion reaction conditions (N_2):** Catalyst (0.01 g), metronidazole (8.5 g, 50 ppm), 5% H_2/N_2 (420 psi), 25% O_2/N_2 (160 psi), 30 °C, 1200 rpm. The $mmol_{metro}$: $mmol_{metal}$ for 10 mg of catalyst and 50 ppm of metronidazole is 3.45.

Table 4.8: The effect time has on the conversion of metronidazole, H_2O_2 concentration and H_2 conversion in the presence of a 0.5 wt.% Au-0.5 wt.% Pd/TiO$_2$ catalyst.

Time (Minutes)	Metronidazole Conversion (%)	H_2O_2 Concentration (ppm)	H_2 Conversion (%)
1	19	130	10
5	21	210	13
10	23	270	18
15	24	270	19
30	23	330	20
60	28	400	31
90	36	460	32
120	39	470	37

Metronidazole conversion reaction conditions (N_2): Catalyst (0.01 g), metronidazole (8.5 g, 50 ppm), 5% H_2/N_2 (420 psi), 25% O_2/N_2 (160 psi), 30 °C, 1200 rpm. The mmol$_{metro}$: mmol$_{metal}$ for 10 mg of catalyst and 50 ppm of metronidazole is 3.45.

Table 4.9: The effect time has on the amount of Au and Pd removed from the surface of a 0.5 wt.% Au-0.5 wt.% Pd/TiO$_2$ catalyst.

| Time	Pd Leached (%)	Pd Leached (ppb)	Au Leached (%)	Au Leached (ppb)
30	2.86	168	0	0
60	3.72	219	0	0
90	4.85	285	0	0
120	6.29	370	0	0

Metronidazole conversion reaction conditions (N_2): Catalyst (0.01 g), 50ppm metronidazole solution (8.5 g), 5% H_2/N_2 (420 psi), 25% O_2/N_2 (160 psi), 30 °C, 1200 rpm.

With the presence of a catalyst, metronidazole conversion after 1 minute is shown to be as high as 19%, with a residual H_2O_2 concentration of 127 ppm observed. This could be explained given the enhanced activity of 1 wt.% AuPd/TiO$_2$ catalyst at low reaction time, as confirmed by Crombie *et. al*[39] with a maximum residual H_2O_2 concentration being observed after 5 min online of 188 µmol$_{H2O2}$ for the oxidation of benzyl alcohol, using an identical AuPd catalyst.

Metronidazole conversion gradually increased, alongside residual H_2O_2 concentration, up to 120 minutes before plateauing at a conversion of 39% and a H_2O_2 concentration of ~470 ppm. The plateauing at 120 minutes for H_2O_2 production, H_2 conversion and metronidazole conversion (Table 4.8) could be assigned to a combination of factors. Firstly, there will be a gradual increase towards the H_2O_2 decomposition rate as there is more H_2O_2 produced in the initial stages of the reaction, as discussed above. There is also the possibility of catalyst deactivation, as even though no Au leaching is observed there is a gradual increase in Pd leaching of up to 6.3% of total Pd being removed from the catalyst support (Table 4.9). However, what we can deduce is that it is not limited by H_2 availability given only 37% of the H_2 present in the system is converted following a 2-hour reaction. Following this study, a reaction time of 2 hours will now be used to get the most out of the catalysts and the reactants.

4.10 The Effect of the Reintroduction of the Gas Mixture on the Conversion of Metronidazole in a Batch Regime.

Following on from the previous study in section 4.6 into the effect that reaction time has on the ability of the catalyst to oxidise metronidazole, it was important to understand and define the reason behind this limited conversion after 2 hours. To comprehend whether this limit was due to catalyst deactivation or gaseous reagent limitations, an 8-hour reaction was set up in which both reactant gases (5% H_2/CO_2 and 25% O_2/CO_2) were re-introduced every 2 hours and the conversion of metronidazole was monitored. The results of this study are presented below in Figure 4.10.
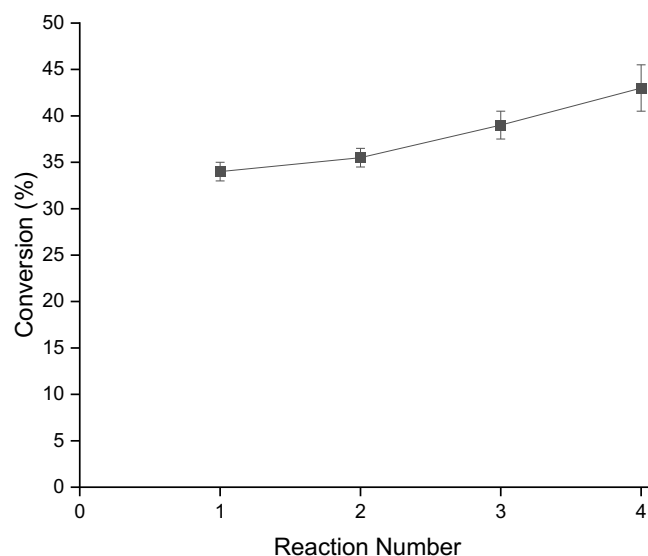
Figure 4.10: The effect the reintroduction of the gas mixture has on the conversion of metronidazole in the presence of a 0.5 wt.% Au-0.5 wt.% Pd/TiO$_2$ catalyst. **Metronidazole conversion reaction conditions (N$_2$):** Catalyst (0.01 g), metronidazole (8.5 g, 50 ppm), 5% H$_2$/N$_2$ (420 psi), 25% O$_2$/N$_2$ (160 psi), 2 h, 30 °C, 1200 rpm. The mmol$_{metro}$: mmol$_{metal}$ for 10 mg of catalyst and 50 ppm of metronidazole is 3.45.
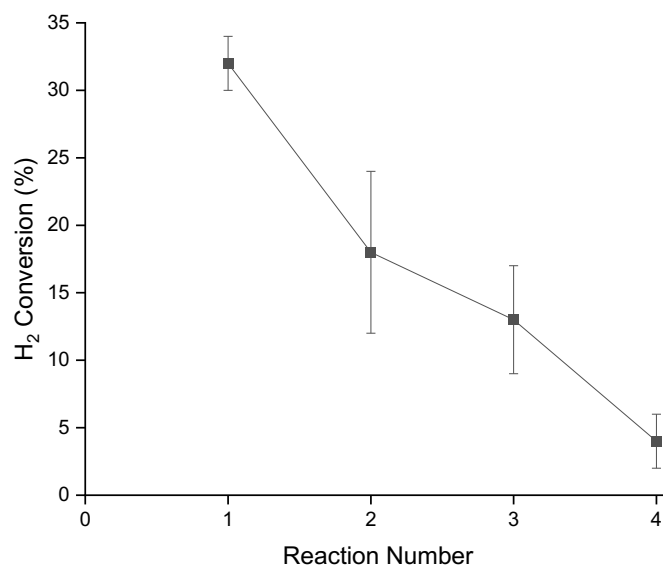
Figure 4.11: The effect the reintroduction of the gas mixture has on the H$_2$ conversion of metronidazole in the presence of a 0.5 wt.% Au-0.5 wt.% Pd/TiO$_2$ catalyst. **Metronidazole conversion reaction conditions (N$_2$):** Catalyst (0.01 g), metronidazole (8.5 g, 50 ppm), 5% H$_2$/N$_2$ (420 psi), 25% O$_2$/N$_2$ (160 psi), 2 h, 30 °C, 1200 rpm. The mmol$_{metro}$: mmol$_{metal}$ for 10 mg of catalyst and 50 ppm of metronidazole is 3.45.

Results showed (Figure 4.10) there was a gradual increase in metronidazole conversion from ~34% up to ~43%, when sequentially adding fresh reactant gas over 4 successive reactions. However, this increase is minimal and alongside the H_2 conversion data for these 4 sequential reactions (Figure 4.11), which shows a large decrease in H_2 conversion from ~33% after reaction 1 down to ~4% after reaction 4, these results point towards catalyst deactivation. The possible contributing factors for the observed catalyst deactivation could be a combination of a change of oxidation of the Pd away from the optimal mixed oxidation state,[40] leaching of metal from the catalyst, and these combining to prevent generation of H_2O_2.

4.11 The Effect of Catalyst Mass on the Conversion of Metronidazole in a Batch Regime.

It is important to comprehend the optimal amount of catalyst that can be used to convert metronidazole before mass transfer limitations present themselves, as well as the cost savings that utilising a lower amount of catalyst will achieve. To comprehend this, catalyst amount was varied from 5-150 mg and the effect this has on the conversion of metronidazole was determined, as well as the amount of residual H_2O_2 produced and H_2 converted (Figure 4.12, Table 4.10).
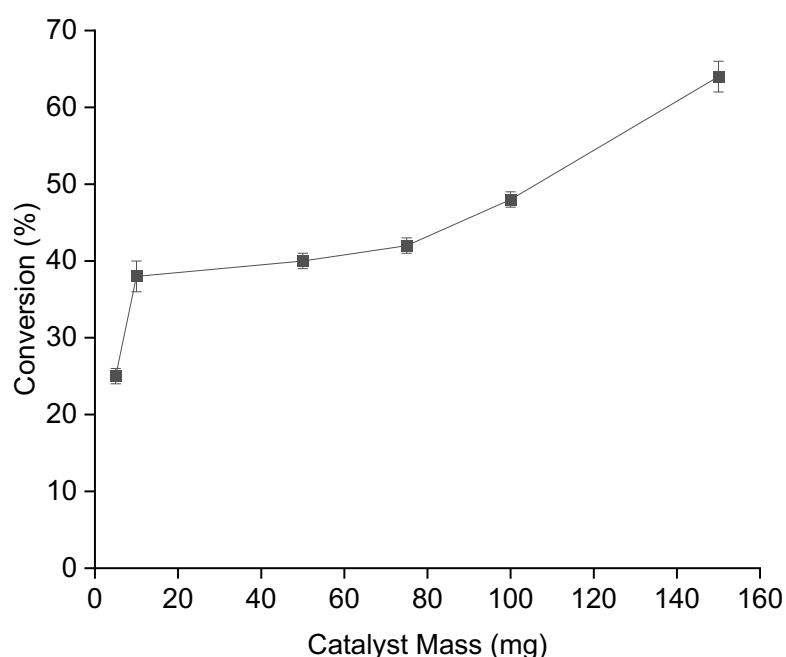
Figure 4.12: The effect catalyst mass has on the conversion of metronidazole using a 0.5 wt.% Au-0.5 wt.% Pd/TiO$_2$ catalyst. **Metronidazole conversion reaction conditions (N$_2$):** metronidazole (8.5 g, 50 ppm), 5% H_2/N_2 (420 psi), 25% O_2/N_2 (160 psi), 2 h, 30 °C, 1200 rpm. The mmol$_{metro}$: mmol$_{metal}$ for 10 mg of catalyst and 50 ppm of metronidazole is 3.45.

Table 4.10: The effect catalyst mass has on the conversion of metronidazole, H_2O_2 concentration and H_2 conversion, in the presence of a 0.5 wt.% Au-0.5 wt.% Pd/TiO$_2$ catalyst.
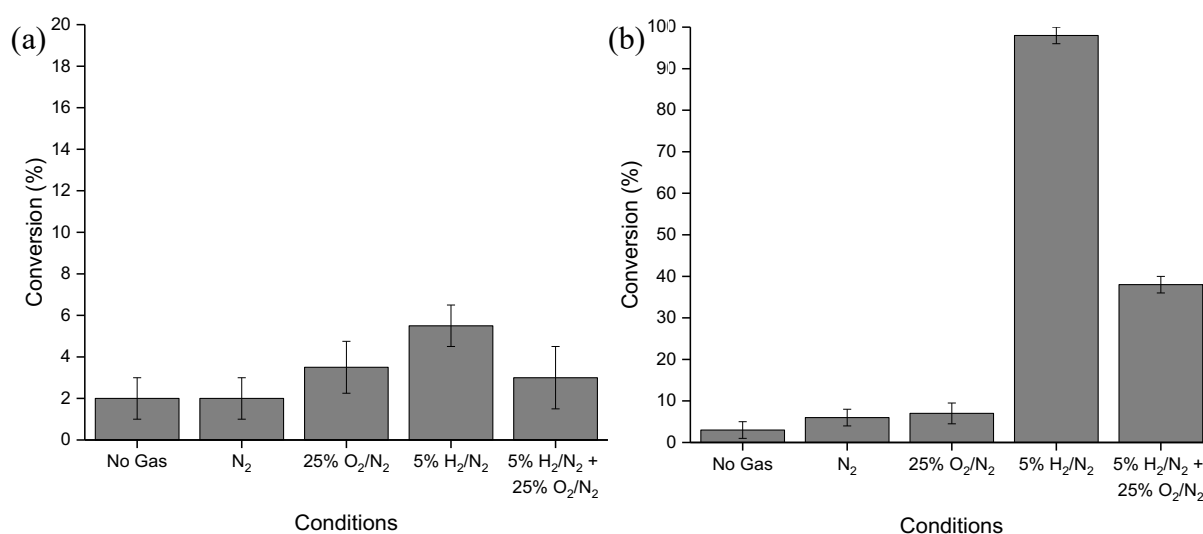
Catalyst Mass (mg)	Metronidazole Conversion (%)	H_2O_2 Concentration (ppm)	Metronidazole Conversion ($mmol_{metronidazole}$ $mmol_{metal}^{-1}h^{-1}$)	H_2 Conversion (%)
5	25	170	8.6×10^{-4}	18
10	37	360	6.4×10^{-4}	31
50	41	520	1.4×10^{-4}	90
75	48	400	1.1×10^{-4}	100
100	54	150	9.3×10^{-5}	100
150	65	80	7.4×10^{-5}	100

Metronidazole conversion reaction conditions (N_2): metronidazole (8.5 g, 50 ppm), 5% H_2/N_2 (420 psi), 25% O_2/N_2 (160 psi), 2 h, 30 °C, 1200 rpm. The $mmol_{metro}$: $mmol_{metal}$ for 10 mg of catalyst and 50 ppm of metronidazole is 3.45.

The gradual increase in the amount of catalyst present in the reaction was shown to increase the concentration of residual H_2O_2 (Table 4.10), in a similar manner to the research by Edwards *et. al*[41]*,* and metronidazole conversion. However, this was observed up until 50 mg where net production of H_2O_2 peaked, while the conversion of metronidazole continued, peaking at 65% for 150 mg. The ideal catalyst amount for metronidazole conversion can be identified as 5 mg given that metronidazole conversion rate was the highest at 8.6×10^{-4} $mmol_{metronidazole}$ $mmol_{metal}^{-1}h^{-1}$ for this mass. This result indicates that there is the possibility of the oxidation of metronidazole, given that H_2O_2 concentration is increasing alongside metronidazole conversion. Oxidation of metronidazole can be confirmed as contributing to metronidazole conversion given that from 75 mg onwards there is no hydrogen left in the system and conversion of metronidazole continues. Furthermore, there could also be a contribution towards conversion via absorption of the antibiotic onto the surface of the support during this catalyst mass amount, given the large amount of catalyst present in the system and that this was proved as a possibility in Chapter 4 Section 5. In addition to this, the reaction could also be limited by mass transfer in which an increase in catalyst mass does not increase H_2O_2 production due to limited reactants, supported by 100% H_2 conversion after 75 mg, and the increase in catalyst amount is being utilised towards the degradation of any *in-situ* formed H_2O_2.

4.12 The Effect of Gas Atmosphere and the Removal of Catalyst on the Conversion of Metronidazole in a Batch Regime.

Following the study into the effect of catalyst mass on H_2O_2 production and metronidazole conversion, the effect of the H_2O_2 synthesis gases $(H_2 + O_2)$, on the conversion of metronidazole was established to aid in identifying the prevalent pathway for metronidazole conversion. An experiment was undertaken in which different gas atmospheres were used while keeping all other reaction conditions the same. Furthermore, the effect of the catalyst was also tested for the different gas atmospheres. The results of these studies are shown below in Figure 4.13.


Figure 4.13 (a +b): (a) The effect gas atmosphere has on the conversion of metronidazole in the absence of catalyst and (b) the effect gas atmosphere has on the conversion of metronidazole in the presence of a catalyst. **Metronidazole conversion reaction conditions (N_2):** metronidazole (8.5 g, 50 ppm), 2 h, 30 °C, 1200 rpm. The $mmol_{metro}$: $mmol_{metal}$ for 10 mg of catalyst and 50 ppm of metronidazole is 3.45.

The data in Figure 4.13a indicates the need for a 0.5 wt.% Au-0.5 wt.% Pd/TiO$_2$ catalyst to allow the degradation of metronidazole. The absence of both the catalyst and the H_2O_2 synthesis gases $(H_2 + O_2)$ from the batch reactor results in minimal metronidazole degradation, with all gas atmospheres registering minimal conversion of metronidazole (< 10%). Thus, confirming that both the presence of the 0.5 wt.% Au-0.5 wt.% Pd/TiO$_2$ catalyst and the H_2O_2 synthesis gases are required for the conversion of metronidazole. Furthermore, the data in Figure 4.13b indicates that the complete removal of H_2 and O_2 from the gas stream, as shown with the N_2 only gas atmosphere, has a drastic effect on the ability of the 0.5 wt.% Au-0.5 wt.%

Pd/TiO$_2$ catalyst to convert metronidazole, which may indicate that the formation of the oxidant species (H$_2$O$_2$ or ROS) may be key to metronidazole conversion. However, when O$_2$ was removed from the gas atmosphere, (5% H$_2$/N$_2$ only), there was complete conversion of metronidazole which would not be expected if the metronidazole degradation proceeded via oxidative pathways as hypothesised. Therefore, this test indicates that metronidazole hydrogenation may be the dominant pathway responsible for the observed conversion.

4.13 The Effect of H$_2$:O$_2$ Ratio on the Conversion of Metronidazole in a Batch Regime.

The H$_2$:O$_2$ ratio has been known to have a dramatic effect on the ability of a catalyst to synthesise *in-situ* H$_2$O$_2$. So, it is therefore important to understand the effect that H$_2$:O$_2$ ratio may have on the conversion of metronidazole, as well if the oxidation pathway is somewhat responsible for the observed conversion of metronidazole. Piccinini *et. al*[37] studied the effect H$_2$:O$_2$ ratio has on the synthesis of H$_2$O$_2$ with these findings indicating that a H$_2$:O$_2$ ratio of 1:1 was optimal for H$_2$O$_2$ production, with production dropping off each side of this value in the shape of an asymmetric parabola (Figure 4.14). The maximum of the graph is flat and indicates that at lower O$_2$ partial pressures the selectivity towards H$_2$O$_2$ deceases more markedly than at lower H$_2$ partial pressures, which subsequently leads to a more favourable production of H$_2$O$_2$ and possibly ROS at a H$_2$:O$_2$ between 0.6-1.
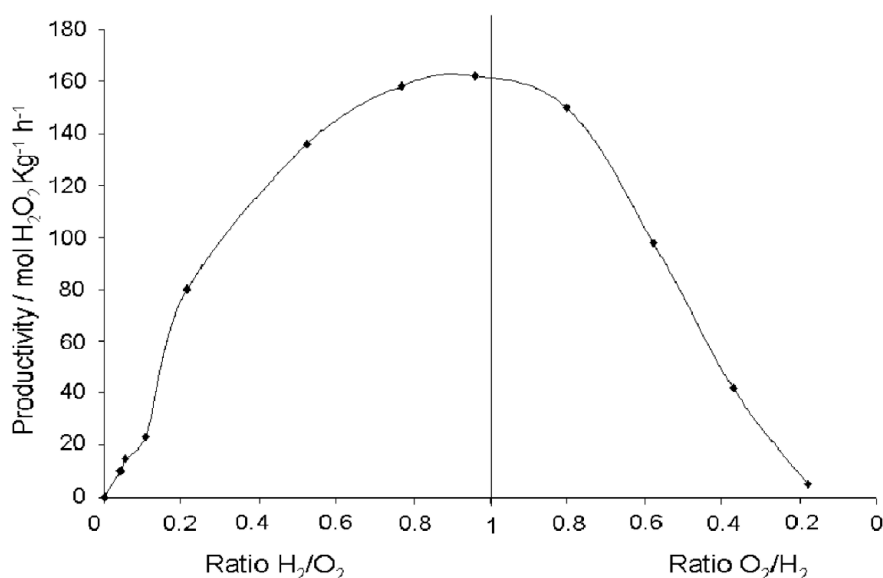
Figure 4.14: Productivity for H$_2$O$_2$ synthesis as a function of gas ratios produced by Marco Piccinini *et. al.* **H$_2$O$_2$ direct synthesis reaction conditions (CO$_2$):** Catalyst (0.01 g), 5% H$_2$/CO$_2$ (420 psi), 25% O$_2$/CO$_2$ (160 psi), 0.5 h, 2 °C, 1200 rpm. Figure use granted in accordance with copyright by Royal Society of Chemistry.[37]

This can be confirmed by a study conducted by Santos *et. al*[42] which concluded that there is a clear variance in H_2O_2 synthesis activity, with the optimal H_2:O_2 ratio being between 0.53-0.96, with net H_2O_2 concentrations declining either side of this ratio, due to limited reagent availability under H_2-lean conditions and an increase in H_2O_2 hydrogenation when the reaction is H_2-rich. Therefore, it may be possible to conclude that a H_2:O_2 ratios of between 0.53 and 0.96 may be optimal for metronidazole conversion via the oxidation pathway.
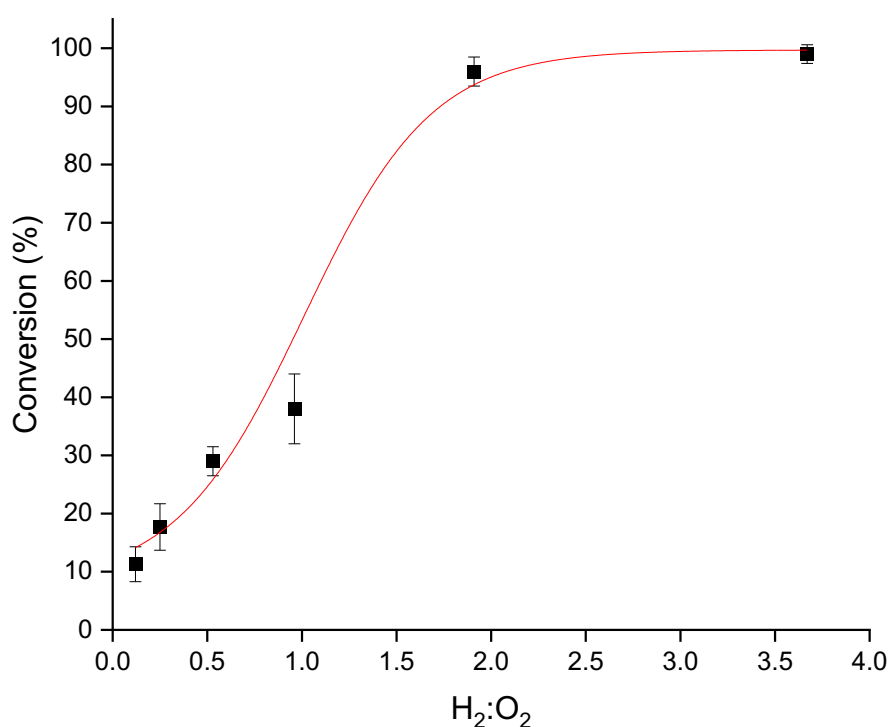
Figure 4.15: The effect H_2:O_2 ratio on the conversion of metronidazole in the presence of a 0.5 wt.% Au-0.5 wt.% Pd/TiO$_2$ catalyst. **Metronidazole conversion reaction conditions (N$_2$):** Catalyst (0.01 g), metronidazole (8.5 g, 50 ppm), 2 h, 30 °C, 1200 rpm. The mmol$_{metro}$: mmol$_{metal}$ for 10 mg of catalyst and 50 ppm of metronidazole is 3.45.

Table 4.11: The effect H_2: O_2 ratio on the conversion of metronidazole, H_2O_2 concentration and H_2 conversion, in the presence of a 0.5 wt.% Au-0.5 wt.% Pd/TiO$_2$ catalyst.

| H_2:O_2	Metronidazole Conversion (%)	H_2O_2 Concentration (ppm)	H_2 Conversion (%)
0.12	11	190	16
0.25	17	250	34
0.53	29	310	35
0.96	39	330	36
1.91	96	100	38
3.67	100	50	40

Metronidazole conversion reaction conditions (N_2): Catalyst (0.01 g), metronidazole (8.5 g, 50 ppm), 2 h, 30 °C, 1200 rpm. The mmol$_{metro}$: mmol$_{metal}$ for 10 mg of catalyst and 50 ppm of metronidazole is 3.45.

The results shown in Figure 4.15 and Table 4.11 indicate that the oxidation of metronidazole may not be contributing to all of the conversion of metronidazole and in fact it is more likely that the hydrogenation of metronidazole is predominant route to its conversion. Opposite to the bell curve observed by Santos *et. al* for H_2O_2 synthesis[42], the effect of the H_2:O_2 ratio on the conversion of metronidazole is more linear, increasing with a shift towards H_2-rich conditions. At low H_2:O_2 ratio, hydrogenation is limited, as expressed by 11% metronidazole conversion. Alongside any potential catalytic oxidation route can also be expected to be limited. As the H_2: O_2 ratio increases any contribution from catalytic oxidation can be expected to increase, until the reaction becomes limited by O_2 availability. However, conversion of metronidazole is seen to increase linearly with H_2 content, as is observed in Figure 4.15 and Table 4.11. With this result indicating that hydrogenation pathways are responsible for the conversion of metronidazole.

4.14 Concluding the Products of the Hydrogenation of Metronidazole.

Subsequently, it is important to confirm what part of the metronidazole molecule may undergo hydrogenation. It has been reported by Chen *et. al*[24] that one possible route is to hydrogenate the nitro group to the corresponding amine, additionally both of the double bonds on the imidazole ring could be hydrogenated, as shown previously in Figure 4.2. With this in mind, the reaction products for both a metronidazole hydrogenation reaction, where the catalyst was

used in conjunction with H_2 only, and the oxidative reaction (proceeding through *in-situ* H_2O_2 generation) were analysed via ^{1}H NMR. The ^{1}H NMR spectra of metronidazole is shown below (Figure 4.16) with the signals below corresponding to; 2.4 ppm – (CH_3, singlet, 4.9) , 3.2 ppm – (+, CH_3OH, singlet, 1.7)[43], 3.8 ppm – (CH_2, triplet, 3.6), 4.4 ppm – (CH_2, triplet, 5.8), 4.5 ppm – (*,OH, singlet) , 7.9 ppm – (CH, singlet, 1.3).[44] The presence of methanol in the sample can be assigned to potential cross contamination, with many reactions in the laboratory containing methanol. Furthermore, the integral values are not completely accurate due to the D_2O swamping the peaks, effecting the values shown.
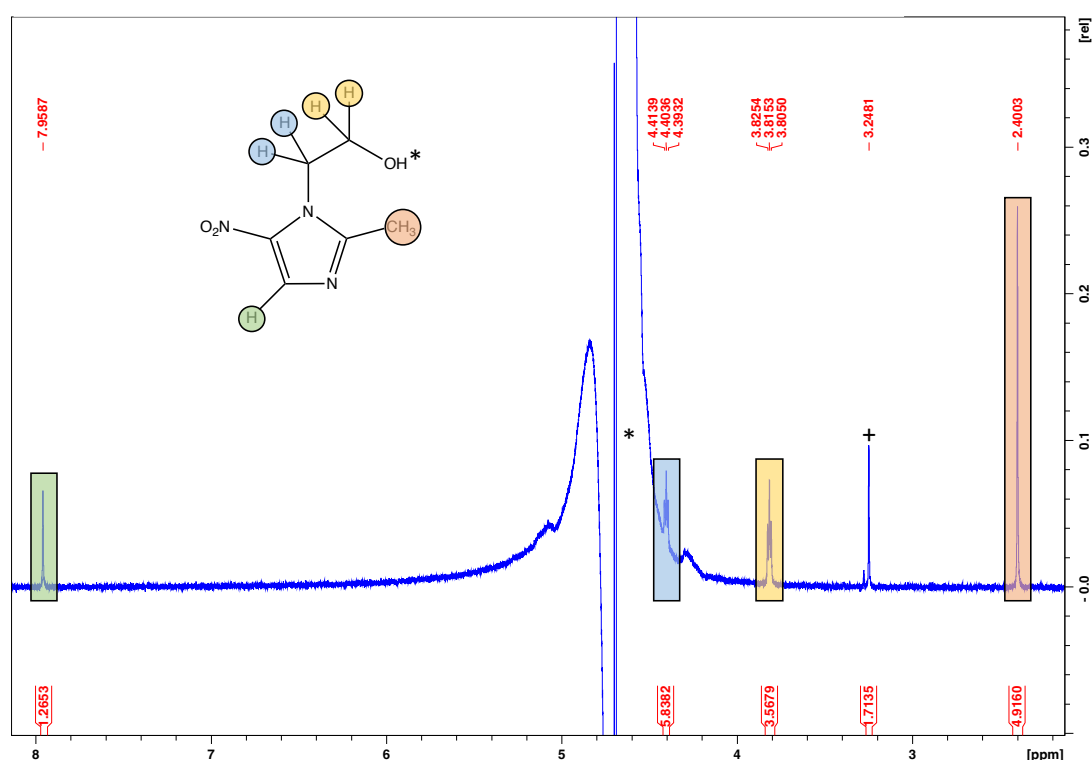
Figure 4.16: ^{1}H NMR for 50 ppm of metronidazole.

Upon identifying the peaks of the metronidazole molecule, it is now possible to identify any product(s) formed upon introducing metronidazole into hydrogenation/direct H_2O_2 synthesis conditions. The ^{1}H NMR spectra for the oxidation of metronidazole is shown below (Figure 4.17) and when compared to that of metronidazole (Figure 4.16) a loss of the peak present at 3.2 ppm in the parent sample is observed, with a gain of a peak at 2.1 ppm. The loss of the peak at 3.2 ppm can be assigned to a loss of the contaminant methanol, while the appearance of the peak at 2.1 ppm can also be assigned to an alternative contaminant, acetone, due to large integration value and chemical shift value.[43] The introduction of acetone can be assigned to incomplete washing of the NMR tubes used to run samples.
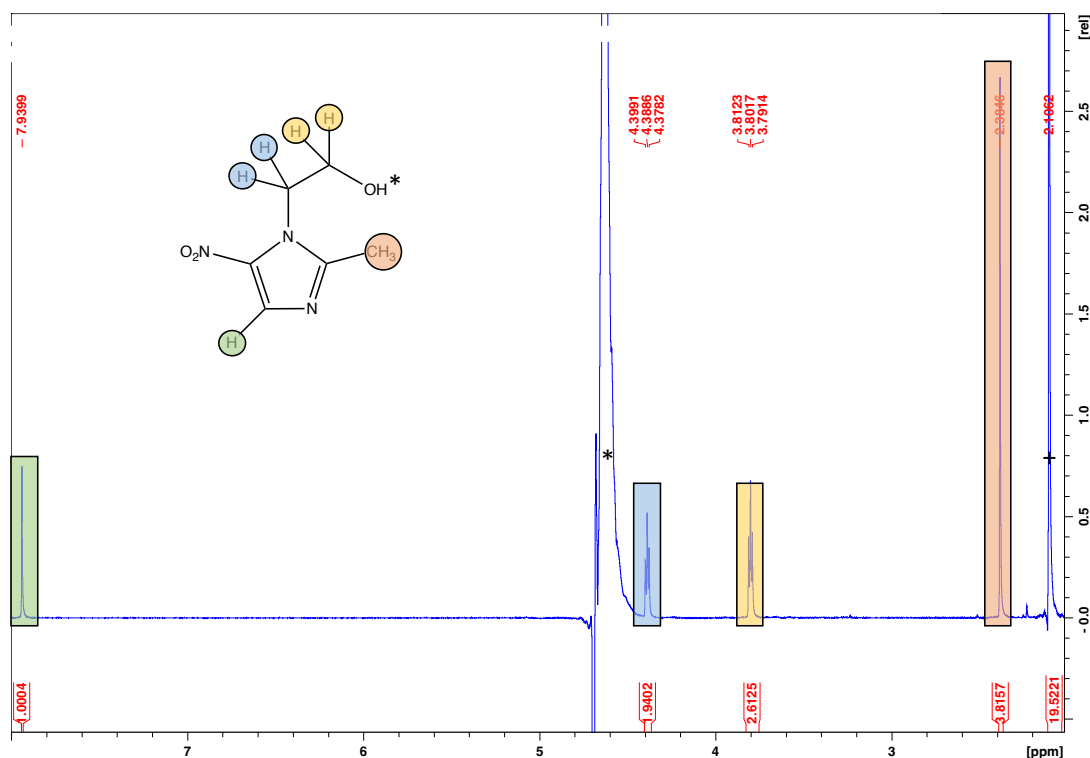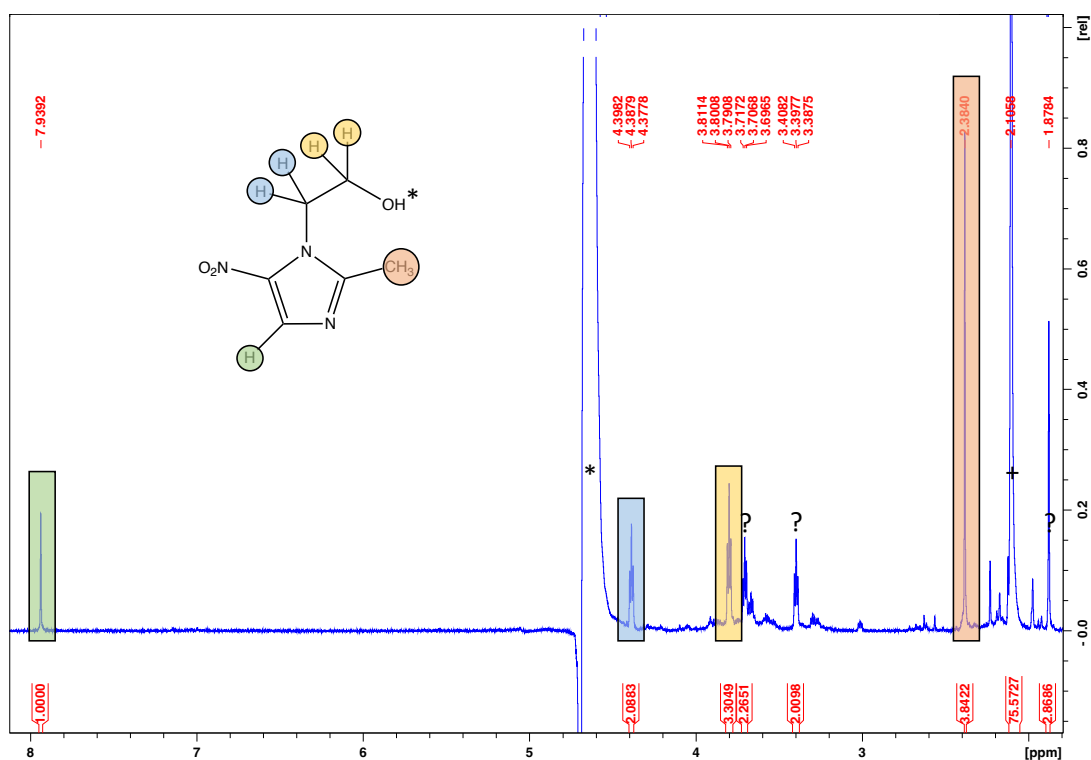
Figure 4.17: ^1H NMR for metronidazole upon being introduced to both H_2O_2 synthesis gases. **Metronidazole conversion reaction conditions (N_2):** Catalyst (0.01 g), metronidazole (8.5 g, 50 ppm), 5% H_2/N_2 (420 psi), 25% O_2/N_2 (160 psi), 2 h, 30 °C, 1200 rpm.

Metronidazole was subsequently reacted with H_2 in the presence of the catalyst to comprehend if any reaction is occurring when O_2 is removed from the reactor system, given that as O_2 is in excess under oxidative conditions (and the high water solubility of O_2 compared to H_2) the subsequent generation of H_2O_2 could act as a competitive reaction pathway for H_2, explaining the limited conversion of metronidazole in the presence on H_2/O_2, as discussed in Chapter 4.12. The ^1H NMR analysis of the post-hydrogenation of metronidazole reaction is shown below (Figure 4.18) and shows a noticeable difference when compared to metronidazole pre-reaction (Figure 4.16). Initially, a peak at 2.1 ppm can be identified, which can be assigned to acetone contamination.

The peaks highlighted can once again be assigned to the starting material, metronidazole. However, there are additional peaks, identified with a ? symbol, which indicates that hydrogenation of the molecule is occurring but where the hydrogen is being added in the

molecule is not confirmed. However, given the position of the additional peaks and the unselective nature of the catalyst used, its most likely that the C=C and/or C=N are being hydrogenated as no peak at ~8.5 ppm is present that would indicate the hydrogenation of the nitro group. This data indicates that all reactions and their observed conversion of metronidazole has been predominately via hydrogenation of metronidazole, as supported by the limited conversion when commercial, pre-formed, H_2O_2 was added alone in Chapter 4 Section 5 and the research done by Shemer et. al.[33]

Figure 4.18: ^{1}H NMR for metronidazole upon being introduced to H_2 only. **Metronidazole conversion reaction conditions (N_2):** Catalyst (0.01 g), metronidazole (8.5 g, 50 ppm), 5% H_2/N_2 (420 psi), 2 h, 30 °C, 1200 rpm.

4.15 Conclusions.

The effect of reaction conditions was investigated by transitioning from ideal conditions of 2 °C, methanol as a solvent and CO_2 diluent gas to 30 °C, water-only solvent and N_2 diluent gas. The results showed that H_2O_2 production is drastically reduced while H_2O_2 degradation increased, however these adjustments must be made to minimise cost if this is to be applied on an industrial scale.

Further examination into catalyst design and reaction conditions supported that the oxidation of metronidazole was the prevalent pathway towards its degradation. Upon alloying Au and Pd together, the "synergetic effect" aids in converting a higher percentage of metronidazole due to the presence of Au releasing the radicals generated from the catalytic surface,[32] given that the 0.5 wt.% Pd/TiO_2 produced more H_2O_2 yet converted less metronidazole. Furthermore, the catalyst also indicated that it was unable to be re-used, possibly due to a combination of a reduction in H_2 conversion, metal particle agglomeration, and the loss of chlorine from the surface of the catalyst, however further testing is needed to confirm. The reaction conditions were shown to have a drastic effect on the conversion of metronidazole, with it being concluded that an increase in reaction temperature, time, and catalyst mass all increase the conversion of metronidazole, with this was hypothesised to be due to an increase in radical production. Furthermore, the effect of time and catalyst mass plateauing H_2O_2 production was hypothesised to due to catalyst deactivation, with this being supported by the reintroduction of gas mixture, and limited H_2 availability respectively.

Finally, the study of the effect of gas atmosphere and H_2:O_2 ratio led to the biggest breakthrough, indicating that upon excluding O_2 and increasing H_2 content inside the reactor vessel increases the conversion towards metronidazole. This result was unexpected, as if oxidation was the primary pathway towards converting metronidazole the greatest conversion of metronidazole would be expected when the H_2:O_2 ratio is around 1. It was identified, via ^1H NMR, that the hydrogenation of the imidazole ring is the most likely pathway leading towards the conversion of metronidazole, rather than an oxidative route that proceeds via H_2O_2 synthesis. However, the limited activity observed when commercial H_2O_2 is used alone, may indicate an oxidative route to metronidazole conversion is present but not the dominant pathway.

4.16 Future Work.

Given additional time and resources I would have pursued the following issues further:

1. Confirm if the hydrogenation products hypothesised in Chapter 4.13, are active as an antibiotic. If the molecule was no longer active as an antibiotic following hydrogenation it may lead to this method of conversion warranting further research.

2. Characterise the surface of the catalyst via TGA-MS, IR following the hydrogenation and oxidation reactions to confirm surface adsorption of the oxygenated/hydrogenated organics reaction products.

3. Investigate alternative routes to catalyst synthesis. The catalysts within this work towards the degradation of metronidazole (prepared via excess chlorine wet co-impregnation methodology), were found to be unstable, with significant loss in activity upon re-use and metal leaching.

4. Test alternative antibiotics to comprehend whether reductive or oxidative methods are better suited for their decomposition as expressed in this chapter with hydrogenation conditions being the favourable route towards the conversion of metronidazole.

5. Investigate into alternative catalysts for the hydrogenation of metronidazole to see if these catalysts can also reduce metronidazole, possibly utilising the catalyst generated by Santos *et. al*[45] for the oxidation of phenol but apply it in a similar manner to (NZVI) catalyst discussed by Chen *et. al.*[46]

4.17 References.

1   M. Oteng-Peprah, M. A. Acheampong and N. K. deVries, *Water. Air. Soil Pollut.*, 2018, **229**, 1-16.

2   D. Fatta-Kassinos, I. K. Kalavrouziotis, P. H. Koukoulakis and M. I. Vasquez, *Sci. Total Environ.*, 2011, **409**, 3555–3563.

3   E. Eriksson, K. Auffarth, A. M. Eilersen, M. Henze and A. Ledin, *Water SA*, 2003, **29**, 135–146.

4   C. N. Aonghusa and N. F. Gray, *J. Environ. Sci. Heal. - Part A Toxic/Hazardous Subst. Environ. Eng.*, 2002, **37**, 1–6.

5   E. Eriksson, S. Srigirisetty and A. M. Eilersen, *Water SA*, 2010, **36**, 139–142.

6   V. Homem and L. Santos, *J. Environ. Manage.*, 2011, **92**, 2304–2347.

7   D. W. Kolpin, E. T. Furlong, M. T. Meyer, E. M. Thurman, S. D. Zaugg, L. B. Barber and H. T. Buxton, *Environ. Sci. Technol.*, 2002, **36**, 1202–1211.

8   K. Kümmerer, *J. Environ. Manage.*, 2009, **90**, 2354–2366.

9   L. S. Shore and M. Shemesh, *Pure Appl. Chem.*, 2003, **75**, 1859–1871.

10   M. Wagil, J. Maszkowska, A. Białk-Bielińska, M. Caban, P. Stepnowski and J. Kumirska, *Chemosphere*, 2015, **119**, S28–S34.

11   L. T. Q. Lien, N. Q. Hoa, N. T. K. Chuc, N. T. M. Thoa, H. D. Phuc, V. Diwan, N. T. Dat, A. J. Tamhankar and C. S. Lundborg, *Int. J. Environ. Res. Public Health*, 2016, **13**, 1–13.

12   J. S. Simms-Cendan, *Prim. Care Update Ob. Gyns.*, 1996, **3**, 153–156.

13   G. Bloom, M. Cruickshank, R. Shaban, M. Oberoi and G. Sandoval, *Who*, 2017, 12–80.

14   J. Koivunen and H. Heinonen-Tanski, *Water Res.*, 2005, **39**, 1519–1526.

15   J. J. R. Márquez, I. Levchuk and M. Sillanpää, *Catalysts*, 2018, **8**, 1-18.

16   M. Farzadkia, E. Bazrafshan, A. Esrafili, J. K. Yang and M. Shirzad-Siboni, *J. Environ. Heal. Sci. Eng.*, 2015, **13**, 1–8.

17   H. Li, Q. Gao, G. Wang, B. Han, K. Xia and C. Zhou, *Chem. Eng. J.*, 2020, **392**, 123819.

18   H. Shemer, Y. K. Kunukcu and K. G. Linden, *Chemosphere*, 2006, 63, 269–276.

19   H. G. Guo, N. Y. Gao, W. H. Chu, L. Li, Y. J. Zhang, J. S. Gu and Y. L. Gu, *Environ. Sci. Pollut. Res.*, 2013, **20**, 3202–3213.

20   H. B. Ammar, M. Ben Brahim, R. Abdelhédi and Y. Samet, *J. Mol. Catal. A Chem.*, 2016, **420**, 222–227.

21   T. Pérez, S. Garcia-Segura, A. El-Ghenymy, J. L. Nava and E. Brillas, *Electrochim. Acta*, 2015, **165**, 173–181.

22   Q. Dai, J. Zhou, M. Weng, X. Luo, D. Feng and J. Chen, *Sep. Purif. Technol.*, 2016, **166**, 109–116.

23   R. J. Knox, R. C. Knight and D. I. Edwards, *Biochem. Pharmacol.*, 1983, **32**, 2149–2156.

24   J. Chen, X. Qiu, Z. Fang, M. Yang, T. Pokeung, F. Gu, W. Cheng and B. Lan, *Chem. Eng. J.*, 2012, **181**–**182**, 113–119.

25   A. Santos, R. J. Lewis, G. Malta, A. G. R. Howe, D. J. Morgan, E. Hampton, P. Gaskin and G. J. Hutchings, *Ind. Eng. Chem. Res.*, 2019, **58**, 12623–12631.

26   D. A. Crole, S. J. Freakley, J. K. Edwards and G. J. Hutchings, *Proc. R. Soc. A Math. Phys. Eng. Sci.*, 2016, 472.

27   S. J. Freakley, M. Piccinini, J. K. Edwards, E. N. Ntainjua, J. A. Moulijn and G. J. Hutchings, *ACS Catal.*, 2013, **3**, 487–501.

28   Z. K. Lopez-Castillo, S. N. V. K. Aki, M. A. Stadtherr and J. F. Brennecke, *Ind. Eng. Chem. Res.*, 2008, **47**, 570–576.

29   C. Samanta, *Applied Catalysis A: General,* 2008, **2**, 133-149.

30   J. K. Edwards, B. Solsona, P. Landon, A. F. Carley, A. Herzing, M. Watanabe, C. J. Kiely and G. J. Hutchings, *J. Mater. Chem.*, 2005, **15**, 4595–4600.

31   P. Tian, L. Ouyang, X. Xu, C. Ao, X. Xu, R. Si, X. Shen, M. Lin, J. Xu and Y. F. Han, *J. Catal.*, 2017, **349**, 30–40.

32   T. Richards, J. H. Harrhy, R. J. Lewis, A. G. R. Howe, G. M. Suldecki, A. Folli, D. J. Morgan, T. E. Davies, E. J. Loveridge, D. A. Crole, J. K. Edwards, P. Gaskin, C. J. Kiely, Q. He, D. M. Murphy, J. Y. Maillard, S. J. Freakley and G. J. Hutchings, *Nat. Catal.*, **4**, 575-585.

33   H. Shemer, Y. K. Kunukcu and K. G. Linden, *Chemosphere*, 2006, **63**, 269–276.

34   J. Brehm, R. J. Lewis, D. J. Morgan, T. E. Davies and G. J. Hutchings, *Catal. Letters*, 2021, **152**, 254-262.

35   Solubility of Gases in Water, https://www.engineeringtoolbox.com/gases-solubility-water-d_1148.html, (accessed 17 September 2021).

36   P. Landon, P. J. Collier, A. F. Carley, D. Chadwick, A. J. Papworth, A. Burrows, C. J. Kiely and G. J. Hutchings, *Phys. Chem. Chem. Phys.*, 2003, **5**, 1917–1923.

37   M. Piccinini, E. Ntainjua N., J. K. Edwards, A. F. Carley, J. A. Moulijn and G. J. Hutchings, *Phys. Chem. Chem. Phys.*, 2010, **12**, 2488–2492.

38   M. Piccinini, PhD Thesis, Cardiff University, 2011.

39   C. M. Crombie, R. J. Lewis, R. L. Taylor, D. J. Morgan, T. E. Davies, A. Folli, D. M. Murphy, J. K. Edwards, J. Qi, H. Jiang, C. J. Kiely, X. Liu, M. S. Skjøth-Rasmussen and G. J. Hutchings, *ACS Catal.*, 2021, **11**, 2701–2714.

40   D. W. Flaherty, *ACS Catal.*, 2018, **8**, 1520–1527.

41   J. K. Edwards, A. Thomas, B. E. Solsona, P. Landon, A. F. Carley and G. J. Hutchings, *Catal. Today*, 2007, **122**, 397–402.

42   A. Santos, R. J. Lewis, G. Malta, A. G. R. Howe, D. J. Morgan, E. Hampton, P. Gaskin and G. J. Hutchings, *Ind. Eng. Chem. Res.*, 2019, **58**, 12623–12631.

43   G. R. Fulmer, A. J. M. Miller, N. H. Sherden, H. E. Gottlieb, A. Nudelman, B. M. Stoltz, J. E. Bercaw and K. I. Goldberg, *Organometallics*, 2010, **29**, 2176–2179.

44   A. A. Salem, H. A. Mossa and B. N. Barsoum, *J. Pharm. Biomed. Anal.*, 2006, **41**, 654–661.

45   A. Santos, R. Lewis, D. J. Morgan, T. Davies, E. Hampton, P. Gaskin and G. Hutchings, *Catal. Sci. Technol.*, 2021, **11**, 7866-7874.

46   Z. Fang, J. Chen, X. Qiu, X. Qiu, W. Cheng and L. Zhu, *Desalination*, 2011, **268**, 60–67.

5   Catalyst Design for H_2O_2 synthesis in a Batch Regime.

5.1   Introduction.

For catalyst design it is important to test catalyst activity towards H_2O_2 synthesis and degradation under the reaction conditions they will be operating under, with these conditions being 30 °C, under N_2 and in H_2O only, to correspond to the industrial scale non-ideal greywater treatment conditions. However, catalyst testing must also occur at optimal conditions to discern changes in catalyst performance that would have previously been masked by non-ideal conditions, therefore testing at 2 °C, under CO_2 and with MeOH allows greater separation for both H_2O_2 productivity and degradation between each catalyst than at 30 °C, under N_2 and in H_2O only.

Previously in Chapter 3 Section 7 the 0.5 wt.% Au-0.5 wt.% Pd/TiO_2 was shown to have high activity towards the synthesis of H_2O_2, producing 84 mol_{H2O2} kg_{cat}^{-1} h^{-1}, while also capable of generating ROS with the ability to act as a biocide for the degradation of *E. coli* to a greater extent than both commercial H_2O_2 and sodium hypochlorite, with a logarithmic reduction of 8.1. In Chapter 4 the catalyst showed minimal degradative potential towards the total oxidation of metronidazole but hydrogenated the antibiotic instead. However, an issue that was identified in Section 3.9 is the catalysts inability to function for any longer than a 30-minute reaction in a flow regime, with this needing to be improved if this approach can be developed on an industrial scale. To change this, this Chapter focuses on catalyst design, looking into cheaper alternative metals to Au, as an alloy for Pd and the effect of the support on catalyst performance, in the hope of potentially increasing H_2O_2 production and increasing catalyst stability. Before transitioning these catalysts to a gas phase reactor with the aim of generating H_2O_2.

While it has been thoroughly reported that Pd has a great activity towards H_2O_2 synthesis it also has a similar propensity to degrade H_2O_2[1–6] and research has shown that through the alloying of additional transition metals and post-transition metals the degradation towards H_2O_2 can be manipulated and reduced.[7] It has been widely documented that Au has the ability to enhance catalytic activity towards H_2O_2 synthesis, when compared to either Pd or Au monometallic catalysts, through what is termed 'synergistic effects'.[8,9] However recently, alternative metals have been researched for their ability to enhance the catalytic efficacy of Pd-based materials such as; Co,[10] Ni,[11,12] Cu,[13] Pt,[14] Zn,[15] Fe[16], and In[17,18]. All these previous

works shows that the introduction of a secondary metal into Pd catalysts leads to an improved H_2O_2 synthesis activity. With this in mind, this Chapter will now investigate the activity of these new materials towards H_2O_2 synthesis in both gas and liquid phase. However, prior to this the catalysts will initially be screened in a batch regime.

Additionally, the choice of support has been demonstrated to play an important role in influencing catalyst activity towards the direct synthesis and subsequent degradation of H_2O_2.[19] The support can do this by influencing the active sites of the supported metals alongside their morphology, potentially decreasing H_2O_2 decomposition and increasing H_2O_2 selectivity.[20] Supports such as CeO_2 have been shown to contribute to the stability of the oxidised Pd sites, which represent an important issue with regard to the decomposition pathway of H_2O_2.[21] Additional studies by Edwards *et. al*[22] investigated the effect the supports isoelectric point (IEP) has on increasing selectivity towards H_2O_2, looking into TiO_2, SiO_2, Carbon, Al_2O_3, CeO_2, Fe_2O_3 and MgO (Figure 5.1). Furthermore, a 0.5 wt.% Pd/ZrO_2 catalyst has shown promise by allowing increased selectivity towards H_2O_2 when compared to a 0.5 wt.% Pd/TiO_2 catalyst.[23] While Nb_2O_5 has been shown to offer high selectivity toward synthesised H_2O_2[24]. All these supports have shown promise for the direct synthesis of H_2O_2 and therefore warrant investigation into their potential effect on resolving the issue of catalyst reusability and/or increasing H_2O_2 production.
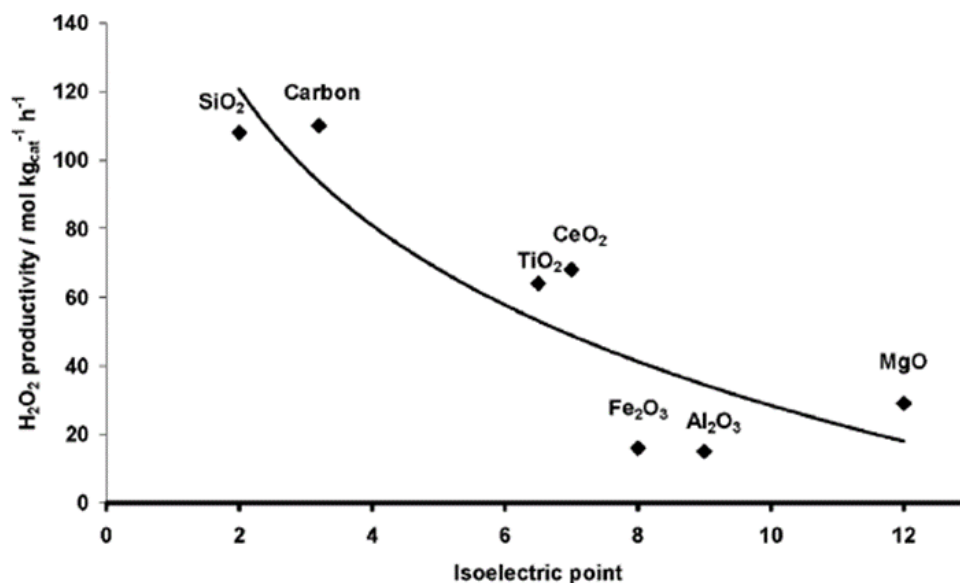
Figure 5.1: The effect that the isoelectric point of a support has on the H_2O_2 productivity of a 2.5 wt.% Au-2.5 wt.% Pd catalyst. **H_2O_2 direct synthesis reaction conditions:** Catalyst (0.01 g), H_2O (2.9 g), MeOH (5.6 g), 5% H_2/CO_2 (420 psi), 25% O_2/CO_2 (160 psi), 0.5 h, 2 °C, 1200 rpm. Figure use granted in accordance with copyright by American Chemical Society.[25]

5.2 The Effect the Various Supports have on the Synthesis and Degradation of H_2O_2 in the Liquid Phase.

Prior to testing the ability of the various 1 wt.% AuPd supported catalysts to synthesise H_2O_2 it is important to comprehend the propensity of the various supports to degrade H_2O_2, as outlined in Chapter 2 Section 3.3. The individual supports were tested for their ability to both synthesise and degrade H_2O_2 under ideal reaction conditions and non-ideal reaction conditions (Chapter 2, Section 3.2-3.5), and the results of this can be found below in Table 5.1 and 5.2.

Table 5.1: The effect the supports have on the degradation of commercial, stabilised H_2O_2, under ideal reaction conditions.

Support	H_2O_2 Productivity ($mol_{H2O2}\ kg_{cat}^{-1}\ h^{-1}$)	H_2O_2 Productivity (wt. %)	H_2O_2 Degradation ($mol_{H2O2}\ kg_{cat}^{-1}\ h^{-11}$)	H_2O_2 Degradation (%)
TiO_2	0	0	12	1
CeO_2	0	0	19	1
ZrO_2	0	0	9	0
SiO_2	0	0	10	0
Al_2O_3	0	0	7	0
Nb_2O_5	0	0	11	1
Carbon	0	0	10	0

H_2O_2 degradation reaction conditions: Support (0.01 g), H_2O_2 (50 wt.% 0.68 g), H_2O (7.82 g), 5% H_2/CO_2 (420 psi), 0.5 h, 2 °C, 1200 rpm.

Table 5.2: The effect the supports have on the degradation of commercial, stabilised H_2O_2, under non-ideal reaction conditions.

| Support	H_2O_2 Productivity ($mol_{H2O2}\ kg_{cat}^{-1}\ h^{-1}$)	H_2O_2 Productivity (wt. %)	H_2O_2 Degradation ($mol_{H2O2}\ kg_{cat}^{-1}\ h^{-1}$)	H_2O_2 Degradation (%)
Blank	0	0	145	8
TiO_2	0	0	184	9
CeO_2	0	0	185	9
ZrO_2	0	0	182	9
SiO_2	0	0	170	8
Al_2O_3	0	0	165	7
Nb_2O_5	0	0	151	8
Carbon	0	0	225	10

H_2O_2 degradation reaction conditions: Support (0.01 g), H_2O_2 (50 wt.% 0.68 g), H_2O (7.82 g), 5% H_2/N_2 (420 psi), 0.5 h, 2°C, 1200 rpm.

It can be observed that the supports display no H_2O_2 productivity and minimal H_2O_2 degradation activity under both ideal and non-ideal conditions. The results are as expected given that under the non-ideal reaction conditions a slightly higher degradation is observed,

given the loss of H_2O_2 stability upon removing methanol as a solvent, CO_2 as a diluent gas and increasing temperature.[26] These results indicate that the supports alone show minimal propensity towards the degradation of H_2O_2 therefore any observed degradation or productivity from the metal loaded supports can be attributed to the metal nanoparticles. This information allows these supports to be used to load the metal upon and in turn allow the synthesis of H_2O_2, while suppressing its degradation, as previously documented,[2,21,22,27,28] as percentage degradation is similar under both sets of conditions.

5.3   The Direct Synthesis of H_2O_2 for Various 1 wt.% AuPd Supported Catalysts in a Batch Regime, under Ideal Reaction Conditions.

It was concluded, in the previous section, that the supports offer negligible activity towards H_2O_2 synthesis and degradation under both ideal and non-ideal reaction conditions. Following this, the effect that support choice has the on H_2O_2 productivity and degradation for a 1 wt.% AuPd supported catalysts was studied. For this study, the catalyst was made again using the excess chloride wet co-impregnation method, outlined in Chapter 2 Section 2, before testing under ideal reactions to allow for discernible changes towards H_2O_2 productivity following the changing of support that would be masked by non-ideal reaction conditions. The results for this study are shown below in Figure 5.2 and Table 5.3.
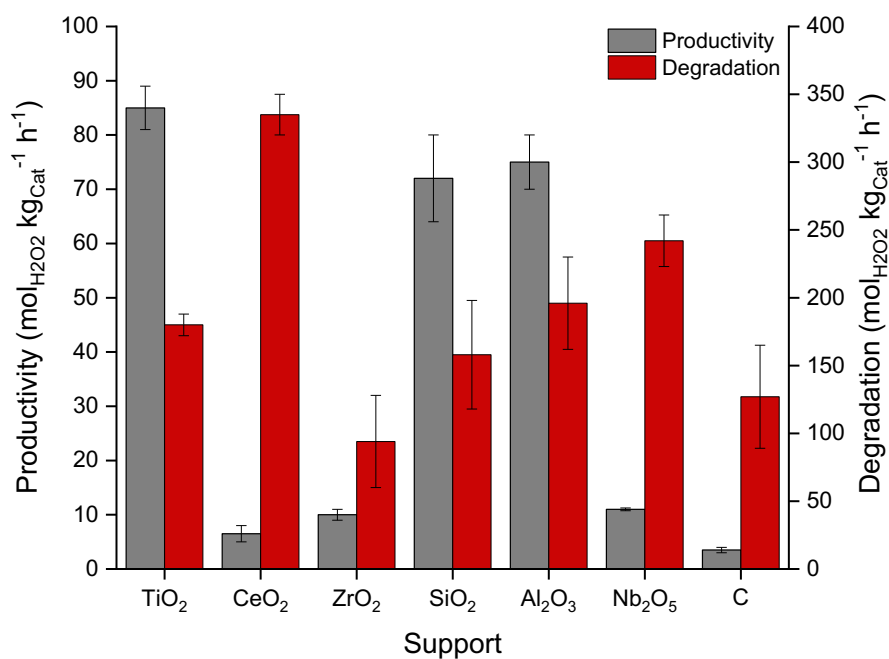
Figure 5.2: The effect the support has on the activity of 0.5 wt.% Au-0.5 wt.% Pd catalysts towards the direct synthesis and degradation of H_2O_2, under ideal reaction conditions. **H_2O_2 direct synthesis reaction conditions:** Catalyst (0.01 g), H_2O (2.9 g), MeOH (5.6 g), 5% H_2/CO_2 (420 psi), 25% O_2/CO_2 (160 psi), 0.5 h, 2 °C, 1200 rpm. **H_2O_2 degradation reaction conditions:** Catalyst (0.01 g), H_2O_2 (50 wt.% 0.68 g), H_2O (2.22 g), MeOH (5.6 g), 5% H_2/CO_2 (420 psi), 0.5 h, 2 °C, 1200 rpm.

Table 5.3: The effect the support has on the 1 wt.% AuPd catalysts towards the H_2 conversion, H_2O_2 productivity and H_2O_2 degradation of a 1 wt.% AuPd catalyst, under ideal reaction conditions.

Support	H_2O_2 Productivity (mol_{H2O2} kg_{cat}^{-1} h^{-1})	H_2O_2 (Wt. %)	H_2 Conversion (%)	H_2O_2 Selectivity (%)	H_2O_2 Degradation (mol_{H2O2} kg_{cat}^{-1} h^{-1})
0.5 wt.% Au-0.5 wt.% Pd/TiO$_2$	85	0.17	19	54	180
0.5 wt.% Au-0.5 wt.% Pd/CeO$_2$	6	0.03	8	45	330
0.5 wt.% Au-0.5 wt.% Pd/ZrO$_2$	10	0.02	7	43	94
0.5 wt.% Au-0.5 wt.% Pd/SiO$_2$	72	0.15	8	53	158
0.5 wt.% Au-0.5 wt.% Pd/Al$_2$O$_3$	75	0.15	13	29	196
0.5 wt.% Au-0.5 wt.% Pd/Nb$_2$O$_5$	11	0.02	5	34	242
0.5 wt.% Au-0.5 wt.% Pd/C	4	0.008	2	38	127

H_2O_2 direct synthesis reaction conditions: Catalyst (0.01 g), H_2O (2.9 g), MeOH (5.6 g), 5% H_2/CO_2 (420 psi), 25% O_2/CO_2 (160 psi), 0.5 h, 2 °C, 1200 rpm. **H_2O_2 degradation reaction conditions:** Catalyst (0.01 g), H_2O_2 (50 wt.% 0.68 g), H_2O (2.22 g), MeOH (5.6 g), 5% H_2/CO_2 (420 psi), 0.5 h, 2 °C, 1200 rpm.
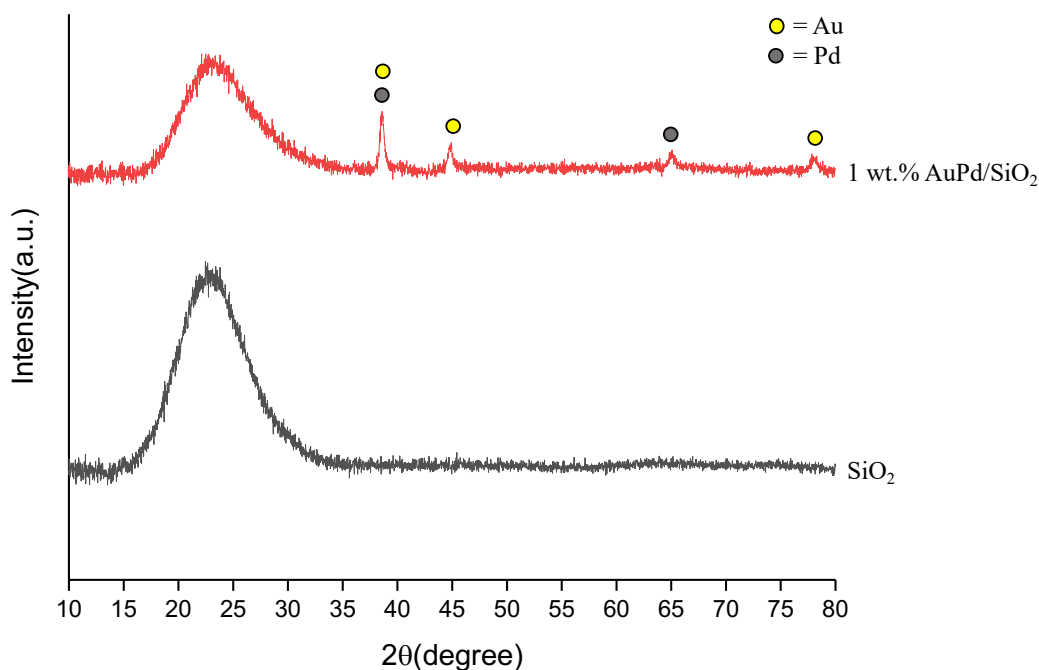
The results show that the choice of support has a considerable effect on the catalytic performance towards the productivity of H_2O_2 in a similar manner to the 5 wt.% AuPd supported catalyst tested by Edwards *et. al,*[29], which illustrates the key role that support choice has on H_2O_2 production. The data in Figure 5.2 and Table 5.3 shows the 1 wt.% AuPd/TiO$_2$ is still the most productive catalyst towards the direct synthesis of H_2O_2 with a value of 85 mol_{H2O2} kg_{cat}^{-1} h^{-1}. The SiO$_2$ and Al$_2$O$_3$ supported catalysts also exhibit promising productivities of 72 and 75 mol_{H2O2} kg_{cat}^{-1} h^{-1}. Furthermore, for the degradation of H_2O_2 it is the CeO$_2$ supported catalyst that has the highest rate of degradation with a value of 335 mol_{H2O2} kg_{cat}^{-1} h^{-1}. Following these results, XPS and BET surface area analysis was undertaken, displayed in Table 5.4 and Table 5.5 respectively, to comprehend the reasoning behind these results.

Table 5.4: The surface composition of 1 wt.% AuPd supported catalysts, as determined by XPS.

Support	Pd: Au	$Pd^{2+}: Pd^0$
0.5 wt.% Au-0.5 wt.% Pd/TiO_2	4.2	0.5
0.5 wt.% Au-0.5 wt.% Pd/CeO_2	4.2	0.7
0.5 wt.% Au-0.5 wt.% Pd/ZrO_2	1.7	All Pd^0
0.5 wt.% Au-0.5 wt.% Pd/SiO_2	2.4	0.5
0.5 wt.% Au-0.5 wt.% Pd/Al_2O_3	6.2	0.9
0.5 wt.% Au-0.5 wt.% Pd/Nb_2O_5	5.0	0.1
0.5 wt.% Au-0.5 wt.% Pd/C	0.6	All Pd^0

Table 5.5: The surface area of the metal oxide and carbon supports with and without the 1 wt.% AuPd, determined by BET.

Support	Surface Area without Metal ($m^2\,g^{-1}$)	Surface Area with Metal ($m^2\,g^{-1}$)
TiO_2	59	50
CeO_2	5	4
ZrO_2	2	2
SiO_2	319	314
Al_2O_3	213	201
Nb_2O_5	6	6
Carbon	1225	1121

Figure 5.3: X-ray diffractograms of powdered 1 wt.% AuPd/SiO$_2$ supported catalysts. ICCD Reference Number: SiO$_2$: 01-078-4812, Pd: 01-087-0638, Au: 01-071-4614.

From the BET data (Table 5.5) it is clear that immobilising the metals leads to a minor reduction in the total surface area available. The poor activity for the ZrO$_2$, CeO$_2$ and Nb$_2$O$_5$ supported catalysts could be explained by poor dispersion of the metal upon the surface of the catalysts, given their relatively low surface areas of 2, 4.4 and 5.9 m^2 g^{-1} respectively. To confirm this XRD was utilised, Appendix Figures 5.16, 5.17, and 5.19. However, none of the supports showed any reflections associated with the immobilised metals, possibly due to low metal loading. If time allowed, TEM could be utilised to confirm that metal dispersion over these catalysts was poor but as catalyst performance was limited this was considered to not be appropriate. The poor activity towards H$_2$O$_2$ synthesis and high degradation of the C supported catalysts can be explained by all the Pd present on the catalyst being Pd^0 only as determined by XPS (Table 5.4), with this offering poor selectivity and activity to H$_2$O$_2$ synthesis, compared to PdO.[3] The high performance of Al$_2$O$_3$ catalyst can be assigned to the high surface area of the support which will allow high metal dispersion, indicated by XRD (Figure 5.18), in addition to the mixed oxidation state of the Pd (Pd^{2+}:Pd^0 ratio of 0.9), which has been reported to aid in increasing both the production and selectivity towards the production of H$_2$O$_2$.[30] However, for the 1 wt.% AuPd/SiO$_2$ supported catalyst the limited performance may be attributed to the

presence of large metal nanoparticles, with clear reflections for immobilised metals observed in the XRD diffractogram shown above, Figure 5.3, with large nanoparticles reported to offer increased H_2O_2 degradation activity.[31]

5.4 The Effect of the Support on the Reusability of Powdered 1 wt.% AuPd Catalysts for the Direct Synthesis of H_2O_2, in a Batch Regime.

For a catalyst to be able to be used on an industrial scale it is imperative that it is stable upon re-use, with the loss of active metals a possible route responsible for deactivation. It would be preferential to study for this under continuous flow conditions, as this would allow the monitoring of H_2 conversion, H_2O_2 concentration, H_2O_2 degradation and productivity over extended reaction time, and under conditions more akin to those likely to be used for real world application. The post reaction effluent could also be continually analysed to identify the extent of metal leaching as a function of rection time. Yet, the main reason continuous flow is preferential as this would allow the real-life application of a catalyst in greywater treatment to be replicated, therefore allowing for a greater comprehension of any future pitfalls. However, within this work catalyst stability was studied using a batch regime due to practicalities associated with catalyst testing. In particular, the removal of leached metal species from a batch system is considerably easier than from a continuous flow system. To determine catalyst stability within this work the catalyst was utilised in a 30-minute H_2O_2 synthesis reaction, the recovered catalyst dried under vacuum for 16 hours at 30 °C. The catalyst was then re-tested for the direct synthesis of H_2O_2, with the results of this re-use being shown below in Table 5.6. While the XPS and ICP data can be found in Table 5.7 and 5.8 respectively

Table 5.6: Reusability of the supported 1 wt.% AuPd catalysts towards the H_2 conversion, H_2O_2 productivity and H_2O_2 degradation at 2 °C.

Catalyst	H_2O_2 Productivity (Use 1) (mol_{H2O2} kg_{cat}^{-1} h^{-1})	H_2O_2 Productivity (Use 2) (mol_{H2O2} kg_{cat}^{-1} h^{-1})	H_2O_2 Productivity Loss/Gain (%)
0.5 wt.% Au-0.5 wt.% Pd/TiO_2	85	45	-47
0.5 wt.% Au-0.5 wt.% Pd/CeO_2	6	36	+600
0.5 wt.% Au-0.5 wt.% Pd/ZrO_2	10	7	-30
0.5 wt.% Au-0.5 wt.% Pd/SiO_2	72	46	-64
0.5 wt.% Au-0.5 wt.% Pd/Al_2O_3	75	7	-93
0.5 wt.% Au-0.5 wt.% Pd/Nb_2O_5	11	4	-36
0.5 wt.% Au-0.5 wt.% Pd/C	6	4	-33

H_2O_2 direct synthesis reaction conditions: Catalyst (0.01 g), H_2O (2.9 g), MeOH (5.6 g), 5% H_2/CO_2 (420 psi), 25% O_2/CO_2 (160 psi), 0.5 h, 2 °C, 1200 rpm.

Table 5.7: The surface composition of 1 wt.% AuPd supported catalysts after use in the direct synthesis of H_2O_2, as determined by XPS.

Support	Pd: Au (Fresh)	Pd: Au (Used)	$Pd^{2+}: Pd^0$ (Fresh)	$Pd^{2+}: Pd^0$ (Used)
0.5 wt.% Au-0.5 wt.% Pd/TiO$_2$	4.2	1.4	0.5	0.5
0.5 wt.% Au-0.5 wt.% Pd/CeO$_2$	4.2	3.1	0.7	0.3
0.5 wt.% Au-0.5 wt.% Pd/ZrO$_2$	1.7	4.0	All Pd^0	All Pd^0
0.5 wt.% Au-0.5 wt.% Pd/SiO$_2$	2.4	7.2	0.5	0.1
0.5 wt.% Au-0.5 wt.% Pd/Al$_2$O$_3$	6.2	16.6	0.9	0.7
0.5 wt.% Au-0.5 wt.% Pd/Nb$_2$O$_5$	5.0	13.6	0.1	0.1
0.5 wt.% Au-0.5 wt.% Pd/C	0.6	0.5	All Pd^0	All Pd^0

H_2O_2 direct synthesis reaction conditions: Catalyst (0.01 g), H_2O (2.9 g), MeOH (5.6 g), 5% H_2/CO_2 (420 psi), 25% O_2/CO_2 (160 psi), 0.5 h, 2 °C, 1200 rpm.

Table 5.8: Leaching of the Au and Pd from the 1 wt.% AuPd supported catalysts following a H_2O_2 direct synthesis reaction, determined by ICP.

Catalyst	Au Leached (%)	Au Leached (ppb)	Pd Leached (%)	Pd Leached (ppb)
0.5 wt.% Au-0.5 wt.% Pd/TiO$_2$	0.0	2.0	0.8	45.0
0.5 wt.% Au-0.5 wt.% Pd/CeO$_2$	0.0	0.0	0.0	1.2
0.5 wt.% Au-0.5 wt.% Pd/ZrO$_2$	0.0	2.0	1.5	87.0
0.5 wt.% Au-0.5 wt.% Pd/SiO$_2$	0.5	26.7	0.4	26.0
0.5 wt.% Au-0.5 wt.% Pd/Al$_2$O$_3$	0.0	0.0	0.0	0.9
0.5 wt.% Au-0.5 wt.% Pd/Nb$_2$O$_5$	0.0	0.0	0.1	5.5
0.5 wt.% Au-0.5 wt.% Pd/C	0.0	0.0	0.0	0.0

H_2O_2 direct synthesis reaction conditions: Catalyst (0.01 g), H_2O (2.9 g), MeOH (5.6 g), 5% H_2/CO_2 (420 psi), 25% O_2/CO_2 (160 psi), 0.5 h, 2 °C, 1200 rpm.
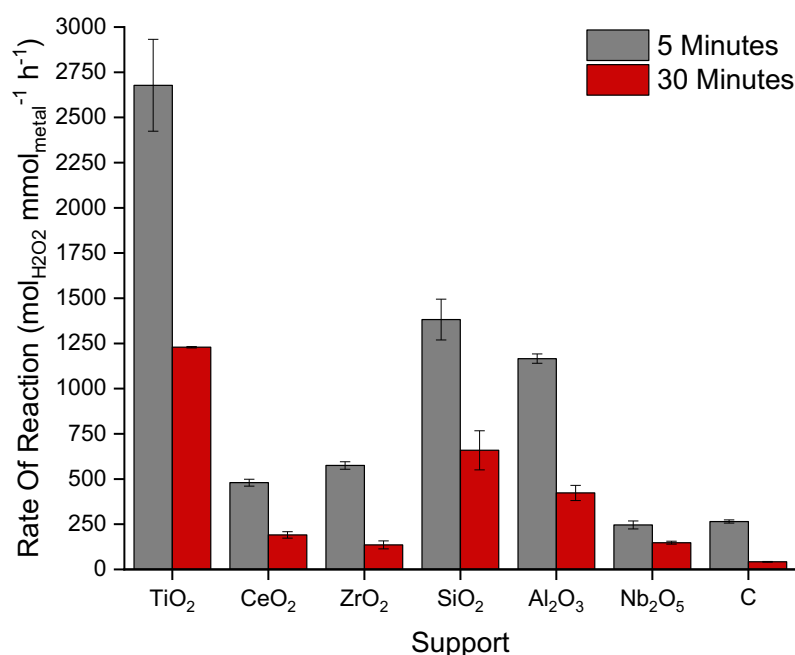
Catalyst activity towards H_2O_2 synthesis was observed to decrease upon re-use for most of the catalysts studied, with the exception of the 1 wt.% AuPd/CeO$_2$ catalyst, with H_2O_2 synthesis activity decreasing by approximately 30-93%. The most probable cause for this observed reduction in catalyst activity upon re-use may be leaching of the Au and Pd upon use. However, as observed in Table 5.8, there is minimal leaching for both Au and Pd across all the catalysts, indicating this is not the cause for the observed instability of the catalysts. As shown in Table 5.7, upon re-using the catalyst there is a reduction in the amount of Pd^{2+} and an increase in the amount of Pd^0, determined by XPS analysis. This increase in Pd^0 and reduction in Pd^{2+} will lead to a decrease in selectivity and activity due to an increase in H_2O_2 decomposition activity, as reported by Choudhary *et. al.*[2], and would explain the expressed reduction in productivity upon re-use. Additionally, the loss of the chlorine from the catalyst could be causing the observed decrease in catalyst productivity. The process of the chlorine being removed from the surface of the catalyst after the initial reaction and following washing could influence productivity, as documented by Brehm *et. al.*[32] The research concluded that the removal of the chlorine could remove the promotional effect that chlorine has on allowing the dispersion of the highly active species, towards the synthesis of H_2O_2, and stable supported Au and Pd nanoparticles. Yet, for the CeO$_2$ supported there was a marked increase in the productivity of the catalyst, up to 36 mol_{H2O2} kg_{cat}^{-1} h^{-1} from 6 mol_{H2O2} kg_{cat}^{-1} h^{-1}. This enhancement could be due to an increase in Pd metal on the catalyst, however without further characterisation to determine the effect re-use has on particle size this result is difficult to conclude.

5.5 The Effect of Pelleting on Initial Rate of Production Towards the Direct Synthesis of H_2O_2 for Various 1 wt.% AuPd Supported Catalysts in a Batch Regime.

Further testing was done to comprehend the initial rate of production for the various 1 wt.% AuPd supported powdered and pelleted catalysts. The catalysts were pelleted by taking the powdered catalyst and pelleting them for 10 seconds under 10 t of pressure before being ground and sieved to a size between 425 – 600 microns using sieves. This study was done as a catalyst needs to sustain its productivity over a prolonged period to have any industrial application, alongside the fact that for most industrial flow reactors powdered catalysts would not be appropriate. To test initial rate of production, the reaction time was reduced to 5 minutes, where the contribution from side reactions is considered to be negligible. In addition, the pellets were reground before testing under the reaction conditions outlined above (Section 5.3). The results for this are shown below in Figure 5.4 and Figure 5.5.
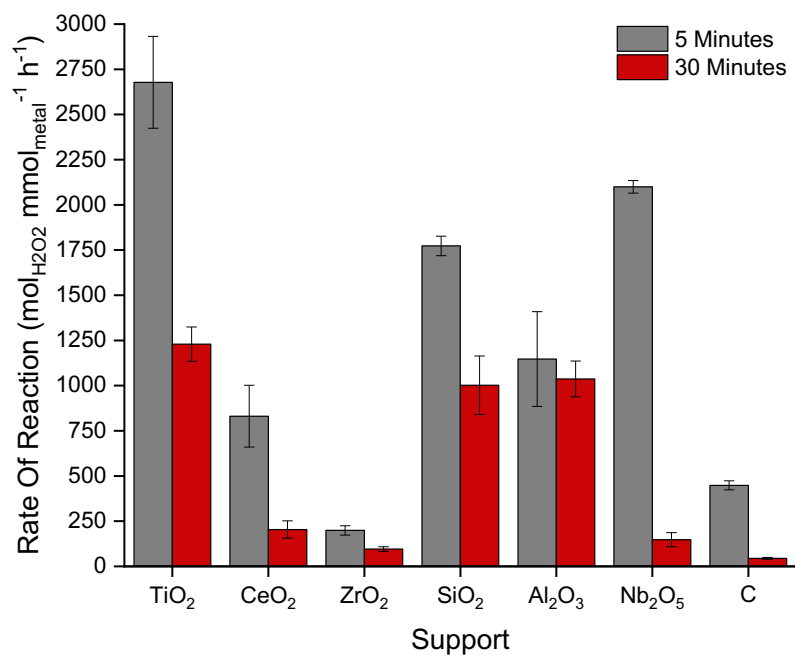
Figure 5.4: Performance of the powdered 1 wt.% AuPd catalysts towards the direct synthesis of H_2O_2 as a function of catalyst support, under ideal conditions. **H_2O_2 direct synthesis reaction conditions:** Catalyst (0.01 g), H_2O (2.9 g), MeOH (5.6 g), 5% H_2/CO_2 (420 psi), 25% O_2/CO_2 (160 psi), 2 °C, 1200 rpm.

Figure 5.5: The effect the support has on the activity of the pelleted 1 wt.% AuPd catalysts for the productivity towards H_2O_2 after 5 minutes, under ideal conditions. **H_2O_2 direct synthesis reaction conditions:** Catalyst (0.01 g), H_2O (2.9 g), MeOH (5.6 g), 5% H_2/CO_2 (420 psi), 25% O_2/CO_2 (160 psi), 0.5 h, 2 °C, 1200 rpm.

Table 5.9: The surface composition of the powdered and reground pellets of the 1 wt.% AuPd supported catalysts, as determined by XPS.

| Catalyst	Pd: Au (Fresh)	Pd: Au (Reground Pellets)	Pd^{2+}: Pd^0 (Fresh)	Pd^{2+}: Pd^0 (Reground Pellets)
0.5 wt.% Au-0.5 wt.% Pd/TiO$_2$	4.2	3.6	0.5	0.5
0.5 wt.% Au-0.5 wt.% Pd/CeO$_2$	4.2	3.8	0.7	2.3
0.5 wt.% Au-0.5 wt.% Pd/ZrO$_2$	1.7	1.4	All Pd^0	0.1
0.5 wt.% Au-0.5 wt.% Pd/SiO$_2$	2.4	2.1	0.5	0.7
0.5 wt.% Au-0.5 wt.% Pd/Al$_2$O$_3$	6.2	1.9	0.9	1.9
0.5 wt.% Au-0.5 wt.% Pd/Nb$_2$O$_5$	5.0	3.8	0.1	0.2
0.5 wt.% Au-0.5 wt.% Pd/C	0.6	0.5	All Pd^0	0.1

The data shows that all the catalysts, powdered and pelleted, have a drop off in activity towards the direct synthesis of H_2O_2 following the initial 5-minute reaction time. The most drastic of the documented drop-offs being the Nb$_2$O$_5$ supported powdered catalysts which sees a decrease in its productivity from 2100 mol_{H2O2} $mmol_{metal}^{-1}$ h^{-1} after 5 minutes to 148 after 30 minutes. However, the Al$_2$O$_3$ supported catalyst shows a promising result maintaining its productivity of 1147 mol_{H2O2} $mmol_{metal}^{-1}$ h^{-1} from the initial 5-minute reaction into 1037 mol_{H2O2} $mmol_{metal}^{-1}$ h^{-1} from the 30-minute reaction. This observed decrease towards the production rate of H_2O_2 can be assigned to an increase in the degradation rates as the reaction proceeds,[33] as the rate of H_2O_2 degradation is proportional to H_2O_2 concentration. As a result there is a deviation in selectivity away from H_2O_2 production,[34] with this leading to a decrease in the rate at which H_2O_2 can be directly synthesised. Furthermore, for the pelleted catalysts, when compared to the powdered catalyst, the majority of the supported catalysts show a loss of production after both 5 and 30 minutes. However, the 1 wt.% AuPd/TiO$_2$ and Al$_2$O$_3$ supported, pelleted catalyst only shows minimal loss of production when compared to its powdered counterpart. The pelleted Al$_2$O$_3$ supported catalyst initial reaction rate after 5 minutes is 1166 mol_{H2O2} $mmol_{metal}^{-1}$ h^{-1} but significantly reduces to 423 mol_{H2O2} $mmol_{metal}^{-1}$ h^{-1} after 30 minutes. This is unfortunate given the promising results expressed above with the powder almost maintaining its productivity over a 30-minute reaction time. The XPS data (Table 5.9) comparing the powder and pellets of the various supported catalysts shows an increase the Pd^{2+}:Pd^0, which indicates

an increase in the amount of Pd^{2+} present on the surface of the catalysts. This documented change in the catalysts Pd speciation supports the decrease in the rate of reaction towards the production of H_2O_2 after both 5-minute and 30-minute reaction times. This being as although the Pd^{2+} is more selective towards the production of H_2O_2 it is also less active towards the conversion of H_2 to both H_2O_2 and its degradation products,[2] with this combination lead to a reduction in the rate of production of H_2O_2.

5.6 The Effect Pelleting has on the Direct Synthesis of H_2O_2 for Various 1 wt.% AuPd Supported Catalysts in a Batch Regime.

The effect pelleting has on the direct synthesis and degradation of H_2O_2 for various 1 wt.% AuPd supported catalysts was studied in a batch regime, prior to trialling in the gas phase reactor. The data is reported below in Figure 5.6 and Table 5.9, while the XPS and ICP data are reported in Table 5.10 and 5.11 respectively.
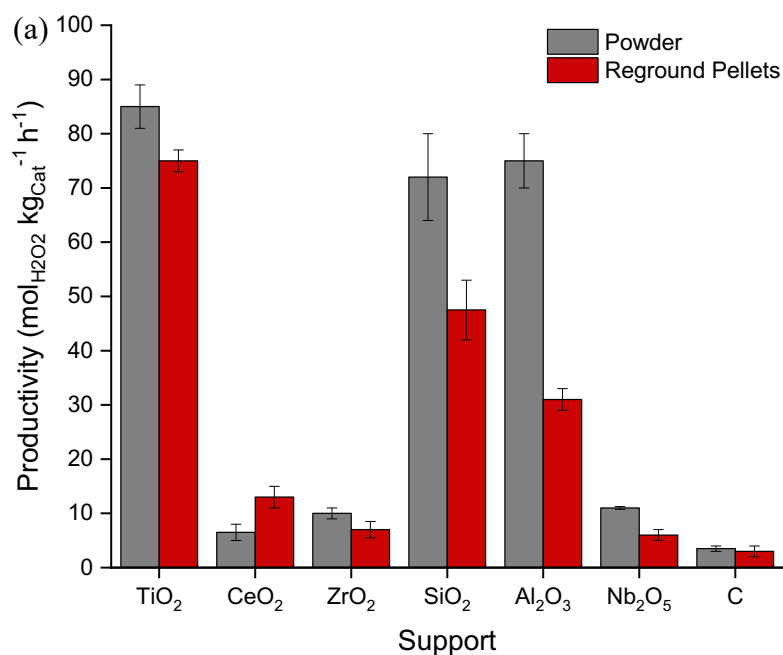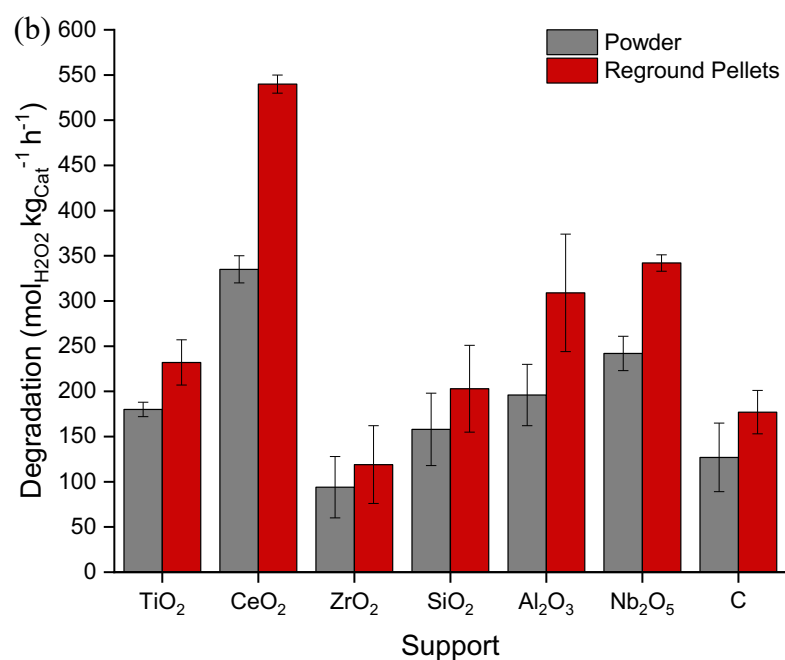
Figure 5.6: The effect the changing of the support has on the activity of pelleted 1 wt.% MPd supported catalyst towards the (a) direct synthesis and (b) degradation of H_2O_2, under ideal reaction conditions. **H_2O_2 direct synthesis reaction conditions:** Catalyst (0.01 g), H_2O (2.9 g), MeOH (5.6 g), 5% H_2/CO_2 (420 psi), 25% O_2/CO_2 (160 psi), 0.5 h, 2 °C, 1200 rpm. **H_2O_2 degradation reaction conditions:** Catalyst (0.01 g), H_2O_2 (50 wt.% 0.68 g), H_2O (2.22 g), MeOH (5.6 g), 5% H_2/CO_2 (420 psi), 0.5 h, 2 °C, 1200 rpm.

Table 5.10: The effect pelleting has on the 1 wt.% AuPd supported catalysts towards the H_2 conversion, H_2O_2 productivity and H_2O_2 degradation, under ideal reaction conditions.

Support	H_2O_2 Productivity ($mol_{H2O2}\ kg_{cat}^{-1}\ h^{-1}$)	H_2O_2 (Wt. %)	H_2 Conversion (%)	H_2O_2 Selectivity (%)	H_2O_2 Degradation ($mol_{H2O2}\ kg_{cat}^{-1}\ h^{-1}$)
0.5 wt.% Au-0.5 wt.% Pd/TiO$_2$	75	0.15	19	54	232
0.5 wt.% Au-0.5 wt.% Pd/CeO$_2$	13	0.026	8	43	540
0.5 wt.% Au-0.5 wt.% Pd/ZrO$_2$	7	0.014	8	41	119
0.5 wt.% Au-0.5 wt.% Pd/SiO$_2$	47	0.095	16	51	203
0.5 wt.% Au-0.5 wt.% Pd/Al$_2$O$_3$	31	0.063	18	24	309
0.5 wt.% Au-0.5 wt.% Pd/Nb$_2$O$_5$	6	0.012	7	27	342
0.5 wt.% Au-0.5 wt.% Pd/C	3	0.005	4	34	177

H_2O_2 direct synthesis reaction conditions: Catalyst (0.01 g), H_2O (2.9 g), MeOH (5.6 g), 5% H_2/CO_2 (420 psi), 25% O_2/CO_2 (160 psi), 0.5 h, 2 °C, 1200 rpm. **H_2O_2 degradation reaction conditions:** Catalyst (0.01 g), H_2O_2 (50 wt.% 0.68 g), H_2O (2.22 g), MeOH (5.6 g), 5% H_2/CO_2 (420 psi), 0.5 h, 2 °C, 1200 rpm.

Table 5.11: Leaching of the Au and Pd from the pelleted 1 wt.% AuPd catalysts following a H_2O_2 direct synthesis reaction, determined by ICP.

| Catalyst	Au Leached (%)	Au Leached (ppb)	Pd Leached (%)	Pd Leached (ppb)
0.5 wt.% Au-0.5 wt.% Pd/TiO$_2$	0.0	2.0	0.1	4.0
0.5 wt.% Au-0.5 wt.% Pd/CeO$_2$	0.0	0.0	4.6	270.0
0.5 wt.% Au-0.5 wt.% Pd/ZrO$_2$	0.0	0.0	1.1	64.0
0.5 wt.% Au-0.5 wt.% Pd/SiO$_2$	0.0	0.0	0.8	46.9
0.5 wt.% Au-0.5 wt.% Pd/Al$_2$O$_3$	0.0	0.0	1.0	60.0
0.5 wt.% Au-0.5 wt.% Pd/Nb$_2$O$_5$	0.0	0.0	0.2	9.0
0.5 wt.% Au-0.5 wt.% Pd/C	0.0	0.0	0.0	0.0

H_2O_2 direct synthesis reaction conditions: Catalyst (0.01 g), H_2O (2.9 g), MeOH (5.6 g), 5% H_2/CO_2 (420 psi), 25% O_2/CO_2 (160 psi), 0.5 h, 2 °C, 1200 rpm.

The data shows an across-the-board decrease in the productivity towards the direct synthesis of H_2O_2 and an increase towards its degradation for all the different supports apart from CeO_2, compared to the as-prepared powdered materials (Table 5.10). With regards to H_2O_2 degradation the CeO_2 supported catalyst shows the largest degradation increase upon pelleting, growing from 130 to 540 mol$_{H2O2}$ kg$_{cat}^{-1}$ h^{-1}. The TiO$_2$ supported catalyst shows the smallest decrease in the activity towards the direct synthesis of H_2O_2, with a loss of 10 mol$_{H2O2}$ kg$_{cat}^{-1}$ h^{-1}, while the Al$_2$O$_3$ supported catalyst shows the largest decrease in productivity of 44 mol$_{H2O2}$ kg$_{cat}^{-1}$ h^{-1}. To understand these trends ICP studies were undertaken, with the results in Table 5.11 showing minimal leaching of Au and Pd for all the supports. However, the XPS data (Table 5.9) comparing the powder and pellets of the various supported catalyst shows an increase in the Pd^{2+}: Pd^0 ratio. This result allows the comprehension of the trends expressed in Figure 5.6, as the catalysts morphology supports the decrease in the production of H_2O_2 as the increase in the presence of Pd^{2+} which is documented to be more selective towards the production of H_2O_2 but less active towards its production.[2] However, this result does not explain the increase in H_2O_2 degradation, yet it is possible that the increase in H_2O_2 degradation could be due to the previously observed (Chapter 3, Figure 3.6) increase in the mean particle size of the 1%AuPd/TiO$_2$ catalyst from 2.9 nm in the powdered catalyst to 4.5 nm in the

pelleted analogue (Chapter 3, Histograms in Figure3.6 (a,b) HAADF-STEM images Figure 3.6 (c (ii-iv)). With this increase in particle size leading to an increase in H_2O_2 degradation, due to the decrease towards H_2O_2 selectivity that is observed with increasing particle size.[31] Yet, as this was only observed for the TiO_2 supported catalyst without further confirmation through TEM of these individual samples this can only be a suggestion. However, for the CeO_2 supported there was a marked increase in the productivity of the catalyst following the pelleting of the catalyst, up to 13 mol_{H2O2} kg_{cat}^{-1} h^{-1} from 6 mol_{H2O2} kg_{cat}^{-1} h^{-1}. This enhancement could be due to an increase in Pd^{2+} (Table 5.9), with this state of Pd being documented as more selective towards the direct synthesis of H_2O_2.[3] However, once again without further characterisation to determine the effect re-use has on particle size this result is difficult to conclude.

5.7   The Direct Synthesis of H_2O_2 for Various 1 wt.% AuPd Supported Catalysts in a Batch Regime under Non-Ideal Conditions.

It is important to understand the efficacy of the catalysts under conditions less conducive to H_2O_2 stability but more likely to be favoured for industrial application. As such testing of the 1 wt.% AuPd supported catalysts was carried out at 30 °C, with N_2 diluted gas feeds and methanol-free solvent mixture, with the results of this study shown below in Figure 5.7 and Tables 5.12 + 5.13.
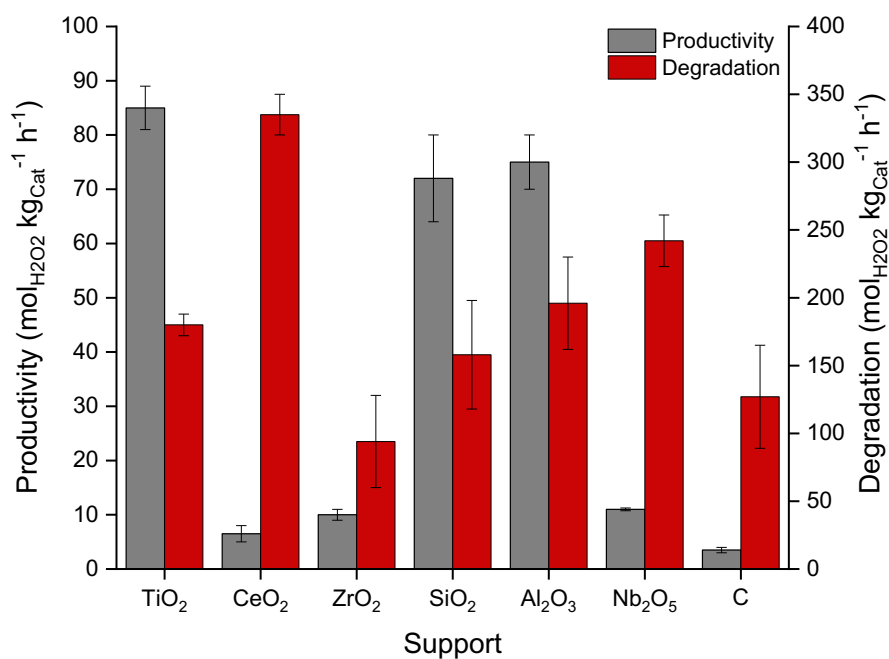
Figure 5.7: The effect the support has on the activity of AuPd catalysts towards the direct synthesis and degradation of H_2O_2, under ideal reaction conditions. **H_2O_2 direct synthesis reaction conditions:** Catalyst (0.01 g), H_2O (2.9 g), MeOH (5.6 g), 5% H_2/CO_2 (420 psi), 25% O_2/CO_2 (160 psi), 0.5 h, 2 °C, 1200 rpm. **H_2O_2 degradation reaction conditions:** Catalyst (0.01 g), H_2O_2 (50 wt.% 0.68 g), H_2O (2.22 g), MeOH (5.6 g), 5% H_2/CO_2 (420 psi), 0.5 h, 2 °C, 1200 rpm.
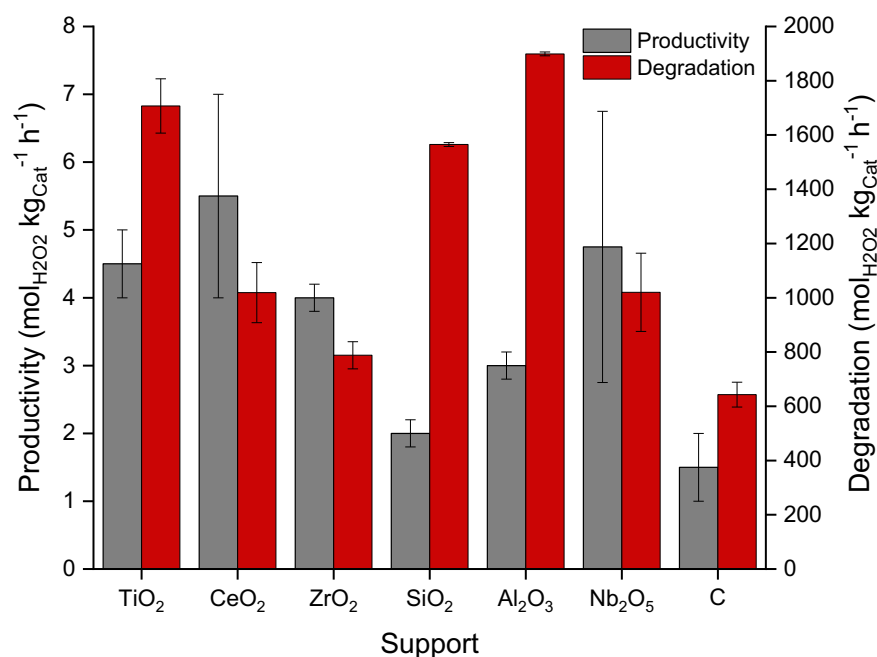
Figure 5.8: The effect the support has on the 1 wt.% AuPd catalyst towards the direct synthesis and degradation of H_2O_2, under non-ideal reaction conditions. **H_2O_2 direct synthesis reaction conditions:** Catalyst (0.01 g), H_2O (8.5 g), 5% H_2/N_2 (420 psi), 25% O_2/N_2 (160 psi), 0.5 h, 30 °C, 1200 rpm. **H_2O_2 degradation reaction conditions:** Catalyst (0.01 g), H_2O_2 (50 wt.% 0.68 g), H_2O (7.82 g), 5% H_2/N_2 (420 psi), 0.5 h, 30 °C, 1200 rpm.

Table 5.12: The effect the support has on the rate of H_2O_2 synthesis using 1 wt.% AuPd catalysts, under non-ideal reaction conditions.

Support	Rate of Reaction ($mol_{H2O2}mmol_{metal}^{-1}h^{-1}$)
0.5 wt.% Au-0.5 wt.% Pd/TiO_2	77
0.5 wt.% Au-0.5 wt.% Pd/CeO_2	90
0.5 wt.% Au-0.5 wt.% Pd/ZrO_2	50
0.5 wt.% Au-0.5 wt.% Pd/SiO_2	28
0.5 wt.% Au-0.5 wt.% Pd/Al_2O_3	39
0.5 wt.% Au-0.5 wt.% Pd/Nb_2O_5	77
0.5 wt.% Au-0.5 wt.% Pd/C	24

H₂O₂ direct synthesis reaction conditions: Catalyst (0.01 g), H_2O (8.5 g), 5% H_2/N_2 (420 psi), 25% O_2/N_2 (160 psi), 0.5 h, 30 °C, 1200 rpm. Rate of reaction calculated using a theoretical metal loading and minimal number of active sites.

Table 5.13: The effect the support has on the 1 wt.% AuPd catalysts towards the H_2 conversion, H_2O_2 productivity and H_2O_2 degradation, under non-ideal reaction conditions.

| Catalyst	H_2O_2 Productivity (mol_{H2O2} kg_{cat}^{-1} h^{-1})	H_2O_2 (Wt. %)	H_2 Conversion (%)	H_2O_2 Selectivity (%)	H_2O_2 Degradation (mol_{H2O2} kg_{cat}^{-1} h^{-1})
0.5 wt.% Au-0.5 wt.% Pd/TiO₂	5	0.010	48	3	1707
0.5 wt.% Au-0.5 wt.% Pd/CeO₂	6	0.014	30	5	1019
0.5 wt.% Au-0.5 wt.% Pd/ZrO₂	4	0.008	22	2	788
0.5 wt.% Au-0.5 wt.% Pd/SiO₂	2	0.004	43	1	1555
0.5 wt.% Au-0.5 wt.% Pd/Al₂O₃	3	0.005	43	1	1899
0.5 wt.% Au-0.5 wt.% Pd/Nb₂O₅	5	0.012	32	3	1020
0.5 wt.% Au-0.5 wt.% Pd/C	2	0.004	39	1	643

H₂O₂ direct synthesis reaction conditions: Catalyst (0.01 g), H_2O (8.5 g), 5% H_2/N_2 (420 psi), 25% O_2/N_2 (160 psi), 0.5 h, 30 °C, 1200 rpm.**H₂O₂ degradation reaction conditions:** Catalyst (0.01 g), H_2O_2 (50 wt.% 0.68 g), H_2O (7.82 g), 5% H_2/N_2 (420 psi), 0.5 h, 30 °C, 1200 rpm.

Upon testing each of the various 1 wt.% AuPd supported catalysts in a batch regime at 30 °C using an N_2 gaseous diluent, minimal H_2O_2 production was observed, while catalytic activity towards H_2O_2 degradation was found to be very high (643-1899 mol_{H2O2} kg_{cat}^{-1} h^{-1}). Furthermore, a similar trend is observed for the rate of reaction, with rates limited and varying from 24-77 $mol_{H2O2} mmol_{metal}^{-1} h^{-1}$ for all the supported catalysts. When comparing the rate of synthesis and degradation testing under ideal reaction conditions the trends between each of the catalysts do not align. This can be affirmed as the CeO_2 supported catalyst now has the highest productivity towards H_2O_2 with a value of 6 mol_{H2O2} kg_{cat}^{-1} h^{-1}, whereas previously it was one of the least efficient catalysts, again producing 6 mol_{H2O2} kg_{cat}^{-1} h^{-1} however under

ideal reaction conditions. This could be explained by the aforementioned non-ideal reaction conditions preventing any discernible changes towards H_2O_2 productivity that the changing of support may induce. These conditions also effect the rate of degradation towards H_2O_2 as a result of the removal of sub-ambient temperatures, an alcohol co-solvent, and the CO_2 diluent (and resulting formation of carbonic acid *in-situ*) all of which contribute to inhibiting H_2O_2 degradation.[26] However, this may not be so much of an issue for real life application given that a flow reactor will most likely be utilised which has a much more limited retention time, seconds compared to minutes, which will substantially reduce degradation activities.

5.8   The Direct Synthesis of H_2O_2 for Various 1 wt.% MPd/TiO$_2$ Supported Catalysts in a Batch Regime under Ideal Reaction Conditions.

In a similar manner to Chapter 5.3 the testing of the various 1 wt.% MPd/TiO$_2$ supported catalysts under ideal conditions was carried out as its easier to discern differences in activity under ideal conditions. The data for this is shown below in Figure 5.9 and Table 5.14, alongside the XPS data and BET surface area analysis in Table 5.15 and 5.16 respectively.
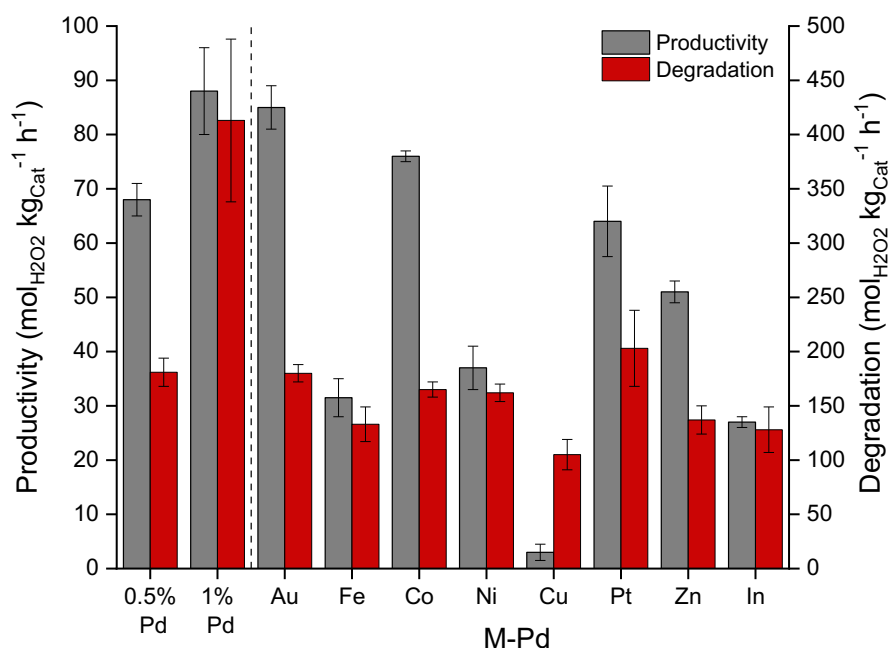
Figure 5.9: The effect of secondary metal inclusion on the activity of Pd catalysts towards the direct synthesis and degradation of H_2O_2, under ideal reaction conditions. **H_2O_2 direct synthesis reaction conditions:** Catalyst (0.01 g), H_2O (2.9 g), MeOH (5.6 g), 5% H_2/CO_2 (420 psi), 25% O_2/CO_2 (160 psi), 0.5 h, 2 °C, 1200 rpm. **H_2O_2 degradation reaction conditions:** Catalyst (0.01 g), H_2O_2 (50 wt.% 0.68 g), H_2O (2.22 g), MeOH (5.6 g), 5% H_2/CO_2 (420 psi), 0.5 h, 2 °C, 1200 rpm.

Table 5.14: The effect of secondary metal catalytic performance towards the direct synthesis and subsequent degradation of H_2O_2, under ideal reaction conditions.

Catalyst	H_2O_2 Productivity (mol_{H2O2} kg_{cat}^{-1} h^{-1})	H_2O_2 (Wt. %)	H_2 Conversion (%)	H_2O_2 Selectivity (%)	H_2O_2 Degradation (mol_{H2O2} kg_{cat}^{-1} h^{-1})
0.5 wt.% Pd/TiO$_2$	68	0.136	14	44	181
1 wt.% Pd/TiO$_2$	88	0.0177	17	38	413
0.5 wt.% Au-0.5 wt.% Pd/TiO$_2$	85	0.17	19	54	180
0.5 wt.% Fe-0.5 wt.% Pd/TiO$_2$	32	0.065	8	39	133
0.5 wt.% Co-0.5 wt.% Pd/TiO$_2$	76	0.152	24	56	165
0.5 wt.% Ni-0.5 wt.% Pd/TiO$_2$	37	0.074	6	32	162
0.5 wt.% Cu-0.5 wt.% Pd/TiO$_2$	3	0.005	5	21	105
0.5 wt.% Pt-0.5 wt.% Pd/TiO$_2$	64	0.123	29	41	203
0.5 wt.% Zn-0.5 wt.% Pd/TiO$_2$	51	0.102	15	68	137
0.5 wt.% In-0.5 wt.% Pd/TiO$_2$	27	0.05	8	53	128

H_2O_2 direct synthesis reaction conditions: Catalyst (0.01 g), H_2O (2.9 g), MeOH (5.6 g), 5% H_2/CO_2 (420 psi), 25% O_2/CO_2 (160 psi), 0.5 h, 2 °C, 1200 rpm. **H_2O_2 degradation reaction conditions:** Catalyst (0.01 g), H_2O_2 (50 wt.% 0.68 g), H_2O (2.22 g), MeOH (5.6 g), 5% H_2/CO_2 (420 psi), 0.5 h, 2 °C, 1200 rpm.

The introduction of a range of transition metals was found to inhibit H_2O_2 degradation rates considerably, compared to the Pd-only analogue (413 mol_{H2O2} kg_{cat}^{-1} h^{-1}), with a corresponding increase in catalytic selectivity towards H_2O_2 during the direct synthesis reaction also observed for many catalyst formulations. Indeed, H_2O_2 degradation rates of many of the Pd-based catalysts were considerably lower than that observed over the 0.5 wt.% Pd-0.5 wt.% Au/TiO$_2$ catalyst (180 mol_{H2O2} kg_{cat}^{-1} h^{-1}). The 1 wt.% AuPd/TiO$_2$ and 1 wt.% CoPd/TiO$_2$ are shown to be the most productive of the bimetallic catalysts for the direct synthesis of H_2O_2 compared to the Pd-only analogue. This incorporation, alongside the increase in the mixed oxidation state of the Pd^0: Pd^{2+} ratio (Table 5.15), is shown to increase both the activity and selectivity towards H_2O_2. The 1 wt.% PtPd/TiO$_2$ catalyst exhibits comparable direct synthesis and degradation of

H_2O_2 when compared to 0.5 wt.% Pd/TiO_2. The 1 wt.% $PtPd/TiO_2$ degrades H_2O_2 at a rate of 203 mol_{H2O2} kg_{cat}^{-1} h^{-1} compared to 181 mol_{H2O2} kg_{cat}^{-1} h^{-1} for the 0.5 wt.% Pd/TiO_2 catalyst, while synthesising H_2O_2 at a rate of 68 mol_{H2O2} kg_{cat}^{-1} h^{-1} compared to 64 mol_{H2O2} kg_{cat}^{-1} h^{-1} for the 0.5 wt.% Pd/TiO_2 catalyst. These results can be assigned to the maintenance of the H_2O_2 selectivity of the catalyst following the introduction of Pt to the surface of the catalyst, alongside the electronic modification towards Pd that Pt can induce optimising the Pd^0: Pd^{2+} ratio. All the other catalysts in this study show a reduction in their ability to both synthesise and degrade H_2O_2 when compared to the 1 wt.% Pd/TiO_2. However for the 1 wt.% $FePd/TiO_2$ this is to be expected given the poor efficacy of the catalyst towards the direct formation of H_2O_2.[35]

Table 5.15: The surface composition of 1 wt.% MPd/TiO_2 catalysts, as determined by XPS.

Catalyst	Pd: M	Pd^{2+}: Pd^0
0.5 wt.% Pd/TiO_2	All Pd	0.2
1 wt.% Pd/TiO_2	All Pd	0.2
0.5 wt.% Au-0.5 wt.% Pd/TiO_2	4.2	0.5
0.5 wt.% Fe-0.5 wt.% Pd/TiO_2	2.6	0.4
0.5 wt.% Co-0.5 wt.% Pd/TiO_2	0.8	0.6
0.5 wt.% Ni-0.5 wt.% Pd/TiO_2	1.0	0.5
0.5 wt.% Cu-0.5 wt.% Pd/TiO_2	0.7	0.2
0.5 wt.% Pt-0.5 wt.% Pd/TiO_2	10.2	0.5
0.5 wt.% Zn-0.5 wt.% Pd/TiO_2	3.3	0.4
0.5 wt.% In-0.5 wt.% Pd/TiO_2	0.8	0.6

Table 5.16: The surface area of supported catalysts, as determined by BET.

Catalyst	Surface Area ($m^2 g^{-1}$)
TiO_2	59
0.5 wt.% Pd/TiO_2	57
1 wt.% Pd/TiO_2	56
0.5 wt.% Au-0.5 wt.% Pd/TiO_2	50
0.5 wt.% Fe-0.5 wt.% Pd/TiO_2	56
0.5 wt.% Co-0.5 wt.% Pd/TiO_2	53
0.5 wt.% Ni-0.5 wt.% Pd/TiO_2	58
0.5 wt.% Cu-0.5 wt.% Pd/TiO_2	52
0.5 wt.% Pt-0.5 wt.% Pd/TiO_2	51
0.5 wt.% Zn-0.5 wt.% Pd/TiO_2	59
0.5 wt.% In-0.5 wt.% Pd/TiO_2	58

While BET analysis of the Pd-based catalysts (Table 5.16) indicates differences in catalytic performance cannot be associated with changes in catalyst surface area, investigation via XPS (Table 5.15) reveals that the incorporation of all secondary metals, with the exception of Cu, significantly enhances the proportion of Pd^{2+}, which correlated well with the observed decrease in H_2O_2 degradation rates. It should be noted that while the 0.5 wt.% Pd-0.5 wt.% Cu/TiO_2 catalyst was found to consist predominantly of Pd^0, catalytic performance towards H_2O_2 production was found to be poor (3 $mol_{H2O2} kg_{cat}^{-1} h^{-1}$). This may be expected given the reported high activity of Pd^0-rich catalysts to H_2O_2 degradation; however, we do not observe such an increase in H_2O_2 degradation with the introduction of Cu into the Pd catalyst. Indeed, H_2O_2 degradation activity of the PdCu catalyst (105 $mol_{H2O2} kg_{cat}^{-1} h^{-1}$) is significantly lower than that of the Pd-only analogue, while determination of H_2 conversion indicates a significant reduction of this metric with the introduction of Cu. As such it is considered that Cu acts as an inhibitor of catalytic activity, with these observations in keeping with previous studies [36]

5.9 Comprehending the Reusability of the Various 1 wt.% MPd/TiO$_2$ Supported Catalysts for the Direct Synthesis of H$_2$O$_2$ in a Batch Regime.

The various 1 wt.% MPd/TiO$_2$ supported catalysts were then tested for their propensity to synthesise H$_2$O$_2$ upon use in a second 30-minute synthesis reaction, as outlined in Chapter 2 section 3.3. The results for this are expressed below in Table 5.16, alongside the XPS data in Table 5.18 and determination of metal leaching via evaluation of the post-reaction solution by ICP-MS (Table 5.19).

Table 5.17: Reusability of the 1 wt.% MPd/TiO$_2$ catalysts towards the H$_2$ conversion, H$_2$O$_2$ productivity and H$_2$O$_2$ degradation at 2°C.

Catalyst	H$_2$O$_2$ Productivity (Use 1) (mol$_{H2O2}$ kg$_{cat}^{-1}$ h^{-1})	H$_2$O$_2$ Productivity (Use 2) (mol$_{H2O2}$ kg$_{cat}^{-1}$ h^{-1})	H$_2$O$_2$ Productivity Loss/Gain (%)
0.5 wt.% Pd/TiO$_2$	68	55	-19
1 wt.% Pd/TiO$_2$	88	72	-18
0.5 wt.% Au-0.5 wt.% Pd/TiO$_2$	85	45	-47
0.5 wt.% Fe-0.5 wt.% Pd/TiO$_2$	32	12	-63
0.5 wt.% Co-0.5 wt.% Pd/TiO$_2$	76	18	-76
0.5 wt.% Ni-0.5 wt.% Pd/TiO$_2$	37	7	-81
0.5 wt.% Cu-0.5 wt.% Pd/TiO$_2$	3	16	+533
0.5 wt.% Pt-0.5 wt.% Pd/TiO$_2$	64	55	-14
0.5 wt.% Zn-0.5 wt.% Pd/TiO$_2$	51	13	-75
0.5 wt.% In-0.5 wt.% Pd/TiO$_2$	27	5	-81

H$_2$O$_2$ direct synthesis reaction conditions: Catalyst (0.01 g), H$_2$O (2.9 g), MeOH (5.6 g), 5% H$_2$/CO$_2$ (420 psi), 25% O$_2$/CO$_2$ (160 psi), 0.5 h, 2 °C, 1200 rpm.

Table 5.18: The surface composition of 1 wt.% MPd/TiO$_2$ catalysts after use in the direct synthesis of H$_2$O$_2$, as determined by XPS.

Catalyst	Pd: M (Fresh)	Pd: M (used)	Pd^{2+}: Pd^0 (Fresh)	Pd^{2+}: Pd^0 (used)
0.5 wt.% Pd/TiO$_2$	All Pd	All Pd	0.2	0.1
1 wt.% Pd/TiO$_2$	All Pd	All Pd	0.2	0.1
0.5 wt.% Au-0.5 wt.% Pd/TiO$_2$	4.2	1.4	0.5	0.5
0.5 wt.% Fe-0.5 wt.% Pd/TiO$_2$	2.6	3.1	0.4	0.2
0.5 wt.% Co-0.5 wt.% Pd/TiO$_2$	0.8	1.1	0.6	0.9
0.5 wt.% Ni-0.5 wt.% Pd/TiO$_2$	1.0	0.8	0.5	0.8
0.5 wt.% Cu-0.5 wt.% Pd/TiO$_2$	0.7	1.1	0.2	0.2
0.5 wt.% Pt-0.5 wt.% Pd/TiO$_2$	10.2	7.9	0.5	0.4
0.5 wt.% Zn-0.5 wt.% Pd/TiO$_2$	3.3	2.4	0.4	0.9
0.5 wt.% In-0.5 wt.% Pd/TiO$_2$	0.8	0.6	0.6	1.2

H$_2$O$_2$ direct synthesis reaction conditions: Catalyst (0.01 g), H$_2$O (2.9 g), MeOH (5.6 g), 5% H$_2$/CO$_2$ (420 psi), 25% O$_2$/CO$_2$ (160 psi), 0.5 h, 2 °C, 1200 rpm.

Table 5.19: Leaching of the M and Pd from the 1 wt.% MPd/TiO$_2$ catalysts following a H$_2$O$_2$ direct synthesis reaction under non-ideal conditions, determined by ICP.

Catalyst	M Leached (%)	M Leached (ppb)	Pd Leached (%)	Pd Leached (ppb)
0.5 wt.% Pd/TiO$_2$	-	-	0.5	32.0
1 wt.% Pd/TiO$_2$	-	-	0.7	76.5
0.5 wt.% Au-0.5 wt.% Pd/TiO$_2$	0.0	2.0	0.1	45.0
0.5 wt.% Fe-0.5 wt.% Pd/TiO$_2$	0.0	0.0	0.0	2.5
0.5 wt.% Co-0.5 wt.% Pd/TiO$_2$	4.5	267.0	0.1	4.0
0.5 wt.% Ni-0.5 wt.% Pd/TiO$_2$	1.9	110.0	0.2	13.0
0.5 wt.% Cu-0.5 wt.% Pd/TiO$_2$	0.5	27.0	0.1	7.4
0.5 wt.% Pt-0.5 wt.% Pd/TiO$_2$	0.0	0.5	0.0	2.0
0.5 wt.% Zn-0.5 wt.% Pd/TiO$_2$	1.3	78.5	0.0	2.0
0.5 wt.% In-0.5 wt.% Pd/TiO$_2$	0.1	5.0	0.1	3.0

H$_2$O$_2$ direct synthesis reaction conditions: Catalyst (0.01 g), H$_2$O (2.9 g), MeOH (5.6 g), 5% H$_2$/CO$_2$ (420 psi), 25% O$_2$/CO$_2$ (160 psi), 0.5 h, 2 °C, 1200 rpm.

Once again, in a similar manner to the 1 wt.% AuPd catalysts immobilised on a range of supports, the dominant trend is a net reduction in the productivity of the catalysts towards the synthesis of H$_2$O$_2$ following an initial 30-minute H$_2$O$_2$ synthesis reaction. The productivity of the catalysts towards the direct synthesis of H$_2$O$_2$ falls between 14 – 81% for all the catalysts apart from 1 wt.% CuPd/TiO$_2$, which sees an 433% increase in its productivity towards H$_2$O$_2$ from 3 to 16 mol$_{H2O2}$ kg$_{cat}^{-1}$ h^{-1}. The ICP data in Figure 5.19 shows < 0.8% Pd metal leaching for all the catalysts alongside almost no leaching of the pairing metal for most of the catalysts except for Co, Ni, and Zn which leach 4.5, 1.9 and 1.3% of their metal loading respectively. This data therefore leads to the conclusion that catalyst deactivation from metal leaching cannot be a large contributor for many of the catalysts. A possible explanation to this trend could be particle agglomeration upon use in the direct synthesis of H$_2$O$_2$, in addition to a potential shift in Pd speciation. The increase in particle size would account for the decreased activity towards the production of H$_2$O$_2$, as smaller nanoparticles are documented as being more catalytically

active.[37,38] Furthermore, the point documented by Brehm *et. al*[32] in which the chlorine is removed from the surface of the catalyst after the initial reaction and following washing could negatively influence productivity could also be contributing. However, for the 1 wt.% CuPd/TiO$_2$ catalyst there is an observed increase in the productivity following catalyst re-use, up to 17 mol H$_2$O$_2$ kg$_{cat}^{-1}$ h^{-1} from 3 mol$_{H2O2}$ kg$_{cat}^{-1}$ h^{-1}. This increase in H$_2$O$_2$ production could be due to the loss of Cu's inhibitory effect towards the direct synthesis of H$_2$O$_2$, [36] which will be lost alongside Cu being removed from the surface of the catalyst.

5.10 The Effect of Pelleting on the Initial Rate of Production Towards the Direct Synthesis of H$_2$O$_2$ for Various 1 wt.% MPd/TiO$_2$ Supported Catalysts in a Batch Regime.

Upon testing the different supported catalysts, the various 1 wt.% MPd/TiO$_2$ supported powdered and pelleted catalysts were then tested for their initial rate of H$_2$O$_2$ production at 5 minutes when compared to the standard 30-minute synthesis reaction. The results for this were expressed below in Figure 5.10. and Figure 5.11.
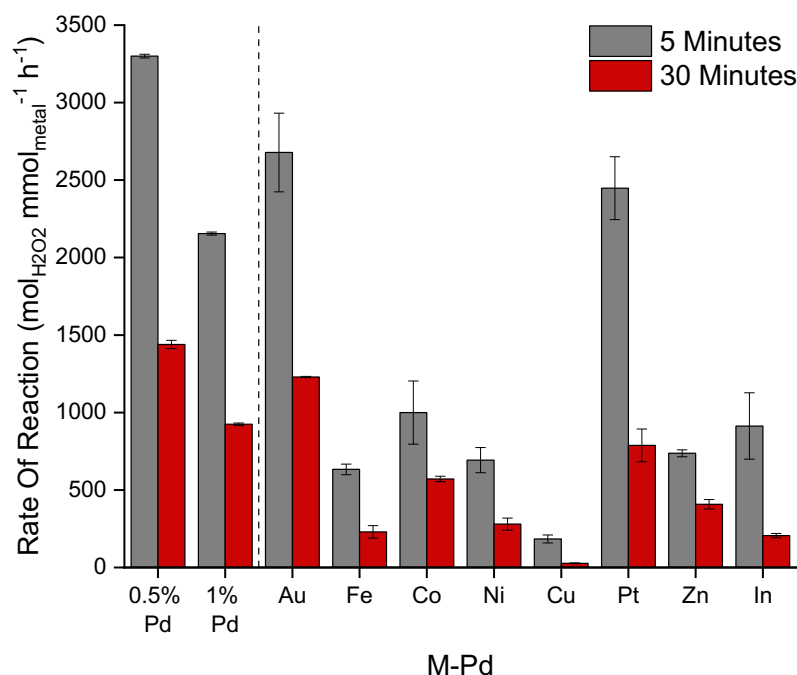
Figure 5.10: The effect the secondary metal has on the activity of the powdered 1 wt.% Pd/TiO$_2$ catalyst for the productivity towards H$_2$O$_2$ after 5 minutes, under ideal conditions. **H$_2$O$_2$ direct synthesis reaction conditions:** Catalyst (0.01 g), H$_2$O (2.9 g), MeOH (5.6 g), 5% H$_2$/CO$_2$ (420 psi), 25% O$_2$/CO$_2$ (160 psi), 0.5 h, 2 °C, 1200 rpm.
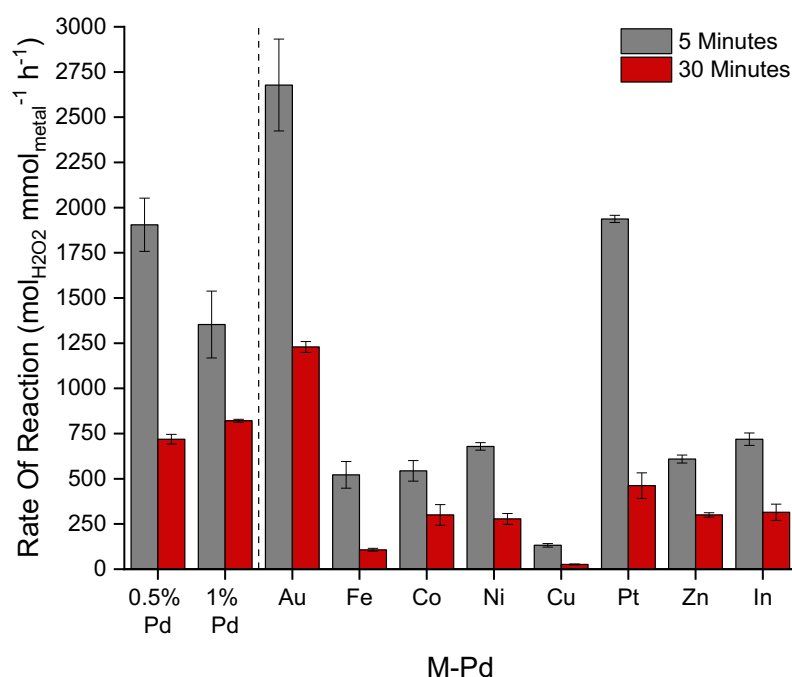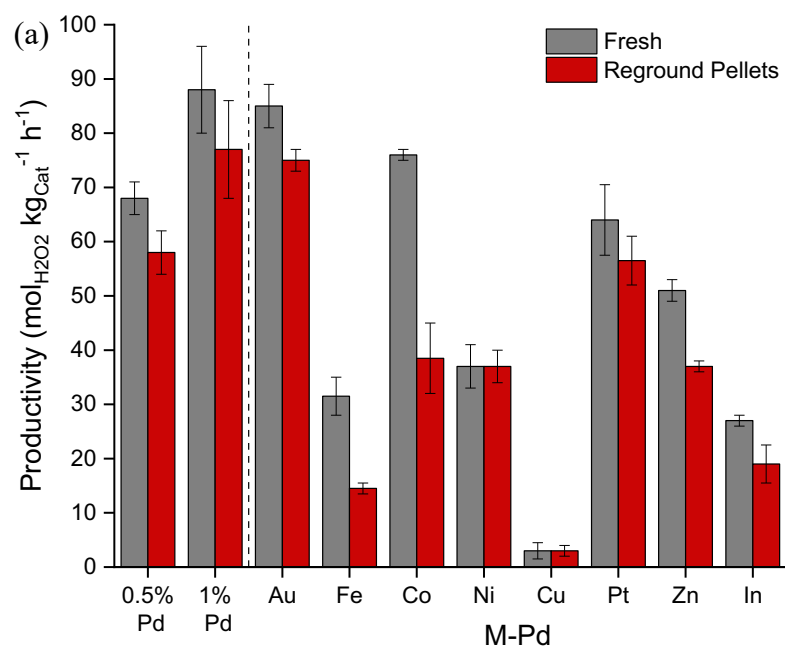
Figure 5.11: The effect the secondary metal has on the activity of the pelleted 1 wt.% Pd/TiO₂ catalyst for the productivity towards H_2O_2 after 5 minutes, under ideal conditions. **H_2O_2 direct synthesis reaction conditions:** Catalyst (0.01 g), H_2O (2.9 g), MeOH (5.6 g), 5% H_2/CO_2 (420 psi), 25% O_2/CO_2 (160 psi), 2 °C, 1200 rpm.

The results show that when comparing the 5-minute production to the 30-minute production towards H_2O_2 there is loss of catalytic performance when loading a secondary metal upon the 1 wt.% MPd/TiO₂ powdered and pelleted catalysts. The 1 wt.% PtPd/TiO₂ powdered catalyst shows a large decrease towards its activity of 81% from 2448 to 462 $mol_{H2O2}mmol_{metal}^{-1}h^{-1}$, however the 1 wt.% ZnPd/TiO₂ powdered catalyst maintains 67% of its activity after a 30-minute reaction. This result can be attributed to the aforementioned increase in the degradation rates as the reaction proceeds[33] and the resultant loss in selectivity towards H_2O_2.[34] Furthermore for the pelleted catalysts, when compared to the powdered catalyst, all of the 10 catalysts show a loss of production after both 5 and 30 minutes. However, the 1 wt.% AuPd/TiO₂ pelleted catalyst only shows minimal loss of production when compared to its powdered counterpart. For the pelleted catalysts, the 1 wt.% PtPd/TiO₂ shows the largest decrease of its activity following pelleting, losing 75% of its initial activity after 5 minutes when reacted for 30 minutes. This observation could be explained by particle agglomeration, in keeping with earlier studies into the AuPd/TiO₂ catalyst (Chapter 3, Figure 3.6), however this cannot be confirmed as TEM has not been done on these catalysts. Finally, this observed trend with the production

rate of H_2O_2 decreasing with time can once again can be assigned to an increase in degradation rate over the pelleted materials and a concurrent loss in catalytic selectivity.[33,34]

5.11 The Effect Pelleting has on the Direct Synthesis of H_2O_2 for Various 1 wt.% MPd/TiO$_2$ Supported Catalysts in a Batch Regime.

It is important to understand the effect that pelleting would also have on the direct synthesis of H_2O_2 before application in a flow reactor. As such the pelleted catalysts were reground to a powder prior to testing, with the data expressed below in Figure 5.12 and Table 5.20, while the XPS and ICP data are expressed in Table 5.21 and 5.22 respectively.

Figure 5.12: The effect the inclusion of a secondary metal has on the activity of pelleted 1 wt.% Pd/TiO_2 catalyst towards the (a) direct synthesis and (b) degradation of H_2O_2, under ideal reaction conditions. **H_2O_2 direct synthesis reaction conditions:** Catalyst (0.01 g), H_2O (2.9 g), MeOH (5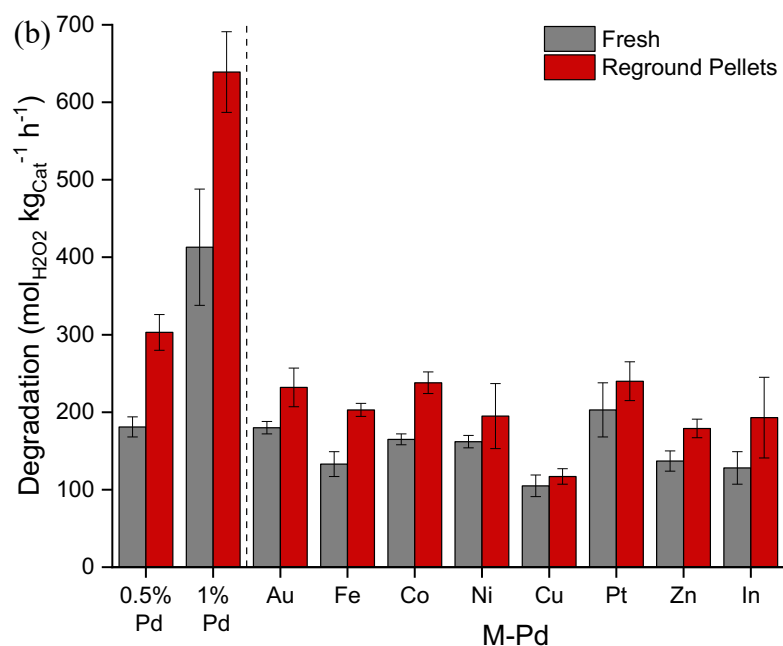.6 g), 5% H_2/CO_2 (420 psi), 25% O_2/CO_2 (160 psi), 0.5 h, 2 °C, 1200 rpm. **H_2O_2 degradation reaction conditions:** Catalyst (0.01 g), H_2O_2 (50 wt.% 0.68 g), H_2O (2.22 g), MeOH (5.6 g), 5% H_2/CO_2 (420 psi), 0.5 h, 2 °C, 1200 rpm.

Table 5.20: The effect pelleting has on the 1 wt.% MPd/TiO$_2$ catalysts towards the H$_2$ conversion, H$_2$O$_2$ productivity and H$_2$O$_2$ degradation, under ideal reaction conditions.

MPd	H$_2$O$_2$ Productivity (mol$_{H2O2}$ kg$_{cat}$$^{-1}$ h^{-1})	H$_2$O$_2$ (Wt. %)	H$_2$ Conversion (%)	H$_2$O$_2$ Selectivity (%)	H$_2$O$_2$ Degradation (mol$_{H2O2}$ kg$_{cat}$$^{-1}$ h^{-1})
0.5 wt.% Pd/TiO$_2$	58	0.116	14	39	303
1 wt.% Pd/TiO$_2$	77	0.155	11	33	639
0.5 wt.% Au-0.5 wt.% Pd/TiO$_2$	75	0.15	19	48	232
0.5 wt.% Fe-0.5 wt.% Pd/TiO$_2$	15	0.03	10	44	203
0.5 wt.% Co-0.5 wt.% Pd/TiO$_2$	39	0.078	9	47	238
0.5 wt.% Ni-0.5 wt.% Pd/TiO$_2$	37	0.074	7	37	195
0.5 wt.% Cu-0.5 wt.% Pd/TiO$_2$	3	0.005	6	18	117
0.5 wt.% Pt-0.5 wt.% Pd/TiO$_2$	56	0.112	19	34	240
0.5 wt.% Zn-0.5 wt.% Pd/TiO$_2$	37	0.074	11	61	179
0.5 wt.% In-0.5 wt.% Pd/TiO$_2$	19	0.038	8	45	193

H$_2$O$_2$ direct synthesis reaction conditions: Catalyst (0.01 g), H$_2$O (2.9 g), MeOH (5.6 g), 5% H$_2$/CO$_2$ (420 psi), 25% O$_2$/CO$_2$ (160 psi), 0.5 h, 2 °C, 1200 rpm. **H$_2$O$_2$ degradation reaction conditions:** Catalyst (0.01 g), H$_2$O$_2$ (50 wt.% 0.68 g), H$_2$O (2.22 g), MeOH (5.6 g), 5% H$_2$/CO$_2$ (420 psi), 0.5 h, 2 °C, 1200 rpm.

Table 5.21: The surface composition of the powdered and reground pellets of the 1 wt.% AuPd supported catalysts, as determined by XPS.

Catalyst	Pd: M (Fresh)	Pd: M (Reground Pellets)	$Pd^{2+}: Pd^0$ (Fresh)	$Pd^{2+}: Pd^0$ (Reground Pellets)
0.5 wt.% Pd/TiO$_2$	All Pd	All Pd	0.2	0.2
1 wt.% Pd/TiO$_2$	All Pd	All Pd	0.2	0.3
0.5 wt.% Au-0.5 wt.% Pd/TiO$_2$	4.2	3.6	0.5	0.5
0.5 wt.% Fe-0.5 wt.% Pd/TiO$_2$	2.6	1.9	0.4	0.5
0.5 wt.% Co-0.5 wt.% Pd/TiO$_2$	0.8	0.6	0.6	0.7
0.5 wt.% Ni-0.5 wt.% Pd/TiO$_2$	1.0	0.9	0.5	0.7
0.5 wt.% Cu-0.5 wt.% Pd/TiO$_2$	0.7	0.5	0.2	0.6
0.5 wt.% Pt-0.5 wt.% Pd/TiO$_2$	10.2	7.5	0.5	0.7
0.5 wt.% Zn-0.5 wt.% Pd/TiO$_2$	3.3	3.0	0.4	0.5
0.5 wt.% In-0.5 wt.% Pd/TiO$_2$	0.8	0.4	0.6	0.7

Table 5.22: Leaching of the M and Pd from the pelleted 1 wt.% MPd/TiO$_2$ catalysts following a H$_2$O$_2$ direct synthesis reaction under ideal conditions, determined by ICP.

Catalyst	M Leached (%)	M Leached (ppb)	Pd Leached (%)	Pd Leached (ppb)
0.5 wt.% Pd/TiO$_2$	-	-	0.0	25.0
1 wt.% Pd/TiO$_2$	-	-	0.3	32.0
0.5 wt.% Au-0.5 wt.% Pd/TiO$_2$	0.0	2.0	0.1	4.0
0.5 wt.% Fe-0.5 wt.% Pd/TiO$_2$	6.0	359.0	1.4	84.0
0.5 wt.% Co-0.5 wt.% Pd/TiO$_2$	52.0	3084.0	0.8	17.0
0.5 wt.% Ni-0.5 wt.% Pd/TiO$_2$	9.5	561.0	0.4	24.0
0.5 wt.% Cu-0.5 wt.% Pd/TiO$_2$	2.1	124.0	0.3	19.0
0.5 wt.% Pt-0.5 wt.% Pd/TiO$_2$	0.3	17.0	0.1	5.0
0.5 wt.% Zn-0.5 wt.% Pd/TiO$_2$	15.9	934.0	0.1	3.5
0.5 wt.% In-0.5 wt.% Pd/TiO$_2$	0.0	0.5	0.2	12.0

H$_2$O$_2$ direct synthesis reaction conditions: Catalyst (0.01 g), H$_2$O (2.9 g), MeOH (5.6 g), 5% H$_2$/CO$_2$ (420 psi), 25% O$_2$/CO$_2$ (160 psi), 0.5 h, 2 °C, 1200 rpm.

In a similar manner to the various supported 1 wt.% AuPd catalysts, the 1 wt.% MPd/TiO$_2$ catalysts also showed a decrease in activity towards the direct synthesis of H$_2$O$_2$ and a concurrent increase towards its degradation after pelleting. It can be observed in Figure 5.12 and Table 5.20 that 1 wt.% CoPd/TiO$_2$ catalyst shows the biggest decrease in its activity upon pelleting losing 49% of its activity, dropping to 39 from 76 mol$_{H2O2}$ kg$_{cat}^{-1}$ h^{-1}. However, in contrast to this the 1 wt.% NiPd/TiO$_2$ catalyst maintains its activity upon pelleting (37 mol$_{H2O2}$ kg$_{cat}^{-1}$ h^{-1}), this can be explained by the selectivity increasing towards H$_2$O$_2$ following pelleting even though H$_2$O$_2$ degradation increases. The general decrease towards H$_2$O$_2$ production could be explained by particle agglomeration, as observed for the 1 wt.% AuPd/TiO$_2$ catalyst (Chapter 3, Figure 3.6). As discussed, the mean particle size of the 1 wt.% AuPd/TiO$_2$ catalyst increased from 2.9 nm in the powdered catalyst to 4.5 nm in the pelleted analogue (Chapter 3, Histograms in Figure 3.6 (a,b) HAADF-STEM images Figure 3.6 (c (ii-iv)). With this increase

in particle size leading to an increase in H_2O_2 degrdation, due to the decrease in particle size leading to an increase towards H_2O_2 selectivity.[31] However, this conclusion would just be an assumption as TEM of all these catalyst would need to be ran to confirm this as the secondary metal paired alongside Pd may effect particle size. Furthmore, the leaching data in Table 5.22 shows minimal leaching of Pd for all of the 1 wt.% MPd catalysts, so could not contribute to the decrease in the productivity towards the direct synthesis of H_2O_2 and a concurrent increase towards its degradation after pelleting. However, the Co, Ni, Zn, and Fe containing bi-metallic catalysts show a large increase in their leaching percentage when comparing the powders to the reground pellets. The Co, Ni and Zn powdered catalyst have a leaching percentage for the powders of 4.5, 1.9 and 1.3%, yet upon pelleting and regrinding these values increase to 52, 9.5 and 15.9%, which can also contribute to the reduced productivity and increased degradation of H_2O_2. The 1 wt.% NiPd/TiO$_2$ catalyst is shown to maintain its productivity, this could be assigned to the catalyst maintaining its H_2O_2 selectivity following pelleting through the maintaince of its mixed oxidation state of Pd preventing the increased H_2O_2 degradation exhibited by the other catalysts.

5.12 The Direct Synthesis of H_2O_2 for Various 1 wt.% MPd/TiO$_2$ Supported Catalysts in a Batch Regime Under Non-Ideal Conditions.

The 1 wt.% MPd/TiO$_2$ supported catalysts, where M represents either Au, Fe, Co, Ni, Cu, Pt, Zn, or In, were subsequently tested for their ability to synthesise and degrade H_2O_2 under non-ideal conditions. Once again it is important to test in these reaction conditions given these are the most probable conditions for industrial use due to the cost applications of the ideal reaction conditions. The results for this study can be found below in Figure 5.14 and Tables 5.23 + 5.24.

Figure 5.13: The effect of secondary metal inclusion on the activity of Pd catalysts towards the direct synthesis and degradation of H_2O_2, under ideal reaction conditions. **H_2O_2 direct synthesis reaction conditions:** Catalyst (0.01 g), H_2O (2.9 g), MeOH (5.6 g), 5% H_2/CO_2 (420 psi)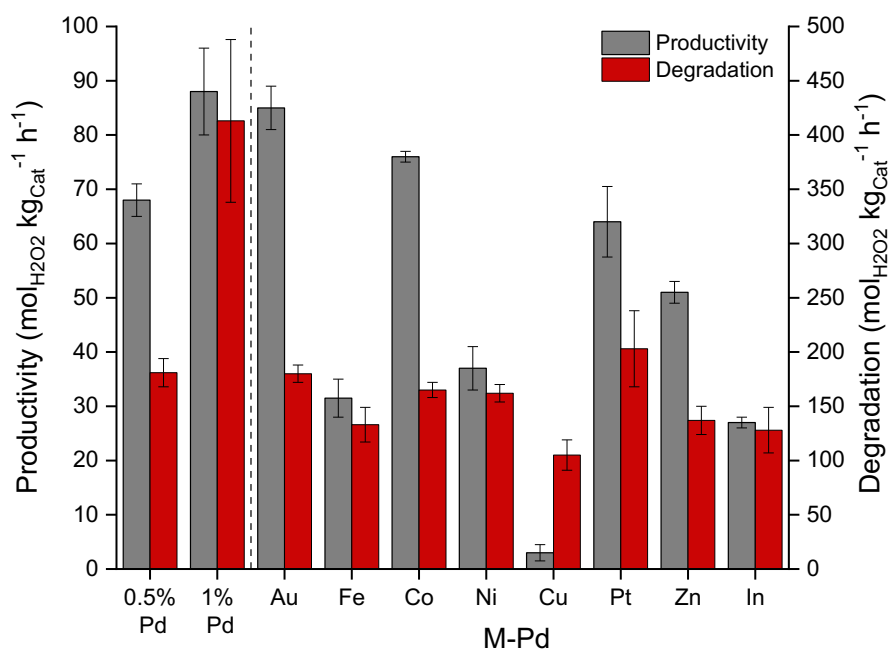, 25% O_2/CO_2 (160 psi), 0.5 h, 2 °C, 1200 rpm. **H_2O_2 degradation reaction conditions:** Catalyst (0.01 g), H_2O_2 (50 wt.% 0.68 g), H_2O (2.22 g), MeOH (5.6 g), 5% H_2/CO_2 (420 psi), 0.5 h, 2 °C, 1200 rpm.
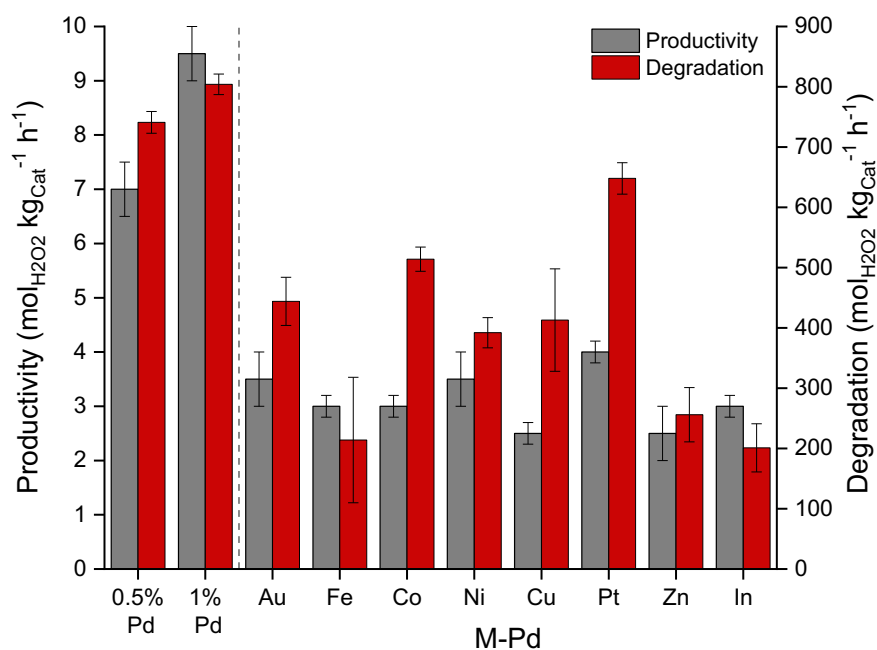
Figure 5.14: The effect the inclusion of a secondary metal has on the activity of a 1 wt.% Pd/TiO_2 catalysts towards the direct synthesis and degradation of H_2O_2, under non-ideal reaction conditions. **H_2O_2 direct synthesis reaction conditions:** Catalyst (0.01 g), H_2O (8.5 g), 5% H_2/N_2 (420 psi), 25% O_2/N_2 (160 psi), 0.5 h, 30 °C, 1200 rpm. **H_2O_2 degradation reaction conditions:** Catalyst (0.01 g), H_2O_2 (50 wt.% 0.68 g), H_2O (7.82 g), 5% H_2/N_2 (420 psi), 0.5 h, 30 °C, 1200 rpm.

Table 5.23: The effect the inclusion of a secondary metal has on the rate of H_2O_2 when using a 1 wt.% Pd/TiO$_2$ catalyst, under non-ideal reaction conditions.

Catalyst	Rate of Reaction $(mol_{H2O2}mmol_{metal}^{-1}h^{-1})$
0.5 wt.% Pd/TiO$_2$	79
1 wt.% Pd/TiO$_2$	213
0.5 wt.% Au-0.5 wt.% Pd/TiO$_2$	77
0.5 wt.% Fe-0.5 wt.% Pd/TiO$_2$	20
0.5 wt.% Co-0.5 wt.% Pd/TiO$_2$	32
0.5 wt.% Ni-0.5 wt.% Pd/TiO$_2$	24
0.5 wt.% Cu-0.5 wt.% Pd/TiO$_2$	19
0.5 wt.% Pt-0.5 wt.% Pd/TiO$_2$	54
0.5 wt.% Zn-0.5 wt.% Pd/TiO$_2$	20
0.5 wt.% In-0.5 wt.% Pd/TiO$_2$	32

H_2O_2 direct synthesis reaction conditions: Catalyst (0.01 g), H_2O (8.5 g), 5% H_2/N_2 (420 psi), 25% O_2/N_2 (160 psi), 0.5 h, 30 °C, 1200 rpm. Rate of reaction calculated using a theoretical metal loading and minimal number of active sites.

Table 5.24: The effect the secondary metal has on the 1 wt.% Pd/TiO_2 catalysts towards the H_2 conversion, H_2O_2 productivity and H_2O_2 degradation, under non-ideal reaction conditions.

Catalyst	H_2O_2 Productivity (mol_{H2O2} kg_{cat}^{-1} h^{-1})	H_2O_2 (Wt. %)	H_2 Conversion (%)	H_2O_2 Selectivity (%)	H_2O_2 Degradation (mol_{H2O2} kg_{cat}^{-1} h^{-1})
0.5 wt.% Pd/TiO_2	7	0.014	32	2	741
1 wt.% Pd/TiO_2	10	0.02	41	1	804
0.5 wt.% Au-0.5 wt.% Pd/TiO_2	5	0.01	48	3	1707
0.5 wt.% Fe-0.5 wt.% Pd/TiO_2	3	0.005	32	3	214
0.5 wt.% Co-0.5 wt.% Pd/TiO_2	4	0.008	24	3	514
0.5 wt.% Ni-0.5 wt.% Pd/TiO_2	4	0.008	28	2	392
0.5 wt.% Cu-0.5 wt.% Pd/TiO_2	3	0.005	26	2	413
0.5 wt.% Pt-0.5 wt.% Pd/TiO_2	4	0.008	52	1	1484
0.5 wt.% Zn-0.5 wt.% Pd/TiO_2	3	0.005	26	2	256
0.5 wt.% In-0.5 wt.% Pd/TiO_2	3	0.005	28	1	201

H_2O_2 direct synthesis reaction conditions: Catalyst (0.01 g), H_2O (8.5 g), 5% H_2/N_2 (420 psi), 25% O_2/N_2 (160 psi), 0.5 h, 30 °C, 1200 rpm. **H_2O_2 degradation reaction conditions:** Catalyst (0.01 g), H_2O_2 (50 wt.% 0.68 g), H_2O (7.82 g), 5% H_2/N_2 (420 psi), 0.5 h, 30 °C, 1200 rpm.

The results seen in Figure 5.14 and Table 5.23 express a similar trend to that reported in Section 5.8, where H_2O_2 synthesis rates were limited while H_2O_2 degradation activity was found to be considerable. For the direct synthesis of H_2O_2 little variability is observed, with the productivity of all the catalysts ranging between 3-10 mol_{H2O2} kg_{cat}^{-1} h^{-1}, as opposed to between 3-88 mol_{H2O2} kg_{cat}^{-1} h^{-1} under ideal reaction conditions (Figure 5.13). Furthermore, a similar trend is observed for the rate of reaction, with rates varying from 19-72 $mol_{H2O2}mmol_{metal}^{-1}h^{-1}$ for all the 1 wt.% catalysts. Yet the 0.5 wt. Pd/TiO_2 catalyst expressed a higher rate of 213 $mol_{H2O2}mmol_{metal}^{-1}h^{-1}$ primarily due to its lower metal loading. For the degradation rate however the opposite is observed, with the degradation ranging between 214 and 1707 mol_{H2O2} kg_{cat}^{-1} h^{-1}, whereas under ideal conditions degradation only ranges between 105 – 413 mol_{H2O2}

kg_{cat}^{-1} h^{-1} (Figure 5.13). As discussed previously, this highlights the crucial role of reaction conditions in promoting H_2O_2 stability. While these reaction conditions are not ideal, they are relevant to future industrial application as well as being most financially affordable for future water treatments plants.

5.13 Conclusions.

This Chapter began by investigating into the role the catalyst support plays on the productivity towards the direct synthesis of H_2O_2. Bare supports were evaluated for both the direct synthesis and degradation of H_2O_2 and revealed the major contribution of the supported metals to catalyse both reactions, rather than the supports alone. It was observed that while the 1 wt.% AuPd/TiO_2 catalyst was still optimal for the direct synthesis of H_2O_2, some other supports and pairing metals showed potential. Following this, the initial H_2O_2 synthesis rate of the various supported powdered, and pelleted catalysts was tested, comparing a 5-minute and 30-minute reaction time, with the productivity towards the synthesis of H_2O_2 decreasing with time. With this being assigned to an increase in the degradation rates with reaction time. However, the Al_2O_3 supported AuPd catalyst was found to offer good stability, with H_2O_2 production rates comparable between 5-30 minutes. The reusability of the supported catalysts was then tested, with the overall trend pointing towards reduction in the Pd^{2+}: Pd^0 ratio. In addition, the effect of pelleting was also studied, with the catalyst needing to be pellet for flow reactor application, with the results indicating that the overall trend of a reduction towards the direct synthesis of H_2O_2 and increase in the degradation of H_2O_2 being due to the aforementioned particle agglomeration, as observed for the AuPd/TiO_2 catalyst (Chapter 3, Figure 3.6). Concluding the testing of the supported catalysts, the effect of transitioning the reaction conditions away from those optimised for H_2O_2 stability towards those likely to be adopted upon any industrial application was evaluated for the various catalysts. In general, a reduction towards the direct synthesis of H_2O_2 and increase in the degradation towards H_2O_2 was observed. This trend was as expected and highlights the crucial role of reaction conditions in promoting H_2O_2 stability, given that ability of sub-ambient temperatures, an alcohol co-solvent, and the CO_2 diluent (and resulting formation of carbonic acid *in-situ*) to inhibit H_2O_2 degradation.

The effect that a second pairing metal has on the productivity towards the direct synthesis of H_2O_2 of a 1 wt.% Pd/TiO_2 catalyst. The PdCo and PdPt catalysts showed a similar ability to directly synthesise H_2O_2 over an initial 30-minute reaction, with a productivity of 76 and 64

$mol_{H2O2} \, kg_{cat}^{-1} \, h^{-1}$ respectively, however these results are still lower than the 84 $mol_{H2O2} \, kg_{cat}^{-1}$ h^{-1} produced by the 0.5 wt.% Au-0.5 wt.% Pd/TiO₂. Furthermore, the PdCo catalyst had some disadvantages, losing a lot of its activity upon reuse and leaching 52% of its cobalt upon pelleting. While the PdPt catalyst maintain 86% of its initial activity upon re-use and showed minimal leaching when pelleted. The Cu catalyst unfortunately lost a lot of its activity upon reapplication while also leaching 52% of its copper upon pelleting. The initial H_2O_2 synthesis rate of the various powdered and pelleted 1 wt.% MPd/TiO₂ catalysts were tested, comparing a 5 minute and 30-minute reaction time, with the productivity towards the synthesis of H_2O_2 once again decreasing with time. With this being assigned to an increase in the degradation rates with reaction time. The reusability of these catalysts was tested alongside the supported catalysts, with the overall trend again pointing towards reduction in the Pd^{2+}: Pd^0 ratio. In addition, the effect of pelleting was also studied, with the results again indicating that the overall trend of a reduction towards the direct synthesis of H_2O_2 and increase in the degradation of H_2O_2 being due to the aforementioned particle agglomeration, as observed for the AuPd/TiO₂ catalyst (Chapter 3, Figure 3.6). To conclude the chapter, the non-ideal reaction conditions were once again tested for their effect on the productivity and degradation of H_2O_2. In a similar manner to the various supported catalysts, a reduction towards the direct synthesis of H_2O_2 and increase in the degradation towards H_2O_2 was observed. This trend was as expected and highlights the aforementioned crucial role of reaction conditions in promoting H_2O_2 stability. This Chapter showed the substantial affect that changing the pairing metal to Pd and support has on the direct synthesis and degradation of H_2O_2 and has identified a few catalysts that might have some propensity to be used in my coming work into trying to produce H_2O_2 in the gas phase.

5.14 Future Work.

Given additional time and resources I would have pursued the following:

1. Investigate further into the reason for catalyst loss of activity following multiple uses, research by Brehm *et. al*[32] has shown that the loss of chlorine through initial use is linked to catalyst deactivation, could be similar issue with this work.

2. Investigate alternative routes to catalyst synthesis. The catalysts within this work (prepared via excess chlorine wet co-impregnation methodology), were found to be unstable, with significant loss in activity upon re-use and metal leaching.

3. Pursue the bimetallic NiPd catalyst further as the catalyst was shown to be stable upon re-use, research by Crole *et. al*[11] has shown that changing the Ni: Pd ratio within the catalyst can increase the production of H_2O_2.

4. Determine the effect that pelleting has on particle size and why this subsequently effects H_2O_2 productivity.

5. Pursue the role of calcination temperature in inhibiting leaching as majority of catalyst have shown leaching upon initial use and research by Edwards *et. al*[39] has shown the positive effect calcination temperature can have on inhibiting metal leaching.

6. Introduction of a third metal at low loadings to a 1 wt.% AuPd/TiO_2 catalyst as positive results were observed by Gong *et. al*[14] in which the incorporation of Pt as a third metal led to an increase in H_2O_2 productivity.

5.15 Appendix.

Powder X-ray diffraction was undertaken for the various 1 wt.% AuPd and 1 wt.% MPd/TiO$_2$ catalysts to provide an indication of particle size. However, for the various 1 wt.% MPd/TiO$_2$ catalysts (Figure 5.15 + 5.16) no reflections that would correspond to individual metal species were identified, with only the reflections associated with the TiO$_2$ support observed. This indicates that the nanoparticles that are generated during the catalyst preparation are too small to be detected. For the various 1 wt.% AuPd supported catalysts shown below (Figure 5.17-21) a similar finding is observed with the powder XRD indicates no presence of these metal nanoparticles, indicating that the formation of large metal nanoparticles may be avoided through the careful selection of catalyst support.
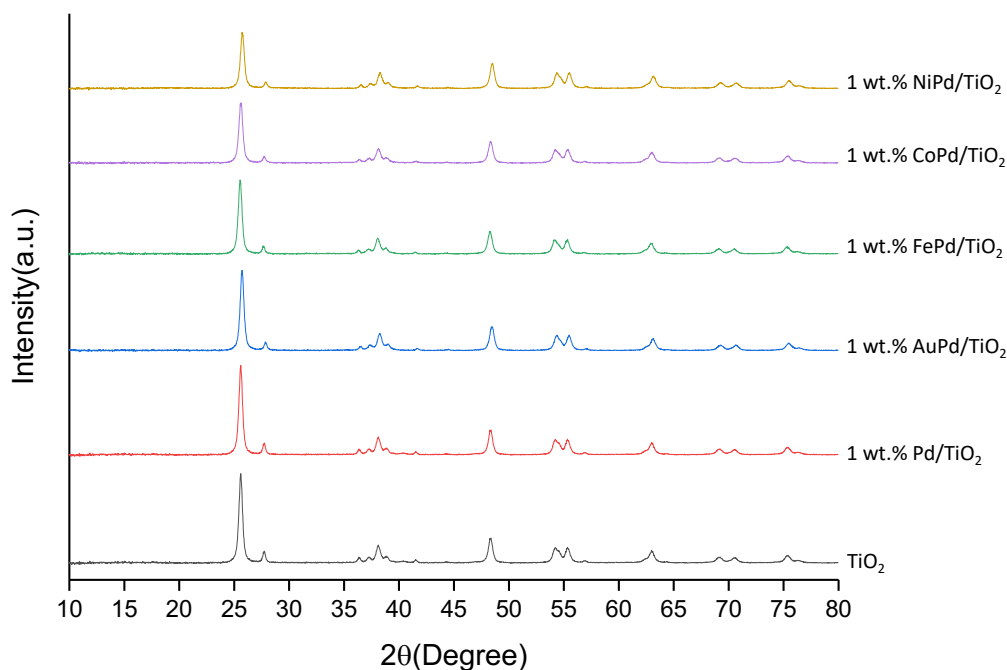
Figure 5.15: X-ray diffractograms of powdered 1 wt.% MPd/TiO$_2$ catalysts, where M is the secondary metal introduced alongside Pd. **ICCD Reference Number:** TiO$_2$: 01-086-1157, Pd: 01-087-0638, Au: 01-071-4614, Fe: 01-086-1354, Co: 01-077-7452 and Ni: 01-089-7129.
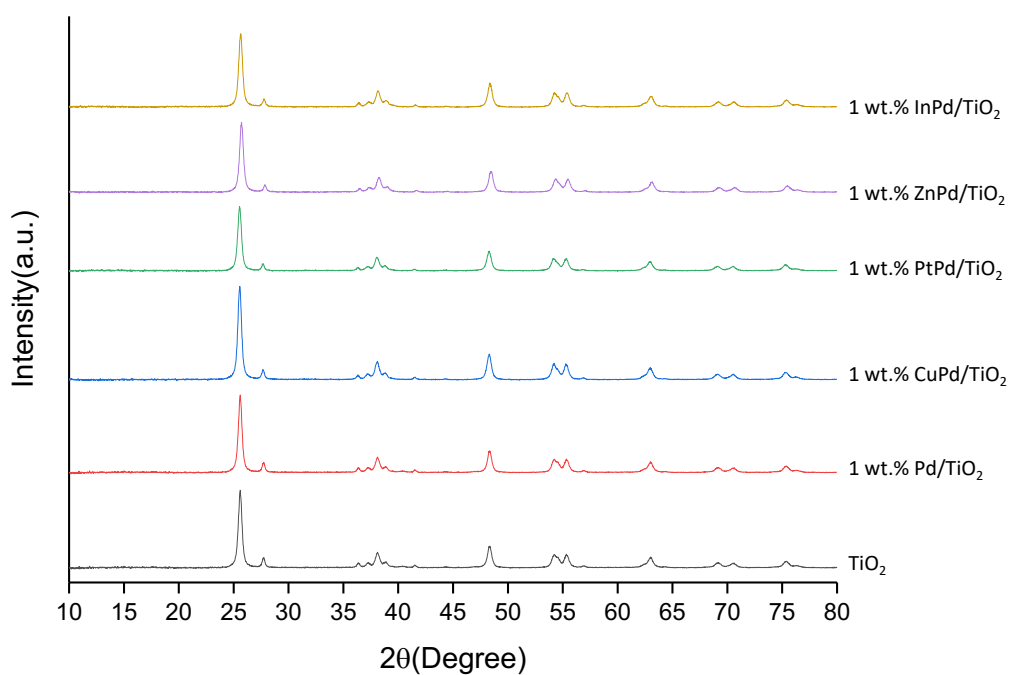
Figure 5.16: X-ray diffractograms of powdered 1 wt.% MPd/TiO$_2$ catalysts, where M is the secondary metal introduced alongside Pd. **ICCD Reference Number:** TiO$_2$: 01-086-1157, Pd: 01-087-0638, Cu: 00-005-0661, Pt: 01-072-2994, Zn: 01-078-7017 and In: 03-065-7421.
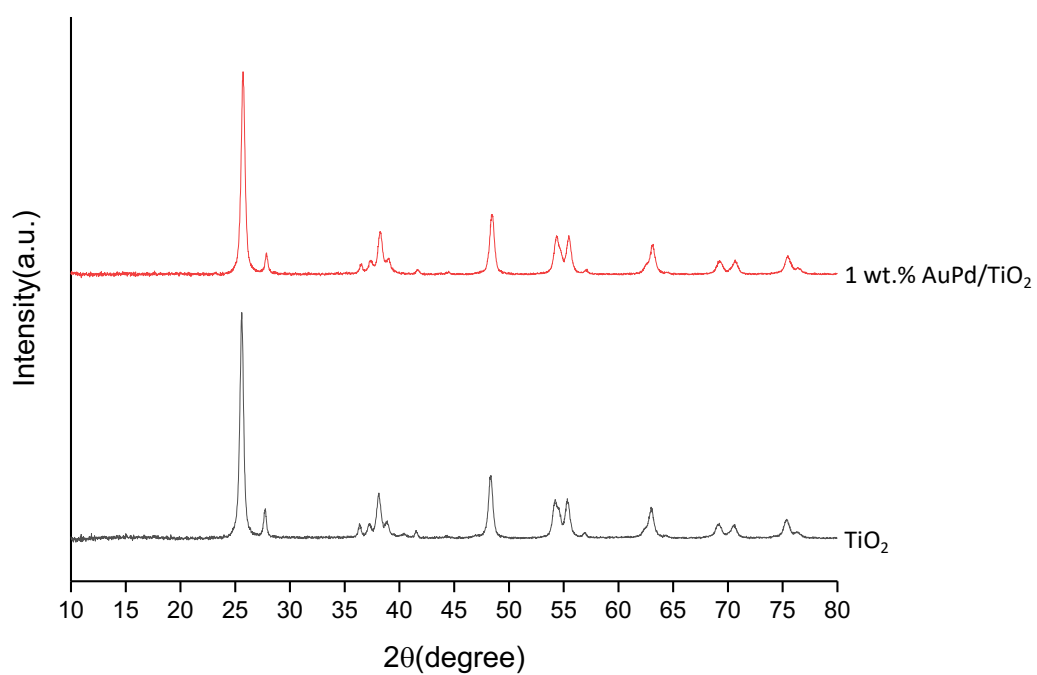
Figure 5.17: X-ray diffractograms of powdered 1 wt.% AuPd/TiO$_2$ supported catalysts. **ICCD Reference Number:** TiO$_2$: 01-086-1157, Pd: 01-087-0638, Au: 01-071-4614.
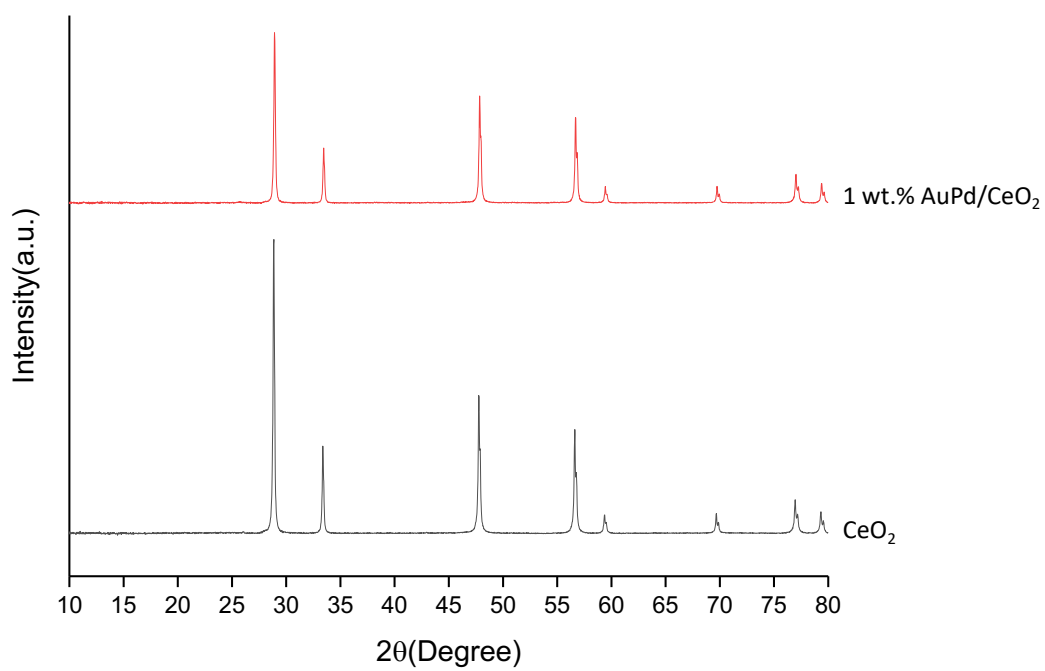
Figure 5.18: X-ray diffractograms of powdered 1 wt.% AuPd/CeO$_2$ supported catalysts. **ICCD Reference Number:** CeO$_2$: 01-081-9325, Pd: 01-087-0638, Au: 01-071-4614.
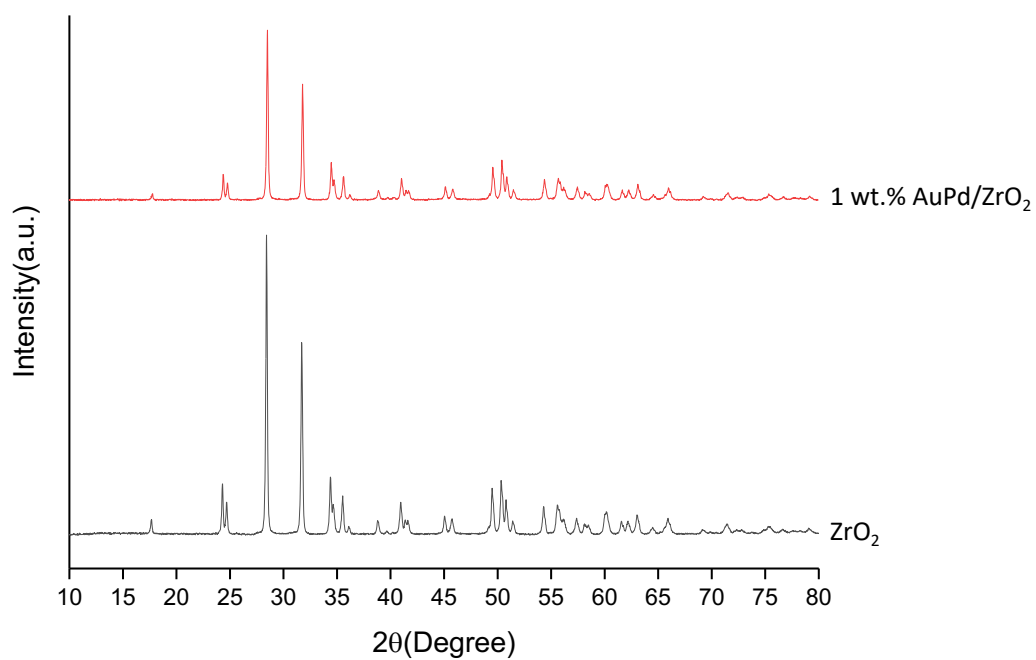
Figure 5.19: X-ray diffractograms of powdered 1 wt.% AuPd/ZrO$_2$ supported catalysts. **ICCD Reference Number:** ZrO$_2$: 01-083-0937, Pd: 01-087-0638, Au: 01-071-4614.
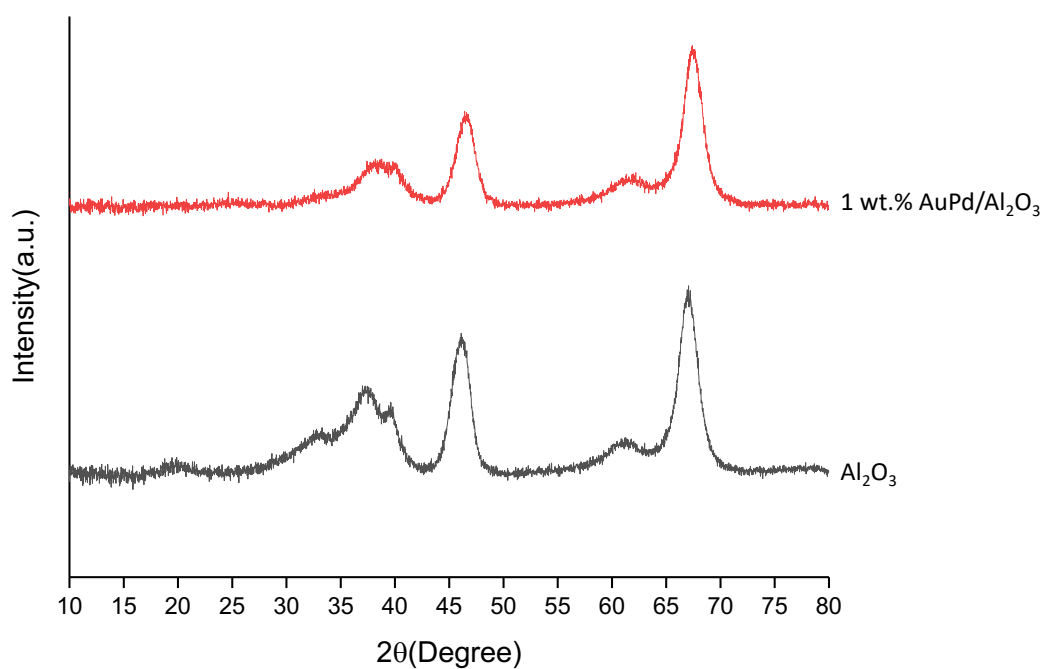
Figure 5.20: X-ray diffractograms of powdered 1 wt.% AuPd/Al_2O_3 supported catalysts. **ICCD Reference Number:** Al_2O_3: 01-083-0937, Pd: 01-087-0638, Au: 01-071-4614.

Figure 5.21: X-ray diffractograms of powdered 1 wt.% AuPd/Nb_2O_5 supported catalysts. **ICCD Reference Number:** Nb_2O_5: 00-027-1003, Pd: 01-087-0638, Au: 01-071-4614.
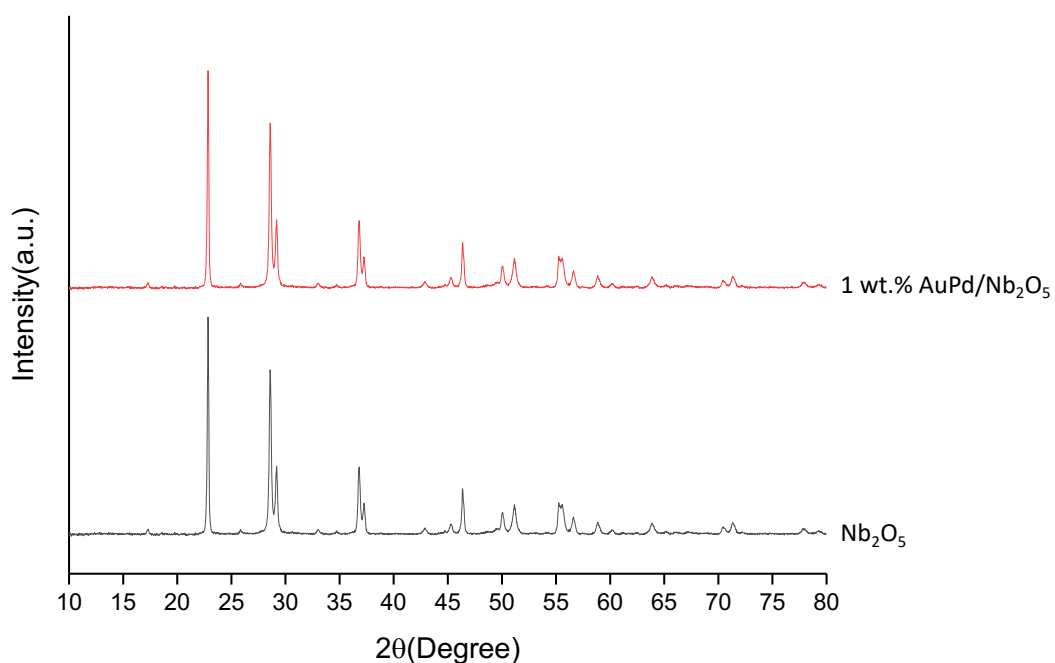
5.16 References.

1   A. Plauck, E. E. Stangland, J. A. Dumesic and M. Mavrikakis, *Proc. Natl. Acad. Sci. U. S. A.*, 2016, **113**, E1973–E1982.

2   V. R. Choudhary, C. Samanta and T. V. Choudhary, *Appl. Catal. A Gen.*, 2006, **308**, 128–133.

3   V. R. Choudhary, A. G. Gaikwad and S. D. Sansare, *Catal. Letters*, 2002, **83**, 235–239.

4   Y. F. Han and J. H. Lunsford, *Catal. Letters*, 2005, **99**, 13–19.

5   Q. Liu and J. H. Lunsford, *Appl. Catal. A Gen.*, 2006, **314**, 94–100.

6   V. R. Choudhary and C. Samanta, *J. Catal.*, 2006, **238**, 28–38.

7   F. Menegazzo, M. Signoretto, E. Ghedini and G. Strukul, *Catalysts*, 2019, **9**, 1-32.

8   J. K. Edwards, S. F. Parker, J. Pritchard, M. Piccinini, S. J. Freakley, Q. He, A. F. Carley, C. J. Kiely and G. J. Hutchings, *Catal. Sci. Technol.*, 2013, **3**, 812–818.

9   J. K. Edwards, B. Solsona, E. N. N, A. F. Carley, A. a Herzing, C. J. Kiely and G. J. Hutchings, *Science*, 2009, **323**, 1037–1041.

10   A. P. Hong, D. W. Bahnemann and M. R. Hoffmann, *J. Phys. Chem.*, 1987, **91**, 2109–2117.

11   D. A. Crole, R. Underhill, J. K. Edwards, G. Shaw, S. J. Freakley, G. J. Hutchings and R. J. Lewis, *Philos. Trans. R. Soc. A Math. Phys. Eng. Sci.*, 2020, 378, 1-11.

12   S. Maity and M. Eswaramoorthy, *J. Mater. Chem. A*, 2016, **4**, 3233–3237.

13   F. Alotaibi, S. Al-Mayman, M. Alotaibi, J. K. Edwards, R. J. Lewis, R. Alotaibi and G. J. Hutchings, *Catal. Letters*, 2019, **149**, 998–1006.

14   X. Gong, R. J. Lewis, S. Zhou, D. J. Morgan, T. E. Davies, X. Liu, C. J. Kiely, B. Zong and G. J. Hutchings, *Catal. Sci. Technol.*, 2020, **10**, 4635–4644.

15   S. Wang, K. Gao, W. Li and J. Zhang, *Appl. Catal. A Gen.*, 2017, **531**, 89–95.

16   C. M. Crombie, R. J. Lewis, D. Kovačič, D. J. Morgan, T. J. A. Slater, T. E. Davies, J. K. Edwards, M. S. Skjøth-Rasmussen and G. J. Hutchings, *Catal. Letters*, 2021, **151**, 2762–2774.

17   S. Wang, R. J. Lewis, D. E. Doronkin, D. J. Morgan, J.-D. Grunwaldt, G. J. Hutchings and S. Behrens, *Catal. Sci. Technol.*, 2020, **10**, 1925–1932.

18   D. E. Doronkin, S. Wang, D. I. Sharapa, B. J. Deschner, T. L. Sheppard, A. Zimina, F. Studt, R. Dittmeyer, S. Behrens and J. D. Grunwaldt, *Catal. Sci. Technol.*, 2020, **10**, 4726–4742.

19   J. K. Edwards, A. Thomas, A. F. Carley, A. A. Herzing, C. J. Kiely and G. J. Hutchings, *Green Chem.*, 2008, **10**, 388–394.

20   J. García-Serna, T. Moreno, P. Biasi, M. J. Cocero, J. P. Mikkola and T. O. Salmi, *Green Chem.*, 2014, **16**, 2320–2343.

21   F. Menegazzo, P. Burti, M. Signoretto, M. Manzoli, S. Vankova, F. Boccuzzi, F. Pinna and G. Strukul, *J. Catal.*, 2008, **257**, 369–381.

22   J. K. Edwards, A. Thomas, B. E. Solsona, P. Landon, A. F. Carley and G. J. Hutchings, *Catal. Today*, 2007, **122**, 397–402.

23   S. Park, J. G. Seo, J. C. Jung, S. H. Baeck, T. J. Kim, Y. M. Chung, S. H. Oh and I. K. Song, *Catal. Commun.*, 2009, **10**, 1762–1765.

24   M. B. Pinto, A. L. Soares, M. C. Quintão, H. A. Duarte and H. A. De Abreu, *J. Phys. Chem. C*, 2018, **122**, 6618–6628.

25   J. K. Edwards, S. J. Freakley, A. F. Carley, C. J. Kiely and G. J. Hutchings, *Acc. Chem. Res.*, 2014, **47**, 845–854.

26   M. Piccinini, J. K. Edwards, J. A. Moulijn and G. J. Hutchings, *Catal. Sci. Technol.*, 2012, **2**, 1908–1913.

27   V. R. Choudhary, C. Samanta and A. G. Gaikwad, *Chem. Commun.*, 2004, **10**, 2054–2055.

28   J. K. Edwards, J. Pritchard, L. Lu, M. Piccinini, G. Shaw, A. F. Carley, D. J. Morgan, C. J. Kiely and G. J. Hutchings, *Angew. Chemie - Int. Ed.*, 2014, **53**, 2381–2384.

29   J. K. Edwards, S. J. Freakley, A. F. Carley, C. J. Kiely and G. J. Hutchings, *Acc. Chem. Res.*, 2014, **47**, 845–854.

30   R. J. Lewis and G. J. Hutchings, *ChemCatChem*, 2019, **11**, 298–308.

31   P. Tian, L. Ouyang, X. Xu, C. Ao, X. Xu, R. Si, X. Shen, M. Lin, J. Xu and Y. F. Han, *J. Catal.*, 2017, **349**, 30–40.

32   J. Brehm, R. J. Lewis, D. J. Morgan, T. E. Davies and G. J. Hutchings, *Catal. Letters*, 2021, **152**, 254-262.

33   R. J. Lewis, PhD Thesis, Cardiff Univeristy, 2016.

34   P. Landon, P. J. Collier, A. F. Carley, D. Chadwick, A. J. Papworth, A. Burrows, C. J. Kiely and G. J. Hutchings, *Phys. Chem. Chem. Phys.*, 2003, **5**, 1917–1923.

35   Z. Fan, Y. H. Kwon, X. Yang, W. Xu and Z. Wu, *Energy Procedia*, 2017, **105**, 1858–1863.

36   M. H. Ab Rahim, R. D. Armstrong, C. Hammond, N. Dimitratos, S. J. Freakley, M. M. Forde, D. J. Morgan, G. Lalev, R. L. Jenkins, J. A. Lopez-Sanchez, S. H. Taylor and

G. J. Hutchings, *Catal. Sci. Technol.*, 2016, **6**, 3410–3418.

37   D. I. Enache, J. K. Edwards, P. Landon, B. Solsona-Espriu, A. F. Carley, A. A. Herzing, M. Watanabe, C. J. Kiely, D. W. Knight and G. J. Hutchings, *Science*, 2006, **311**, 362–365.

38   J. K. Edwards, A. F. Carley, A. A. Herzing, C. J. Kiely and G. J. Hutchings, *Faraday Discuss.*, 2008, **138**, 225–239.

39   J. K. Edwards, J. Pritchard, M. Piccinini, G. Shaw, Q. He, A. F. Carley, C. J. Kiely and G. J. Hutchings, *J. Catal.*, 2012, **292**, 227–238.

6   Conclusions and Future Work.

6.1   Conclusion

The direct synthesis of H_2O_2 represents an economical and environmental alternative to the anthraquinone process, with the route to H_2O_2 production being potentially 100% atom efficient and able to utilise non-toxic solvents, with both of these factors being major drawbacks of the current industrial route to commercial H_2O_2 manufacture. While monometallic catalysts have expressed the ability to synthesise H_2O_2, including Pt[1,2] and Pd[3,4], it is the bimetallic catalysts that have shown promise, with AuPd systems perhaps the most extensively studied.[5–8] The synergistic enhancement in activity of AuPd systems, in comparison to their monometallic analogues, are often to the ensemble effect, which dilutes Pd ensembles known to be active for H_2O_2 decomposition pathways, and the ligand effect, in which electron donation from Au into Pd d-band is able to inhibit O-O bond scission[9], and the resulting formation of H_2O. Due to these effects AuPd catalyst have been well documented for the direct synthesis of H_2O_2[7,10–13] as well as other reactions such as phenol[14] and benzyl alcohol oxidation.[11] However, an increasing amount of interest has focused on the use of H_2O_2 use as a chemical oxidant for us in the treatment of wastewater,[15,16] with such focus typically utilising Advanced Oxidation Processes (AOPs),[17–21] where pre-formed H_2O_2 is utilised in addition to UV-light,[17–19] Ozone,[22,23] Fentons active metals[20,21] or a combination thereof. However, there are numerous limitations to these approaches that would prevent their practical application, not least the presence of the chemical stabilisers used to prolong the shelf life of H_2O_2. The direct synthesis of H_2O_2 from the dilute stream of H_2 and O_2 has the potential to overcome many of the drawbacks associated with the application of AOPs and allow for on-site water remediation.

While considerable attention has been placed on the evolution of H_2O_2 synthesising catalysts using batch regimes,[24–26] owing in-part to rapidity of catalyst screening which such systems allow, for application in the treatment of water streams the use of flow systems are likely to be favoured.

Indeed, while not as prevalent in the literature there have been some works that have studied the direct synthesis of H_2O_2 under a flow regime.[27,28] In particular, Freakley *et. al*[29] has investigated the efficacy of a 1 wt.% AuPd/TiO$_2$ catalyst towards H_2O_2 synthesis, under a range of reaction conditions. Using optimal conditions, which utilised a methanol co-solvent, which

would clearly not be suitable for water treatment, and dilute reagent streams it was possible to synthesise 760 ppm. Over 30 minutes on-stream. Building on this earlier study, the work in this thesis has demonstrated that it is still possible to synthesise considerable concentrations of H_2O_2 (202 ppm), using an identical catalyst to that used by Freakley *et. al*[29], despite the removal of the alcohol co-solvent.

With the recent drive towards the use of H_2O_2 as a chemical oxidant for water treatment, due to its production of non-toxic by-products upon application (only H_2O), its high redox potential and oxidative properties, it was important to comprehend if this system had any biocidal activity. This was confirmed when an 8 $\log_{10}$ concentration of *E. coli* (JM109) was passed through the system, with results confirming a 7 $\log_{10}$ reduction with the 0.5 wt.% Au-0.5 wt.% Pd/TiO$_2$ catalyst once again. The efficacy of the *in-situ* generated H_2O_2 towards greywater remediation was then compared against current disinfectants such as commercial H_2O_2, un-stabilised preformed H_2O_2 and sodium hypochlorite, with concentrations varying from 5-10000 ppm. The results further supported the enhanced biocidal efficacy of the *in-situ* generated H_2O_2, with the commercial disinfectants observed to result in no more than a 1 $\log_{10}$ reduction of the *E. coli* (JM109). The species responsible for this enhanced activity was then deduced to be the reactive oxygen species (ROS) generated on route to H_2O_2, a combination of $HO^{\bullet}$, $HOO^{\bullet}$ and $O_2^{\bullet-}$, which was confirmed via EPR and spin trapping experimentation. Notably, the presence of Au in the catalyst was required to promote the release of these radical species from the catalyst surface, with EPR studies indicating the presence of the ROS in the reaction solution, as supported by earlier theoretical work by Ishihara *et. al*[30] who reported the role of Au in promoting the release of H_2O_2 during the direct synthesis reaction.

Chemical pollutants have also shown susceptibility to ROS, with Koivunen *et. al*[17] and Marquez *et. al*[31] identifying the ability of H_2O_2 to oxidise viruses and pesticides respectively. While there is great interest in the removal of these pollutants, the treatment of antibiotics can be considered to be of equal/greater importance given the ever-growing use of these chemicals in both humans and livestock. Previous work has indicated the susceptibility of ROS, generated during advanced oxidation processes, in the oxidative degradation of antibiotics.[32–35] In particular, the remediation of metronidazole, a common antibiotic, has been demonstrated to be highly susceptible to treatment via ROS generated by AOPs[33,36]. Building on these works, the *in-situ* generation of H_2O_2, and its radicals, were then trialed for there ability to degrade metrondazole (50 ppm). The 0.5 wt.% Au-0.5 wt.% Pd/TiO$_2$ catalyst was shown to convert

23% of metronidazole after 30 minutes of reaction, with this metric increasing to 39% after 2 hours of reaction time. Further investigation of the propensity of bare TiO_2 and commercial H_2O_2 for to absorb/degrade metronidazole respectively, revealed minimal conversion (< 10%), indicating the potential ability of *in-situ* H_2O_2 and ROS to convert metronidazole. However, further testing revealed that the method to which the metronidazole was being converted may not be dominated by oxidative degradation. When oxygen was removed from the reaction (5% H_2/N_2 only), complete conversion of metronidazole was observed, suggesting metronidazole hydrogenation was the dominant for the degradation of the molecule. This was confirmed through additional studies into the effect of the $H_2:O_2$ ratio on the conversion of metronidazole, which revealed that the less oxygen present in the system the greater the extent of conversion. ^1H NMR was then utilised to aid in determining the extent of oxidative and hydrogenation products of metronidazole. The analysis of post-reaction solutions indicated that following the application of H_2/O_2 gaseous reagents no noticeable oxidative degradation occurred. By comparison, when metronidazole was subjected to H_2 alone NMR analysis indicated the hydrogenation of metronidazole at both double bond's present in the imidazole ring, as indicated by the range of NMR signals between 3-5 ppm, while the absence of a signal at ~8.5 ppm ruled out the hydrogenation of the nitro group withing the molecule.

The preferential hydrogenation of metronidazole over oxidation, utilising a AuPd catalyst, may not have been unexpected. Recent investigations by Santos *et. al*[14] in to the oxidative degradation of phenol via the *in-situ* production of H_2O_2 indicated the negligible activity of AuPd catalysts to oxidise phenol. Indeed, other bimetallic catalysts, such as $PdFe/TiO_2$, were shown to greatly outperform the AuPd analogue. Thus, indicating that while H_2O_2 and ROS may have the ability to oxidise chemical contaminants, such as metronidazole AuPd systems are likely to not be prime candidates for further study. Additional research by Crombie *et. al*[37] indicated that the combination of Pd with Fentons active metals may offer enhanced activity for radical-based feedstock valorisation, while Ntainjua *et. al*[8] reported the promotive effect that can be achieved through the careful selection of catalyst support on H_2O_2 formation rates. With these earlier studies in mind, and with the need to find alternative catalytic systems to those based around AuPd, which would offer comparable H_2O_2 synthesis rates which also offering improved activity to radical based oxidation, an extensive catalyst design investigation was undertaken, using a batch regime. With an aim to further study optimal candidates for both H_2O_2 synthesis and *E. coli* remediation in a flow regime. Initially a range of common oxides were investigated as supported for AuPd nanoparticles, with TiO_2, Al_2O_3 and SiO_2 based

materials demonstrating promising results producing $H_2O_2 > 70$ mol_{H2O2} kg_{cat}^{-1} h^{-1}. However, upon re-use all catalysts were shown to be unstable, exhibiting a loss of activity, in the region of 45-95%. As no metal leaching was observed via ICP-MS analysis of post reaction solutions the loss of chlorine (a known promoter of H_2O_2 synthesis) from the surface of the catalyst was considered to be the underlying cause of deactivation, with Brehm *et. al*[38] reporting similar findings for analogously prepared catalyst.

The replacement of Au with a range of secondary metals (Fe, Co, Ni, Pt, Zn, and In), was also studied, with these metals previously identified to promote catalytic performance of Pd-based catalysts prepared via alternative synthesis procedures that are used within this work.[2,25–32] These studies demonstrated the efficacy of the 1 wt.% CoPd/TiO$_2$, and 1 wt.% PtPd/TiO$_2$ catalysts, which offered H_2O_2 synthesis rates greater than 60 mol_{H2O2} $kg_{cat}^{-1}h^{-1}$. However, once again upon re-use, these catalysts were found to be unstable, losing between 14-76% of their initial activity, likely due to the aforementioned loss of chlorine from the surface of the catalyst.

6.2 Further Work.

Catalyst stability for both the synthesis of H_2O_2 and the *in-situ* oxidative degradation of both *E. coli* and Metronidazole has been identified as an issue throughout this research, with all catalysts unable to retain their initial activity. The insufficient reusability of these materials, prepared via an excess-chloride wet co-impregnation procedure is attributed to the loss of surface chloride during initial use of the material, as demonstrated by Brehm *et. al*.[38] This earlier work further established that spent catalysts could be regenerated through the addition of Cl, in the form of CaCl$_2$ or MgCl$_2$. This information leads to the conclusion that the excess-chloride wet co-impregnation preparation method is not suitable for the prolonged production of H_2O_2 due to the dependence on Cl to modify Pd active sites. Therefore, alternative routes to catalyst preparation should be studied further, with the synthesis of AuPd catalysts by co-impregnation, sol-immobilisation and deposition precipitation all previously investigated for H_2O_2 synthesis, catalysts prepared by these routes should be studied for their efficacy in the remediation of wastewater.

A further theme throughout this work is metal leaching, although the metal leaching is not substantial (<5%), leaching of any kind will prevent the adsorption of a catalytic route to water treatment on an industrial scale. Yet again the use of alternative routes to catalyst synthesis may be a resolution to this problem, Indeed, Solsona *et. al*[39] have reported that a 2.5 wt.% Au-

2.5% wt.% Pd/Al_2O_3 catalyst prepared by a wet co-impregnation procedure and calcined at 400 °C for 16 hours does not leach any metal during use in the direct synthesis of H_2O_2 reaction, while also maintaining its initial activity towards H_2O_2 production. This finding is promising, given that this catalyst has a higher total metal loading than the ones used in my research, yet is still able to prevent any leaching into the reaction solution. Given this result the data points towards moving towards a wet co-impregnation preparation method may be the key to preventing precious metal leaching and allowing future industrial application. Furthermore, the application of zeolites could be a route to generating a catalyst active for the direct synthesis of H_2O_2 while not leaching any metal. Jin *et. al*[40] have reported the stability of a $AuPd@SiO_2$ catalyst was crystallised into an MFI zeolite framework for methane oxidation to methanol using in-situ generated H_2O_2.

A previously mentioned issue with the application of commercial H_2O_2 is the need for solutions to be concentrated, stored, and then transported and diluted upon requirement, with acidic stabilisers often employed to promote shelf-life. While all these steps lead to an increase in cost, the presence of stabilisers is a key factor to focus on, particularly as they have been shown to limit catalyst stability, decrease reactor lifetime through corrosion, and generate substantial costs associated with removal of these stabilizers from product streams.[41] Likewise, all chemical transformations that use pre-formed H_2O_2 suffer from these drawbacks to a certain degree. Common stabilisers used for this process include colloidal stannate, sodium pyrophosphate, organophosphates, nitrates, and phosphoric acid, however the quantities of these stabilisers present in solution are unknown given their industrial application but can range anywhere from a 1:10,000 to 1:1 ratio of stabiliser to H_2O_2.[42] From this, it is clear that the use of commercial H_2O_2 for the treatment of greywater has many adverse effects and the *in-situ* generation of H_2O_2 and its ROS for the same treatment of greywater could overcome this issue given further research. Furthermore, it could be of interest to investigate into alternative ways of preventing degradation of commercial H_2O_2, inexpensive ways to which the stabilizers can be removed and stabilizers in which catalyst stability is not affected.

A key finding of Chapter 4 was the identification of the potential role of hydrogenation pathways chemical conversion. The competition between oxidative and hydrogenation pathways may be a concern when it comes to the treatment of real-world contaminated water streams. As such detailed analysis of product streams may be necessary to identify the extent to which contaminants are truly denatured or their hazardous properties inhibited.

It should be noted that pathogens other than *E. coli* can be found in greywater and have also been shown to be susceptible to the oxidative degradation. This was confirmed by Zuorro *et. al*[43] in which the application of UV/H_2O_2 was successful for the treatment of Staphylococcus aureus. Antibiotics and herbicides can also be found in greywater effluent and fortunately have also expressed susceptibility to oxidative degradation via O_3, O_3/H_2O_2 and Fe^{2+}/H_2O_2 [18,21,44,45]. Likewise, steroids and hormones have also been identified as greywater contaminants of growing concern. Fortunately, all have been receptive to oxidative degradation via either UV/TiO_2, H_2O_2[46] or UV/H_2O_2[47], and therefore are likely candidates for remediation with the *in-situ* H_2O_2 based systems. These results indicate that while oxidative degradation of greywater contaminants seem to be the dominant pathway, the findings of Chapter 4 indicates that some pollutants may be more susceptible to a hydrogenation degradation pathway. While the reactor system used within this work might not be optimal for such an application, given that it operates in a H_2:O_2 ratio of 1:1, it would be of interest to design a system in which both hydrogenation and oxidation pathways can be utilised in the same system without competing for H_2. One possible method to overcome this could be the application of reactor capable of decoupled electrolysis of water. This reactor system could allow greywater to be both hydrogenated and oxidized in tandem without the competition between both pathways.

With the ability of the 0.5 wt.% Au–0.5 wt.% Pd/TiO_2 catalyst to generate H_2O_2 alongside ROS, the further application of such systems outside water treatment should also be investigated. Previous work by Akram *et. al*[48] has indicated that a similar AuPd/TiO_2 catalyst is able to generate 95 ppm of H_2O_2 in the gas phase and under atmospheric pressure. This illustrates the possibility using such systems for the gas phase valorisation of chemical feedstocks and the purification of air.

Furthermore, the *in-situ* liquid phase generation of H_2O_2 could also have many other areas of application. Previous work has indicated that *in-situ* generated H_2O_2 could be used for the oxidation of methane to methanol[40,49], the oxidation of benzyl alcohol[25], the degradation of phenol[14] and as an oxidant for a urea fuel cell[50] to name but a few. With all this work indicating that the catalytic system developed during this research has many avenues of research that could be pursued.

6.3   References.

1   J. K. Edwards, J. Pritchard, L. Lu, M. Piccinini, G. Shaw, A. F. Carley, D. J. Morgan, C. J. Kiely and G. J. Hutchings, *Angew. Chemie - Int. Ed.*, 2014, **53**, 2381–2384.

2   Q. Liu, J. C. Bauer, R. E. Schaak and J. H. Lunsford, *Appl. Catal. A Gen.*, 2008, **339**, 130–136.

3   D. P. Dissanayake and J. H. Lunsford, *J. Catal.*, 2003, **214**, 113–120.

4   D. P. Dissanayake and J. H. Lunsford, *J. Catal.*, 2002, **206**, 173–176.

5   R. J. Lewis, K. Ueura, Y. Fukuta, S. J. Freakley, L. Kang, R. Wang, Q. He, J. K. Edwards, D. J. Morgan, Y. Yamamoto and G. J. Hutchings, *ChemCatChem*, 2019, **11**, 1673–1680.

6   A. Villa, S. J. Freakley, M. Schiavoni, J. K. Edwards, C. Hammond, G. M. Veith, W. Wang, D. Wang, L. Prati, N. Dimitratos and G. J. Hutchings, *Catal. Sci. Technol.*, 2016, **6**, 694–697.

7   J. K. Edwards, S. F. Parker, J. Pritchard, M. Piccinini, S. J. Freakley, Q. He, A. F. Carley, C. J. Kiely and G. J. Hutchings, *Catal. Sci. Technol.*, 2013, **3**, 812–818.

8   E. Ntainjua N., J. K. Edwards, A. F. Carley, J. A. Lopez-Sanchez, J. A. Moulijn, A. A. Herzing, C. J. Kiely and G. J. Hutchings, *Green Chem.*, 2008, **10**, 1162–1169.

9   F. Gao and D. W. Goodman, *Chem. Soc. Rev.*, 2012, **41**, 8009–8020.

10   J. A. Lopez-Sanchez, N. Dimitratos, P. Miedziak, E. Ntainjua, J. K. Edwards, D. Morgan, A. F. Carley, R. Tiruvalam, C. J. Kiely and G. J. Hutchings, *Phys. Chem. Chem. Phys.*, 2008, **10**, 1921–1930.

11   J. Pritchard, L. Kesavan, M. Piccinini, Q. He, R. Tiruvalam, N. Dimitratos, J. A. Lopez-Sanchez, A. F. Carley, J. K. Edwards, C. J. Kiely and G. J. Hutchings, *Langmuir*, 2010, **26**, 16568–16577.

12   J. K. Edwards, N. N. Edwin, A. F. Carley, A. A. Herzing, C. J. Kiely and G. J. Hutchings, *Angew. Chemie - Int. Ed.*, 2009, **48**, 8512–8515.

13   E. Ntainjua N., M. Piccinini, J. C. Pritchard, J. K. Edwards, A. F. Carley, J. A. Moulijn and G. J. Hutchings, *ChemSusChem*, 2009, 2, 575–580.

14   A. Santos, R. Lewis, D. J. Morgan, T. Davies, E. Hampton, P. Gaskin and G. Hutchings, *Catal. Sci. Technol.*, 2021, **11**, 7866-7874.

15   Y. Xie, *Disinfection Byproducts in Drinking Water: Formation, Analysis and Control*, Taylor & Francis, 2003.

16   C. Xia, Y. Xia, P. Zhu, L. Fan and H. Wang, *Science.*, 2019, **366**, 226–231.

17   J. Koivunen and H. Heinonen-Tanski, *Water Res.*, 2005, **39**, 1519–1526.

18   B. A. Wols, C. H. M. Hofman-Caris, D. J. H. Harmsen and E. F. Beerendonk, *Water Res.*, 2013, **47**, 5876–5888.

19   H. G. Guo, N. Y. Gao, W. H. Chu, L. Li, Y. J. Zhang, J. S. Gu and Y. L. Gu, *Environ. Sci. Pollut. Res.*, 2013, **20**, 3202–3213.

20   D. Spuhler, J. Andrés Rengifo-Herrera and C. Pulgarin, *Appl. Catal. B Environ.*, 2010, **96**, 126–141.

21   G. F. Ijpelaar, R. T. Meijers, R. Hopman and J. C. Kruithof, *Ozone Sci. Eng.*, 2000, **22**, 607–616.

22   H. Li, X. Zhu and J. Ni, *Electrochim. Acta*, 2011, **56**, 9789–9796.

23   N. Hassanshahi and A. Karimi-Jashni, *Ecotoxicol. Environ. Saf.*, 2018, **161**, 683–690.

24   A. Santos, R. J. Lewis, G. Malta, A. G. R. Howe, D. J. Morgan, E. Hampton, P. Gaskin and G. J. Hutchings, *Ind. Eng. Chem. Res.*, 2019, **58**, 12623–12631.

25   C. M. Crombie, R. J. Lewis, R. L. Taylor, D. J. Morgan, T. E. Davies, A. Folli, D. M. Murphy, J. K. Edwards, J. Qi, H. Jiang, C. J. Kiely, X. Liu, M. S. Skjøth-Rasmussen and G. J. Hutchings, *ACS Catal.*, 2021, **11**, 2701–2714.

26   D. A. Crole, R. Underhill, J. K. Edwards, G. Shaw, S. J. Freakley, G. J. Hutchings and R. J. Lewis, *Philos. Trans. R. Soc. A Math. Phys. Eng. Sci.*, 2020, 378, 1-11.

27   D. E. Doronkin, S. Wang, D. I. Sharapa, B. J. Deschner, T. L. Sheppard, A. Zimina, F. Studt, R. Dittmeyer, S. Behrens and J. D. Grunwaldt, *Catal. Sci. Technol.*, 2020, **10**, 4726–4742.

28   W. Ratchananusorn, D. Gudarzi and I. Turunen, *Chem. Eng. Process. Process Intensif.*, 2014, **84**, 24–30.

29   S. J. Freakley, M. Piccinini, J. K. Edwards, E. N. Ntainjua, J. A. Moulijn and G. J. Hutchings, *ACS Catal.*, 2013, **3**, 487–501.

30   J. Li, T. Ishihara and K. Yoshizawa, *J. Phys. Chem. C*, 2011, **115**, 25359–25367.

31   J. J. R. Márquez, I. Levchuk and M. Sillanpää, *Catalysts*, 2018, **8**, 1-18.

32   V. Homem and L. Santos, *J. Environ. Manage.*, 2011, **92**, 2304–2347.

33   M. Farzadkia, E. Bazrafshan, A. Esrafili, J. K. Yang and M. Shirzad-Siboni, *J. Environ. Heal. Sci. Eng.*, 2015, **13**, 1–8.

34   Q. Dai, J. Zhou, M. Weng, X. Luo, D. Feng and J. Chen, *Sep. Purif. Technol.*, 2016, **166**, 109–116.

35   H. Shemer, Y. K. Kunukcu and K. G. Linden, *Chemosphere*, 2006, 63, 269–276.

36   H. B. Ammar, M. Ben Brahim, R. Abdelhédi and Y. Samet, *J. Mol. Catal. A Chem.*,

2016, **420**, 222–227.

37   C. M. Crombie, R. J. Lewis, D. Kovačič, D. J. Morgan, T. J. A. Slater, T. E. Davies, J. K. Edwards, M. S. Skjøth-Rasmussen and G. J. Hutchings, *Catal. Letters*, 2021, **151**, 2762–2774.

38   J. Brehm, R. J. Lewis, D. J. Morgan, T. E. Davies and G. J. Hutchings, *Catal. Letters*, 2021, **152**, 254-262.

39   B. E. Solsona, J. K. Edwards, P. Landon, A. F. Carley, A. Herzing, C. J. Kiely and G. J. Hutchings, *Chem. Mater.*, 2006, **18**, 2689–2695.

40   Z. Jin, L. Wang, E. Zuidema, K. Mondal, M. Zhang, J. Zhang, C. Wang, X. Meng, H. Yang, C. Mesters and F. S. Xiao, *Science.*, 2020, **367**, 193–197.

41   G. Gao, Y. Tian, X. Gong, Z. Pan, K. Yang and B. Zong, *Chinese J. Catal.*, 2020, **41**, 1039–1047.

42   EU Pat., 0351772A2, 1889.

43   A. Zuorro, M. Fidaleo, M. Fidaleo and R. Lavecchia, *J. Environ. Manage.*, 2014, **133**, 302–308.

44   O. Merih, *Chemosphere,* 2003, **50**, 85–95.

45   Y. Pan, Y. Zhang, M. Zhou, J. Cai and Y. Tian, *Water Res.*, 2019, **153**, 144–159.

46   F. K. Hashem AlAani, Shahir Hashem, *Int. J. ChemTech Res.*, 2017, **10**, 1061–1070.

47   X. Ma, C. Zhang, J. Deng, Y. Song, Q. Li, Y. Guo and C. Li, *Int. J. Environ. Res. Public Health*, 2015, **12**, 12016–12029.

48   A. Akram, S. J. Freakley, C. Reece, M. Piccinini, G. Shaw, J. K. Edwards, F. Desmedt, P. Miquel, E. Seuna, D. J. Willock, J. A. Moulijn and G. J. Hutchings, *Chem. Sci.*, 2016, **7**, 5833–5837.

49   S. Sun, A. J. Barnes, X. Gong, R. J. Lewis, N. F. Dummer, T. Bere, G. Shaw, N. Richards, D. J. Morgan and G. J. Hutchings, *Catal. Sci. Technol.*, 2021, **11**, 8052–8064.

50   Z. Fan, Y. H. Kwon, X. Yang, W. Xu and Z. Wu, *Energy Procedia*, 2017, **105**, 1858–1863.